

**ADSORPTION FROM FLOODING SOLUTIONS IN POROUS MEDIA**

**A Study of Interactions of Surfactants and Polymers  
with Reservoir Minerals—Annual Report**

Date Published—February 1980

Work Performed for the Department of Energy  
Under Contract DE-AC19-79BC10082

School of Engineering and Applied Science  
Columbia University  
New York, N.Y.



**U. S. DEPARTMENT OF ENERGY**

## NOTICE

This report was prepared as an account of work sponsored by an agency of the United States Government. Neither the United States nor any agency thereof, nor any of their employees, makes any warranty, expressed or implied, or assumes any legal liability or responsibility for any third party's use or the results of such use of any information, apparatus, product or process disclosed in this report, or represents that its use by such third party would not infringe privately owned rights.

Printed in the United States of America  
Available from  
National Technical Information Service  
U.S. Department of Commerce  
5285 Port Royal Road  
Springfield, VA 22161

### NTIS price codes

Printed copy: \$9.50  
Microfiche copy: \$3.00

ADSORPTION FROM FLOODING SOLUTIONS IN POROUS MEDIA

A Study of Interactions of Surfactants  
and Polymers with Reservoir Minerals

Annual Report

Professor P. Somasundaran  
Principal Investigator  
School of Engineering and Applied Science  
Columbia University  
New York, NY 10027

Robert L. Berg  
Technical Project Officer  
San Francisco Operations Office  
Fossil Energy Division  
Oakland, CA 94612

Date Submitted--December 1979  
Date Published--January 1980

Work Performed for the Department of Energy  
Under Contract DE-AC19-79BC10082

ADSORPTION FROM FLOODING SOLUTIONS IN POROUS MEDIA--  
A Study of Interactions of Surfactants  
and Polymers with Reservoir Minerals

Annual Report Submitted by  
Professor P. Somasundaran

to

The Department of Energy  
The National Science Foundation  
Amoco Production Company  
Chevron Oil Field Research Company  
Exxon Research and Engineering Company  
Gulf Research and Development Company  
Marathon Oil Company  
Mobil Research and Development Company  
Shell Development Company  
Texaco, Inc.  
Union Oil Co. of California

Principal Investigator: Professor P. Somasundaran  
Co-Investigator: Professor C.C. Gryte  
Research Staff: K.P. Ananthapadmanabhan  
L.K. Anderson  
S. Ayril  
M.S. Celik  
A. Goyal (until February, 79)  
A.F. Hollander  
Dr. I.B. Ivanov  
M.A. Ivanova  
D. Karmakar  
Dr. E.D. Manev  
B.M. Moudgil  
S.V. Sazdanova-Maneva

DOE Contract Number: DE-AC19-79BC 10082

NSF Grant Number: ENG-78-11776

School of Engineering and Applied Science  
Columbia University in the City of New York

July 1979

## CONTENTS

CONVERSION FACTORS . . . . .	vi
LIST OF FIGURES . . . . .	vii
SUMMARY . . . . .	xiv
I. ADSORPTION OF SURFACTANTS ON RESERVOIR MINERALS . . . . .	1
A. Introduction . . . . .	1
B. Materials and Methods . . . . .	3
B.1. MINERALS . . . . .	3
B.2. SURFACTANTS AND OTHER CHEMICALS . . . . .	4
B.3. EXPERIMENTAL PROCEDURES . . . . .	11
B.3.a. Purification of Na-Dodecylbenzene- sulfonate . . . . .	11
B.3.b. Adsorption Experiments . . . . .	28
C. Results and Discussion . . . . .	33
C.1. KINETICS OF ABSTRACTION OF NaDDBS ON Na-KAOLINITE . . . . .	33
C.2. PRECIPITATION, ABSTRACTION AND ADSORPTION . . . . .	35
C.3. EFFECT OF PURITY AND CHEMICAL COMPOSITION OF THE SURFACTANT . . . . .	43
C.4. EFFECT OF OIL ON THE ADSORPTION ON PURIFIED NaDDBS ON Na-KAOLINITE . . . . .	51
D. Conclusions . . . . .	57
LIST OF SYMBOLS AND ABBREVIATIONS . . . . .	59
II. SOLUTION CHEMISTRY OF SURFACTANTS . . . . .	60
A. Chemical Equilibria in Surfactant Solutions and Their Role in Adsorption at Interfaces . . . . .	60
A.1. INTRODUCTION . . . . .	60
A.2. SURFACE ACTIVITIES OF SURFACTANT COMPLEXES . . . . .	61
A.3. THERMODYNAMICS OF SURFACE TENSION OF SYSTEMS CONTAINING SURFACTANT COMPLEXES . . . . .	72
A.4. EXPERIMENTAL . . . . .	85
A.5. RESULTS AND DISCUSSION . . . . .	88
B. Precipitation/Redissolution Phenomena . . . . .	94
B.1. INTRODUCTION . . . . .	94
B.2. KINETICS OF PRECIPITATION . . . . .	94

B.3.	PRECIPITATION AND REDISSOLUTION WITH MULTIVALENT IONS. . . . .	99
B.4.	ADDITION OF MONO AND MULTIVALENT SALT MIXTURES. . . . .	104
C.	Mechanisms of Precipitation/Redissolution Phenomena: Surface Tension Studies . . . . .	107
C.1.	INTRODUCTION. . . . .	107
C.2.	THEORY. . . . .	108
C.3.	EXPERIMENTAL. . . . .	114
C.4.	RESULTS AND DISCUSSION. . . . .	114
C.5.	CONCLUSIONS . . . . .	120
D.	Surfactant-Polymer Interactions . . . . .	122
D.1.	INTRODUCTION. . . . .	122
D.2.	RELATIVE VISCOSITY MEASUREMENTS . . . . .	122
D.3.	SURFACE TENSION STUDIES . . . . .	123
	LIST OF SYMBOLS AND ABBREVIATIONS . . . . .	128
III.	DYNAMIC STUDIES OF THE INTERACTION OF POLYMER AND SUR- FACTANT WITH CORE MINERALS. . . . .	131
A.	Adsorption Characteristics of Poly(acrylamides) on Sodium Kaolinite. . . . .	131
A.1.	INTRODUCTION . . . . .	131
A.2.	EXPERIMENTAL PROCEDURES . . . . .	132
A.2.a.	Preparation of Acrylamide Copolymers. . . . .	132
A.2.b.	Preparation of Sodium Kaolinite . . . . .	134
A.2.c.	Procedure for Polymer Adsorption. . . . .	135
A.3.	DISCUSSION OF RESULTS . . . . .	136
B.	Polymeric Flow Distributions in Consolidated Sandstone . . . . .	163
B.1.	INTRODUCTION. . . . .	163
B.2.	EXPERIMENTAL DEVELOPMENT. . . . .	165
B.2.a.	Background. . . . .	165
B.2.b.	Apparatus . . . . .	167
B.2.c.	Experiments . . . . .	169
B.2.d.	Results and Discussion. . . . .	171
B.3.	MODEL DEVELOPMENT . . . . .	175
B.3.a.	Background. . . . .	175
B.3.b.	Mathematical Development. . . . .	177
B.3.c.	Theoretical Results and Discussion. . . . .	184

C.	Tomographic Observation of Oil Displacement . . . .	195
C.1.	INTRODUCTION . . . . .	195
C.2.	PROCEDURE . . . . .	196
	C.2.a. Calibration of CAT Scan . . . . .	196
	C.2.b. CAT Scan of Oil Displacement . . . . .	196
C.3.	DISCUSSION OF RESULTS . . . . .	199

CONVERSION FACTORS

Conversion Factor  
(Multiply Cust-  
omary Unit by  
Factor to get the  
SPE-Preferred

<u>Quantity</u>	<u>SPE Preferred SI Unit</u>	<u>Customary Unit</u>	<u>SI Unit)</u>
Abstraction Precipitation Adsorption	mol/Kg	M/g	$10^{-3}$
Concentration	$\text{mol/m}^3$	M/l	$10^{-3}$
Surface tension	mN/m	dyne/cm	1
Time	h	min.	60
Wave Numbers	$\text{m}^{-1}$	$\text{cm}^{-1}$	$10^{-2}$

## LIST OF FIGURES

### Chapter I

1. Surface tension of recrystallized and LC-purified Na-dodecylbenzenesulfonate as a function of concentration...	5
2. Surface tension of Na p(1, butyloctyl) benzenesulfonate ( Texas #2) as a function of concentration .....	6
3. Vapor phase chromatogram (VPC) of n-octane.....	7
4. Vapor phase chromatogram (VPC) of n-decane.....	8
5. Vapor phase chromatogram (VPC) of n-dodecane.....	9
6. Surface tension of NaCl aqueous solutions as a function of concentration.....	10
7. Chromatograms of as-received and purified Na-dodecylbenzenesulfonate.....	14
8. ALC chromatogram of deoiled Na-dodecylbenzenesulfonate.....	15
9. Prep LC chromatogram of as-received Na-dodecylbenzenesulfonate (10 g/100 ml).....	16
10. ALC chromatogram of recrystallized Na-dodecylbenzenesulfonate.....	17
11. ALC chromatogram of peak #2 from Figure I.9.....	18
12. IR spectrum of as-received Na-dodecylbenzenesulfonate.....	20
13. IR spectrum of peak #1 from Figure I.9 (trisubstituted benzene ring).....	21
14. NMR of peak #1 from Figure I.9 (trisubstituted benzene ring).....	22
15. IR spectrum of peak #2 from Figure I.9 (purified Na-dodecylbenzenesulfonate).....	23

16. NMR of peak #2 from Figure I.9 (purified Na-dodecylbenzenesulfonate).....	24
17. Total ionic current pattern of p-NaDDBS, elluent #2.....	25
18. Total ionic current pattern of p-NaDDBS, elluent #2 (repeat analysis).....	25
19. Fragmentation pattern of p-NaDDBS, scan #129 from Figure I.17.....	26
20. Fragmentation pattern of p-NaDDBS, scan #168 from Figure I.18.....	27
21. Calibration curve for titration of recrystallized Na-dodecylbenzenesulfonate with hexadecyltrimethylammonium bromide (HTAB).....	29
22. Calibration curve for titration of Na p(1, butyloctyl) benzenesulfonate (Texas #2) with hexadecyltrimethylammonium bromide (HTAB).....	30
23. Abstraction kinetics of Na-dodecylbenzenesulfonate on Na-kaolinite.....	34
24. Abstraction, precipitation and adsorption of LC-purified Na-dodecylbenzenesulfonate on Na-kaolinite as a function of concentration.....	36
25. Surface tension of LC-purified Na-dodecylbenzenesulfonate in 0.1 M/l NaCl and in clay supernatant prepared in 0.1 M/l NaCl.....	38
26. Abstraction isotherms of LC-purified NaDDBS on Na-kaolinite at constant ionic strength and at constant concentration of NaCl added.....	41
27. Residual concentration of Na-dodecylbenzenesulfonate in 1 M/l NaCl as a function of the initial concentration in the presence and in the absence of Na-kaolinite.....	42
28. Abstraction, adsorption and precipitation isotherms of as-received NaDDBS on Na-kaolinite. Adsorption isotherm is compared to that of LC-purified NaDDBS.....	45
29. Abstraction isotherms of recrystallized and LC-purified NaDDBS on Na-kaolinite in 0.1 M/l NaCl.....	46

30. Abstraction isotherms of Na-p(1, butyloctyl) benzene-sulfonate (Texas #2) on Na-kaolinite.....	48
31. Abstraction isotherms of a mixture of recrystallized NaDDBS and Na-p(1, butyloctyl) benzenesulfonate at various molar ratios.....	49
32. Abstraction of a mixture of recrystallized NaDDBS and Na-p(1, butyloctyl) benzenesulfonate (Texas #2) as a function of molar ratio .....	50
33. Effect of addition of n-octane on the adsorption of Na-dodecylbenzenesulfonate on Na-kaolinite.....	53
34. Effect of addition of n-dodecane on the adsorption of Na-dodecylbenzenesulfonate on Na-kaolinite.....	54
35. Effect of addition of n-decane on the abstraction of Na-dodecylbenzenesulfonate on Na-kaolinite.....	55

## Chapter II

1. Species Distribution Diagram of Potassium Oleate Solutions as a function of pH at $C_T = 3 \times 10^{-5}$ M. The constants used in computing this diagram are: $pK_s = 7.6$ , $pK_a = 4.95$ , $pK_D = -4.0$ and $pK_{AD} = -4.95$ .....	62
2. Species Distribution Diagram as a function of pH for Na-dodecylsulfonate solutions at $C_T = 10^{-4}$ M. The constants used in computing this diagram are: $pK_a = -1.3$ , $pK_D = -3.0$ and $pK_{AD} = -4.48$ .....	64
3. Species Distribution Diagrams as a function of pH for Na-dodecylsulfate solutions at $C_T = 10^{-4}$ M. The constants used in computing this diagram are: $pK_a = -3.0$ , $pK_D = -2.39$ and $pK_{AD} = -3.88$ .....	65
4. A schematic diagram of an apparatus for measuring surface potential. E-Radio Active Electrode, R-Reference Electrode.	86
5. Correlation of the calculated surface tension with the experimentally obtained values as a function of oleate concentration at pH 11.4. Buffer is $K_2HPO_4/KOH$ .....	89
6. Adsorption Density of oleate at the Liquid/Air Interface as a function of its concentration showing an anomaly in the absence of premicellar aggregation.....	91

7.	Kinetics of precipitation as measured by optical density for Texas #2 solutions in the presence of different concentrations of $\text{CaCl}_2$ .....	96
8.	Percent light transmission as a function of added salt concentration in the presence of $1.44 \times 10^{-3} \text{M}$ deoiled sodium dodecylbenzenesulfonate.....	98
9.	Percent transmission of Texas #2 sulfonate solutions as a function of its concentration in the presence of $7.5 \times 10^{-3} \text{M}$ $\text{CaCl}_2$ .....	100
10.	Percent light transmission as a function of added Na-dodecylbenzenesulfonate and $\text{AlCl}_3$ concentrations.....	101
11.	Percent light transmission as a function of added $\text{CaCl}_2$ concentration in the presence of different concentrations of Texas #2 sulfonate.....	103
12.	Percent light transmission as a function of added concentration of NaCl for two concentrations of sodium dodecylbenzenesulfonate in the presence of $5 \times 10^{-3} \text{M}$ $\text{CaCl}_2$ .....	105
13.	Surface tension as a function of the total concentration of NaDDBS in the presence of $10^{-3} \text{M}$ $\text{CaCl}_2$ .....	115
14.	Surface tension as a function of the total concentration of NaDDBS in the presence of $5 \times 10^{-4} \text{M}$ $\text{Al}(\text{NO}_3)_3$ .....	118
15.	Relative viscosity of 1,000 ppm of polyacrylamide (PAM) as a function of concentration of sodium dodecylsulfonate (NaDDS).....	124
16.	Surface tension of sodium dodecylsulfonate (NaDDS) in the presence of 1,000 ppm of polyacrylamide (PAM).....	126

### Chapter III

1.	(a) Intrinsic viscosity of poly(acrylamide) and the copolymer PAMS as a function of ionic strength. Electrolyte: NaCl; Temperature $30^\circ\text{C}$ , (b) Effect of solution pH on the intrinsic viscosity of poly(acrylamide) and its copolymers Temperature $30^\circ\text{C}$ .....	149
2.	Relative viscosity of a 2000 ppm PAM solution as a function of equilibration time without agitation.....	151
3.	Kinetics of PAM adsorption on sodium kaolinite at the conditions indicated	

( I is concentration of NaCl in ppm; C is the initial PAM concentration in ppm; S is the solid to liquid ratio and H is the initial solution pH).....	152
4. Equilibrium adsorption of PAM on sodium kaolinite as a function of final polymer concentration. (Temperature is 30°C; S is 0.1; equilibrium time is 72 hours; indicated pH is final equilibrium value).....	153
5. Equilibrium adsorption of PAMS on sodium kaolinite as a function of final solution polymer concentration. (conditions as in Figure 4).....	158
6. Equilibrium adsorption of acrylamide copolymers as a function of ionic strength (final polymer concentration 100 ppm; other conditions as in Figure 4).....	160
7. Effect of temperature on the adsorption of acrylamide copolymers on sodium kaolinite.....	161
8. Schematic Representation of Experimental System.....	168
9. Core Permeability Tests with Nitrogen Gas.....	168
10. Typical Sucrose and Polymer Core Residence Time Distribution Profiles that Result from Pulse Injection into Berea Core.....	174
11. Schematic Representation of Repeating Unit for Proposed Model of Core Transport.....	180
12. Modified Repeating Unit wherein Series CFSTR Units Simulate Capillary Plug Flow.....	180
13. Informational Flow Diagram Relating the Experimental Results with the Core Model.....	183
14. Effect of Number of Stages on Model Predicted Exit Concentration Profile.....	185
15. Effect of Mixing Volume Fraction PM on Model.....	185
16. Comparison of Experimental Results and Model Prediction.....	187
17. Sensitivity to Model Parameters $M$ , $Q_1$ and PM.....	187
18. Effect of Flow Rate Distribution on Output for Model with 10 Stages.....	188

19. Effect of Mixing Volume Fraction, PM on Output from Single Stage.....	188
20. Effects of Systems Parameters.....	190
21. Modified and Original Model Compared.....	190
22. Simulated Output from Cores of Different Length from Pulse Injection of Sucrose.....	191
23. Sucrose and Polymer Signals.....	191
24. The Effects of Adsorption on Output Signal.....	192
25. CT Numbers as a Function of Solution Composition for Sand Packed Beds.....	197
26. Berea Sandstone Core used for CAT Scan Experiments...	198
27. CAT Scan of Water-Flooded Berea Sandstone Core.....	201

19. Effect of Mixing Volume Fraction, PM on Output from Single Stage.....	188
20. Effects of Systems Parameters.....	190
21. Modified and Original Model Compared.....	190
22. Simulated Output from Cores of Different Length from Pulse Injection of Sucrose.....	191
23. Sucrose and Polymer Signals.....	191
24. The Effects of Adsorption on Output Signal.....	192
25. CT Numbers as a Function of Solution Composition for Sand Packed Beds.....	197
26. Berea Sandstone Core used for CAT Scan Experiments...	198
27. CAT Scan of Water-Flooded Berea Sandstone Core.....	201

## SUMMARY

### I. Adsorption of Surfactants on Reservoir Minerals

Our previous studies have shown considerable adsorption of the sulfonates on reservoir rocks, the extent of adsorption being dependent on several system parameters such as pH, temperature, ionic strength, type of inorganic cations and anions, etc. The adsorption isotherms were also found to exhibit a maximum in the region around critical micelle concentration under certain conditions. Most importantly, the nature of adsorption or depletion (which also includes the surfactant that is lost by precipitation, entrapment or any other process from the liquid phase) was found to depend markedly on the pretreatment received by minerals as well as the surfactant. It was clear that in as much as adsorption (depletion) of surfactants with reservoir rock minerals is a complex phenomenon involving several types of interactions, a reliable understanding of it is possible only with well characterized mineral/surfactant systems. As none of the sulfonates that were obtained from commercial or academic circles was found to be isomerically pure, a procedure was developed during the last year, with considerable effort, for the purification of the sulfonate using high performance liquid chromatography.

Adsorption experiments conducted with the purified and the as-received sulfonate indicated purification to reduce,

but not eliminate, the extent of maximum. The extent of abstraction of the sulfonate due to precipitation was also determined under certain conditions and found to contribute differently for the purified and unpurified systems. Also adsorption experiments with a mixture of surfactants (normal and branched chain sodium dodecylbenzenesulfonate) showed the latter to act as an impurity in controlling adsorption when present in smaller amounts.

Since precipitation was often observed during the adsorption experiments, its role on the shape of the isotherm was investigated. Results showed that the surfactant when added to solutions containing inorganic electrolytes first precipitates and then, depending on the type of the inorganic ions present, redissolves as surfactant concentration is increased. The redissolution of the precipitate is being investigated now in detail and is considered to be due to solubilization by the micelles. Interestingly, the maximum in precipitation was found to correlate with the maximum in the abstraction isotherm. Adsorption isotherm obtained by isolating precipitation from abstraction still exhibited a maximum, although less sharp.

The effect of the presence of oil in the system was investigated under certain conditions this year. A study of three systems (Na-kaolinite/Na-dodecylbenzenesulfonate/n-octane, n-decane, n-dodecane) that has already been completed showed the addition of oil to decrease both the adsorption and pre-

cipitation. Increase in the chain length of the oil also decreased the adsorption of sulfonate considerably. As the effect of oil is possibly the most important one determining the surfactant loss in reservoir systems, it will be studied in detail with relevant mineral/surfactant/oil systems.

## II. Solution Chemistry of Surfactants

### A. Chemical Equilibria in Surfactant Solutions and Their Role in Adsorption at Interfaces

Solution chemistry of surfactants has a major role in determining various interfacial processes such as adsorption and it is the objective of this work to study such solution chemistry by analyzing the chemical equilibria in surfactant solutions. Towards this goal, most importantly, a basic understanding of various associative interactions in surfactant solutions, especially in the pre and near micellar concentration range is necessary.

In this study, species distribution diagrams have been obtained for some of the most widely used surfactants such as Na-dodecylsulfonate using the thermodynamic data that are available in the literature and the estimates of energy of interaction between molecules. A model has been developed for the comparison of the surface activities of certain types of surfactant complexes.

It is shown that some of the complexes such as acid-soap and dimer can play an important role in governing the inter-

facial adsorption even when the concentration of such complexes in solution is six or eight orders of magnitude lower than that of the monomers.

A thermodynamic model of the surface tension behavior of surfactant solutions incorporating the formation of association complexes such as dimers as a function of pH and total concentration has been developed. It has been shown that the general equation can be reduced to simpler forms depending upon solution conditions. These equations are used to evaluate the formation constants of association complexes under selected conditions.

Surface tension behavior of potassium oleate solutions under high pH and ionic strength conditions has been explained using the thermodynamic model developed here. Also the dimerization constant for this system has been evaluated using the present data. Surface tension results in combination with surface potential values suggest the saturation of liquid/air interface at concentrations that are an order of magnitude lower than the CMC. Hence the changes in slope of  $\gamma$  vs.  $\log C_T$  above this concentration region have been attributed to dimerization in the bulk.

The above results clearly show the importance of the above model for developing a complete understanding of the chemical equilibria in surfactant solutions and in further elucidating the mechanisms governing processes such as adsorption.

## B. Precipitation/Redissolution Phenomena

The effect of inorganic electrolytes on the behavior of surfactants in porous media is of considerable interest because reservoir fluids contain significant amounts of various mono and multivalent inorganic ions. Interaction of these ions with the surfactant species in the bulk solution during chemical flooding can lead to surfactant precipitation and in turn to substantial amount of surfactant depletion and possibly even plugging of reservoir cores.

It was found earlier that multivalent species such as those of Ca and Al can cause precipitation of sulfonate and subsequent redissolution at some concentration above its equivalent concentration of sulfonate. Unlike multivalent ions, the precipitate obtained with monovalent ions, however, did not redissolve in the concentration range studied. In order to gain a better understanding of the precipitation and redissolution phenomena, a systematic study was initiated this year.

Kinetics of precipitation was also studied this year as a function of electrolyte concentration. The rate of formation of precipitates is found to be dependent on experimental conditions. An equilibrium can be obtained within a few minutes or in several hours, depending on the type of ions present and the degree of stirring.

Monovalent salts,  $\text{Na}^+$  and  $\text{K}^+$ , have lesser degree of salt tolerance than  $\text{NH}_4^+$  and  $\text{Li}^+$  salts indicating the role

of the size of the ion. The solubility products of the Ca and Al salts of sulfonate were determined from turbidity measurements.

Possible mechanisms suggested for the redissolution are: solubilization of precipitates in sulfonate micelles, aggregation of charged micelles and their redispersion, and redissolution by complexation. Surface tension results obtained in the presence of  $10^{-3} \text{ M CaCl}_2$  support the mechanism of solubilization in micelles since precipitation occurs before micellization. On the other hand, in the presence of  $5 \times 10^{-4} \text{ M Al(NO}_3)_3$  the surface tension curves exhibit an apparent micellization region before precipitation. Experiments are in progress at present to confirm the above behavior under controlled conditions such as pH.

### C. Surfactant-Polymer Interactions

Surfactant-polymer interactions can lead to reduced oil displacement efficiency of the micellar flood and additional loss of surfactant in the reservoir rock. Earlier results had shown that while increased additions of the surfactant, sodium dodecylbenzenesulfonate, resulted in only a nominal decrease in the adsorption of the polymer polyacrylamide on kaolinite, the addition of polymer produced a marked decrease on the adsorption of surfactant. This year, surface tension of sodium dodecylsulfonate has been found to decrease significantly in the presence of polyacrylamide indi-

cating an increase in the concentration of surface active species at the liquid-gas interface. Relative viscosity measurements also suggest the significance of surfactant-polymer interactions in the mobility of different phases involved. From the preliminary investigations conducted so far, it can be concluded that it is important to investigate the modifications in the bulk and interfacial properties due to surfactant-polymer interactions that can lead to minimum surfactant losses. Adsorption/desorption studies, relative viscosity, surface tension and conductivity measurements are planned to study the mechanism of surfactant-polymer interaction and its implications in surfactant losses during micellar flooding.

### III. Dynamic Studies of the Interaction of Polymer and Surfactant with Core Minerals

This part of the work focuses on three major problem areas: an analysis of the residence time distribution of pulse injected polymer solutions in Berea sandstone cores; the adsorption characteristics of poly(acrylamide) copolymers on sodium kaolinite; and the observation of oil displacement using computer-aided tomography.

A Berea sandstone core (approximately 300 millidarcy permeability) was inserted in a liquid chromatography system in place of a normal column. Using an injection loop, a

pulse of solute (in volume less than 1% of the core void volume) was injected into the core. Two test solutes were investigated, sucrose, a non-interacting solute permeable to all regions of the core, and poly(acrylamide). All of the solutes were in 2000 ppm NaCl solution. The exit concentration profile of the solutes (representing residence time distributions in the core) were measured with a differential refractometer. From these experiments, total retention of the solute, accessible pore volume and the solute residence time distribution were obtained. A model was constructed to allocate solute permeability and adsorption to the different flow domains within the core.

Since retention within the core is, at least in part, the result of adsorption of polymer, a study was undertaken to characterize in detail the interaction between sodium kaolinite and poly(acrylamide). In order to isolate the relative importance of hydrogen bonding interactions with the surface and those due to electrostatic interactions both a homopolymer of acrylamide and a copolymer containing 6.8% by mole of a sulfonate monomer were used. Analysis was made by labeling the polymers with carbon-14. Adsorption measurements were made as a function of ionic strength, solution pH and temperature.

Preliminary experiments were carried out using the technique of computer assisted tomography to observed displacement of an oil with a 1 N KI solution in a filled Berca core.

The electron dense KI solution was clearly observable in the tomographic plane. With the salt solution, about 30% of the pore oil was recovered from the core. This solution passed through large channels, leaving much of the core still filled with oil. Surprisingly, fingers seemed to be oriented in a manner that indicated some stratification in the seemingly homogeneous Berea material.

A. Introduction

An understanding of the phenomenon of surfactant adsorption has indeed been recognized to be of vital importance in investigations related to enhanced oil recovery using micellar flooding. The past studies have however shown that the adsorption of surfactants on clays is a very complex process. Furthermore, proper interpretation of the experimental data for adsorption is made difficult due to large variations that are possible in the characteristics of mineral and surfactant samples. The experience has thus clearly shown the need for careful characterization of the starting materials used in the adsorption study. During our past work we have placed emphasis on proper monitoring of the system in terms of composition and purity of the minerals, surfactants and other chemicals used as well as experimental conditions such as the type and concentration of the added inorganic electrolyte, pH, contact time, temperature etc. This past year we have placed additional emphasis on further purifying the surfactants and on studying the effect of such purification of surfactants and then addition of oil to such purified systems.

The oil present in the reservoir being flooded can also be expected to influence the surfactant adsorption. A study of the effect of addition of oil on adsorption of Na-dodecylbenzenesulfonate on Na-Kaolinite was therefore conducted.

---

\* The list of symbols and abbreviations is given at the end of the chapter.

Adsorption experiments with a series of hydrocarbons of different chain length were carried out.

Finally, adsorption from solution of a mixture of surfactants (normal and branched dodecylbenzenesulfonates) on Na-Kaolinite in dependence on the surfactant composition and concentration was also studied in order to ascertain the effect of variation in the surfactant composition.

A phenomenon that has been found to be of much theoretical and practical interest is the presence of maximum and sometimes even a minimum in the isotherms. The presence of maximum has been attributed in the past to mechanisms involving micellar exclusion from interfacial region due to electrostatic repulsion or structural incompatibility, presence of impurities, surfactant composition, adsorbent morphology, etc. None of these explanations is, however, fully substantiated to be considered as a confirmed mechanism for surfactant adsorption from concentrated solutions particularly due to possibilities for serious experimental artifacts arising from such processes as precipitation and entrapment. Indeed more than one mechanism can be operating in different systems or in the same system under even slightly different conditions.

Since precipitation is often observed during adsorption tests, the role of it in determining the nature of the isotherms was further investigated. In many cases the phenomenon of precipitation was found to be responsible to a great extent for the amount of adsorption as well as its maximum, although it could not fully account for the latter under all conditions.

## B. Materials and Methods

### B.1. MINERAL

The mineral used in the adsorption test was kaolinite. Its preparation which has been described in the previous annual report (July 1978) is given here in greater detail since such details are now considered important to the experiment.

Kaolinite used was from a well crystallized sample purchased from the clay repository at the University of Missouri. The surface area of this sample was determined by nitrogen adsorption and was found to be  $8.35 \text{ m}^2/\text{g}$ . From this sample the homoionic "Na-Kaolinite" was prepared in the following manner:

As received clay was treated with distilled water for 15 minutes with a high speed (1750 r.p.m.) mixer at a solid to liquid ratio of 1:2 by weight. The product was diluted with distilled water to about 1:30 solid to liquid and then allowed to settle for 24 hours. The clear supernatant liquid was then discarded. This process of washing was repeated 10-12 times until there was a negligible change in conductivity of the supernatant solution. The washed kaolinite was repulped with 2M NaCl solution and agitated at high solid to liquid ratio (1:2 to 1:3) for 15 minutes, and then diluted with distilled water to about 1:30. Washing procedure was repeated 10-12 times until a pH of 7 was reached and the conductivity of the suspension remained constant. NaCl treated product was repulped in

1M NaCl at pH 3 and agitated at high solid to liquid ratio (1:2 to 1:3) and then diluted and washed as before 10-12 times until a pH of 7 was reached. During the last washing steps, the fine clay particles were separated from the coarse impurities. The resultant Na-Kaolinite was freeze dried and then stored dry in a desiccator.

## B.2. SURFACTANTS AND OTHER CHEMICALS

Samples of sodium dodecylbenzenesulfonate, specified to be 90% pure by Lachat Chemicals, were purified by deoiling, recrystallization and liquid chromatographic techniques as discussed further on in this chapter.

Pure sodium P(1, butyloctyl) benzenesulfonate (Texas #2) purchased from University of Texas was used as received.

Surface tension versus concentration curves obtained for n-dodecylbenzenesulfonate: recrystallized (Fig.I.1), purified by liquid chromatography (Fig.I.1) as well as the branched P(1, butyloctyl) benzenesulfonate (Fig. I.2) did not indicate the presence of a minimum.

Organic solvents used for purification were A.C.S. certified reagents which were distilled before use.

Hydrocarbons, specified to be 99+% (Gold Label), were purchased from Aldrich Chemical Company, Inc. Vapor phase chromatographic analysis of the batches purchased confirmed their purity (Figures I.3 - 5).

Inorganic salts used to adjust the ionic strength, pH

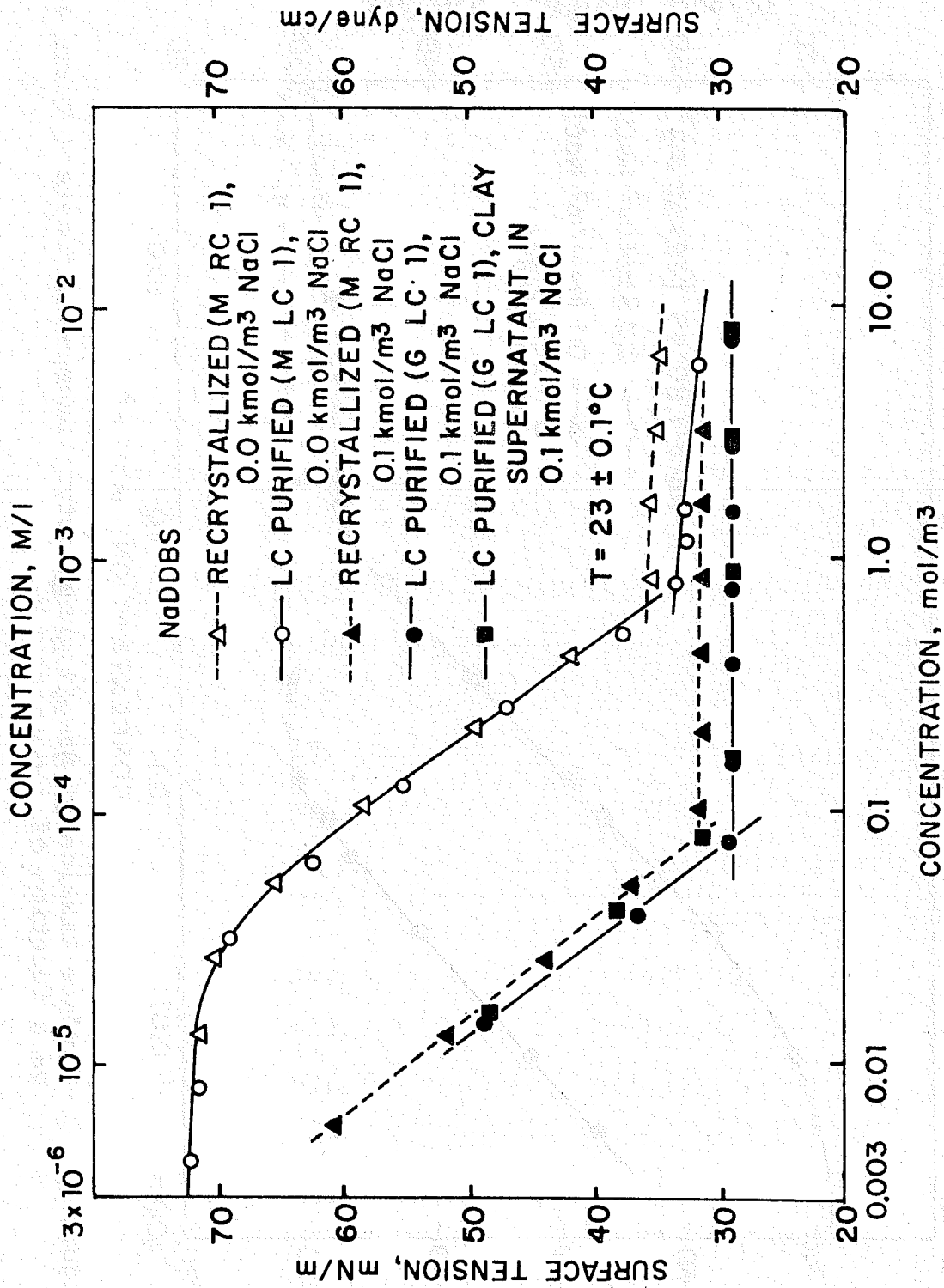


Figure I. 1. Surface tension of recrystallized and LC-purified Na-dodecylbenzenesulfonate as a function of concentration.

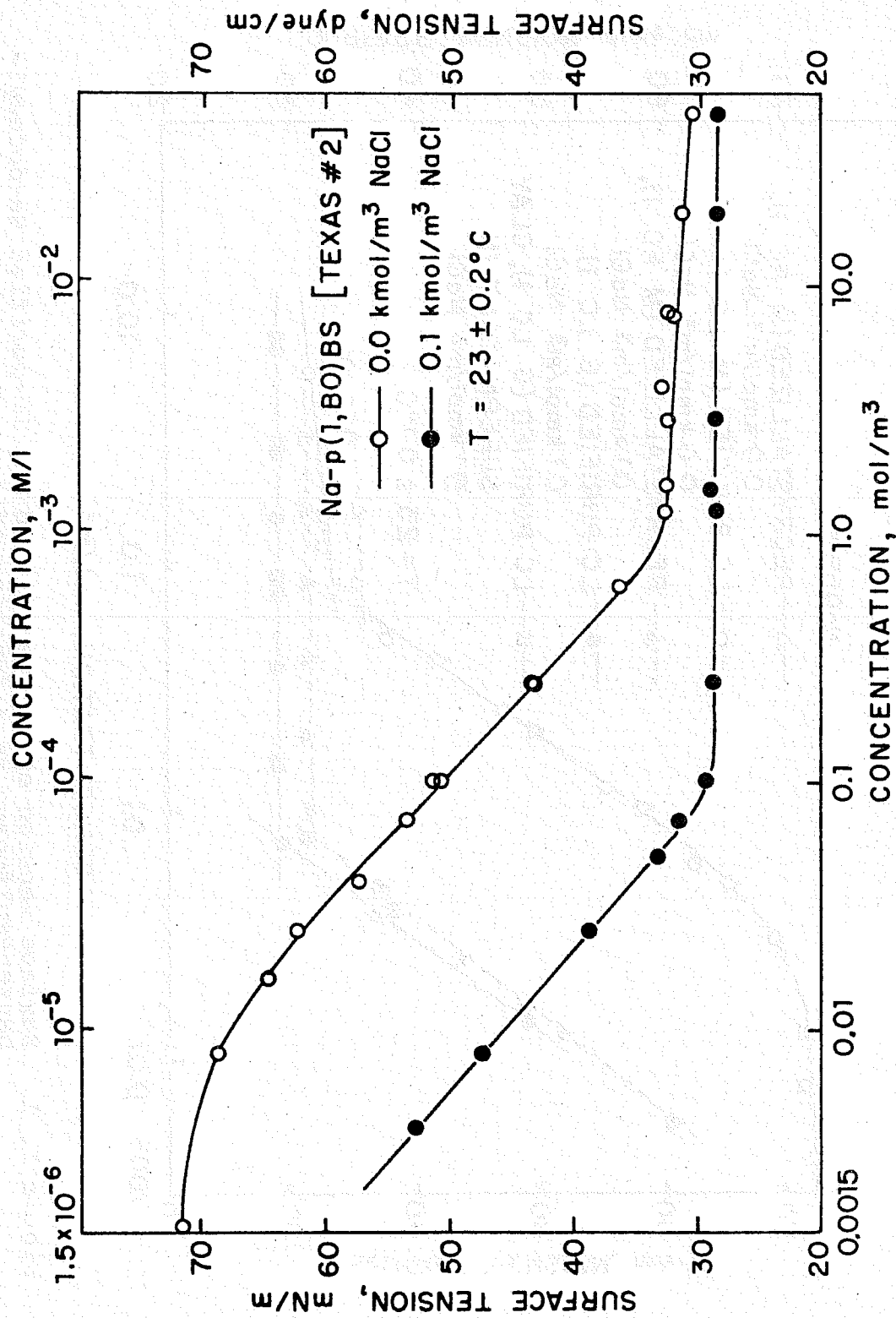


Figure I. 2. Surface tension of Na-p(1, butyloctyl) benzenesulfonate ( Texas #2) as a function of concentration.

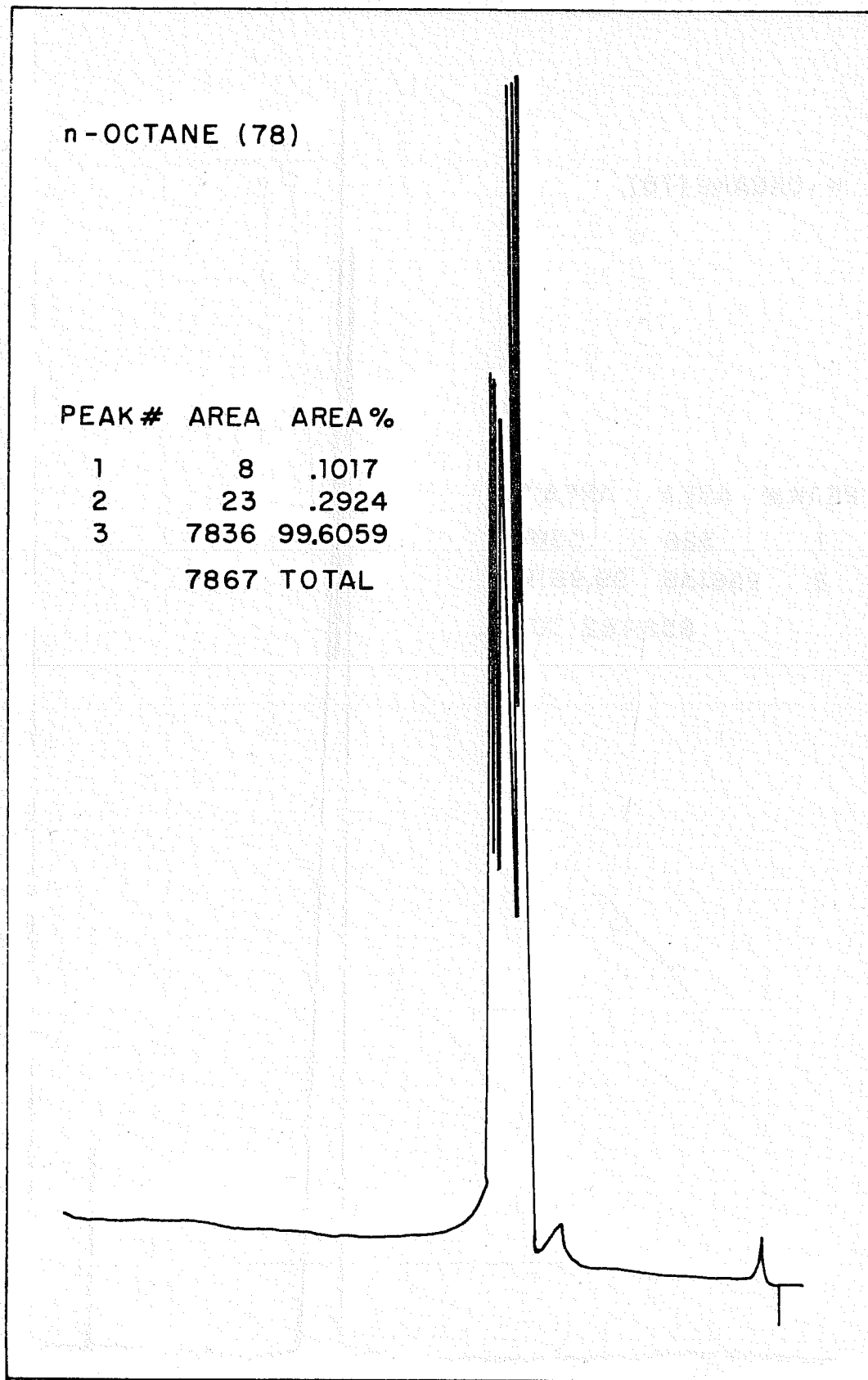


Figure I. 3. Vapor phase chromatogram (VPC) of n-octane.

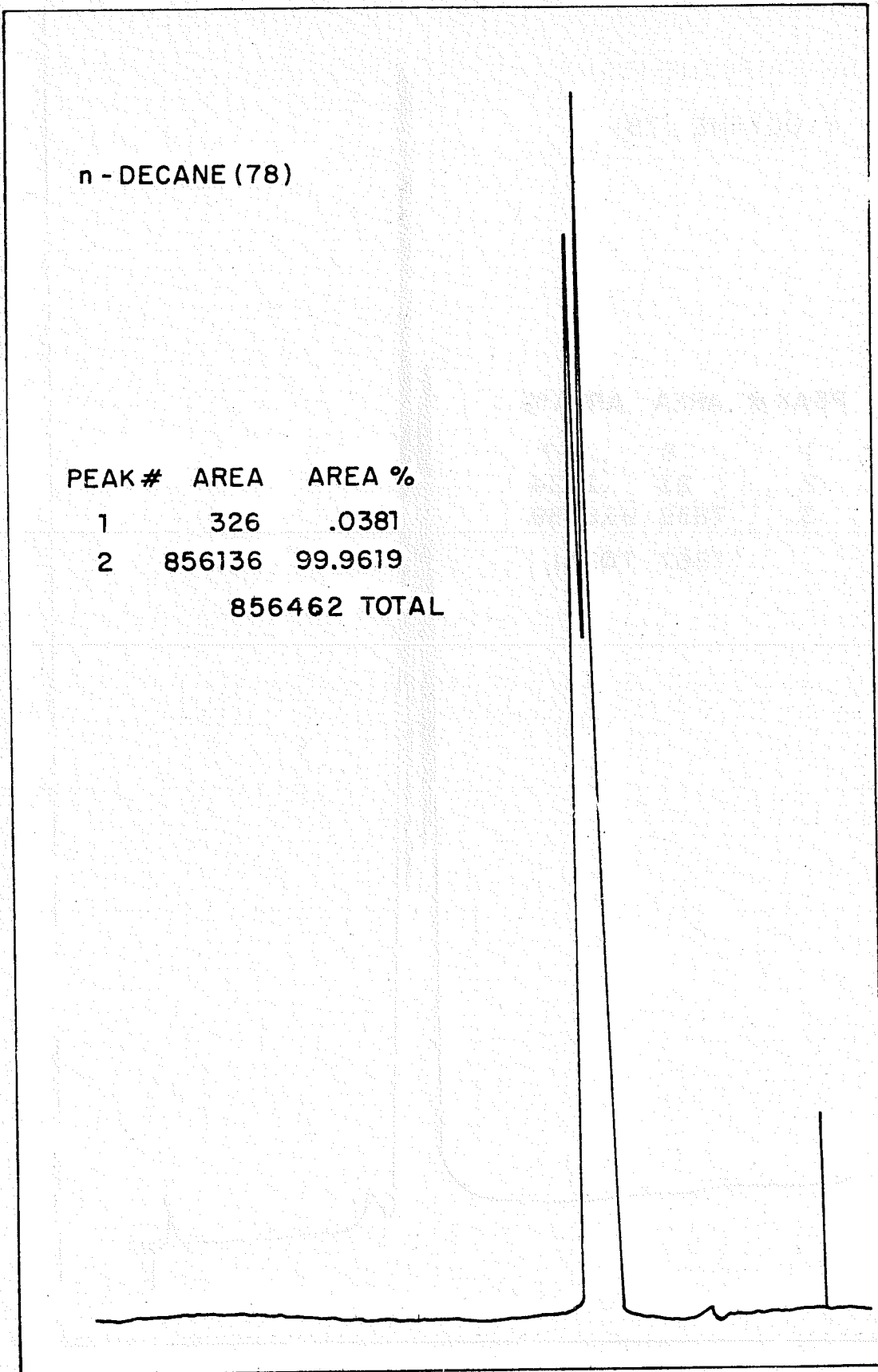


Figure I. 4. Vapor phase chromatogram (VPC) of n-decane.

n-DODECANE (78)

PEAK #	AREA	AREA %
1	762	.0417
2	8858	.4847
3	1814920	99.3211
4	2784	.1523

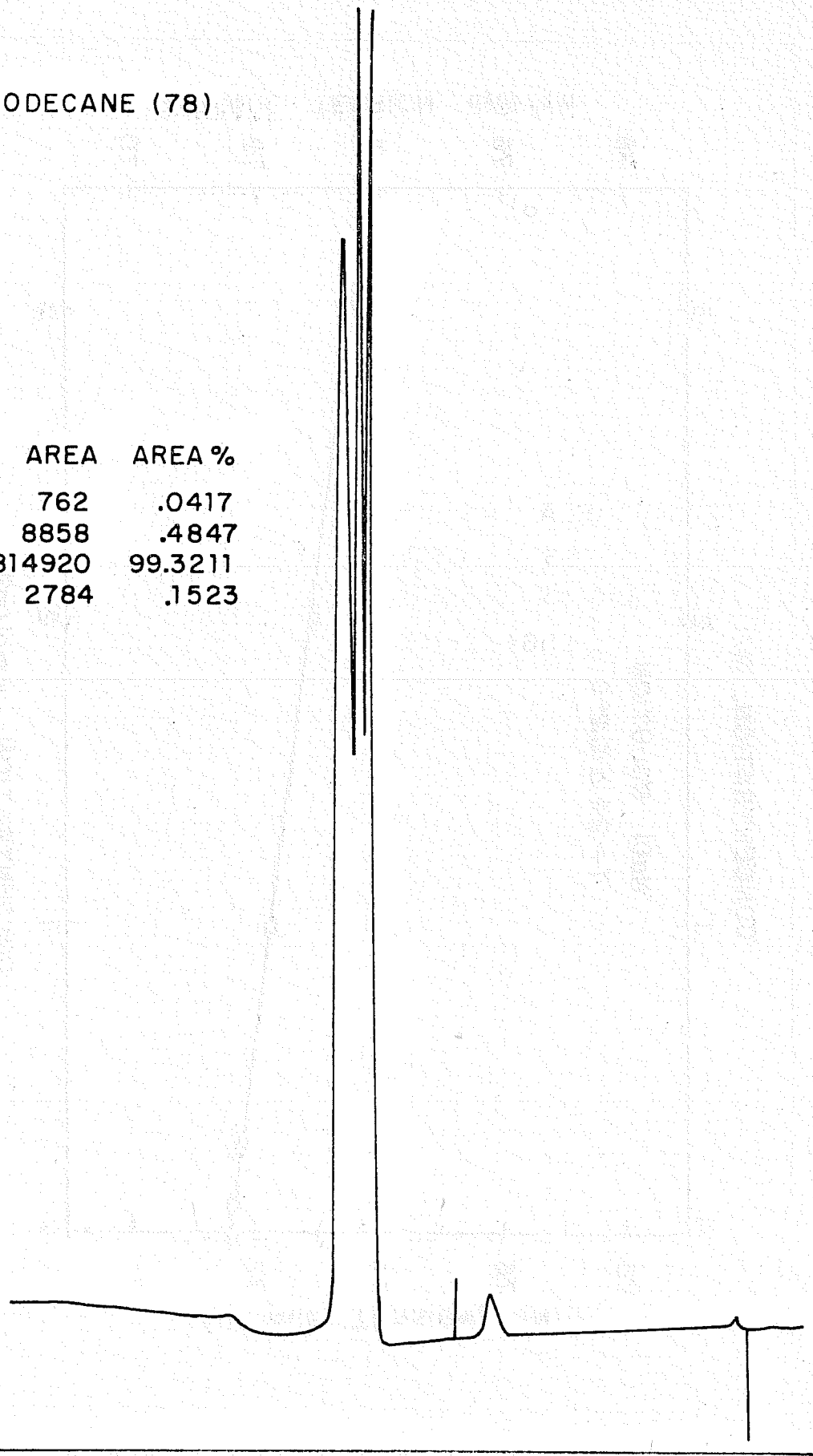


Figure I. 5. Vapor phase chromatogram (VPC) of n-dodecane.

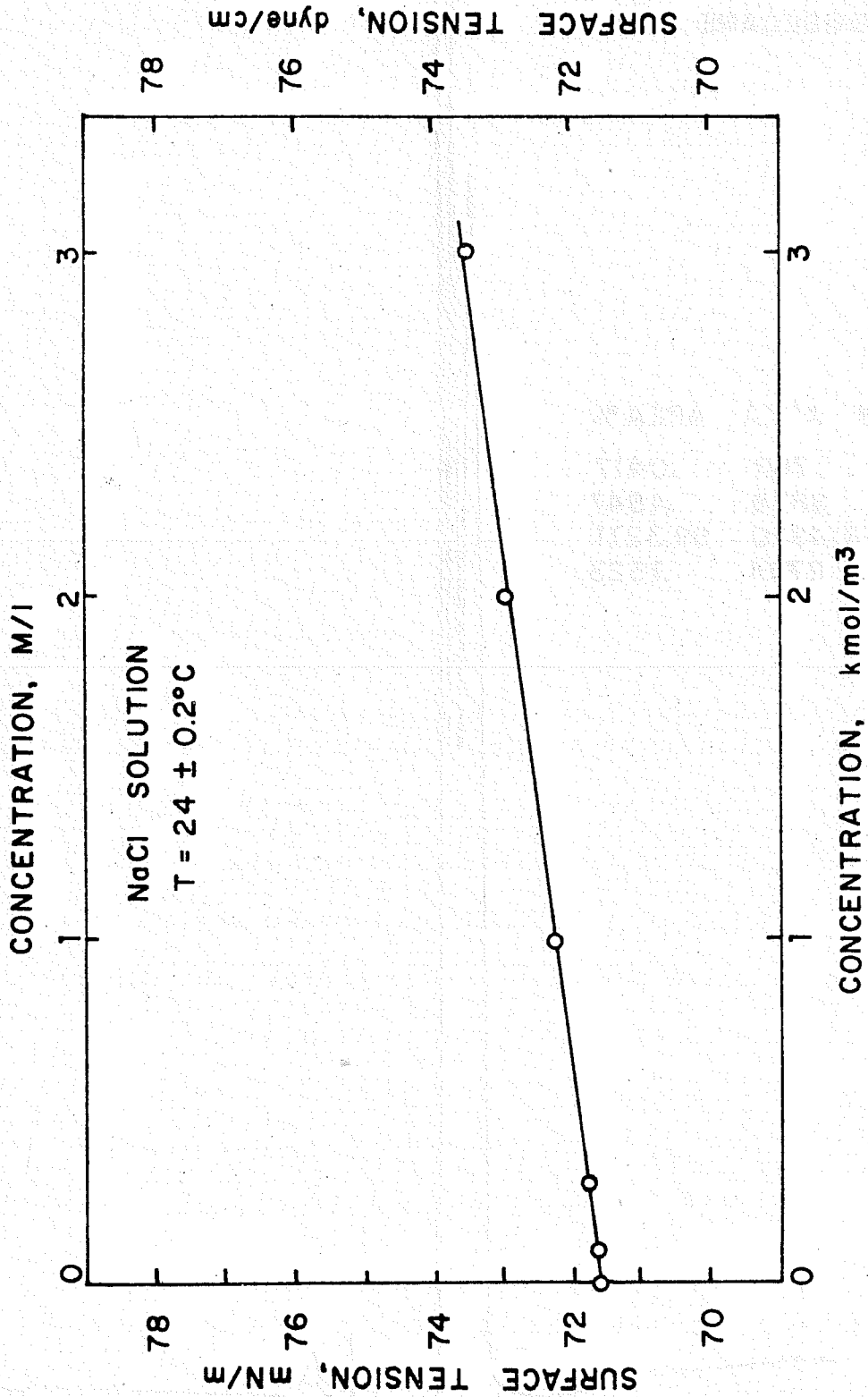


Figure I. 6. Surface tension of NaCl aqueous solutions as a function of concentration.

and in the precipitation experiments were of A.R. Grade. The dependence of the surface tension on the concentration of the NaCl used was also obtained (Fig. I.6).

Triply distilled water was used in all experiments.

### B.3. EXPERIMENTAL PROCEDURES

#### B.3.a. Purification of Na Dodecylbenzenesulfonate

Sodium dodecylbenzenesulfonate purchased from Lachat Chemicals and specified to be 90% pure was first freed from non-polar organic impurities by the following deoiling procedure.

A 75 grams sample of NaDDBS was dissolved in 375 ml 1:1 mixture of distilled methanol and triply distilled water in a large beaker using a magnetic stirrer. The light yellow solution obtained was consequently extracted with three 200 ml portions of petroleum ether. The sulfonate remains in the polar water/methanol phase while oil is extracted into the petroleum ether phase. The colorless petroleum ether phase after evaporation and drying yielded 3.3% oil by weight of the total sample.

Using a rotavapor, the water/methanol solvent was evaporated at 50°C and 160 mm Hg pressure until a very viscous solution is obtained which was used for further purification by means of recrystallization and liquid chromatography.

For recrystallization the residual viscous yellow

substance was dissolved in 250 ml acetone and left overnight in a freezer at about  $-25^{\circ}\text{C}$ . The white crystals were filtered and dried at  $50^{\circ}\text{C}$ . Most of the sulfonate remained dissolved in the acetone; the yield was only about 15% of the starting materials. Recrystallization had been originally considered to be inadequate by itself for the purpose of purification since isomeric impurities can be expected to crystallize along with the desired p-isomer of the DDBS. However, surface tension, precipitation and adsorption experiments as well as analytical liquid chromatography (Figures I.10-11) showed its behavior to be very similar to that of the purified by liquid chromatography. Since recrystallization procedure is much simpler and faster, such sulfonate was prepared in larger quantities and subsequently used in some of the experiments as indicated.

The development of preparatory LC procedure for purification of sulfonates using Waters Associates' Prep LC/System 500 Liquid Chromatograph was based on guidelines established with the help of Analytical Liquid Chromatograph (ALC), as these two techniques are identical in principle. The purification step itself involved injection of sodium dodecylbenzenesulfonate solution into a pre-equilibrated BONDAPAK  $\text{C}_{18}$  column. Scale up work showed that 3 grams of sulfonate was the maximum amount that could be injected into the column without losing the resolution. The eluted components were analyzed using a refractometer. Distilled and filtered solvents were always used to prepare the mobile phase.

The major aspects of purification of sodium dodecylbenzenesulfonate by preparative liquid chromatography are described below.

Initially solutions of methanol or isopropanol in water at various concentrations were used to establish the optimum conditions for the separation of the sulfonate components. The exploratory work conducted at Water Associates indicated that the addition of 1% acetic acid to a solution of 50% methanol in triply distilled water as solvent would produce satisfactory resolution. Acetic acid, by lowering the pH, reduces the dissociation of sulfonate which in turn causes a decrease in the adsorption of it on this column and thus produces a better resolution. Using this solvent, analytical work was done on deoiled sodium salt of the dodecylbenzenesulfonic acid, as received sodium dodecylbenzenesulfonate and sodium dodecylbenzenesulfonate previously purified in our laboratory. Figures I.7-8 indicate that purified sulfonate is not significantly different in chemical composition from the as received sulfonate. Indeed oil is present in the as received sulfonate but it is not seen in the chromatogram since it is retained on the C-18 ALC column. Hence the similarity of the chromatograms is not considered in this case to indicate that the two samples are identical in chemical composition. The chromatograms also show that the purified sulfonate has one

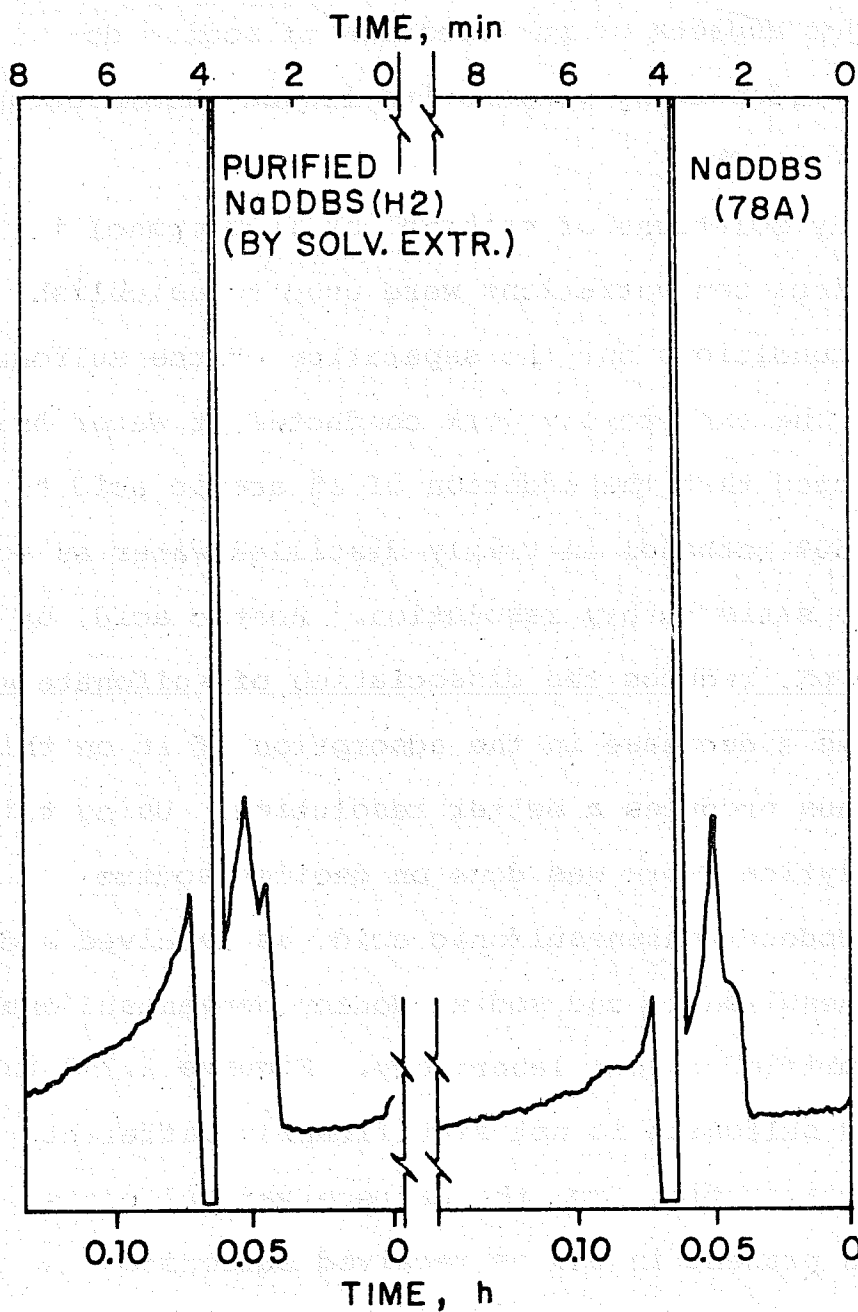


Figure I. 7. Chromatograms of as-received and purified Na-dodecylbenzene-sulfonate.

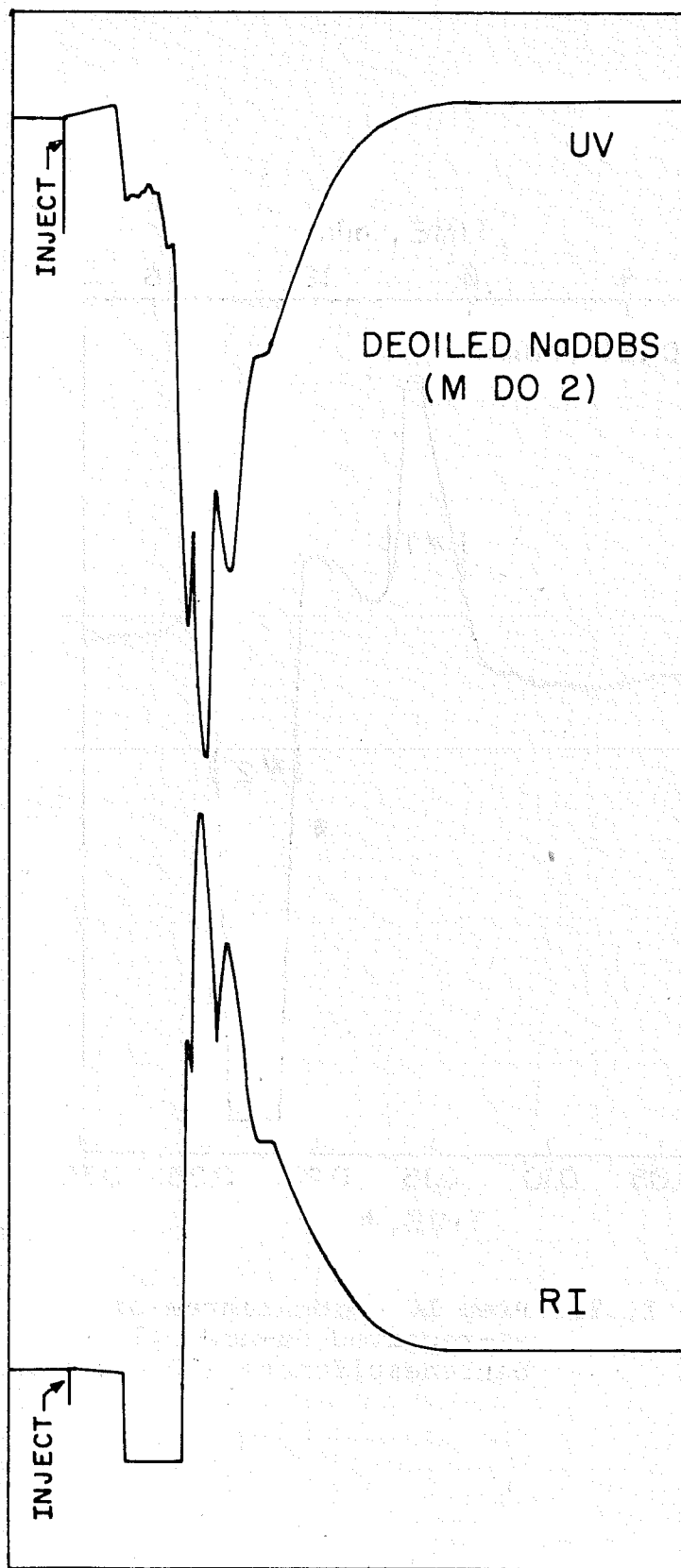


Figure I. 8. ALC chromatogram of deoiled Na-dodecylbenzenesulfonate.

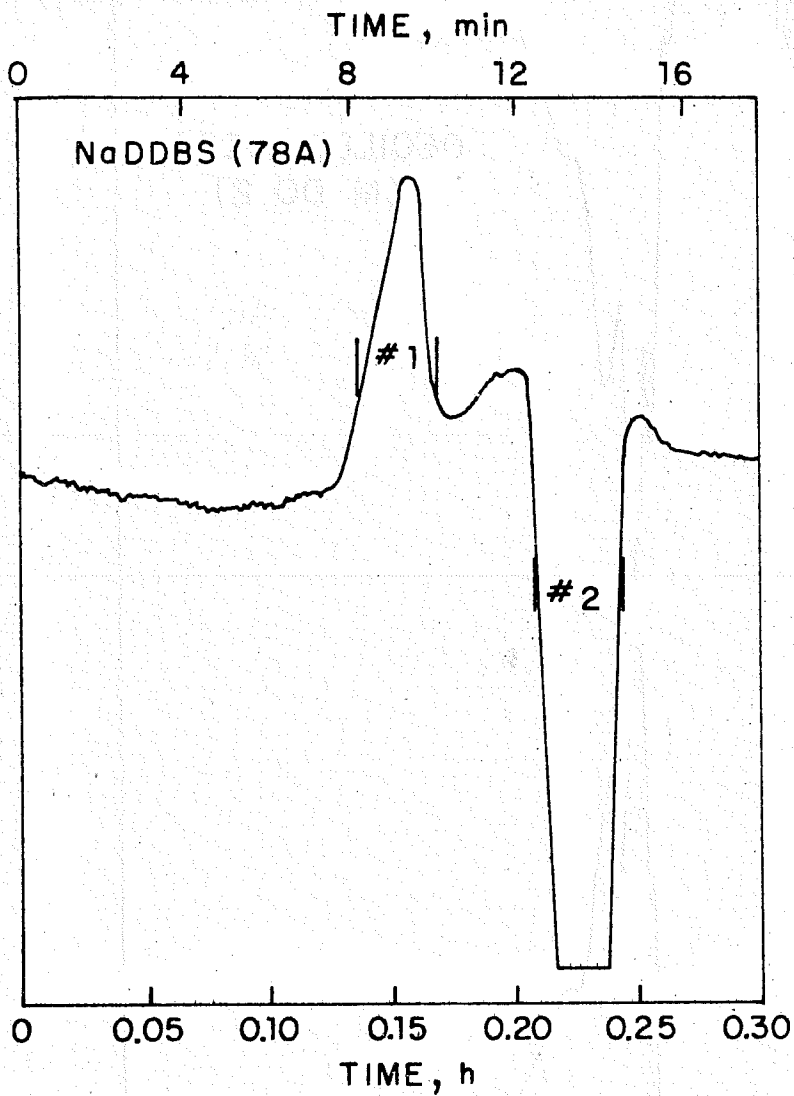


Figure I. 9. Prep LC chromatogram of as-received Na-dodecylbenzenesulfonate (10 g/100 ml).

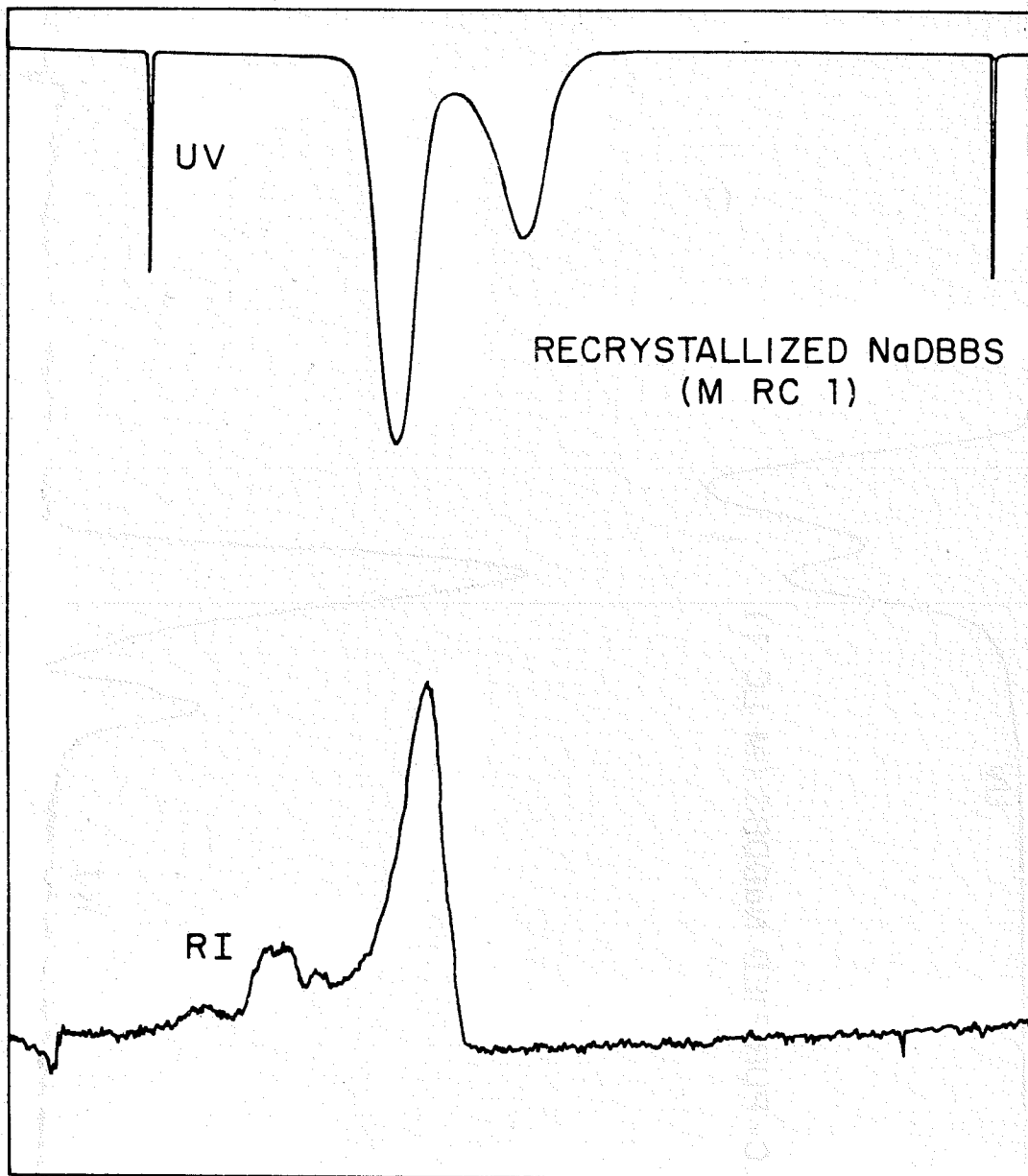


Figure I. 10. ALC chromatogram of recrystallized Na-dodecylbenzenesulfonate.

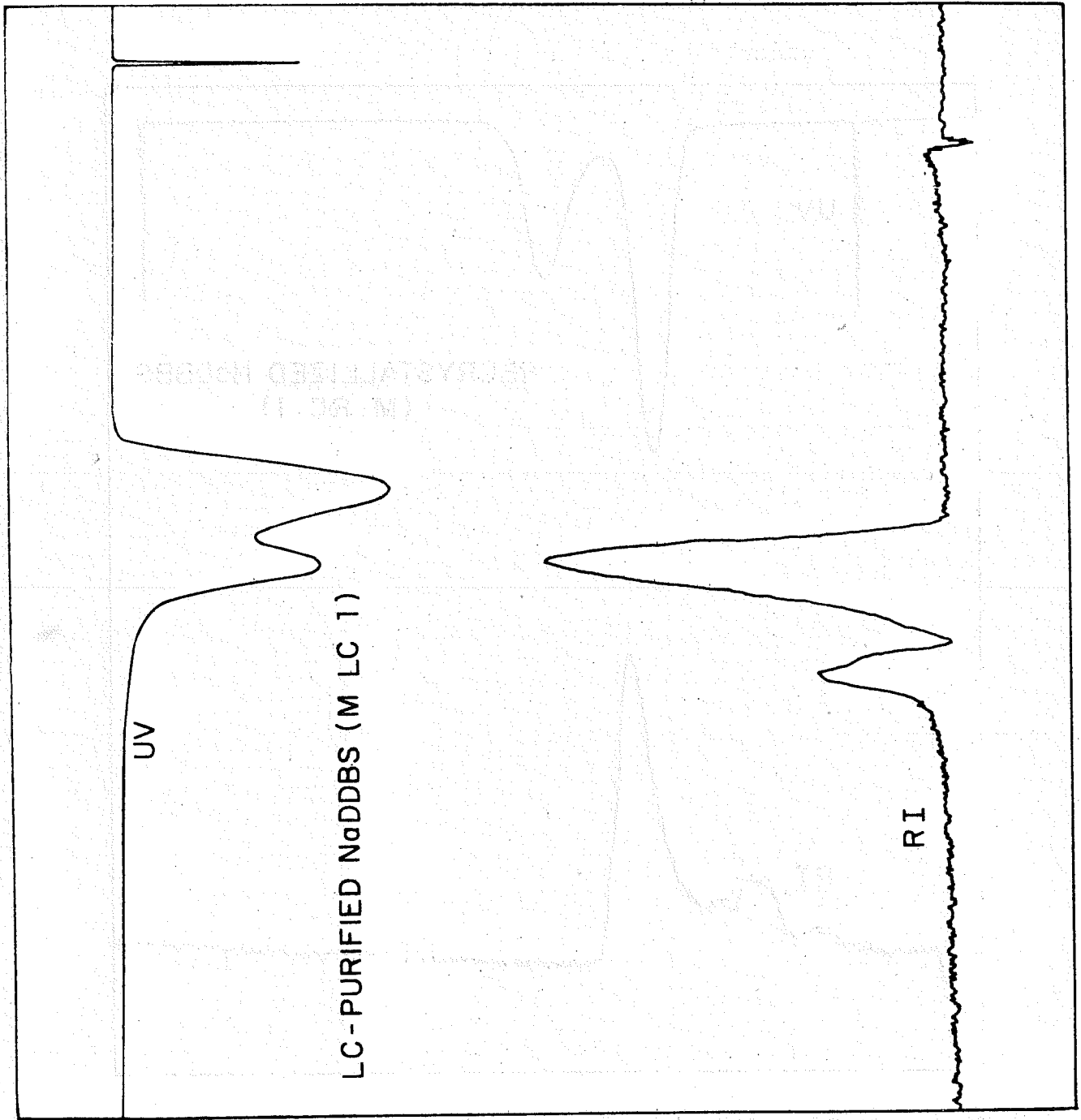


Figure I. 11. ALC chromatogram of peak #2 from Figure I. 9.

component in larger concentrations than the as-received sulfonate, which could possibly be due to the conversion of one of the components to its isomer upon continuous heating of the sulfonate sample during Soxhlet extraction.

Since as received sulfonate was considerably purer than the sulfonic acid purchased separately and was very similar to the purified sulfonate except for the presence of oil in it, as received sulfonate after deoiling was used for the preparation of pure dodecylbenzenesulfonate on Prep LC 500 with  $\mu$  Bondapak C-18 column.

Elluents #1 and #2 (indicated in Figure I.9) were collected. Residues after evaporation of the solvent were analyzed by Infrared Spectroscopy (IR) and Nuclear Magnetic Resonance Spectroscopy (NMR). Analysis indicated that elluent #1 is a tri-substituted benzene ring (Figures I.13-14), while elluent #2 is the p-NaDDBS that is of interest for the present study (Figure I.15-16). IR of as received NaDDBS is given for comparison in Figure I.12.

An attempt was made to confirm the structure and molecular weight of the purified p-NaDDBS, the elluent #2, using Mass Spectroscopy. Two separate analyses of the same batch of sulfonate showed quite different Total Ionic Current Patterns (Figures I.17-18) as well as different fragmentation patterns (Figures I.19-20). The data in those figures show that the sulfonate, instead of giving a fixed fragmentation pattern, disintegrates rapidly. Molecular weight or the structure could not therefore be confirmed by this technique;

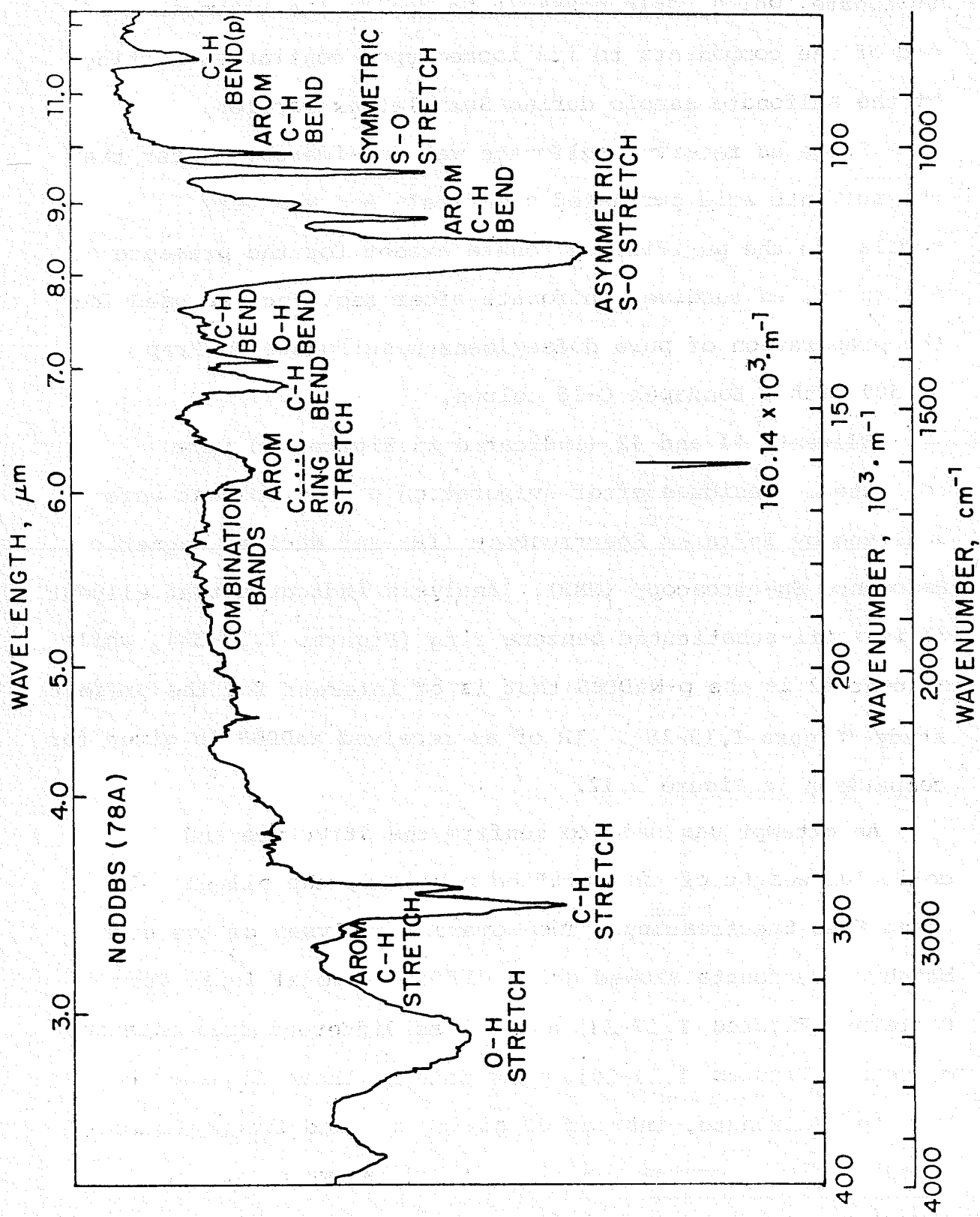


Figure I. 12. IR spectrum of as-received Na-dodecylbenzenesulfonate.

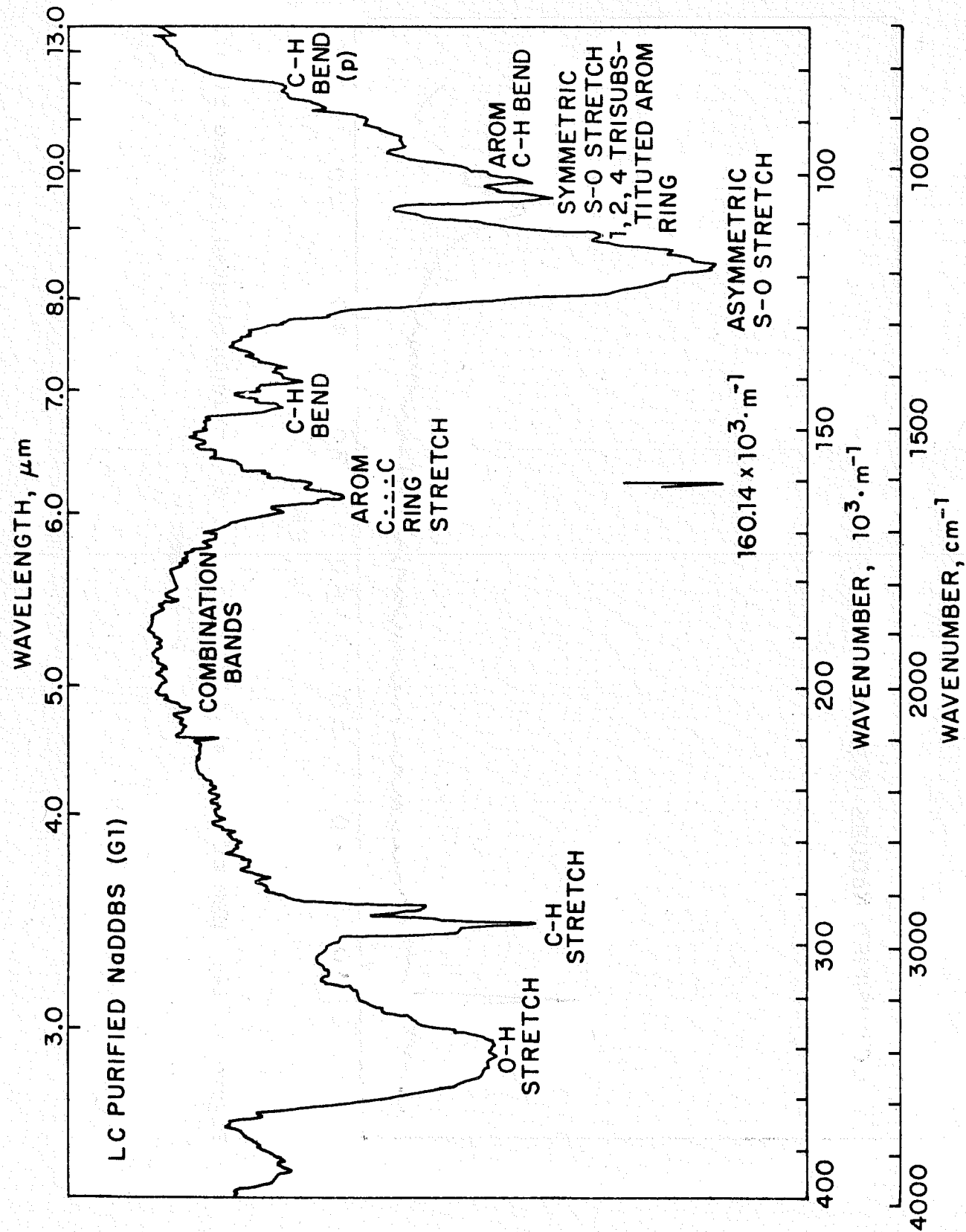


Figure I. 13. IR spectrum of peak #1 from Figure I. 9 (trisubstituted benzene ring).

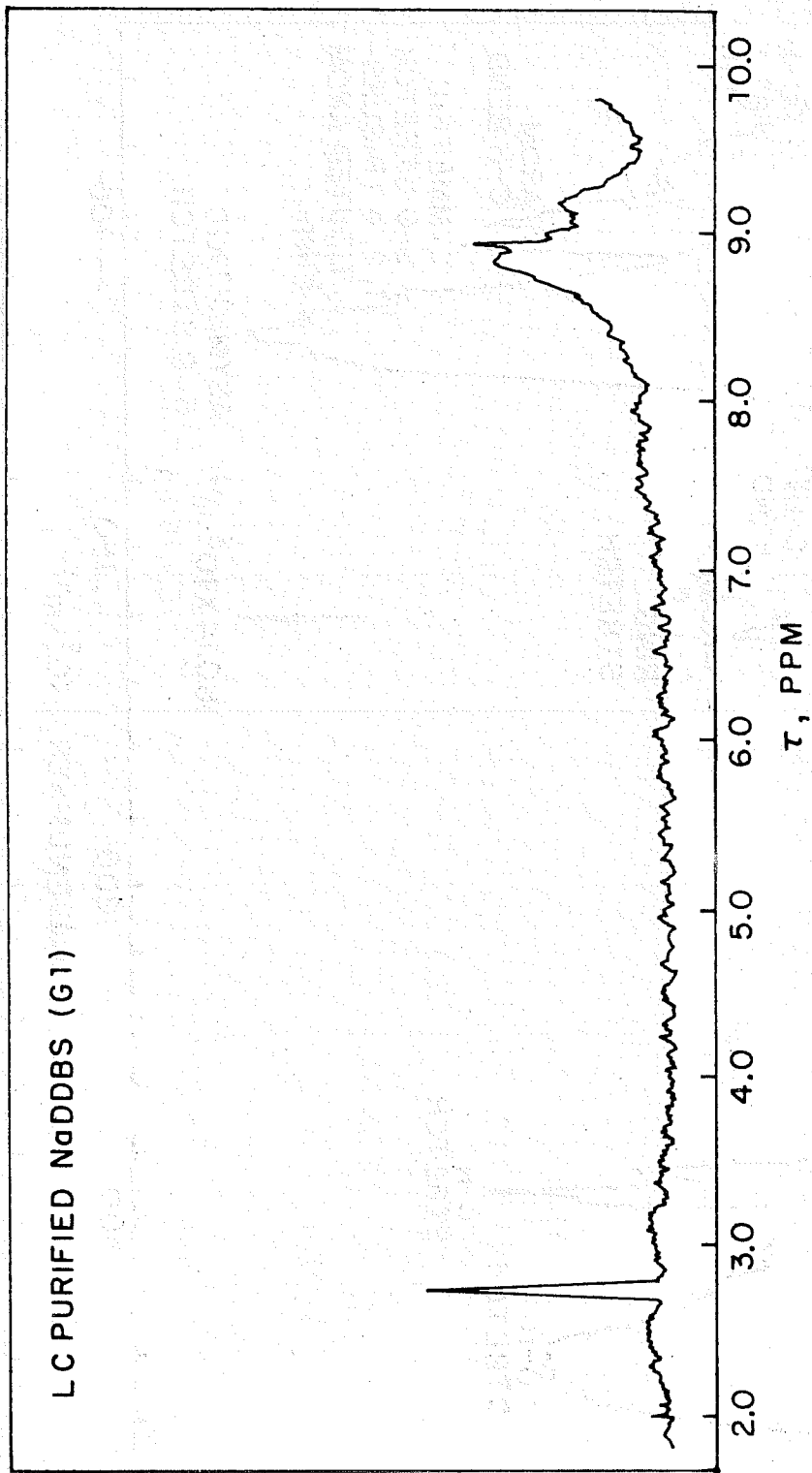


Figure I. 14. NMR of peak #1 from Figure I. 9 (trisubstituted benzene ring).

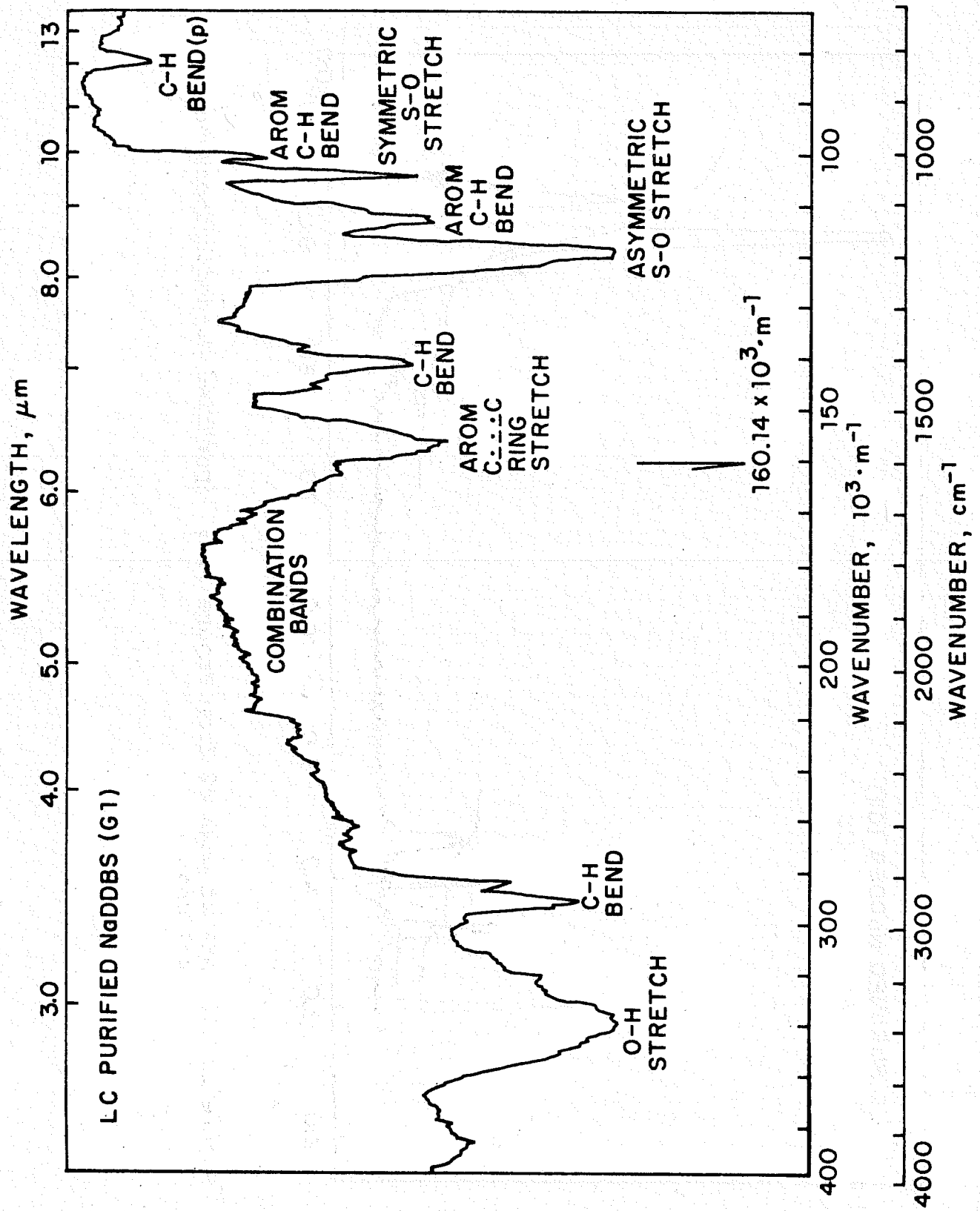


Figure I. 15. IR spectrum of peak # 2 from Figure I. 9 (purified Na-dodecylbenzene-sulfonate).

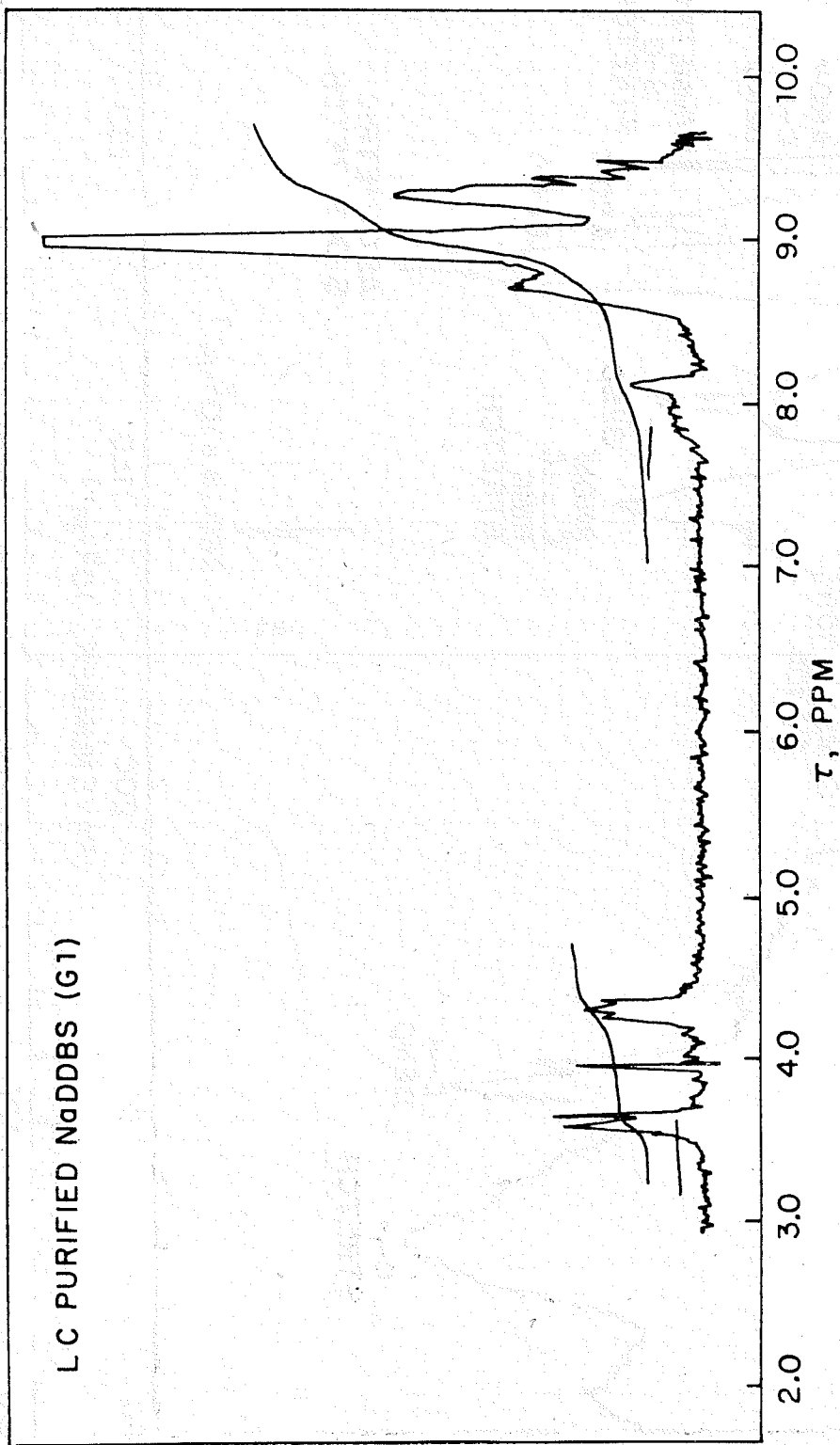


Figure I. 16. NMR of peak #2 from Figure I. 9 (purified Na-dodecylbenzene-sulfonate).

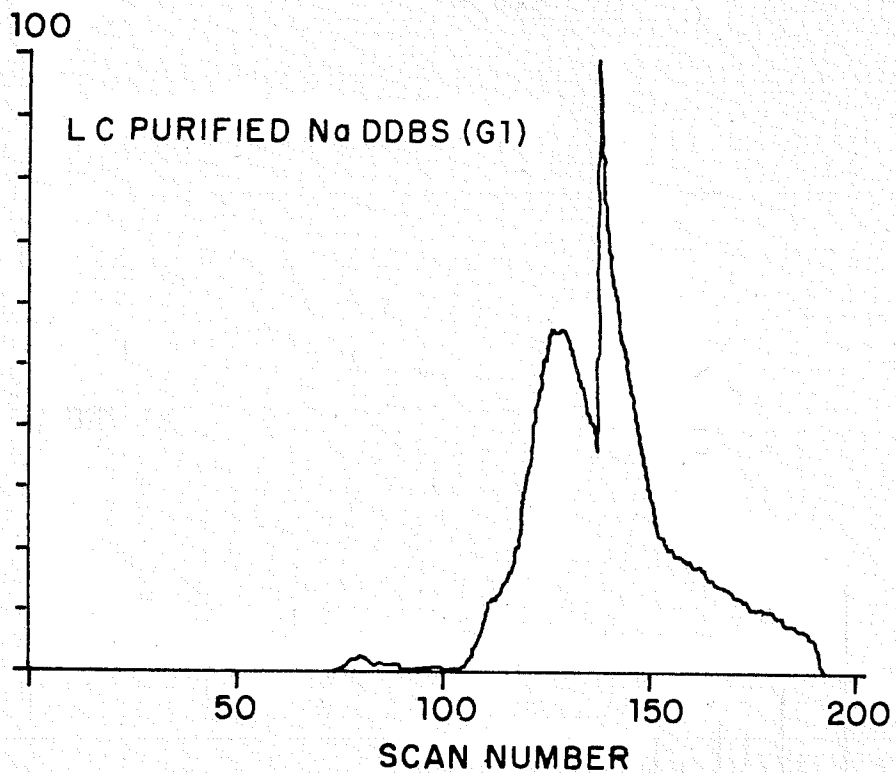


Figure I. 17. Total ionic current pattern of p-NaDDBS, elluent #2.

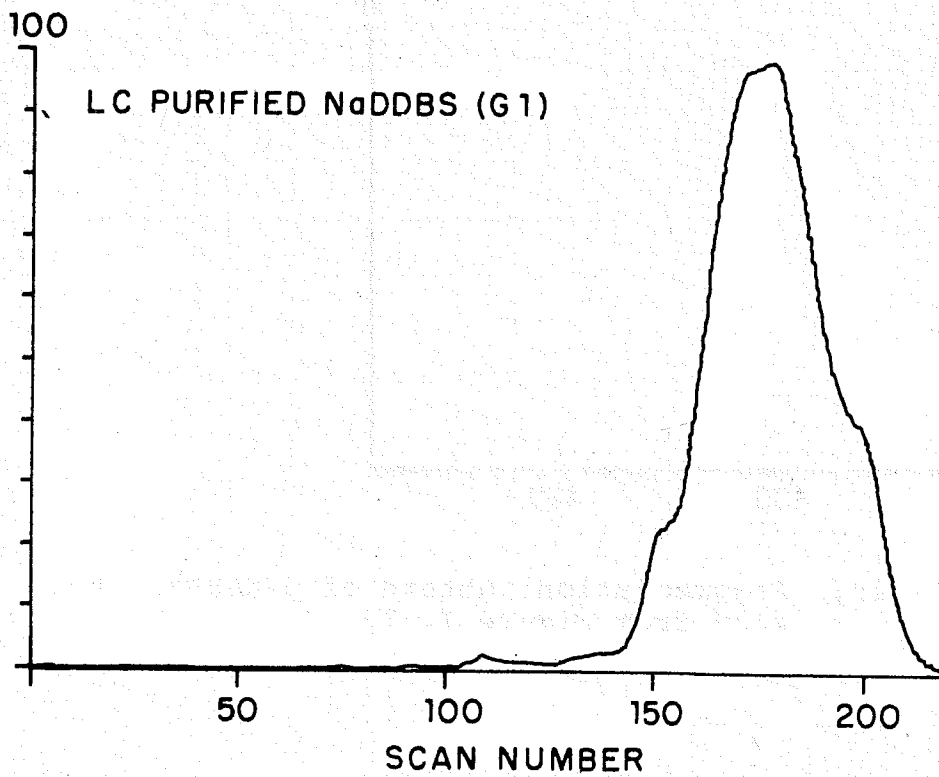


Figure I. 18. Total ionic current pattern of p-NaDDBS, elluent #2 (repeat analysis).

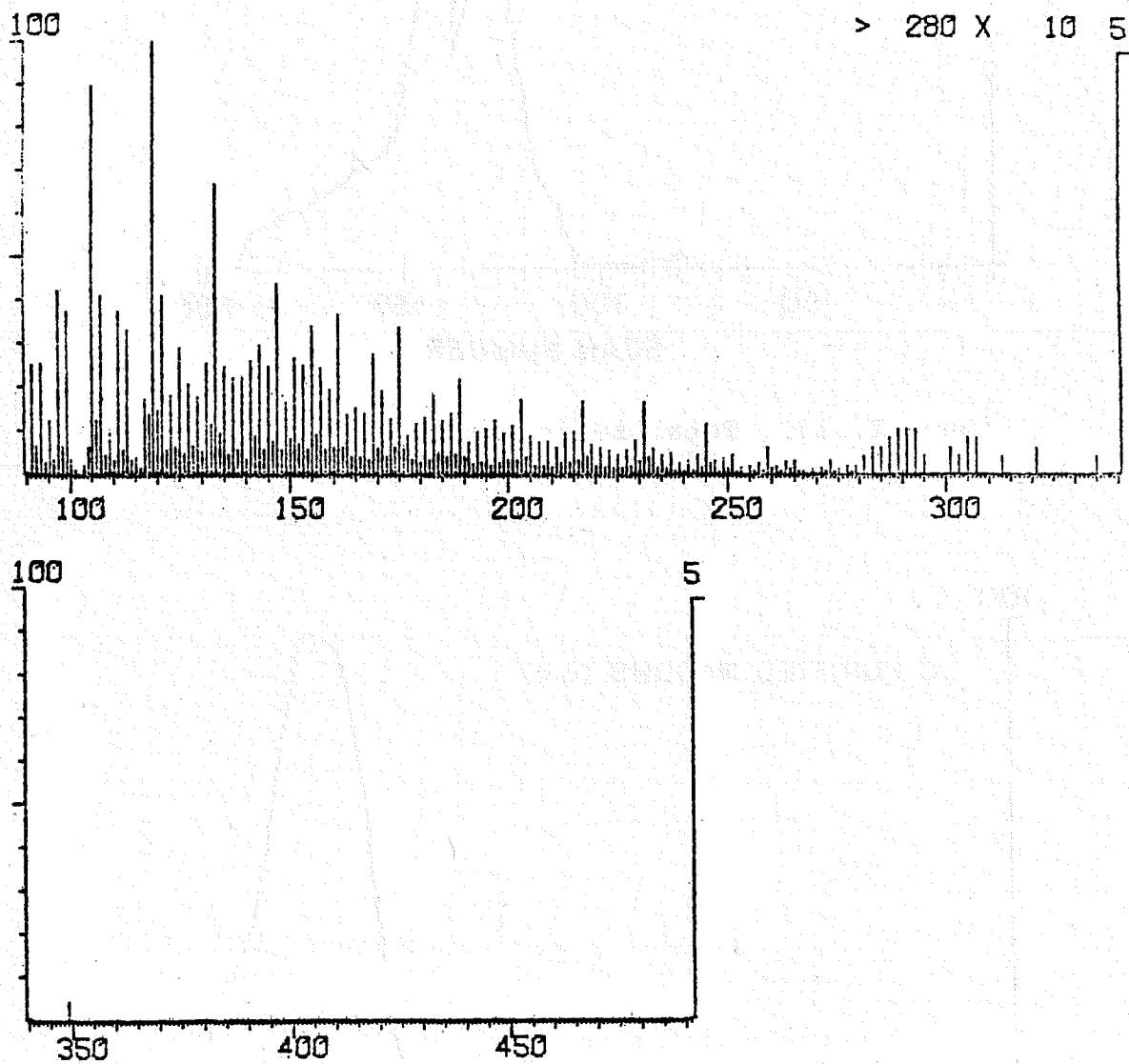


Figure I. 19. Fragmentation pattern of p-NaDDBS, scan #129 from Figure I. 17.

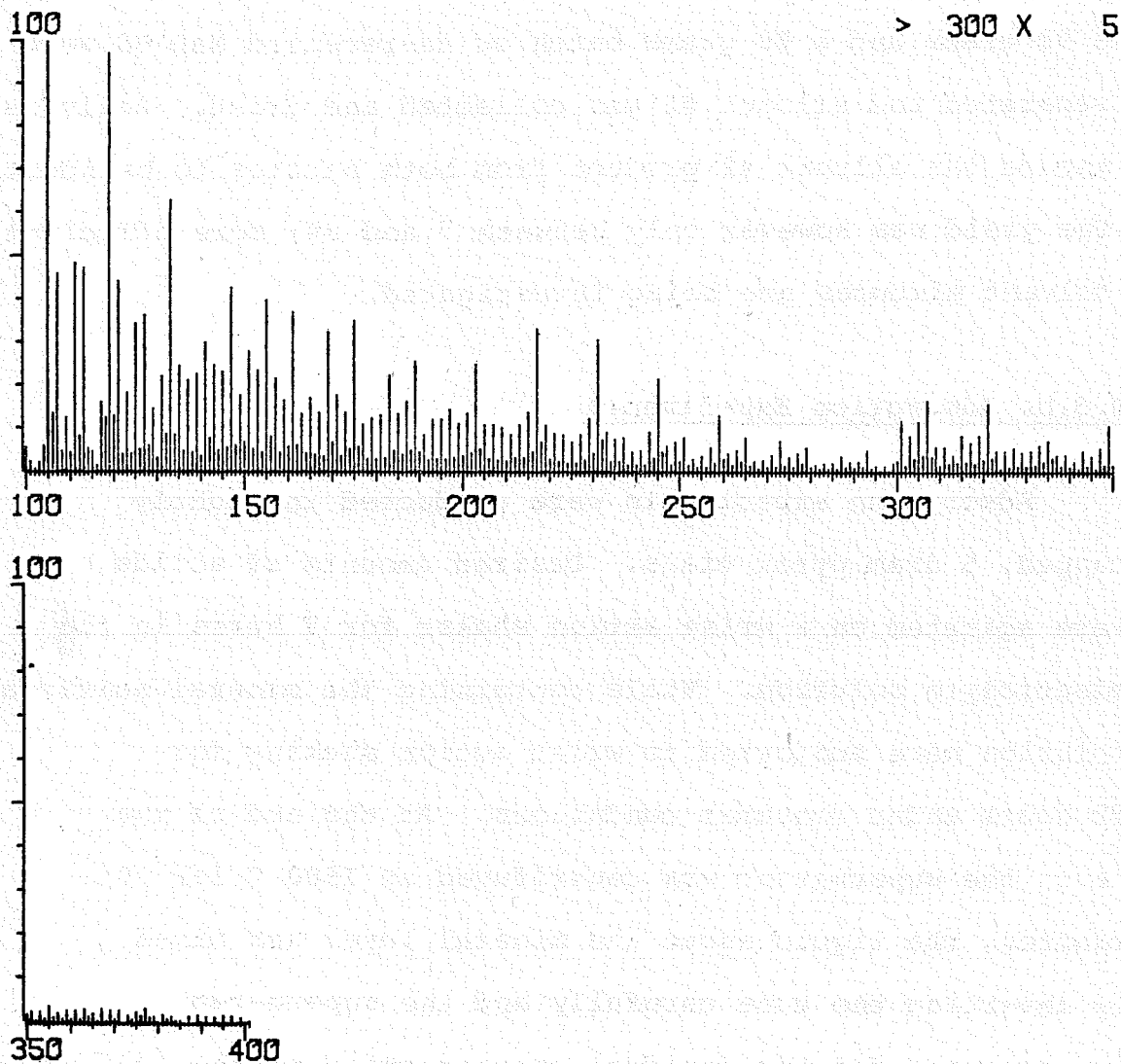


Figure I. 20. Fragmentation pattern of p-NaDDBS, scan #168 from Figure I. 18.

mass spectroscopy cannot be used for compounds that decompose before fragmenting.

Using the chromatographic procedure described above, a 90 grams and a 60 grams batch of as-received NaDDBS were separated and elluent #2 was collected and dried. Analysis showed the elluent #2 product from both batches to be identical. The yield was however only between 7 and 8%; more efficient solvent mixtures are being investigated.

### B.3.b. Adsorption Experiments

Adsorption experiments were conducted in tightly capped, 5 dram pyrex vials. Desired amounts of solids were agitated on a wrist action shaker for 2 hours in the electrolyte solution. Vials containing the mineral/surfactant solution were subjected to wrist action shaking for 72 hours under constant conditions. At the end of the test, the supernatant was centrifuged at 1500 G for 20 minutes, the liquid above the mineral layer was mixed by inverting the tube carefully and the supernatant was analyzed for the residual concentration of the sulfonate by the two phase titration technique using the dimidium bromide/disulphine blue mixed indicator as described by Powers (1) and Reid et. al. (2,3).

Calibration curves obtained for the titration of

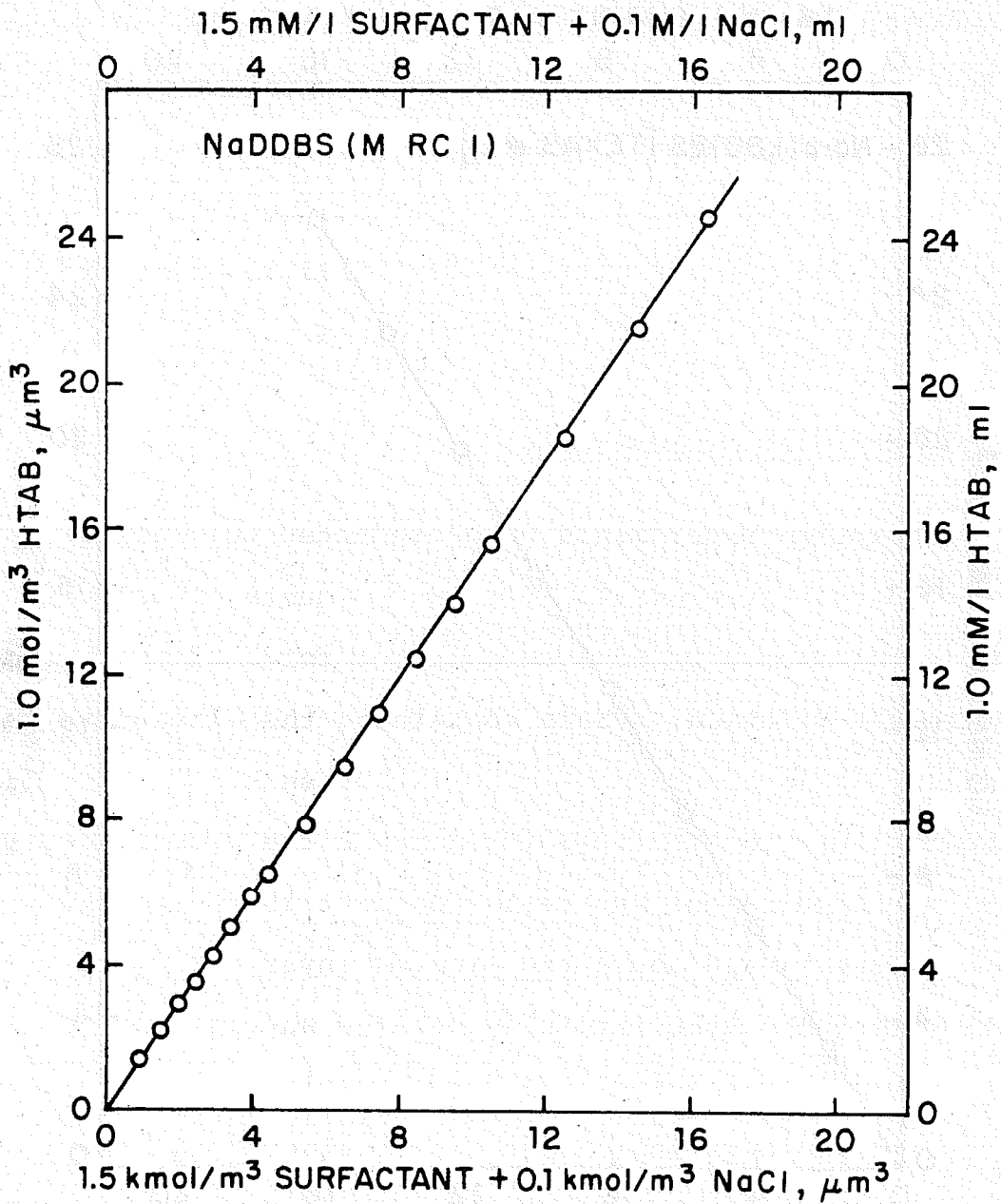


Figure I. 21. Calibration curve for titration of recrystallized Na-dodecylbenzenesulfonate with hexadecyltrimethylammonium bromide (HTAB).

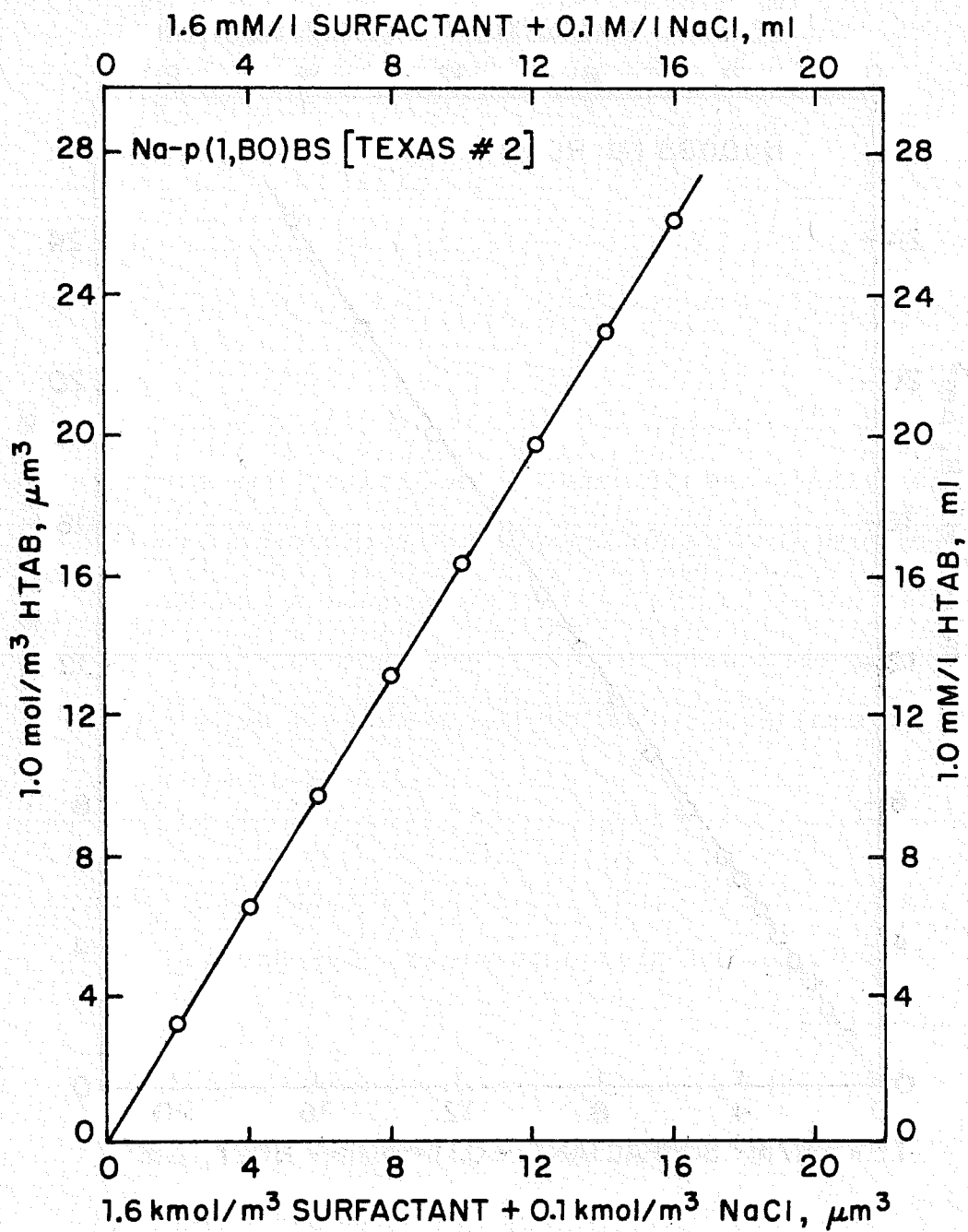


Figure I. 22. Calibration curve for titration of Na-p(1, butyloctyl) benzenesulfonate (Texas #2) with hexadecyltrimethylammonium bromide (HTAB).

normal (Fig. I.21) and branched (Fig. I.22) dodecylbenzenesulfonates in 0.1N NaCl with  $10^{-3}$ M HTAB, are linear up to about 20  $\mu$  moles of surfactant. In order to keep the quantity of HTAB used always in the same range (about 5  $\mu$  moles), the amount of surfactant sample was varied according to its concentration. Adsorption density was calculated from the difference in initial and final values of sulfonate concentration and amount of clay used.

In order to investigate the effect of oil on adsorption of sodium dodecylbenzenesulfonate on kaolinite, the surfactant solutions were prepared as follows. Desired amount of oil was weighed and added to the surfactant solution and was subjected to ultrasonication for a given time for the formation of an emulsion. Some of the resultant solutions were still turbid, but they did clear during adsorption tests.

Precipitation of surfactant during adsorption experiments by the ions present in the clay supernatant was studied in the following manner.

The supernatant was prepared under conditions similar to those used in adsorption tests as described above. Na-Kaolinite was equilibrated with the desired electrolyte solution at a solid to liquid ratio of 0.2 for seventy-two hours and then the kaolinite was removed by centrifugation for 20 minutes. In order to avoid any dilution effects, the supernatant was evaporated to dryness (except in the

cases where the oil was not added, in which case the surfactant solution was evaporated) and the desired volume of surfactant solution was added. The test solution was then agitated on a wrist-action shaker for twelve hours and the residual concentration of it was determined after centrifugation for 20 minutes. Precipitation density was calculated from the differences between the initial and final values of sulfonate concentration. In certain cases, the turbidity of the sulfonate-supernatant mixture was measured using the Brinkmann colorimeter.

## C. Results and Discussion

### C.1. KINETICS OF ABSTRACTION OF NaDDBS ON Na-KAOLINITE

Kinetics of abstraction of surfactant on pre-wetted kaolinite was described in 1977 annual report (p. 14). Here we give additional results obtained for the rate of change of abstraction in the presence of oil. Fig.I.23 shows the results for three concentrations of sodium dodecylbenzenesulfonate with different amounts of two hydrocarbons. Surfactant concentrations were selected so that the final sulfonate concentration would be in the region below that of the anticipated maximum in one case, in the region of the maximum in another, and above this region in the third case. Chain length and the amounts of oils were selected in accordance with the high and low values used in our studies. In all the three cases, abstraction kinetic curves exhibited two distinct plateaus, the final one being attained only in about fifty hours. It can be seen that the time required to reach equilibrium is longer for the system with higher surfactant and oil concentrations. Seventy-two hours of equilibration time was selected as in all of our adsorption studies.

The two-step kinetics curve obtained for the abstraction of sulfonate by kaolinite is similar to what was obtained previously by us (4). Such a behavior was attributed to the slow release of exchangeable aluminum ions from the mineral.

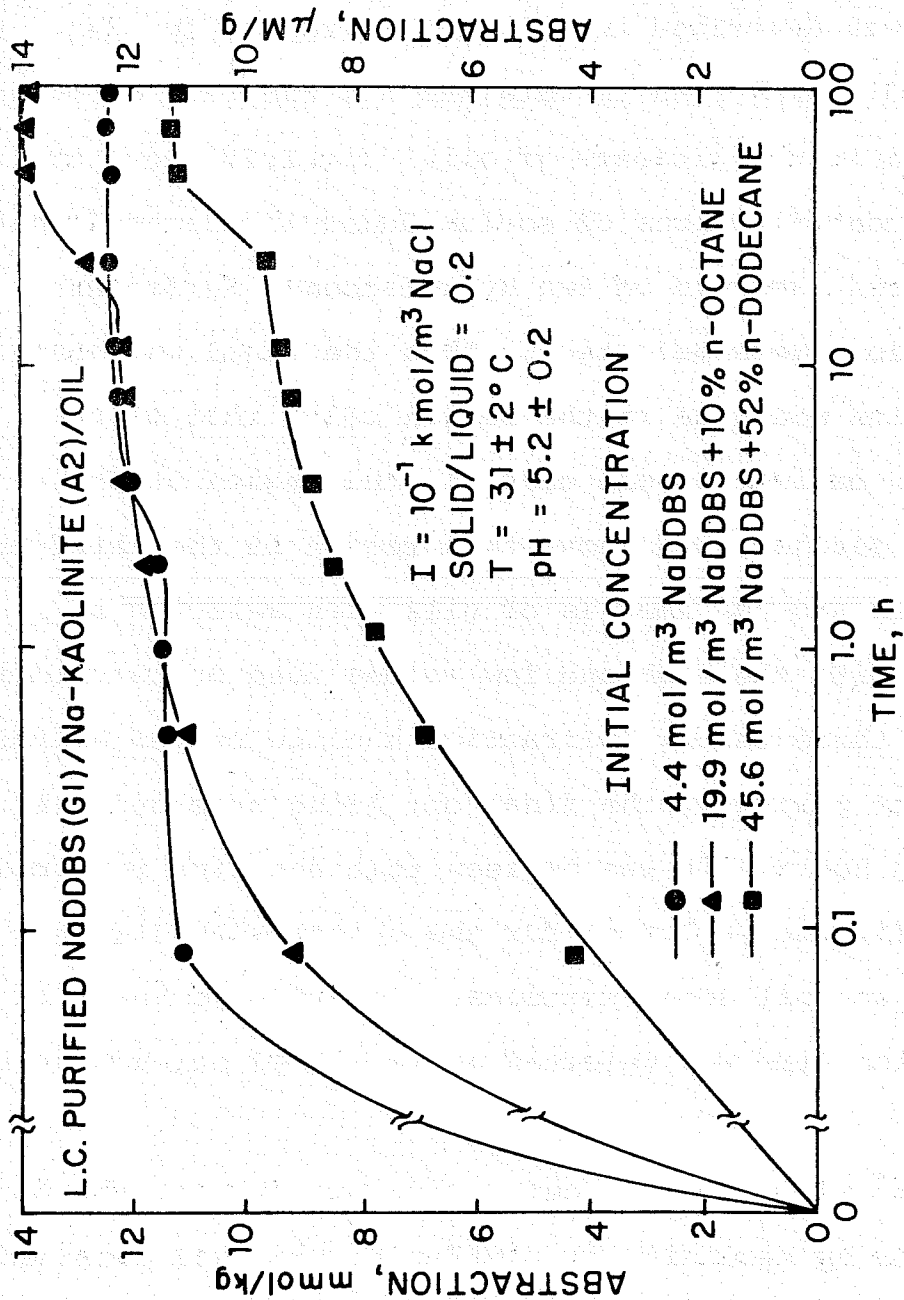


Figure I. 23. Abstraction kinetics of Na-dodecylbenzenesulfonate on Na-kaolinite.

## C.2. PRECIPITATION, ABSTRACTION AND ADSORPTION

Results obtained for abstraction of isomerically pure sodium dodecylbenzenesulfonate from a solution upon the equilibration of it with homoionic Na-Kaolinite are given in Figure I.24. It can be seen that this isotherm is characterized by the presence of a maximum. The data for sulfonate abstraction upon contacting it with the supernatant from a kaolinite suspension as well as the data for light transmission of the sulfonate supernatant mixtures before centrifugation are also given in this figure. They show a good correlation; both the precipitation and transmission curves exhibit maxima in the concentration region of the abstraction maximum.

It is recognized that the amount of sulfonate that will precipitate due to interaction of it with dissolved mineral species in the presence of kaolinite need not be equal to that which will precipitate in a supernatant from which kaolinite has been removed, due to elimination of the possibility for continuous equilibration of kaolinite with the solution in the latter case. It is also to be noted that the natural pH values obtained during precipitation tests were slightly higher than those obtained in the abstraction tests, again due to lack of continuous equilibration in the presence of kaolinite. Assuming these two effects to be minimal, adsorption isotherm was calculated from the difference between the two isotherms and is given in Figure I.24.

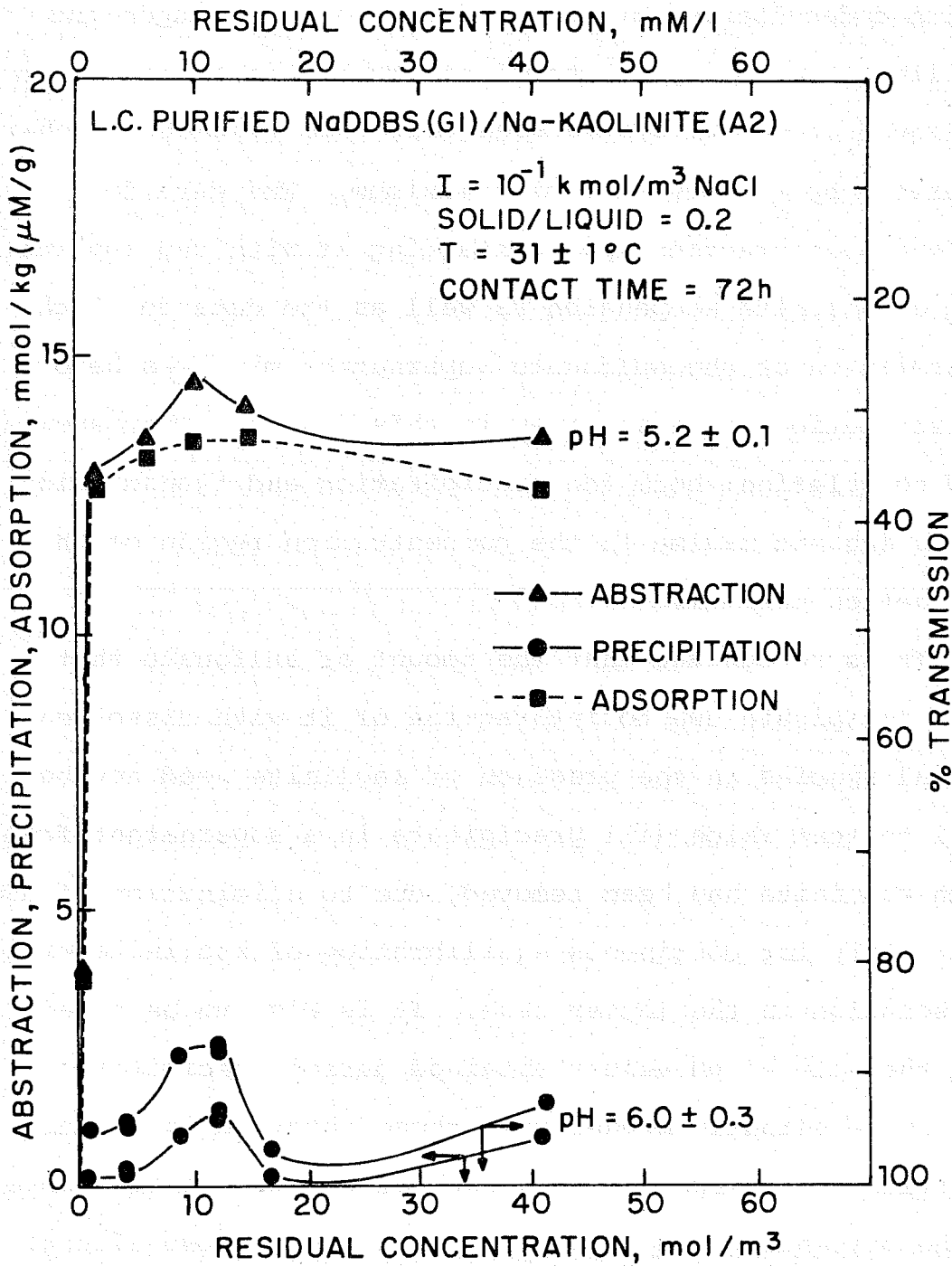


Figure I. 24. Abstraction, precipitation and adsorption of LC-purified Na-dodecylbenzenesulfonate on Na-kaolinite as a function of concentration.

Release of mineral species is also confirmed by the surface tension measurements made in the electrolyte solution and the supernatant solution prepared in a similar manner as for precipitation experiments. With the dissolution of the mineral, ionic strength would increase, thus the CMC of the sulfonate solution should decrease. The opposite was observed (Figure I.25), CMC in the supernatant solution is slightly higher than in the NaCl solution. This, it seems, is due to the fact that precipitation of sulfonate occurs in the supernatant solution. Since precipitation is a competing phenomenon, and also a separate phase, monomer concentration would not increase until precipitation is completed, thus higher surfactant concentration would be required to reach CMC. Because precipitation amount is very small, plateau in surface tension due to precipitation is missed.

It can be seen that the major peak giving rise to the maximum is considerably reduced in the case of the adsorption isotherm (Figure I.24) suggesting that the precipitation of sulfonate with the dissolved mineral species does indeed contribute towards determining the shape of the adsorption isotherm for the system considered here. It is to be noted that the resultant adsorption isotherm does still exhibit a maximum, even though much less prominent. The presence of such a maximum could be attributed to other mechanisms which have been suggested, but it is possible that this is due to the absence of kaolinite in the precipitation experiments.

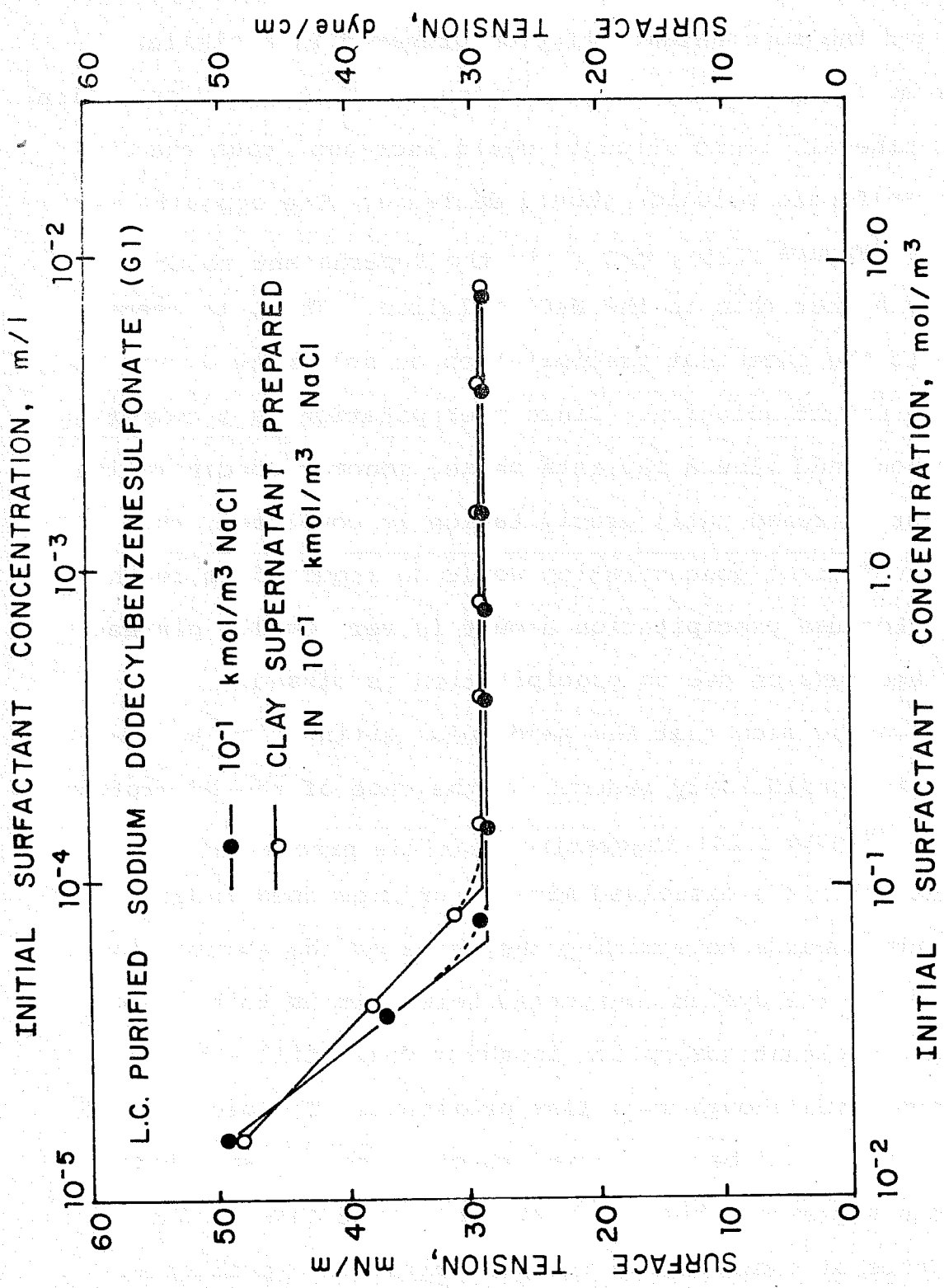


Figure I. 25. Surface tension of LC-purified Na-dodecylbenzenesulfonate in 0.1 M/1 NaCl and in clay supernatant prepared in 0.1 M/1 NaCl.

As sulfonate precipitates, when kaolinite is present in the system, and consumes the dissolved mineral species, more ions would be expected to be released from the mineral due to the offset of equilibrium conditions. This suggests that in the abstraction experiments precipitation can be higher than what is observed during precipitation experiments. Release of ions can also be higher when the initial precipitation is rapid rather than when it is slow. This can cause the decrease in the abstraction density to be higher for the rapid precipitation region than for other regions, which can possibly even then eliminate the maximum completely.

The decrease in precipitation as the surfactant concentration is increased can be due to the solubilization of the precipitate by the micelles. Mechanism for such precipitate redissolution is still not known, but it could be due to the detergency action of micellar solutions. Micellar solutions are known to bring into solution, otherwise insoluble, organic molecules. The solubilized material can be incorporated into the micelle itself due to the nonpolar environment of its interior (5). Since surfactant precipitate will be unionized, it can be expected to behave as a nonpolar compound, and thus get solubilized by the micelles.

Precipitation curve is also characterized by an increase in precipitation after the initial decrease as surfactant concentration is further increased. This could possibly be due to the salting out of the surfactant as ionic strength increases in the region where surfactant concentration

is only an order of magnitude lower than the concentration of supporting electrolyte. Precipitation in this region is observed at concentrations above the region of maxima in several systems. Results obtained during an abstraction experiment, where the total ionic strength of the surfactant solution was therefore maintained at a constant value by adjusting the NaCl addition to the system, are shown in Figure I.26. Since salting out, caused by a change in ionic strength, has been eliminated here, decreasing abstraction is indeed observed. A plateau in the abstraction isotherm might be expected if the experiments had been carried out at still higher surfactant concentrations, whereas, at constant NaCl concentration a minimum would be expected. The abstraction isotherm is very similar to the adsorption isotherm in Figure I.24 at high surfactant concentrations. Figure I.26 also illustrates the excellent reproducibility which was achieved for abstraction experiments conducted several days apart. Due to the salting out effect of the inorganic electrolyte, the role of precipitation should increase with the increase of the electrolyte concentration in the system. The results of the adsorption experiments carried out with recrystallized sodium dodecylbenzenesulfonate in 1 M/l NaCl at three different values of pH are shown in Fig. I.27. As it was expected, precipitation strongly affects the abstraction of surfactant from the solution under such conditions. The residual concentrations measured in the clay supernatant after 72 hours were very low (curves 1, 2, 3). However

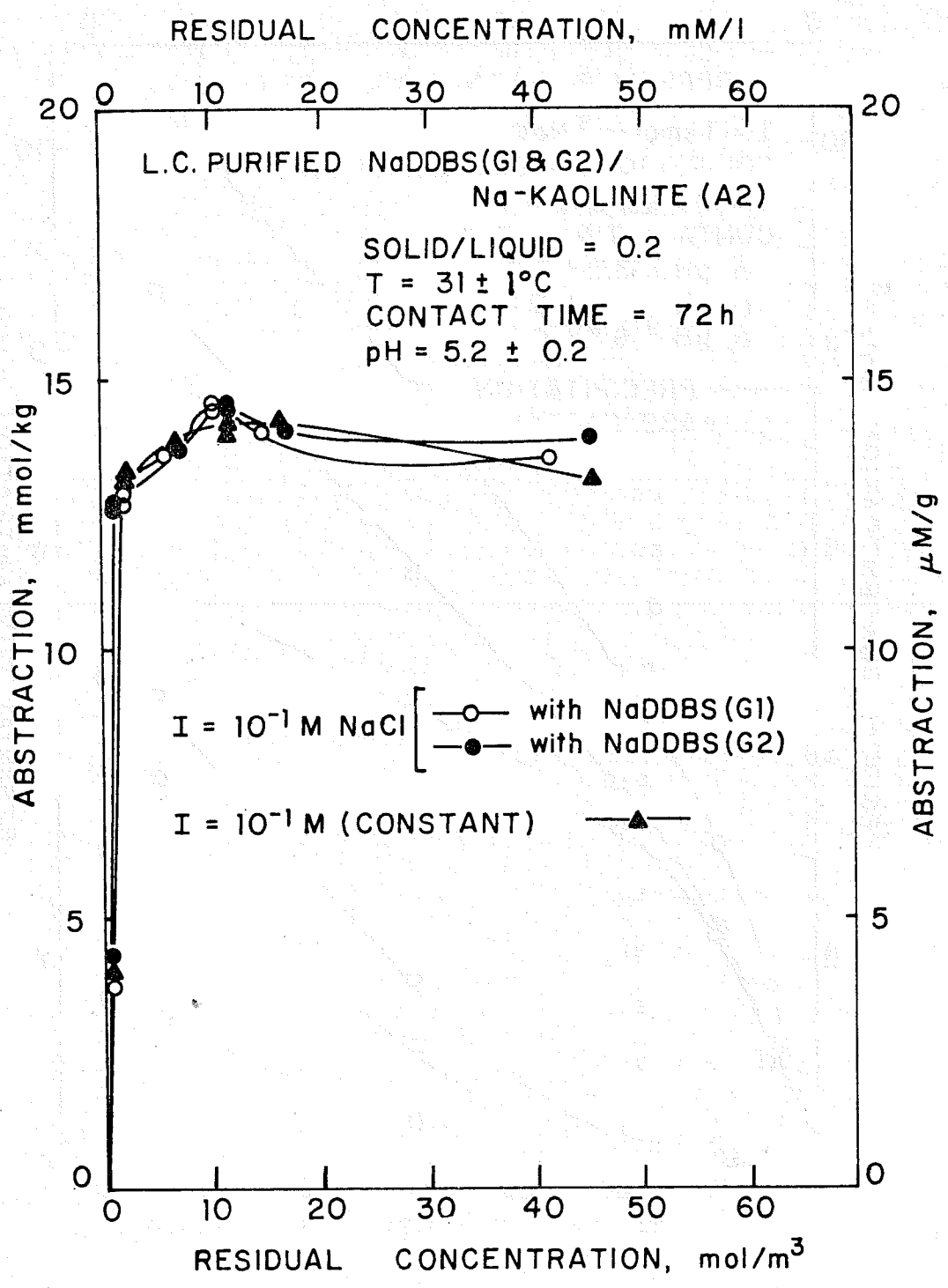


Figure I. 26. Abstraction isotherms of LC-purified Na-DDBS on Na-kaolinite at constant ionic strength and at constant concentration of NaCl added.

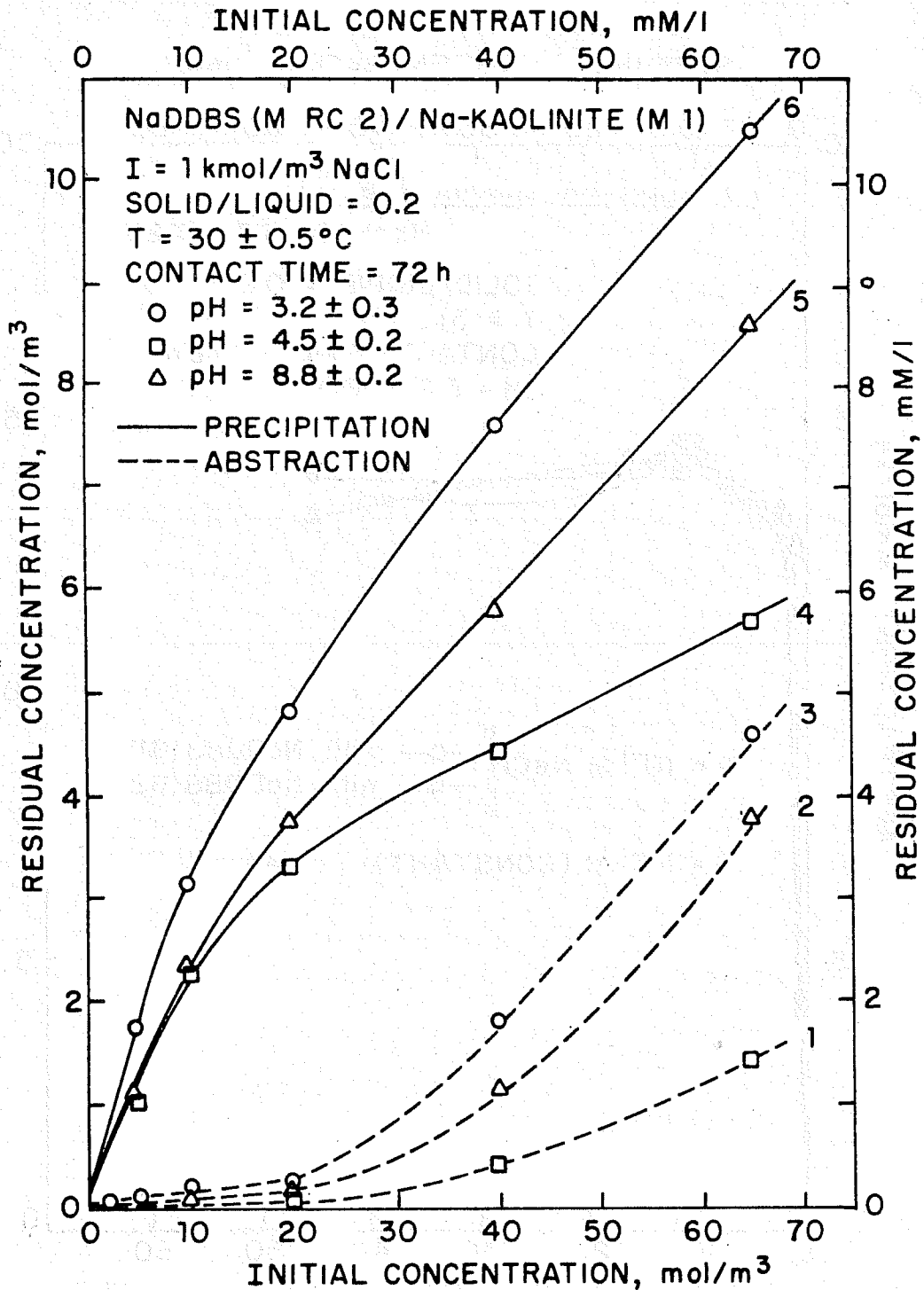


Figure I. 27. Residual concentration of Na-dodecylbenzenesulfonate in 1M/l NaCl as a function of the initial concentration in the presence and in the absence of Na-kaolinite.

most of the surfactant (80% or more in all cases) was precipitated even in the absence of clay by the inorganic electrolyte itself (curves 4,5,6 in Figure 27).

The data obtained also show dependence of the precipitation and of the total abstraction on pH. Both in the presence and in the absence of clay there is a minimum in the residual concentration corresponding to the "natural" pH which was about 4.5.

It is clear from these results that surfactants of the sulfonate type can undergo precipitation and redissolution upon interacting with solutions containing dissolved inorganic ions and that such phenomenon can play a major role in producing a maximum in abstraction isotherms.

### C.3. EFFECT OF PURITY AND CHEMICAL COMPOSITION OF THE SURFACTANT

The results discussed in the previous section (C.2) showed that the presence of a maximum in the adsorption isotherm of purified sulfonate on clays can be accounted for to a large extent by taking their precipitation into consideration. However, for adsorption of sulfonates that are not purified, other mechanisms can also contribute towards the extent of adsorption as well as the presence of maximum. In fact, the data given in Figure I.28 shows that while taking precipitation into account can reduce the extent of the maximum, it does not eliminate it completely. When adsorption isotherms for the unpurified and purified surfactant systems are compared, it is clear that purification also helps to

reduce the extent of maximum significantly. As received dodecylbenzenesulfonate contains at least unsulfonated oil as well as a trisubstituted benzene ring sulfonate (see Figures I.13 and I.14). These compounds can be expected to have properties, e.g. CMC values and adsorption constants, that are considerably different from the properties of pure dodecylbenzenesulfonate itself. Binary mixture theories of Mysels and Otter (6), Trogus et. al. (7,8), which are based upon such vast differences, and the explanations that have been put forward by Kitchener (9) on the role of impurities can possibly explain the presence of maximum in the adsorption isotherms of unpurified sulfonates. Isomers of the surfactant, if still present in the purified NaDDBS, are less likely to produce a maximum in the isotherm.

The experiments with recrystallized sulfonate and that purified by liquid chromatographic separation carried out under identical solution conditions (ionic strength, solid/liquid ratio, temperature) confirm this assumption. As Figure I.29 shows the dependences abstraction vs. concentration obtained with two recrystallized and two LC-purified surfactant samples differ very little (less than 20% with respect to abstraction) and these differences can in fact be easily explained by the previously reported by us (4 and 10) dependence of the adsorption on pH.

Results of the adsorption experiments obtained with branched sodium dodecylbenzenesulfonate (Texas #2) under the

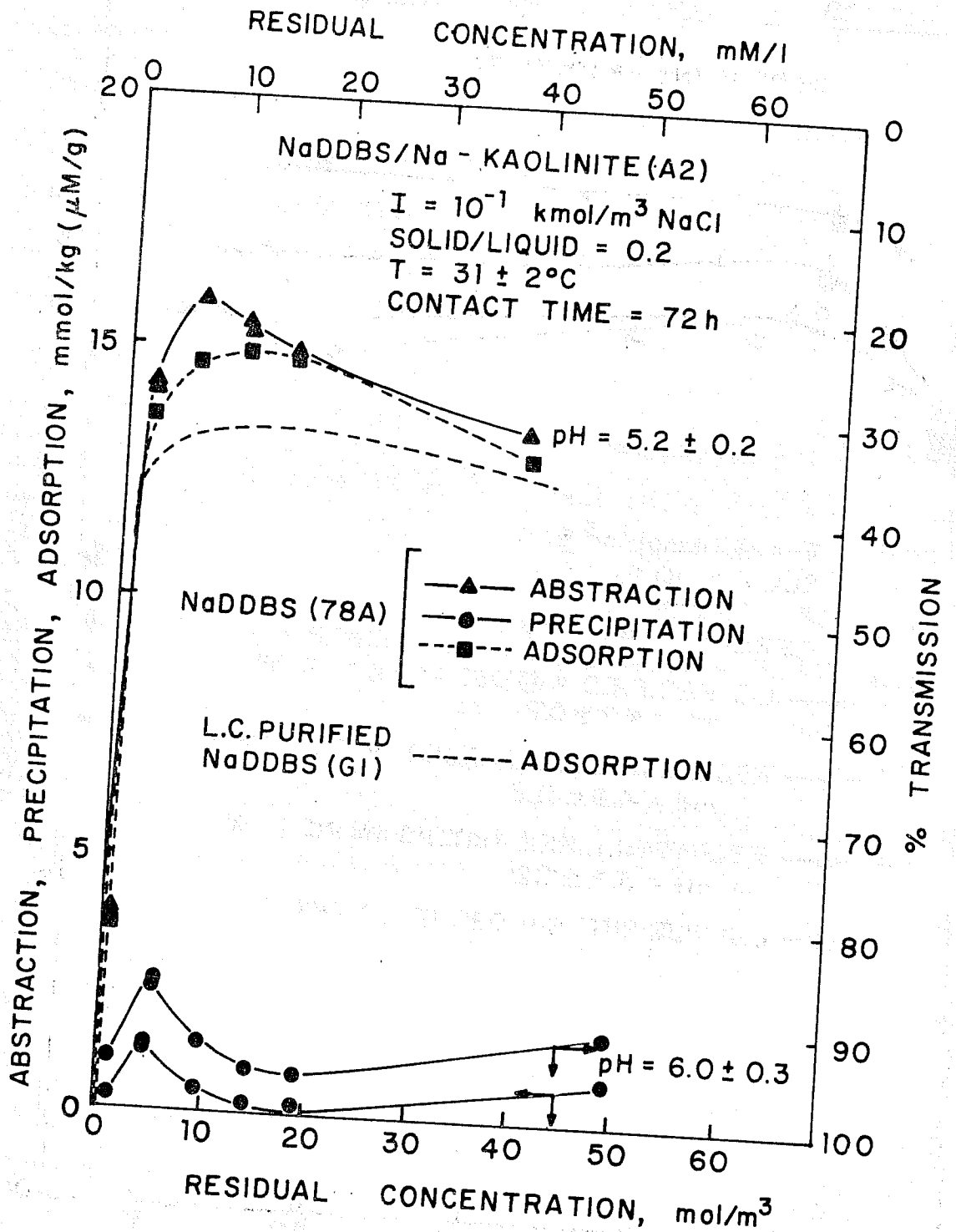


Figure I. 28. Abstraction, adsorption and precipitation isotherms of as-received NaDDBS on Na-kaolinite. Adsorption isotherm is compared to that of LC-purified NaDDBS.

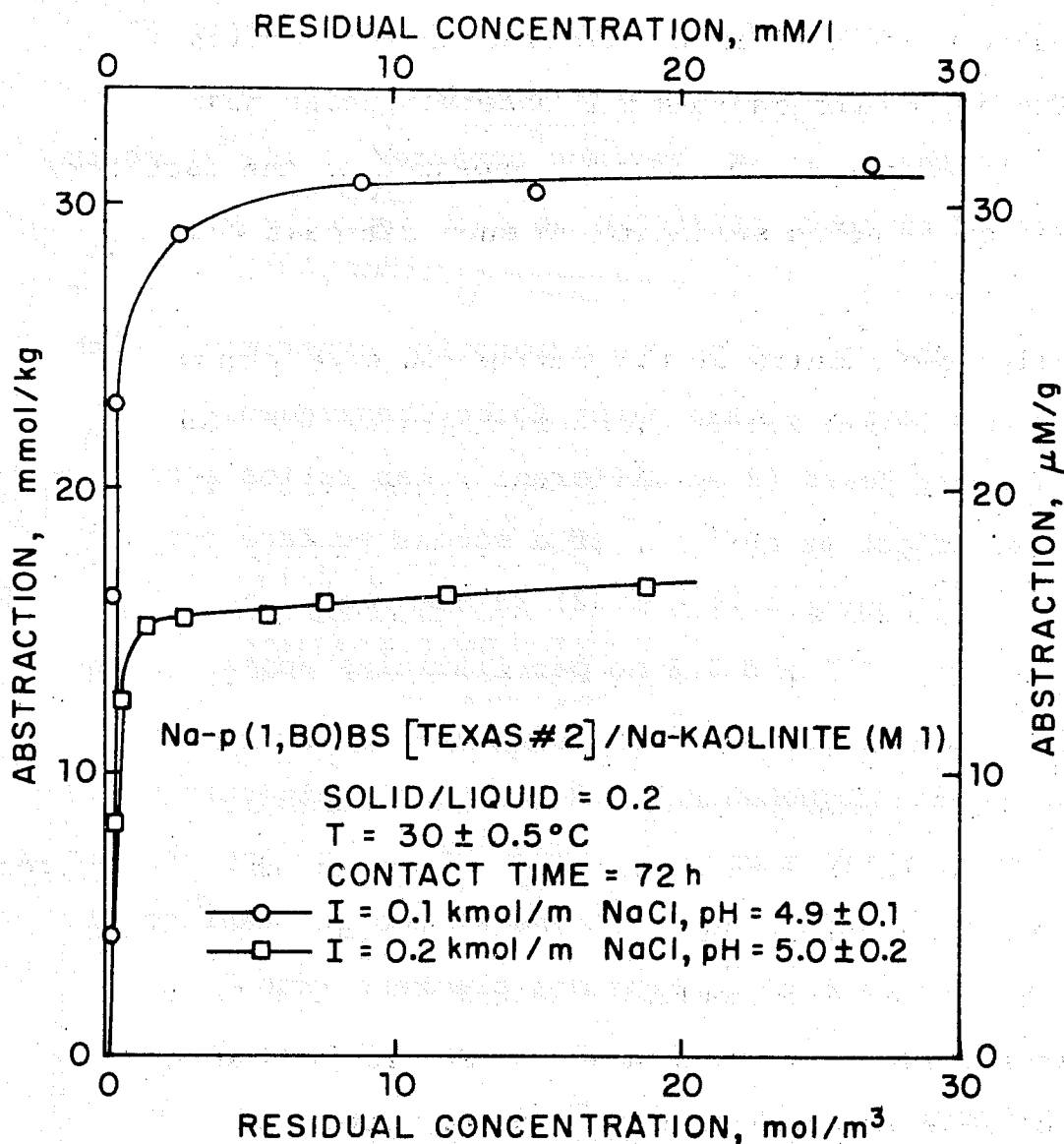


Figure I. 30. Abstraction isotherms of Na-p(1, butyloctyl) benzenesulfonate (Texas #2) on Na-kaolinite.

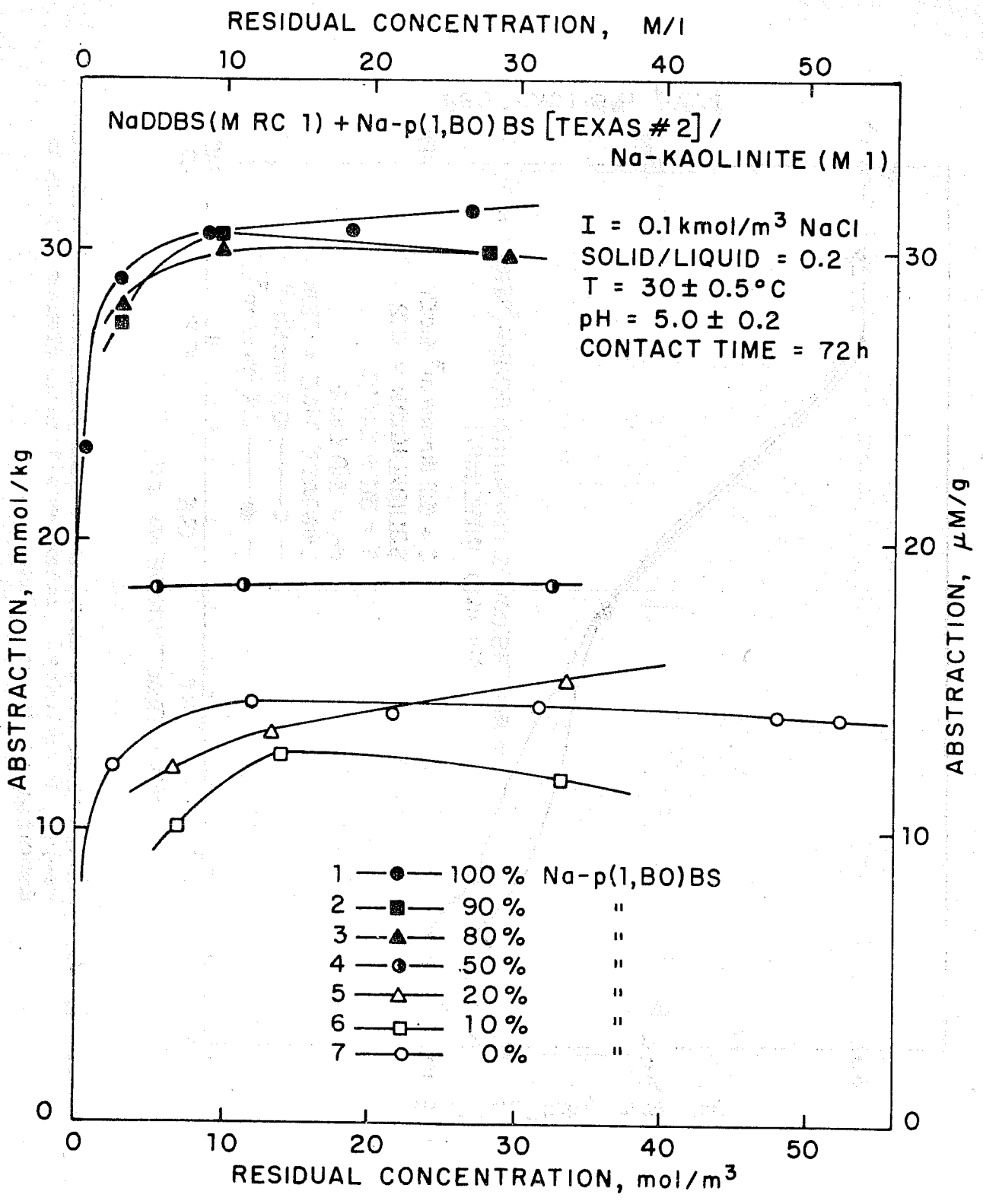


Figure I. 31. Abstraction isotherms of a mixture of recrystallized NaDDBS and Na-p(1, butyloctyl) benzenesulfonate at various molar ratios.

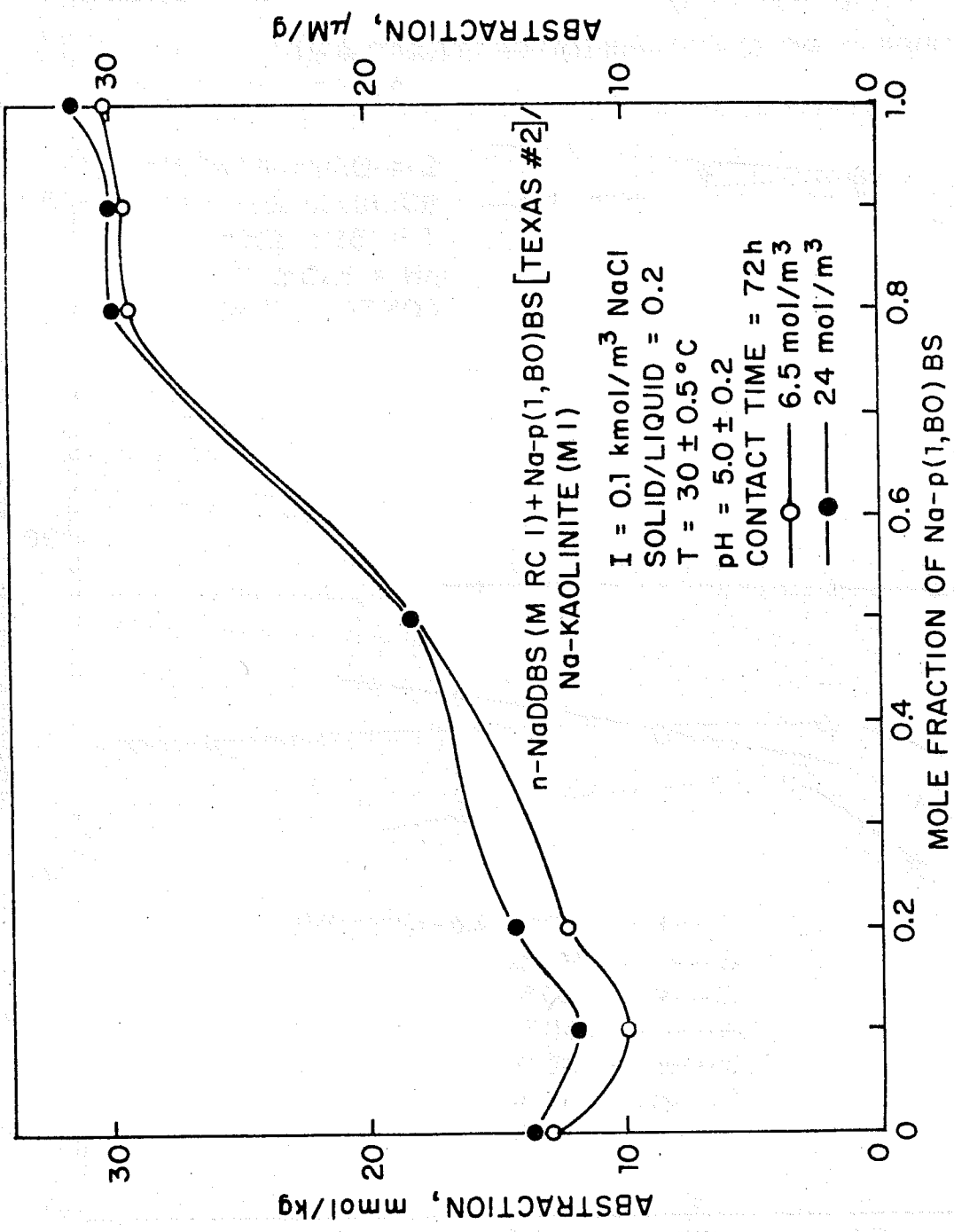


Figure I. 32. Abstraction of a mixture of recrystallized NaDDBS and Na-p(1, butyloctyl) benzenesulfonate (Texas #2) as a function of molar ratio.

smaller amount in the mixture acts as an impurity thus altering the behavior of the system. However, it is difficult to judge to what extent these results correspond to the theoretical predictions since the two sulfonates differ very little with respect to CMC (see Figures I.1 and I.2), the latter having been the crucial parameter in the theories proposed in the past.

#### C.4. EFFECT OF OIL ON THE ADSORPTION OF PURIFIED NaDDBS ON Na-KAOLINITE

Results obtained for the effect of presence of a series of pure hydrocarbons on the abstraction, precipitation and adsorption of sodium dodecylbenzenesulfonate on Na-Kaolinite are given in Figures I.33-35. It is to be noted that no two abstraction isotherms are of similar shape. Addition of oil has decreased the extent of abstraction in all cases, except in the case of 10% n-octane. Systems with 10% n-octane showed the most peculiar behavior, in that its adsorption isotherm exhibited two maxima and a minima. This is due to the fact that the abstraction maximum and the precipitation maximum do not correlate in this case. Such a behavior has not been observed in the past, to our knowledge. This interesting observation suggests the need for a detailed study in order to elucidate the mechanisms for such behavior. One possibility exists that the difference in pH might have caused the observed shift in precipitation maximum, for some reason, 10% n-octane system

being more sensitive to such pH change. At higher pH values, cation exchange of mineral will be lower and thus precipitation will commence at a higher surfactant concentration.

An interesting phenomenon can be noticed from the precipitation experiment, i.e. addition of oil (except for the case of 10% n-octane) has eliminated the precipitation in the low surfactant concentration region. Precipitation at higher concentration may be due to salting out, as discussed earlier. The elimination of precipitation could be due to either the partitioning of the surfactant species into a separate oil phase present in the system or the dissolution of the precipitate in the oil present in the form of microemulsion. In the former case, surfactant species can get partitioned between the separate oil and aqueous phases thus reducing the surfactant concentration in the aqueous phase and consequently reducing also the precipitation. The latter case is similar to the micellar solution discussed earlier. The difference between the two is that microemulsions can form below CMC and as a result, solubilization can commence at surfactant concentrations below such CMC, thus reducing precipitation and maybe even eliminating it. Further work is needed to verify this hypothesis.

Results given in Figures I.33-35 show that the presence of oil does affect the sulfonate adsorption on kaolinite. Adsorption was less in the presence of oil for all cases except for that of 10% n-octane. Data also indicate a dependence of this decrease on the chain length of the oils and their con-

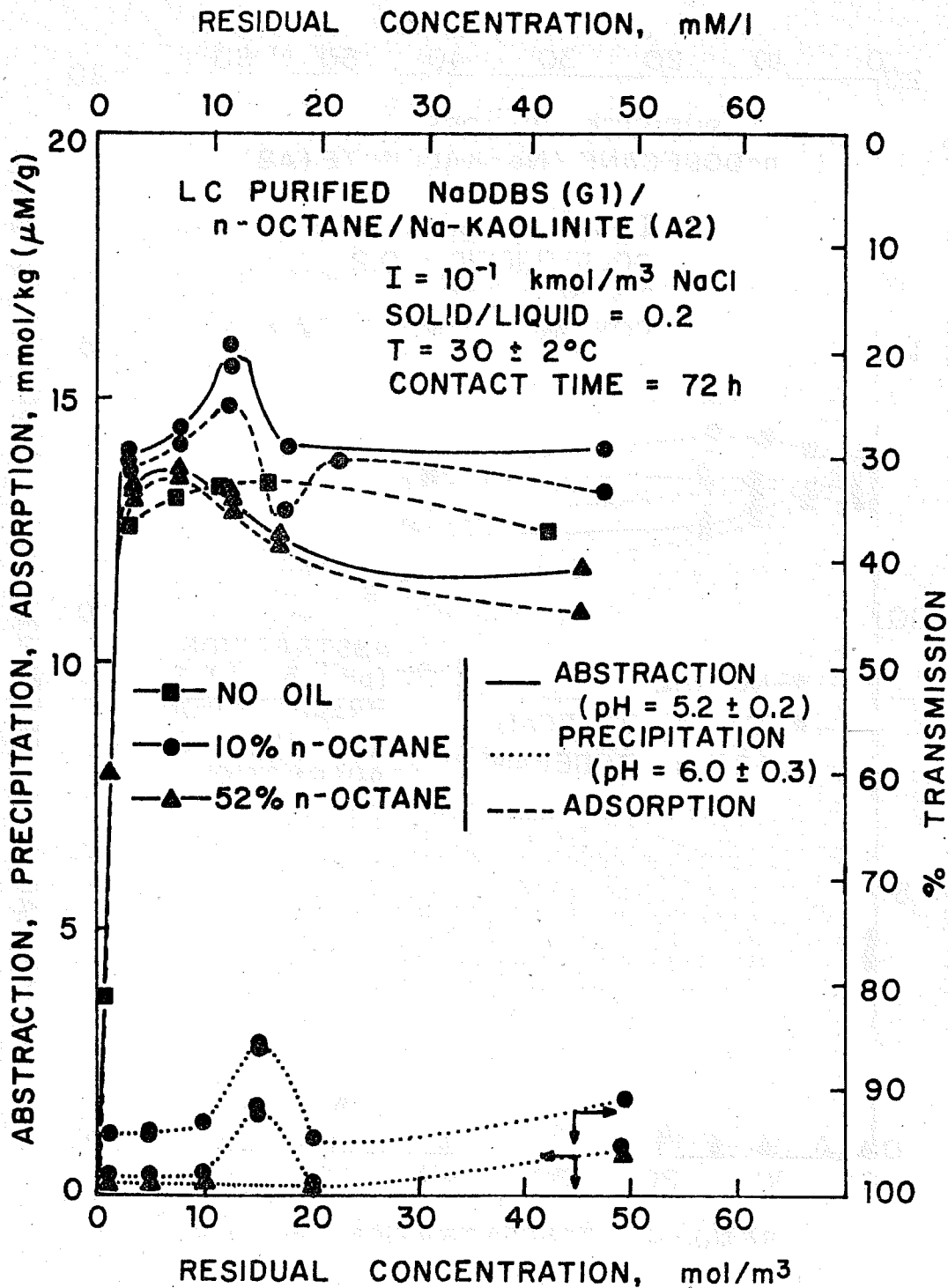


Figure I. 33. Effect of addition of n-octane on the adsorption of Na-dodecylbenzene-sulfonate on Na-kaolinite.

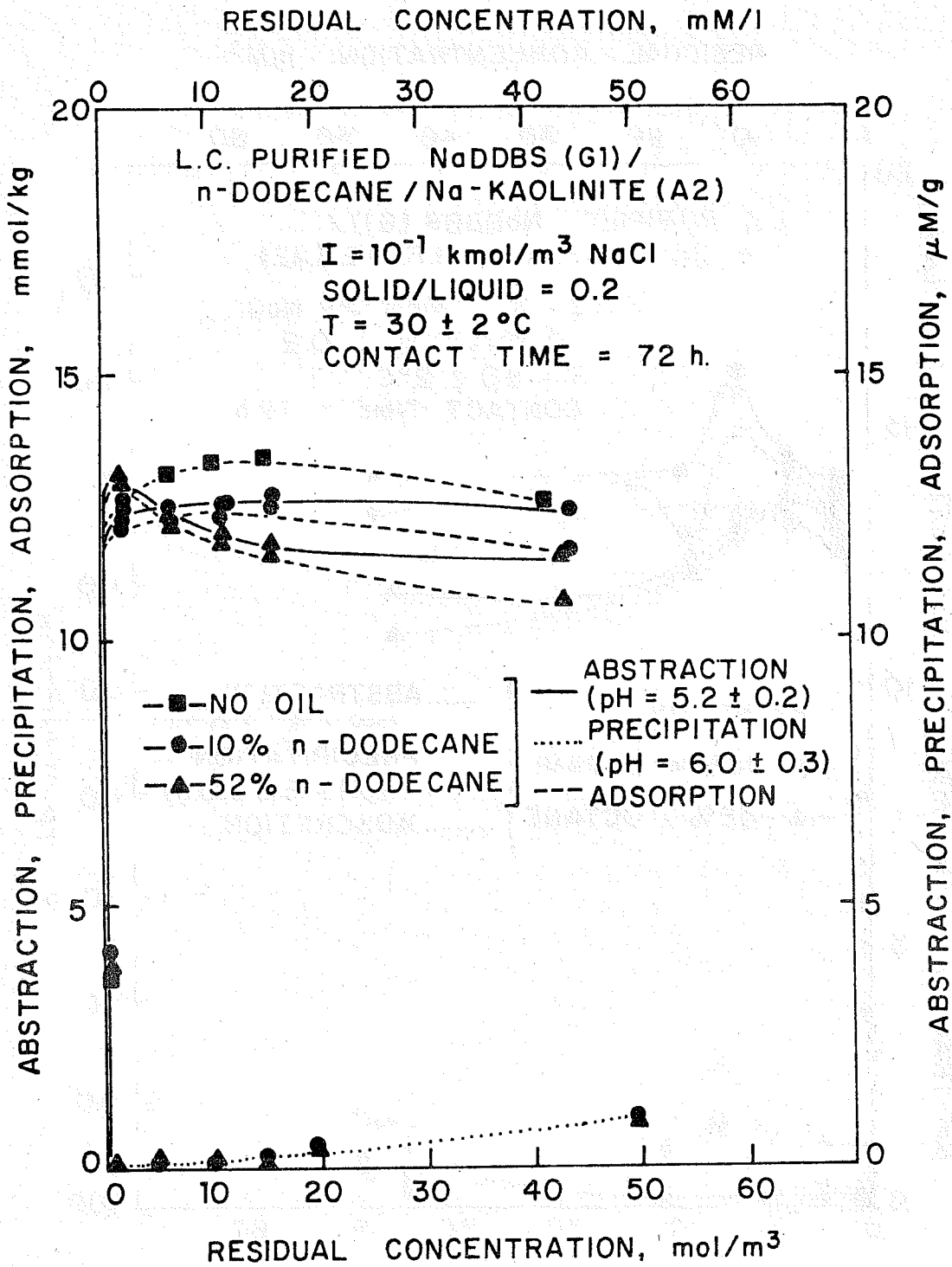


Figure I. 34. Effect of addition of n-dodecane on the adsorption of Na-dodecylbenzenesulfonate on Na-kaolinite.

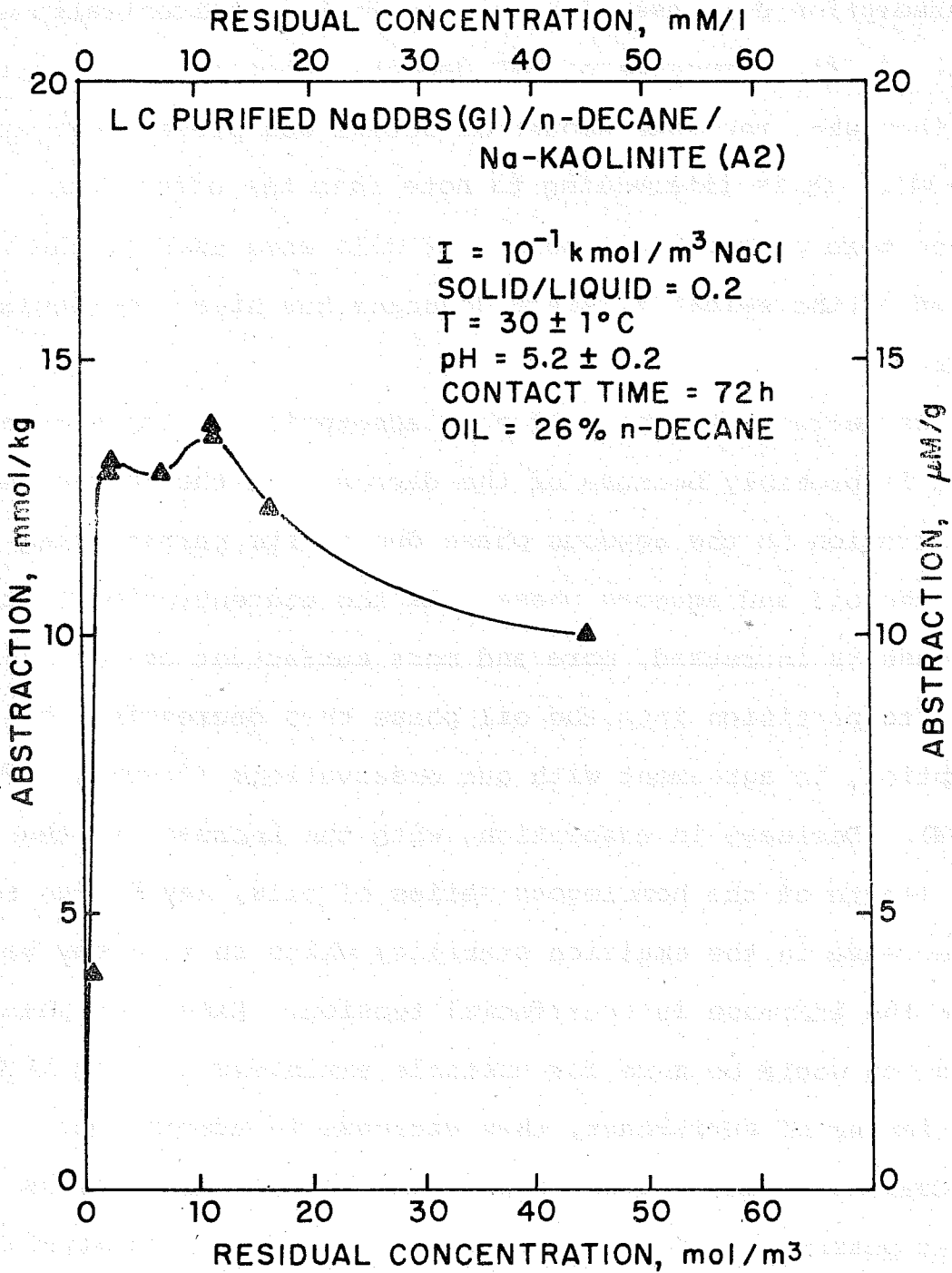


Figure I. 35: Effect of addition of n-decane on the abstraction of Na-dodecylbenzene-sulfonate on Na-kaolinite.

centration. As concentration of oil is increased from 0% to 52% adsorption decreases for most surfactant concentrations (Figure I.34). Presence of 52% dodecane decreased adsorption more than when the same amount of octane was present (Figures I.33-34). It is interesting to note that the effect can be even more prominent if mole % of oils were used as the basis instead of the weight %, since dodecane has higher molecular weight.

The decrease in the sulfonate adsorption in the presence of oil is probably because of the decrease in the surfactant concentration in the aqueous phase due to its partitioning between the oil and aqueous phase. As the concentration of the oil phase is increased, more and more surfactant can be expected to partition into the oil phase thus decreasing the adsorption, in agreement with our observations (Figures I.33 & I.34). Decrease in adsorption, with the increase in the chain length of the homologous series of oils, may be due to the decrease in the emulsion stability which in turn may be due to the increase in interfacial tension. Extent of phase separation would be more for unstable emulsions causing higher partitioning of surfactant, thus decrease in adsorption.

Coating or adsorption of oils on the kaolinite may be another possibility for the decrease of sulfonate adsorption in the presence of oil. Such a coating would indeed increase with an increase in oil concentration. One or both of these mechanisms might be operating in the present system.

#### D. Conclusions

The results of the experiments presented in this chapter demonstrate the importance of studying well characterized systems in order to identify the precise mechanism of adsorption of surfactant. Presence of impurities in the system can cause a maximum in the adsorption isotherm. Results indicate the effect of longer chain (less polar) impurities to be stronger. Presence of shorter chain impurities in the recrystallized sulfonate did not produce such an effect. Also experiments with addition of hydrocarbons to the system confirmed this possibility. In the presence of nonpolar components more pronounced maximum is found to appear in the adsorption isotherm. Oil decreases surfactant adsorption and even completely eliminates precipitation of surfactant in most of the cases studied. Increase in chain length or concentration of the homologous series of oils also decreased adsorption.

Precipitation of surfactant due to its interaction with the dissolved mineral species contributes to the presence of maxima observed in the adsorption isotherm. It is necessary to conduct precipitation and abstraction experiments under identical environments in order to infer adsorption densities from them.

Adsorption experiments conducted with the purified and as-received sulfonates indicated that purification also can reduce the extent of the maximum. There is indeed a dire

need for work to continue in this direction so that better solvents can be developed for improving the efficiency of purification by liquid chromatography and/or for further purifying the sodium dodecylbenzenesulfonate.

Symbols and Abbreviations

ALC	Analytical Liquid Chromatography.
LC	Liquid Chromatography.
HPLC	High Performance Liquid Chromatography.
NaDDBS	sodium dodecylbenzenesulfonate.
Na p(1, BO)BS	sodium p(1, butyloctyl)benzenesulfonate.
RC	Recrystallized.
VPC	Vapor Phase Chromatography.

## II. SOLUTION CHEMISTRY OF SURFACTANTS\*

### A. Chemical Equilibria in Surfactant Solutions and their Role in Adsorption at Interfaces

#### A.1. INTRODUCTION

A fundamental characteristic of surfactant species is their amphiphilic nature, i.e. the presence of nonpolar and polar moieties in the same molecule or ion. This dual nature gives rise to their adsorption at various interfaces. The same amphiphilic tendency causes them to also undergo associative interactions in aqueous solutions to form micelles. Similarly, formation of low molecular weight aggregates such as dimers have been postulated in the past. Analysis of the literature on pre-micellar aggregation, however, revealed the conflicting nature of the existing information. For example, the species distribution computed as a function of pH for potassium oleate solutions using different sets of available data as well as the estimates of energy of interactions between various species for the formation of complexes showed that the ratio of acid-soap to monomer ( $R_2H^-$  to  $R^-$ ) varied from  $10^{-6}$  to 10 depending upon the set of data used. Since the complexes such as dimers and acid-soaps are expected to have different surface activities, a knowledge of the relative abundance of these species and their surface activities is important in understanding the mechanism of adsorption at various interfaces. Our investigation aimed towards identifying

---

\*List of symbols and abbreviations is given at the end of the chapter.

such complexes and towards determining the relevant thermodynamic data for them involved the measurement of surface tension of surfactant solutions under selected solution conditions such as pH. Preliminary results presented in last year's annual report indicated the aggregation of surfactants in the premicellar region in potassium-oleate solutions. A minimum possible value for the dimerization constant was also evaluated during the above study.

A general thermodynamic model incorporating the formation of association complexes such as dimers for the dependence of surface tension of surfactant solutions as a function of concentration and pH was developed during the current year. A model was suggested for the purpose of comparing the surface activities of certain major types of surfactant complexes. In addition, surface tension measurements were extended to other solution conditions. Surface potential was also measured simultaneously with surface tension. The combination of surface tension and surface potential proved to be a powerful technique for the investigation of solution chemistry of surfactants.

#### A.2. SURFACE ACTIVITIES OF SURFACTANT COMPLEXES

Species distribution as a function of pH for potassium oleate solutions presented in the 1978 Annual report and reproduced in Figure II.1 indicates the maximum ratio of acid-soap to monomer ( $R_2H^-$  to  $R^-$ ) to be about  $10^{-4}$  -  $10^{-3}$  in the neutral pH region. Similar distribution computed as a function of pH using the literature value of dimerization constant and

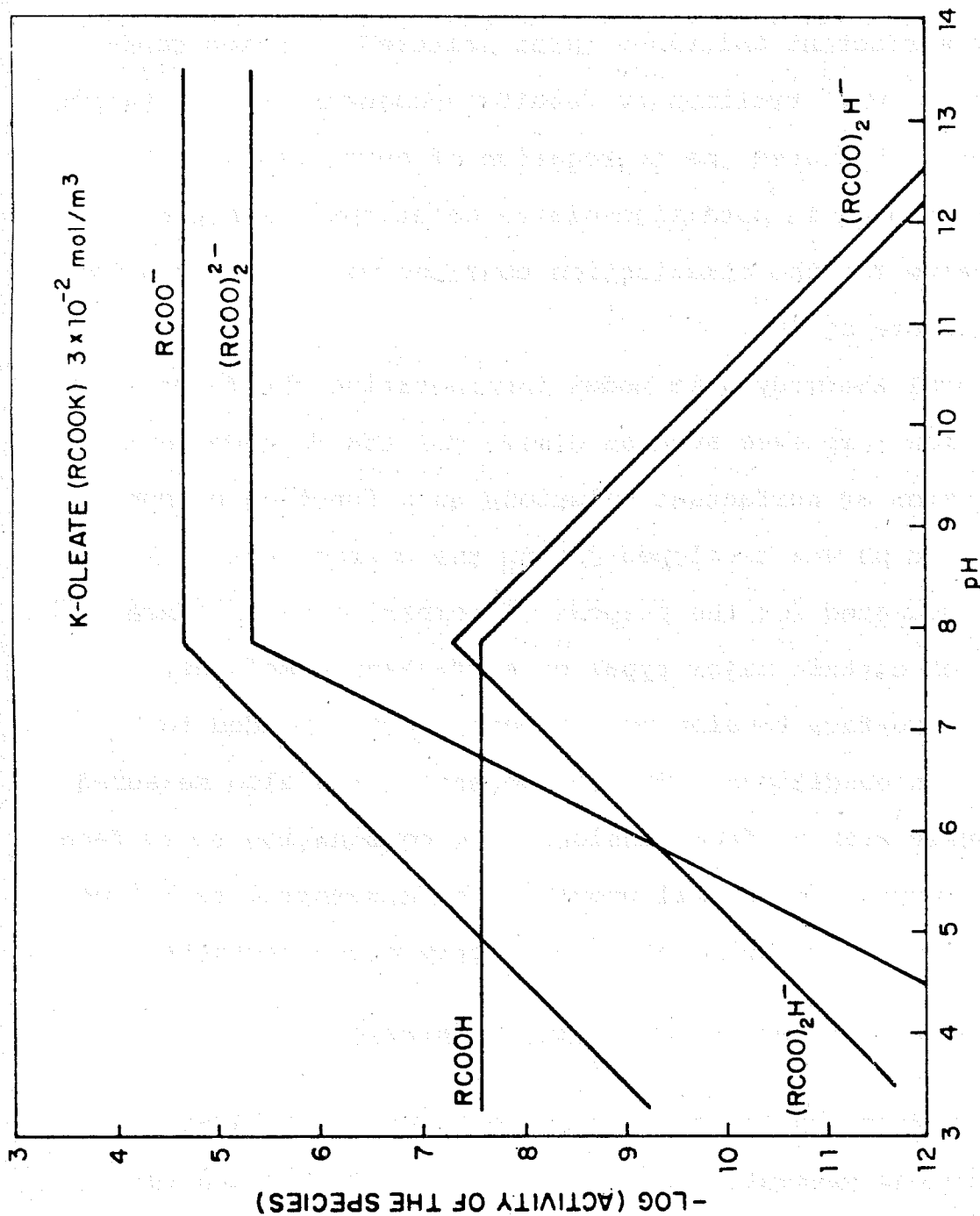


Figure II. 1. Species Distribution Diagram of Potassium Oleate Solutions as a function of pH at  $C_T = 3 \times 10^{-5} M$ . The constants used in computing this diagram are:  $pK_s = 7.6$ ,  $pK_a = 4.95$ ,  $pK_D = -4.0$  and  $pK_{AD} = -4.95$ .

the estimated value for acid-soap formation constant for sodium dodecylsulfonate and sodium dodecylsulfate are presented in Figures II.2 and II.3. They both indicate the presence of significant amounts of  $R_2^{2-}$  along with  $R^-$  throughout the pH region, with acid-soap and neutral acid being present in comparable amounts at very low pH values.

An interesting question in determining the role of the above species is what would the relative concentrations of various species be for the solution properties to be affected to a significant extent. In this section an attempt is made to compare the surface activities of  $RH$ ,  $R^-$  and  $R_2H^-$ . Oleic acid is used as a specific example to point out the importance of association complexes.

Boltzmann's equation for adsorption of various species at the interface is given by

$$c_s = c_b \text{ Exp } (-\Delta G_{ad}^{\circ}/RT) \quad (1)$$

where  $c_s$  = concentration of the species at the interface

$c_b$  = concentration of the species in the bulk

$\Delta G_{ad}^{\circ}$  = free energy change due to the transfer of a surfactant from bulk to interface

$\Delta G_{ad}^{\circ}$  for the case where the adsorbed molecules do not interact with each other can be written as (3) :

$$\Delta G_{ad}^{\circ} = n \cdot \phi_{CH_2} + \lambda_P + Ze\psi_0 \quad (2)$$

where

$n$  = no. of  $-CH_2$  groups in the hydrocarbon chain

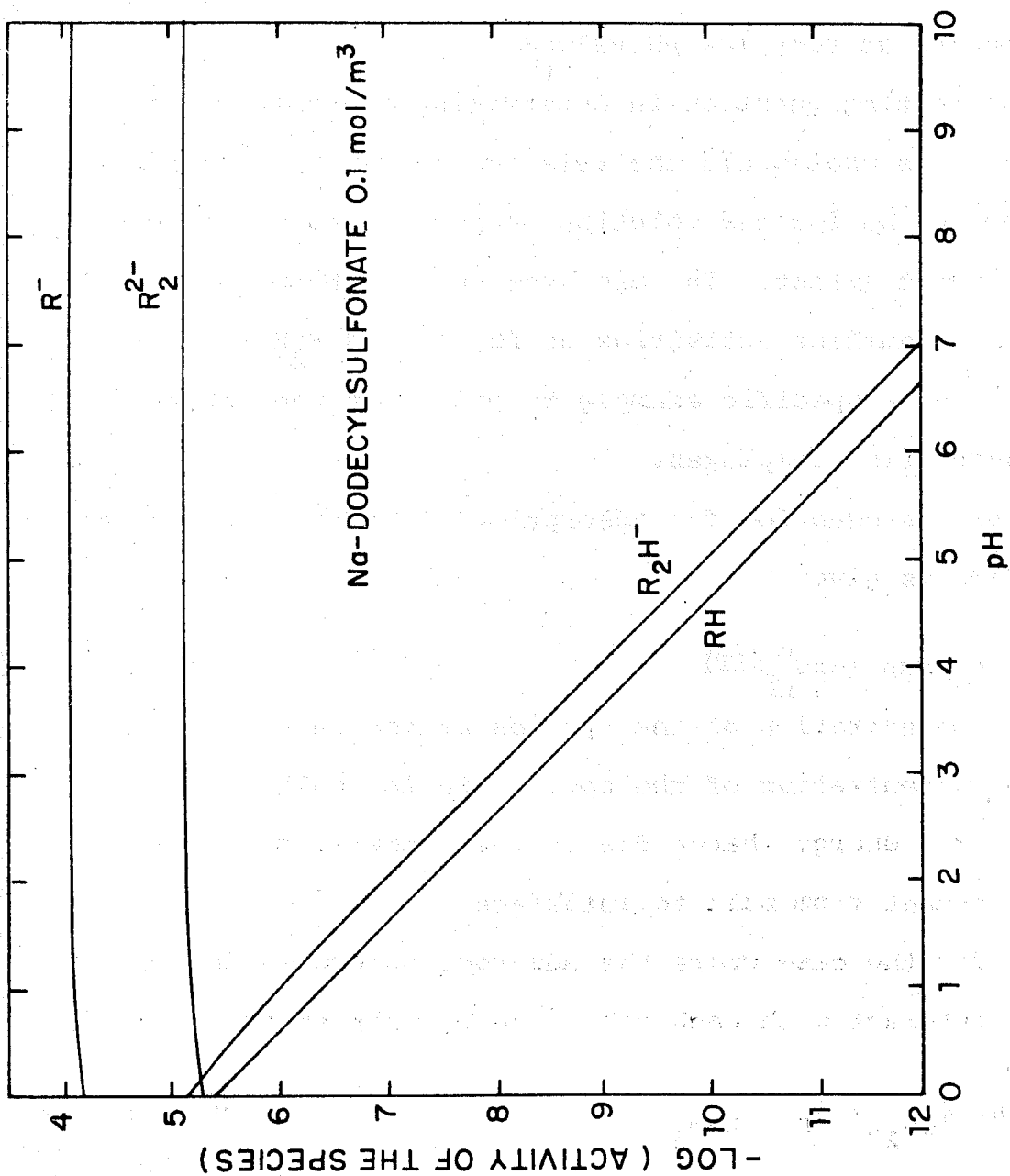


Figure II. 2. Species Distribution Diagrams as a function of pH for Na-dodecylsulfonate solutions at  $C_T = 10^{-4} M$ . The constants used in computing this diagram are:  $pK_a = -1.3$ ,  $pK_D = -3.0$  and  $pK_{AD} = -4.48$ .

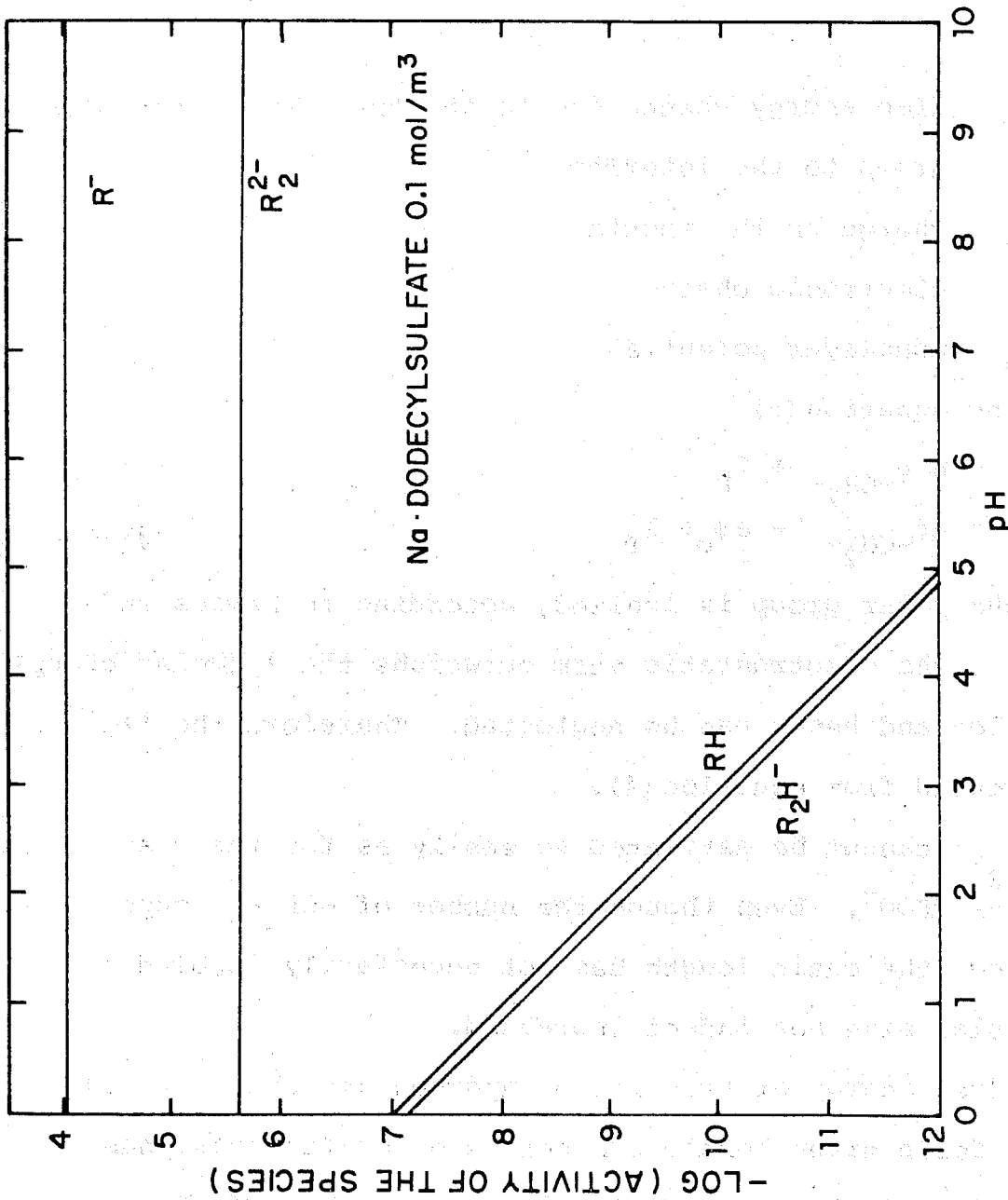


Figure II. 3. Species Distribution Diagrams as a function of pH for Na-dodecylsulfate solutions at  $C_T = 10^{-4} M$ . The constants used in computing this diagram are:  $pK_a = -3.0$ ,  $pK_D = -2.39$  and  $pK_{AD} = -3.88$ .

$\phi_{\text{CH}_2^-}$  = free energy change due to the transfer of a single  
 $-\text{CH}_2-$  group to the interface

$\lambda_p$  = free energy change due to the transfer of the polar  
group to the interface

Z = charge on the species

e = electronic charge

and  $\psi_0$  = monolayer potential.

Using equation (2)

$$\Delta G_{\text{RH}}^{\circ} = n \phi_{-\text{CH}_2^-} + \lambda_p \quad (3)$$

$$\Delta G_{\text{R}^-}^{\circ} = n \phi_{-\text{CH}_2^-} - e \psi_0 + \lambda_p \quad (4)$$

If the polar group is ionized, according to Davies and Rideal (3), the electrostatic term outweighs the  $\lambda_p$  (polar group) contribution and hence can be neglected. Therefore the ' $\lambda_p$ ' can be dropped from equation (4).

$\Delta G_{\text{R}_2\text{H}^-}^{\circ}$  cannot be estimated so easily as for the case of  $\text{RCOOH}$  or  $\text{RCOO}^-$ . Even though the number of  $-\text{CH}_2-$  groups has doubled, the chain length has not necessarily doubled, the molecular size has indeed increased.

The free energy of transfer of hydrocarbon chains to the interface for a given homologous series of surfactants, has been established to be proportional to the number of  $-\text{CH}_2-$  groups in the chain. (3) This can be examined from another point of view.

Since the tendency of hydrocarbon molecules is to decrease the interfacial area exposed to water, it is reason-

able to expect the hydrophobic energy involved in such an interaction to be proportional to the interfacial area, i.e.

$$\text{Hydrophobic free energy} = A \cdot \phi'_{\text{CH}_2}$$

where A is the interfacial area and  $\phi'_{\text{CH}_2}$  the free energy change per unit area.

For a long chain hydrocarbon, the hydrophobic area can be expressed as (neglecting the one end area as it would be negligible in comparison to the lateral area):

$$A = 2\pi r n l_0$$

where

r is the diameter of the hydrocarbon chain, and

$l_0$  the length of a single  $-\text{CH}_2-$  group.

For a given homologous series of surfactants (assuming straight chain),  $2\pi r l_0$  remains constant and hence the variation in free energy among the homologous series will be proportional to the number of  $-\text{CH}_2-$  groups in the surfactant. Thus, the use of the concept of interfacial area to be a property that is proportional to the change in free energy as opposed to the number of carbon atoms is in no contradiction to the existing results. Hence,

$$A_{\text{RH}} \cdot \phi'_{\text{CH}_2} = n_{\text{RH}} \cdot \phi_{\text{CH}_2} \tag{6}$$

Using this approach, it is possible to evaluate the number of effective  $-\text{CH}_2-$  groups in an acid-soap molecule as follows,

$$A_{\text{R}_2\text{H}^-} \cdot \phi'_{\text{CH}_2} = n_{\text{R}_2\text{H}^- \text{eff.}} \cdot \phi_{\text{CH}_2} \tag{7}$$

which leads to,

$$n_{R_2H^- \text{ eff.}} = \frac{A_{R_2H^-}}{A_{RH}} \cdot n_{RH} \tag{8}$$

where  $A_{RH}$  and  $A_{R_2H^-}$  represent the interfacial area of RH and  $R_2H^-$  respectively.

Thus, a knowledge of the changes in interfacial area due to association is necessary to use this approach. A good estimate of area can be obtained by using molecularly scaled models (4).

Assuming that  $\phi_{-CH_2-} = 700$  cal/mole  $\lambda_p = 437$  cal/mole(3) and on the basis of solubility considerations, approximating oleic acid, the  $C_{18}$  fatty acid with a double bond to be equivalent to a  $C_{16}$  straight chain fatty acid

$$\Delta G_{R_2H}^{\circ} = -11637 \text{ cal/mole.}$$

Assuming that the monolayer potential is about 100 mv which according to the Gouy theory corresponds to a system where area for ionogenic molecule is about  $100A^{\circ 2}$  and the ionic strength is  $10^{-1}M$

$$\Delta G_R^{\circ-} = -8895 \text{ cal/mole.}$$

Normally the area per molecule can be expected to be lower than  $100A^{\circ 2}$ , resulting in a higher monolayer potential and hence a higher electrostatic repulsion for the adsorption of ionic groups.

$A_{RH}$  and  $A_{R_2H^-}$  taken from estimates of interfacial area made on molecularly scaled models are  $275A^{\circ 2}$  and  $490A^{\circ 2}$  respectively (4). This yields the value of n to be 28 and

$$\Delta G_{R_2H^-}^{\circ} = -17730 \text{ cal/mole.}$$

Therefore at  $25^{\circ}C$

$$c_{s-RH} = c_{b-RH} \{ \exp (19.5) \} \quad (9)$$

$$c_{s-R^-} = c_{b-R^-} \{ \exp (19.5) \} \quad (10)$$

and 
$$c_{s-R_2H^-} = c_{b-R_2H^-} \{ \exp (29.7) \} \quad (11)$$

For equal adsorption of RH and  $R_2H^-$  the concentration ratio in the bulk will be

$$\frac{c_{b-R_2H^-}}{c_{b-RH}} = \exp(-10.2) = 3.7 \times 10^{-5} \quad (12)$$

$$c_{b-RH}$$

Similarly

$$\frac{c_{b-R_2H^-}}{c_{b-R^-}} = \exp(-14.8) = 3.73 \times 10^{-7} \quad (13)$$

$$c_{b-R^-}$$

The above simple calculation shows that even if  $R_2H^-$  concentration is five orders of magnitude lower than that of RH or seven orders of magnitude lower than that of  $R^-$  its adsorption at the liquid/air interface can be significant. These calculations can be modified by considering other factors such as the induction effect that minimizes the contribution of the  $-CH_2-$  group near the ionic/polar group to hydrophobicity. Most importantly, the above calculations illustrate the point that the adsorption of  $R_2H^-$  can be very significant even if its relative concentration is very low.

Examination of Figure II.1 shows that around the neutral pH region,  $c_{R_2H^-}/c_{R^-}$  is about  $10^{-3} - 10^{-4}$  and hence the adsorption can be expected to be much higher than that of  $R^-$ .

$R_2^{2-}$  on the other hand, has ionic heads at the opposite ends, and hence a direct comparison of its surface activity with other species becomes difficult. At low coverages  $R_2^{2-}$  can adsorb at the water/oil or water/air interface with an inverted 'U' configuration, thereby allowing the ionic heads to be in aqueous solution and the hydrocarbon chains in oil or air. At high surface coverages however it is reasonable to expect the adsorption of this dimer to be less probable compared to that of individual monomers. On the contrary, adsorption of  $R_2^{2-}$  at the solid/liquid interface can always be considered to be energetically favorable, as it can orient one hydrophilic end toward the mineral and the other towards the bulk solution. In fact, it is interesting to note that such effects can possibly contribute to the decrease in mineral non-wettability often observed at higher surfactant concentrations. In the past, this has been attributed to a number of factors such as the adsorption of a second layer of surfactant with a reverse orientation, decrease in the size of droplet or bubble and the saturation of the surface of the droplet or the bubble and solid/liquid interfaces with surfactants which can possibly make the droplet and the bubble incompatible with the hydrophobic surface of the mineral.

Distribution diagrams presented above give an estimate of the activities of various species in solution. Estimation of the surface activities of these species show that the

association complexes even if present in very small amounts, can make significant contributions to the adsorption characteristics of the surfactants. This suggests the need for a careful study as well as experimentation for obtaining reliable values for the thermodynamic constants of association complexes.

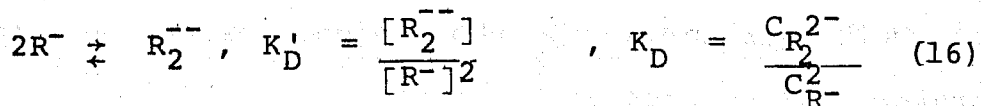
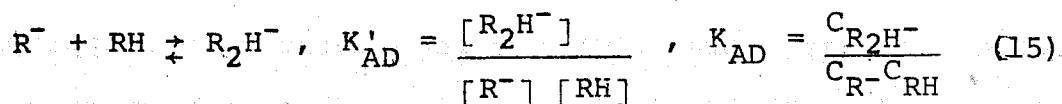
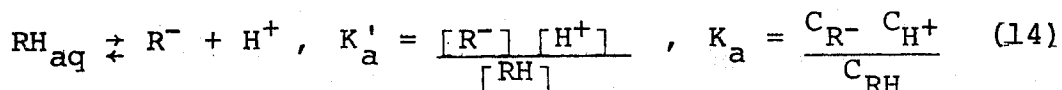
### A.3 THERMODYNAMICS OF SURFACE TENSION OF SYSTEMS CONTAINING SURFACTANT COMPLEXES

A number of solution properties of surfactants such as conductivity, molar volume and hydrolysis can yield information on bulk chemical equilibria. Yet another property which has not been exploited for this purpose fully is the surface tension behavior of surfactant solutions. This method can reveal not only information on the bulk equilibria but also on the surface activities of different species. Surface tension has been known to be highly sensitive to surface active impurities. As a result, this method is normally avoided lest there are complications arising from possible contamination. On the other hand, if the property is very sensitive to the presence of even traces of impurities, it should be possible to exploit the changes in it for detecting associations in the system. With this view, a thermodynamic model taking into account the formation of dimers and acid-soaps is developed for the surface tension behavior of surfactant solutions. This model discussed below is a more generalized one than that described earlier(1).

#### Theory

Let us consider an anionic surfactant RH in an aqueous solution in the presence of an indifferent electrolyte MX. Species to be considered in this system are: RH,  $R^-$ ,  $R_2H^-$ ,  $R_2^{2-}$ ,  $M^+$ ,  $X^-$ ,  $H_2O$ ,  $H^+$  and  $OH^-$ . Multimers such as trimers and tetramers have not been considered in this treatment at this

stage, as they are not likely to exist in significant amounts (below CMC), because of the accentuated repulsion between the charged heads which must now be placed closer to one another. If necessary, higher multimers can however be easily included in this treatment. The following bulk chemical equilibria and the corresponding equilibrium constants can be written for this system:



where terms in the square brackets indicate the respective activities and 'C<sub>i</sub>' refers to the bulk concentration of species 'i'. The Gibbs equation for adsorption of various species at the interfacial region at constant temperature can be written as:

$$-\partial\gamma = \sum_i \Gamma_i \partial\mu_i \quad (19)$$

where  $\gamma$  is the surface tension,  $\Gamma_i$  and  $\mu_i$  are the Gibbs excess and the chemical potential of the species 'i' respectively.

Gibbs equation for this system with the standard convention

$\Gamma_{H_2O} = 0$  is:

$$\begin{aligned}
 -\partial\gamma = & \Gamma_{RH} \partial\mu_{RH} + \Gamma_{R^-} \partial\mu_{R^-} + \Gamma_{R_2H^-} \partial\mu_{R_2H^-} & (20) \\
 & + \Gamma_{R_2^{--}} \partial\mu_{R_2^{--}} + \Gamma_{H^+} \partial\mu_{H^+} + \Gamma_{OH^-} \partial\mu_{OH^-} \\
 & + \Gamma_{M^+} \partial\mu_{M^+} + \Gamma_{X^-} \partial\mu_{X^-}
 \end{aligned}$$

Assuming that the chemical potential of the solvent does not change appreciably and incorporating the appropriate relations for the chemical potential of various species from bulk equilibria, the above equations can be simplified to obtain:

$$\begin{aligned}
 -\partial\gamma = & \left[ \Gamma_{RH} + 2\Gamma_{R_2H^-} + 2\Gamma_{R_2^{--}} + \Gamma_{R^-} \right] \partial\mu_{RH} & (21) \\
 & + \left[ \Gamma_{H^+} - \Gamma_{R_2H^-} - 2\Gamma_{R_2^{--}} - \Gamma_{R^-} - \Gamma_{OH^-} \right] \partial\mu_{H^+} \\
 & + \Gamma_{M^+} \partial\mu_{M^+} + \Gamma_{X^-} \partial\mu_{X^-}
 \end{aligned}$$

This equation involves the chemical potential of only a single surfactant species namely, RH. It will be convenient to rewrite this in terms of the total surfactant concentration and this can be done as follows. Since the adsorption at the interface can be considered not to affect the bulk con-

centration appreciably, one can write:

$$C_T = C_{RH} + C_{R^-} + 2C_{R_2H^-} + 2C_{R_2^{--}} \quad (22)$$

where  $C_T$  represents the total surfactant concentration in solution. Using Equations 14-18 and 22,  $C_T$  can be expressed as:

$$C_T = C_{RH} + K_a \frac{C_{RH}}{C_{H^+}} + 2K_{AD} K_a \frac{C_{RH}^2}{C_{H^+}} + 2K_D K_a^2 \left( \frac{C_{RH}}{C_{H^+}} \right)^2 \quad (23)$$

Solving this quadratic equation for  $C_{RH}$  and noting that  $C_{RH}$  is  $>0$ ,

$$C_{RH} = \frac{-(1 + K_H) + \sqrt{(1 + K_H)^2 + 8C_T Z}}{4Z} \quad (24)$$

where

$$Z = K_{AD} K_H + K_D K_H^2 \quad (25)$$

and

$$K_H = K_a / C_{H^+} \quad (26)$$

The expression for  $C_{RH}$  can be differentiated to yield

$$\partial \ln C_{RH} = \alpha \partial \ln C_T + \beta \ln C_{H^+} \quad (27)$$

where  $\alpha$  and  $\beta$  are given by

$$\alpha = \frac{1}{2} + \frac{1}{2} \frac{1 + K_H}{\sqrt{(1 + K_H)^2 + 8ZC_T}} \quad (28)$$

$$\beta = \frac{1}{2} - \frac{1}{2} \frac{1 - K_H}{\sqrt{(1 + K_H)^2 + 8ZC_T}} \quad (29)$$

$$+ K_D K_H^2 \left[ \frac{1}{2Z} - \frac{1 + K_H}{2Z \sqrt{(1+K_H)^2 + 8ZC_T}} \right]$$

Thus,  $C_{RH}$  depends upon  $C_T$  and  $C_{H^+}$  as indicated above.

Noting that

$$\partial \mu_{RH} = RT \partial \ln C_{RH} + RT \partial \ln f \quad (30)$$

and assuming that  $\partial \ln f = 0$  for dilute solutions,

$$\begin{aligned} - \frac{\partial \gamma}{RT} = & \Gamma_{R-T} \left[ \alpha \partial \ln C_T + \beta \partial \ln C_{H^+} \right] \quad (31) \\ & + \left[ \Gamma_{H^+} - \Gamma_{R^-} - \Gamma_{R_2H^-} - 2\Gamma_{R_2^{2-}} - \Gamma_{OH^-} \right] \partial \ln C_{H^+} \\ & + \Gamma_{M^+} \partial \ln C_{M^+} + \Gamma_{X^-} \partial \ln C_{X^-} \end{aligned}$$

where  $\Gamma_{R-T} = \Gamma_{RH} + \Gamma_{R^-} + 2\Gamma_{R_2H^-} + 2\Gamma_{R_2^{2-}}$

This general equation describes the surface tension behavior of aqueous surfactant solutions as a function of pH and concentration. Coefficients  $\alpha$  and  $\beta$  account for all the associative interactions. It would therefore be interesting to evaluate their limiting values.

a. Complete Association

$$K_{AD} \cdot K_H + K_D K_H^2 = Z \rightarrow \infty \quad (32)$$

$$\lim_{Z \rightarrow \infty} \alpha = \frac{1}{2}.$$

b. No Association (Z → 0)

$$\lim_{Z \rightarrow 0} \alpha = 1. \quad (33)$$

The value of 'α' lies between 1 and ½, the former corresponding to no association and the latter to complete association.

Similarly the value of 'β' for the case of no association is

$$\lim_{Z \rightarrow 0} \beta = 1 - \frac{1}{1 + K_H} \quad (34)$$

This latter limit of β depicts the situation where only RH and R<sup>-</sup> are the surfactant species in solution.

Thus, α and β reflect the degree of association in the bulk. Equation 31 can be simplified for certain cases. Some of the possible cases are discussed below.

a. High pH Conditions (also for highly ionizable surfactants)

Z can be written as

$$Z = K_D K_H^2 (1 + K_{AD}/K_D K_H) \quad (35)$$

As discussed earlier,  $K_{AD}/K_D$  is not known very accurately, but can be as high as  $10^4$  (1). Using this high value, above pH 11,

$$K_{AD}/K_D \cdot K_H \approx 10^4 \cdot 10^{-11}/10^{-5} \ll 1.$$

$$Z = K_D \cdot K_H^2 \tag{36}$$

Similarly,  $1 + K_H \approx K_H$  (37)

and

$$K_{AD} + 2K_D K_H \approx 2K_D K_H \tag{38}$$

With these simplifications,  $\alpha$  and  $\beta$  can be written as,

$$\alpha = \frac{1}{2} + \frac{1}{2} \frac{1}{\sqrt{1 + 8K_D C_T}} \quad \beta = 1. \tag{39}, \tag{40}$$

Equation 31 then becomes,

$$\begin{aligned} - \frac{\partial \gamma}{RT} = & \Gamma_{R-T} \left[ \frac{1}{2} + \frac{1}{2} \frac{1}{\sqrt{1 + 8K_D C_T}} \right] \partial \ln C_T \tag{41} \\ & + \left[ \Gamma_{H^+} + \Gamma_{RH} + \Gamma_{R_2H^-} - \Gamma_{OH^-} \right] \partial \ln C_{H^+} \\ & + \Gamma_{M^+} \partial \ln C_{M^+} + \Gamma_{X^-} \partial \ln C_{X^-} \end{aligned}$$

For constant  $C_T$  conditions the first term in (41) can be dropped. Similarly the second can be dropped for constant pH.

Under high pH conditions  $\Gamma_{RH}$  and  $\Gamma_{R_2H^-}$  can be expected to be small since  $C_{RH}$  and  $C_{R_2H^-}$  are present in negligible amounts. If  $C_T$  is also maintained constant,

$$\begin{aligned} - \frac{\partial \gamma}{RT} = & (\Gamma_{H^+} - \Gamma_{OH^-}) \partial \ln C_{H^+} \tag{42} \\ & + \Gamma_{M^+} \partial \ln C_{M^+} + \Gamma_{X^-} \partial \ln C_{X^-} \end{aligned}$$

This equation is applicable also for the case of highly ionizable surfactants such as sulfonates and sulfates under most pH conditions where hydrolysis reactions can be assumed to be negligible. Variations in  $\gamma$  with the total surfactant concentration for highly ionizable surfactants and for hydrolyzable anionic surfactants under high and constant pH conditions can be written as

$$-\frac{\partial \gamma}{RT} = \Gamma_{R-T} \left[ \frac{1}{2} + \frac{1}{2} \frac{1}{\sqrt{1 + 8K_D C_T}} \right] \partial \ln C_T \quad (43)$$

$$+ \Gamma_{M^+} \partial \ln C_{M^+} + \Gamma_{X^-} \partial \ln C_{X^-}$$

Equation 43 can be used for cationic surfactants also under conditions of complete ionization. In fact, the equation derived by Rignout(5) for hexadecyltrimethylammonium bromide is similar to 43 and is a special case of 31.

b. Constant adsorption density conditions

It has been suggested that the adsorption density at the liquid/air interface attains a constant value at concentrations as low as 1/3 cmc(5). The manner in which this situation can be exploited to yield information on associative interaction has been discussed in the earlier reports. Briefly, under high ionic strength, high pH conditions, if  $\Gamma_{R-T}$  remains constant,

$$\frac{-\partial \gamma}{2.3RT} = \Gamma_{R-T} \left[ \frac{1}{2} + \frac{1}{2} \frac{1}{\sqrt{1 + 8K_D C_T}} \right] \partial \ln C_T \quad (44)$$

At very low concentrations, when  $8K_D C_T \ll 1$ ,  $\alpha$  (term in the square bracket) = 1, and as the concentration increases,

$\alpha$  begins to decrease resulting in a decrease of the product  $\Gamma_{R-T} \cdot \alpha$ . This suggests that when  $\gamma$  vs  $\log C_T$  is plotted one may observe a constant slope region followed by a region where a decrease in slope as cmc is approached. Thus, the changes in the slope of  $\gamma$  vs  $\log C_T$  can be used for determining  $K_D$ .

Equation 44 can be integrated to yield,

$$-\frac{\gamma}{2.3 RT\Gamma_{R-T}} = \frac{1}{2} \log \left[ \frac{C_T \sqrt{1 + 8K_D C_T} - 1}{\sqrt{1 + 8K_D C_T} + 1} \right] + \text{constant.} \quad (45)$$

This equation describes the surface tension behavior as a function of  $C_T$  under constant high pH, high ionic strength and constant temperature conditions.

Using the maximum slope as the limiting value of  $\Gamma_{R-T}$  and assuming the observed decrease in the slope at higher concentrations to be due to the decrease in  $\alpha$ , it is possible to estimate the minimum possible value for  $K_D$ . The constant slope region in fact could have resulted from the compensating effects of increase in  $\Gamma_{R-T}$  and decrease in  $\alpha$ . In other words, the limiting  $\Gamma_{R-T}$  calculated from the constant slope region in fact could be lower than the actual saturation adsorption density. This would make the  $K_D$  from these calculations "the minimum."

This possibility raises an interesting question as to whether the constant slope often reported in the literature

is due to constant adsorption or due to the compensating effects discussed above. Measurement of surface tension combined with other techniques such as surface potential (for ionized monolayers) or direct measurement of adsorption at interfaces should yield more information on this problem.

Dependence of Surface Tension on pH

a. Conditions of precipitation of RH:

If RH is precipitating, then

$$\partial \mu_{RH} = 0 \tag{46}$$

Equation 21 then becomes,

$$-\partial \gamma = \left[ \Gamma_{H^+} - \Gamma_{R_2H^-} - 2\Gamma_{R_2^{2-}} - \Gamma_{R^-} - \Gamma_{OH^-} \right] \partial \mu_{H^+} + \Gamma_{M^+} \partial \mu_{M^+} + \Gamma_{X^-} \partial \mu_{X^-} \tag{47}$$

using the electrical neutrality condition for the interface,

$$\Gamma_{H^+} + \Gamma_{M^+} = \Gamma_{R^-} + 2\Gamma_{R_2^{2-}} + \Gamma_{R_2H^-} + \Gamma_{OH^-} + \Gamma_{X^-} \tag{48}$$

$$-\partial \gamma = \left[ \Gamma_{X^-} - \Gamma_{M^+} \right] \partial \mu_{H^+} + \Gamma_{M^+} \partial \mu_{M^+} + \Gamma_{X^-} \partial \mu_{X^-} \tag{49}$$

under high ionic strength conditions,

$$-\partial \gamma = \left[ \Gamma_{X^-} - \Gamma_{M^+} \right] \partial \mu_{H^+}$$

or

$$\frac{\partial \gamma}{2.3 RT \partial pH} = \Gamma_{X^-} - \Gamma_{M^+} \tag{50}$$

Since the ionic strength of the solution is relatively high,

$$C_{M^+} \approx C_{X^-} \quad (51)$$

Also,

$$\Gamma_{X^-} = C_{X^-} \cdot d \cdot \text{Exp} \left( \frac{e\psi_0}{kT} \right) \quad (52)$$

and

$$\Gamma_{M^+} = C_{M^+} \cdot d \cdot \text{Exp} \left( \frac{-e\psi_0}{kT} \right) \quad (53)$$

where  $\psi_0$  is the monolayer potential and 'd' is a parameter similar to the thickness of the adsorbed layer.

$$\frac{\partial \gamma}{2.3RT \partial \text{pH}} = 2C_{M^+} \cdot d \cdot \text{Sinh} \left( \frac{e\psi_0}{kT} \right) \quad (54)$$

Since the monolayer potential will be negative for anionic surfactants,

$$\frac{\partial \gamma}{\partial \text{pH}} < 0 \quad (55)$$

Thus,  $\gamma$  should decrease with increase in pH under the precipitation conditions for RH.

This is in agreement with the reported surface tension measurements (6).

The sign of  $\frac{\partial \gamma}{\partial \text{pH}}$  can be similarly obtained in the alkaline range in the following manner.

b. No Precipitation:

Under high pH, high ionic strength and constant  $C_T$  conditions,

$$\begin{aligned} \frac{-\partial \gamma}{RT} &= \Gamma_{R-T} \partial \ln C_{H^+} + \left[ \Gamma_{H^+} - \Gamma_{R^-} - \Gamma_{R_2H^-} - 2\Gamma_{R_2^{2-}} - \Gamma_{OH^-} \right] \partial \ln C_{H^+} \\ &= \left[ \Gamma_{H^+} + \Gamma_{RH} + \Gamma_{R_2H^-} - \Gamma_{OH^-} \right] \partial \ln C_{H^+} \end{aligned} \quad (56)$$

$$\frac{\partial \gamma}{2.3RT \partial \text{pH}} = \Gamma_{H^+} + \Gamma_{RH} + \Gamma_{R_2H^-} - \Gamma_{OH^-} \quad (57)$$

Since the righthand side sum is positive for an anionic surfactant,

$$\frac{\partial \gamma}{\partial \text{pH}} > 0 \quad (58)$$

Since  $\partial \gamma / \partial \text{pH}$  is negative on one side and positive on the other, a minimum in  $\gamma$  vs pH can be expected. The exact position of the minimum and the corresponding value of  $\gamma$  will depend upon the adsorption of various species including that of surfactant complexes. The reported data for  $\gamma$  vs pH in fact exhibits a minimum, in accordance with the above predictions (6). At high pH values, neglecting  $\Gamma_{RH}$  and  $\Gamma_{R_2H^-}$  and noting that  $C_{H^+} = K_w / C_{OH^-}$

$$\frac{\partial \gamma}{2.3RT \partial \text{pH}} = d \cdot C_{H^+} \text{Exp}\left(\frac{-e\psi_0}{kT}\right) - \frac{K_w d}{C_{H^+}} \cdot \text{Exp}\left(\frac{e\psi_0}{kT}\right) \quad (59)$$

Surface tension dependence on pH in the intermediate range under constant  $C_T$  and high ionic strength conditions can be written as:

$$-\frac{\partial \gamma}{RT} = \left[ \Gamma_{R-T} \beta + C_{M+} 2d \cdot \text{Sinh} \left( \frac{e\psi_0}{kT} \right) \right] \partial \ln C_{H+} \quad (60)$$

$$+ \frac{\partial \gamma}{2.3RT \partial \text{pH}} = \left[ \Gamma_{R-T} + 2C_{M+} d \cdot \text{Sinh} \left( \frac{e\psi_0}{kT} \right) \right] \quad (61)$$

where  $\beta$  is given by Equation 29. This simple derivation assumes that only electrostatic forces bind the counter ions to the interface.

In Equation 61, both  $\Gamma_{R-T}$  and  $\psi_0$  can be measured experimentally (for e.g.,  $\Gamma_{R-T}$  using labelled surfactants and  $\psi_0$  by measuring surface potential). These results, along with the surface tension vs. pH data, can be used to evaluate  $\beta$ . Since  $K_D$  can be determined independently under high pH conditions, 61 can be used to estimate  $K_{AD}$ . On the other hand,  $\gamma$  vs.  $\log C_T$  in the neutral pH region (around pH 8.5) can also be used to estimate  $\alpha$  and thus  $K_{AD}$ .

Equations have been derived for the dependence of surface tension on pH and surfactant concentration. Possible experimental conditions under which the thermodynamic constants can be evaluated are also discussed. The above analysis shows that studies of surface tension can reveal bulk association and this technique, coupled with surface potential and surface adsorption can be a powerful experimental tool in studying the chemical equilibria in surfactant solutions and the adsorption characteristics of surfactants at interfaces.

## A.4 EXPERIMENTAL

### Methods

#### Surface Tension

Wilhelmy plate technique described in detail in the earlier reports was used to determine the surface tension.

#### Surface Potential

The potential difference measured between a reference electrode in solution and an air electrode just above the solution surface is the surface potential. At a clean surface of pure water, the measured potential corresponds to that of the dipoles at the surface. In the presence of an ionized monolayer the potential will be the sum of the contributions due to the charges and the dipoles of the surfactant and the solvent.

Most of the past work on surface potential has been on spread monolayers as opposed to adsorbed monolayers as is in the present investigation. One of the techniques to measure the surface potential is the so-called "ionization electrode technique" in which a radioactive air electrode and a reference electrode are used in combination with a high impedance electrometer. Preliminary experiments in the case of adsorbed monolayers also showed that the above technique yielded reproducible results.

A schematic diagram of the equipment used is given in Figure II.4. Air electrode-Am<sup>241</sup> was placed about 5 mm. from

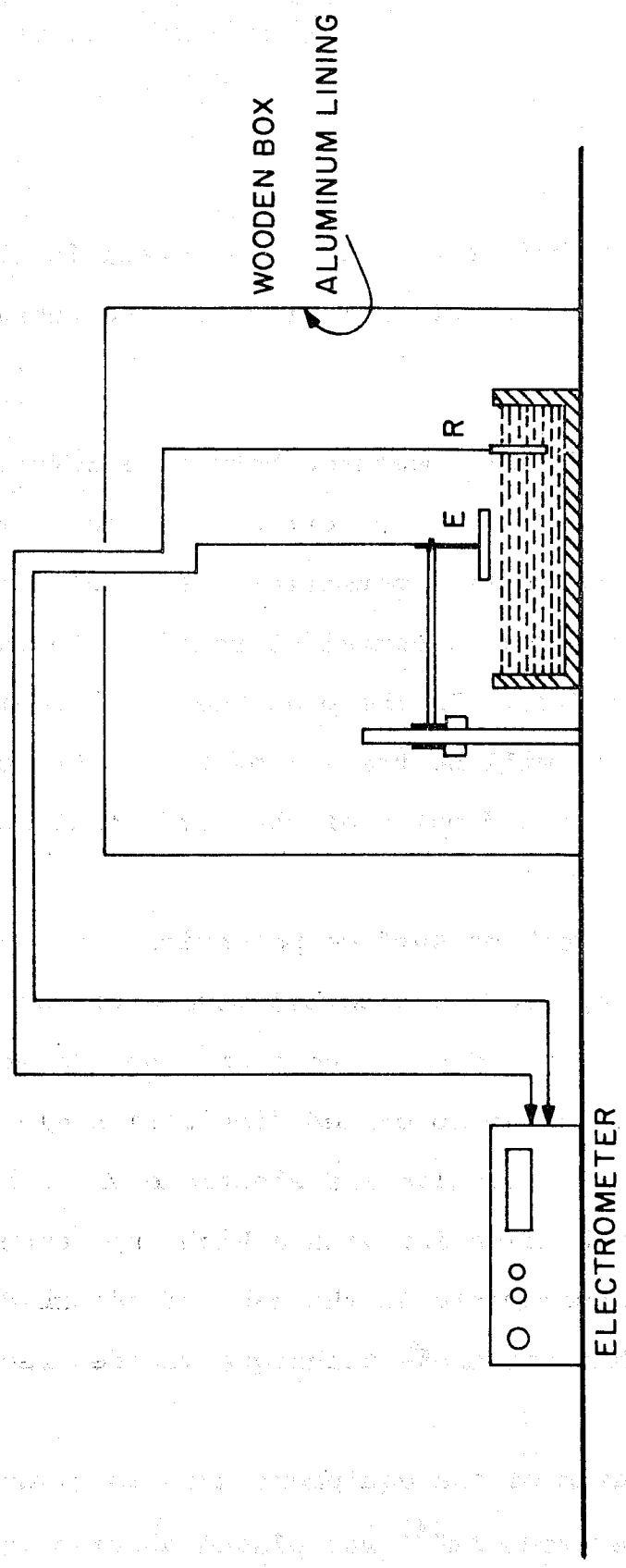


Figure II. 4. A schematic diagram of an apparatus for measuring surface potential.  
E-Radio Active Electrode, R-Reference Electrode.

the solution surface.  $\text{Am}^{241}$  emits  $\beta$ -rays which ionizes the air between the electrode and the solution surface. A silver wire coated with AgCl (obtained by the electrolysis of HCl between two silver wires at a voltage of about 1.5v) was used as the reference electrode in solution. The voltage developed between the air and the reference electrode was measured using a high impedance electrometer (Keithly-603), the output of which was recorded using a Sargent recorder.

To avoid the interference from all the external electrical noises, it was necessary to isolate the system totally from the surroundings. The cell assembly was placed inside a wooden box lined with an aluminum sheet and was well grounded. Similarly, the leads from the electrometer were also covered with aluminum foil and grounded.

The difference between the measured voltages of the solution containing surfactant and the one without it under identical conditions with respect to other parameters such as pH and salt concentration (reference solution) was taken as the surface potential of the surfactant solution. It was necessary to check the potential of the base solution frequently during a series of measurements since it was found to drift over a period of hours.

Poisoning of the reference electrode by surfactant adsorption was checked frequently by measuring its voltage against a clean Ag wire in distilled water.

Volume of solution (40 ml.) taken for each test was kept

constant so that the distance from the electrode to the solution surface is not altered.

### Materials

Oleic acid of > 99.9% purity according to the manufacturer's chromatographic analysis was purchased from Applied Science Laboratories and was used without further purification. All other inorganic chemicals, (KOH, HNO<sub>3</sub>, and K<sub>2</sub>HPO<sub>4</sub>), were of reagent grade purchased from Fisher Scientific Company.

All the aqueous solutions were prepared using deaerated triple distilled water. Potassium oleate stock solutions of  $6.5 \times 10^{-3}$  m/l concentration were stored under a nitrogen atmosphere in the refrigerator.

### A.5 RESULTS AND DISCUSSION

Surface tension results of potassium oleate solutions in the presence of K<sub>2</sub>HPO<sub>4</sub>/KOH buffer at pH 11.4 is given in Figure II.5. Surface potential values obtained from tests conducted under identical conditions using the same solution are also plotted in Figure II.5. An examination of the surface tension curve indicates a linear region in certain concentration region followed by a decrease in slope at higher surfactant concentration. Surface potential however reaches a plateau above a certain concentration and remains constant even under conditions where a decrease in slope of  $\gamma$  vs  $\log C_T$  is observed. This behavior of surface potential suggests a constant adsorption density at the liquid/air

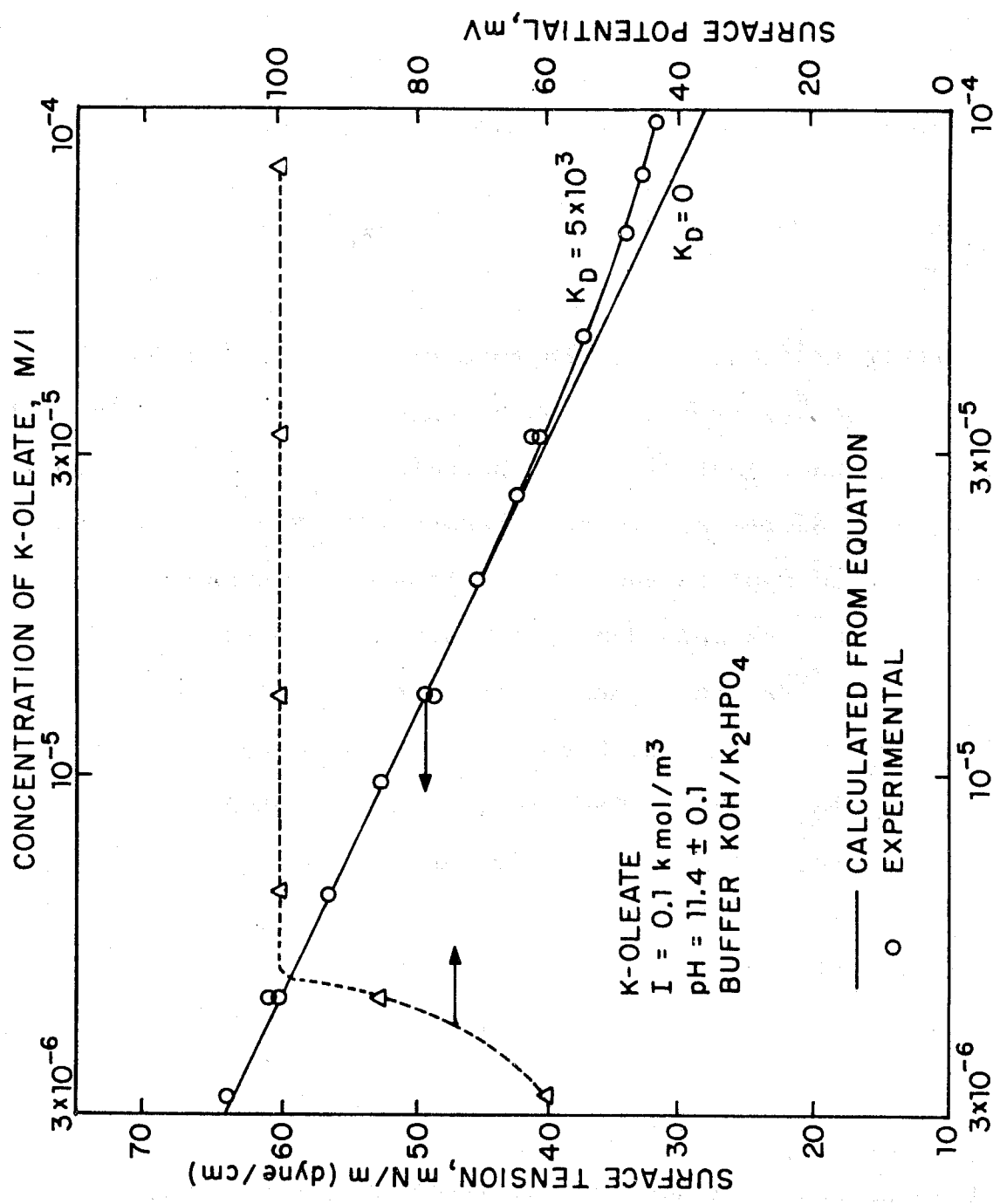


Figure II. 5. Correlation of the calculated surface tension with the experimentally obtained values as a function of oleate concentration at pH 11.4. Surface potential measured under the same conditions is also plotted. Buffer is  $\text{K}_2\text{HPO}_4/\text{KOH}$ .

interface. Therefore, the decrease in the slope of  $\gamma$  vs  $\log C_T$  curve at higher surfactant concentration is attributed to dimerization in the bulk. According to Equation 44, which governs the surface tension behavior under these conditions,

$$\frac{-\partial\gamma}{RT\partial\ln C_T} = \Gamma_{R-Tot} \left[ \frac{1}{2} + \frac{1}{2} \frac{1}{\sqrt{1 + 8K_D C_T}} \right] \quad (44)$$

At low concentrations where the term  $8K_D C_T$  is not appreciable in comparison to unity,  $\partial\gamma/\partial\ln C_T$  can be expected to remain constant. As the term  $8K_D C_T$  increases with the increase in  $C_T$ ,  $\alpha$  will decrease and  $\partial\gamma/\partial\ln C_T$  will decrease. In the present case Equation 45 can therefore be used to explain the surface tension behavior with concentration. This has been done by trial and error by using various values of  $K_D$  and the slope in the linear region of  $\gamma$  vs.  $\log C_T$  curve.  $K_D = 5 \times 10^3$  fits the curve well and quality of the fit can be seen from Figure II.5. This is in good agreement with the value  $6 \times 10^3$  estimated from our earlier measurements (1). The fact that a single  $K_D$  can explain the complete curve up to cmc indicates the absence of higher multimers in significant amounts at larger concentrations. Otherwise, a continuously increasing  $K_D$  would have been required to fit the curve up to cmc.

If the formation of dimers is not taken into consideration in this system, an apparent adsorption density would have resulted from calculations using the  $\gamma$  vs.  $\log C_T$  data curve and this is shown in Figure II.6. The curve in Figure shows a maximum in adsorption density which cannot normally

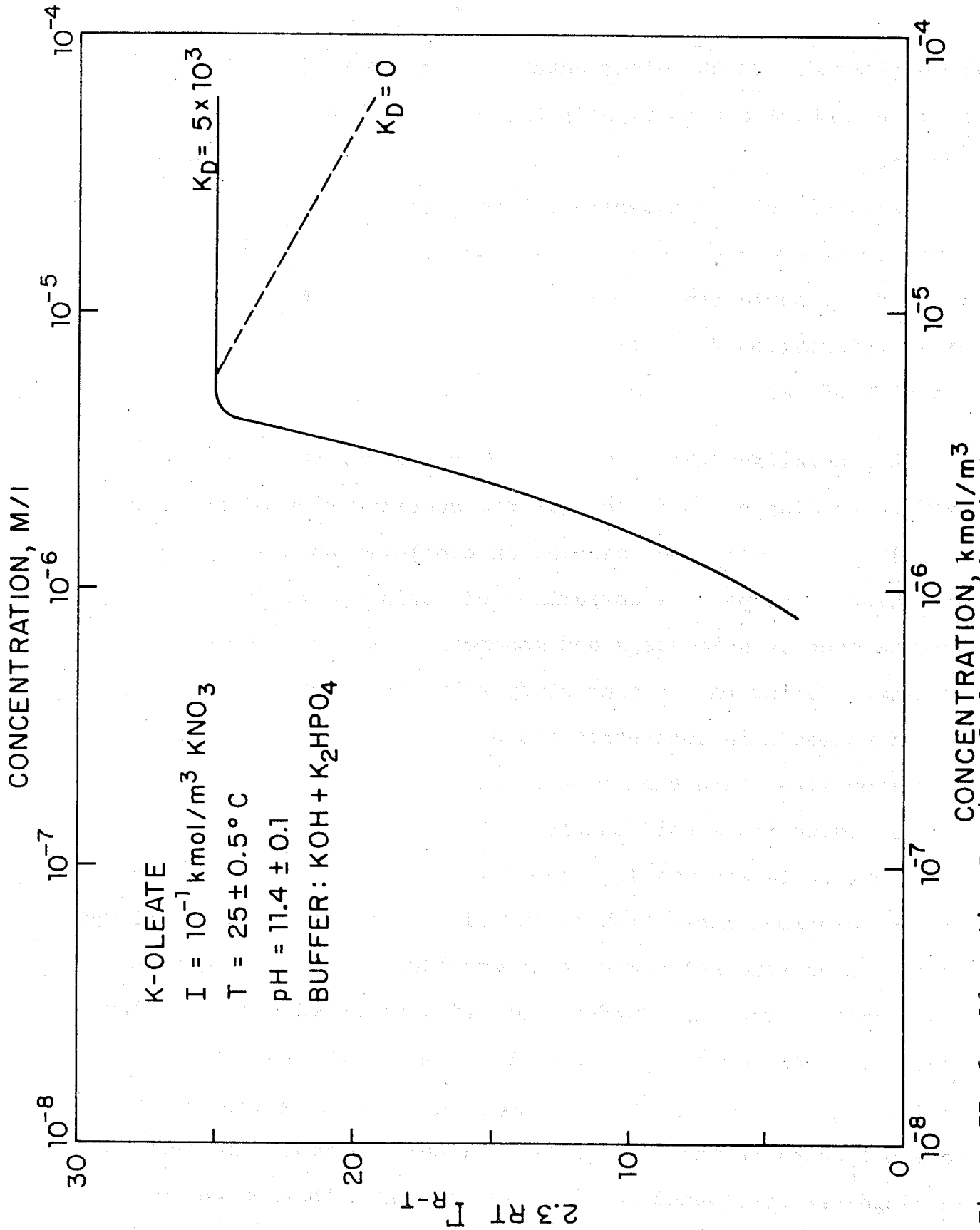


Figure II. 6. Adsorption Density of oleate at the Liquid/Air Interface as a function of its concentration showing an anomaly in the absence of premicellar aggregation.

be explained. On the other hand, the consideration of dimerization enables one to explain the anomalous behavior of the system.

Analysis of the experimental results using the thermodynamic procedure discussed earlier has proved to be fruitful for identifying surfactant complexes and for obtaining thermodynamic information for them.

#### A.6 CONCLUSIONS

A generalized thermodynamic treatment for the dependence of surface tension on pH as well as the concentration of surfactants in solutions containing association complexes such as dimers have been developed. A comparison of surface activities of species such as acid-soaps and monomers by a new technique suggested during the present study shows that certain complexes even if present in concentrations seven or eight orders of magnitude lower than that of the monomer, can affect the interfacial adsorption significantly.

Surface tension vs log concentration curves for potassium oleate solutions under high pH and high ionic strength conditions exhibited an abnormal decrease in  $\partial\gamma/\partial \log C_T$  above a certain concentration region. Surface potential measured under the same conditions however remained constant even in the region where  $\partial\gamma/\partial \log C_T$  decreased. This suggests the association of surfactant species in the bulk prior to micellization. The decrease in slope was attributed to dimerization and a thermodynamic

constant for the formation of dimers was estimated.

Surface tension measurements are being extended to other surfactants such as sulfonates and sulfates.

## B. Precipitation/Redissolution Phenomena

### B.1 INTRODUCTION

Our earlier studies on solution chemistry led to the confirmation of the precipitation/redissolution phenomenon with the increase in the concentration of the surfactant in the case of dodecylbenzenesulfonate/multivalent ion system. The role of this phenomenon in determining the nature and the shape of the isotherms of adsorption on clay is discussed in chapter I (section C.2). The investigation of the precipitation/redissolution process itself was continued during the current year with the aim of understanding the mechanism involved. Precipitation studies were extended to sulfonate systems containing different ions such as aluminum, calcium, and ammonium. Early experiments showed that the formation of precipitates and their growth were time dependent processes and hence kinetics of precipitation was also tested under selected conditions. In addition, surface tension of surfactant solutions in the presence of multivalent ions, which may possibly yield some information on the interaction of multivalent ions with the surfactant species causing precipitation and redissolution, is also being pursued at present. These aspects are discussed in the following sections.

### B.2 KINETICS OF PRECIPITATION

The rate of formation of precipitates is dependent on

experimental conditions such as the concentration of both surfactant and inorganic electrolytes added, the type of ions present and the degree of stirring. The extent of precipitation was determined by measuring turbidity using a Brinkman PC-600 probe calorimeter according to the procedure described in our earlier report (1). Figure II.7 illustrates the development of turbidity as measured by absorbance as a function of time. As indicated in this Figure,  $10^{-3}$  M/l of Texas #2 sulfonate is mixed with solutions containing various concentration of  $\text{CaCl}_2$ . It was observed that at higher concentrations of electrolyte additions development of turbidity is almost instantaneous and an equilibrium is reached in a few minutes. At lower concentrations, however, the initial rate of the turbidity development is relatively slow and an equilibrium is reached only in hours. At very low concentrations of  $\text{Ca}^{++}$  ( $< 10^{-4}$  M/l) precipitate is found to appear only after several days. Similar observations were made when the surfactant concentration was varied with the  $\text{Ca}^{++}$  concentration kept constant. The results show the difficulty in arriving at an equilibrium time interval that is suitable under all concentration conditions. For most concentrations where turbidity development was relatively fast, an equilibrium time of 30 minutes was found to be adequate. Ottewil et al. (7) have also reported similar kinetic studies for tetradecylsulfate/barium nitrate system. However, in their case it was assumed that equilibrium was reached within 90 seconds.

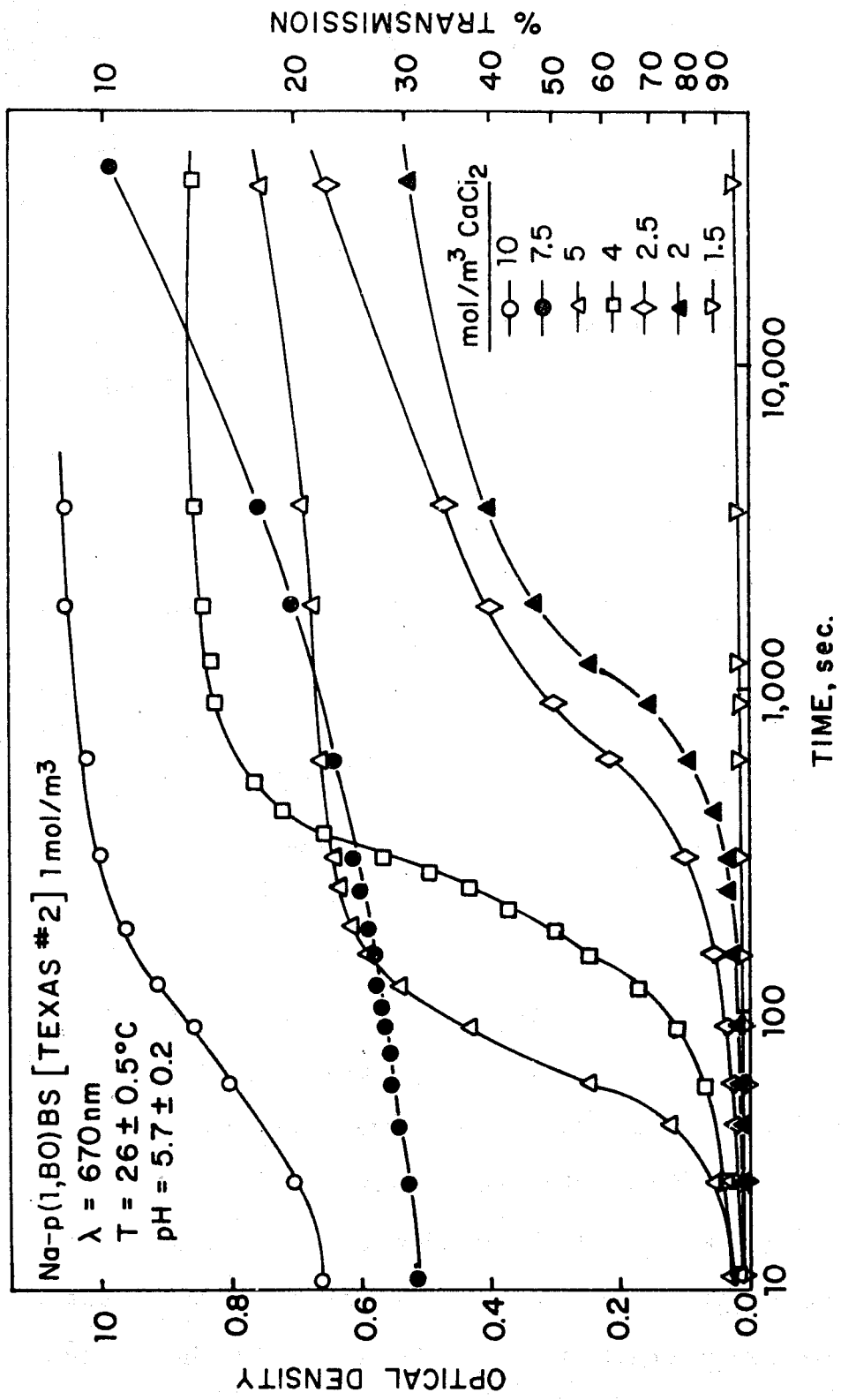


Figure II. 7. Kinetics of precipitation as measured by optical density for Texas #2 solutions in the presence of different concentrations of CaCl<sub>2</sub>.

The rate of stirring is another factor which can produce considerable effects since it can enhance the coagulation of the precipitate particulates that are already formed. In the present study the system was maintained under static conditions to eliminate such possible artifacts.

It is interesting to note from the results obtained here that it might not be possible to use the data obtained for the concentration at which the turbidity becomes appreciable for the evaluation of the solubility products of the sulfonates unless special care is taken during the initial stages of turbidity development. Because of such low turbidities the accuracy of the method is not enough.

#### Precipitation of Sulfonates with Monovalent Ions

Results obtained for the light transmission of sodium dodecylbenzenesulfonate solutions in the presence of various monovalent ions are given in Figure II.8. It can be seen that  $\text{Na}^+$  and  $\text{K}^+$  ions behave quite similarly, but interestingly,  $\text{NH}_4^+$  and  $\text{Li}^+$  salts exhibit much larger degree of salt tolerance. Similar differences were also obtained previously with  $\text{NaCl}$  and  $\text{NH}_4\text{NO}_3$  solutions to which different amounts of sodium dodecylbenzenesulfonate were added.

There are no established mechanisms yet for the presence of such differences in salt tolerances. It is however possible that the size of ions which in turn can influence their interactions with the surfactant species is a major contributing factor.

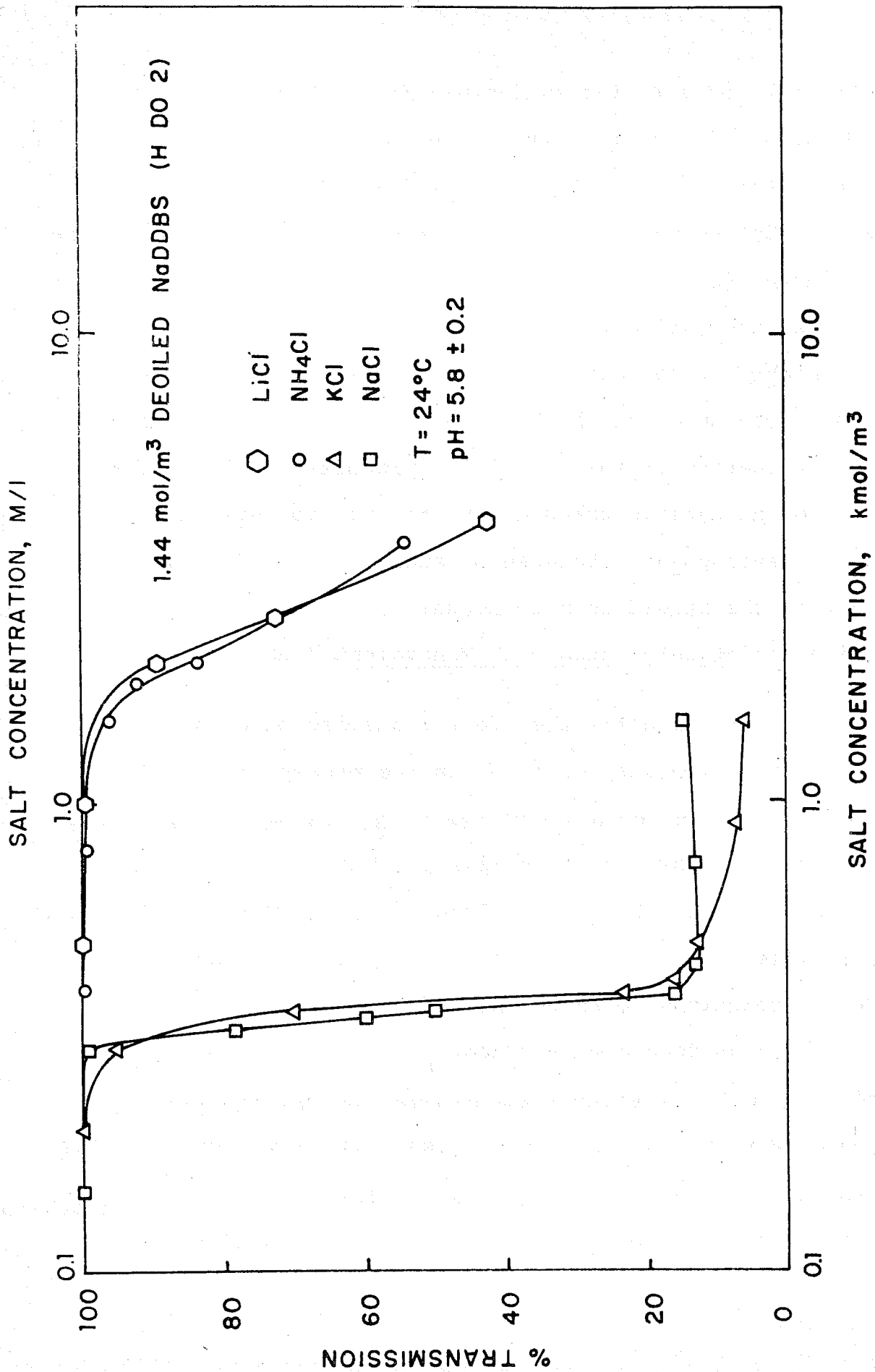


Figure II. 8. Percent light transmission as a function of added salt concentration in the presence of 1.44x10<sup>-3</sup>M deoiled sodium dodecylbenzenesulfonate.

### B.3 PRECIPITATION AND REDISSOLUTION OF SULFONATES WITH MULTIVALENT IONS

As discussed earlier, a precipitate was found to be formed upon adding increasing amount of sulfonate to salt solutions with the precipitate redissolving in the case of salt containing multivalent cations. The redissolution of the precipitate was at a concentration of sulfonate that is higher than the equivalent concentrations of the cation. In addition, the precipitate obtained in monovalent solutions did redissolve when water was added. However, addition of water did not interestingly cause immediate redissolution of the multivalent ion sulfonate precipitate.

Results obtained for the light transmission of  $7.5 \times 10^{-3}$  M/l  $\text{CaCl}_2$  solution as a function of sulfonate (Texas #2) concentration are given in Figure II.9 where precipitation/redissolution phenomenon is clearly seen. It is to be noted that the decrease in turbidity begins at about equivalent quantities of sulfonate to calcium, while complete redissolution takes place only at sulfonate concentration that is several times ( $\sim 5$ ) higher than that of the calcium.

Trivalent ions such as aluminum also undergo precipitation/redissolution phenomenon as illustrated in Figure II.10. Although the concentration required for precipitation in this case was much lower than that was required for  $\text{Ca}^{++}$  ions, the complete redissolution occurred only at much higher sulfonate

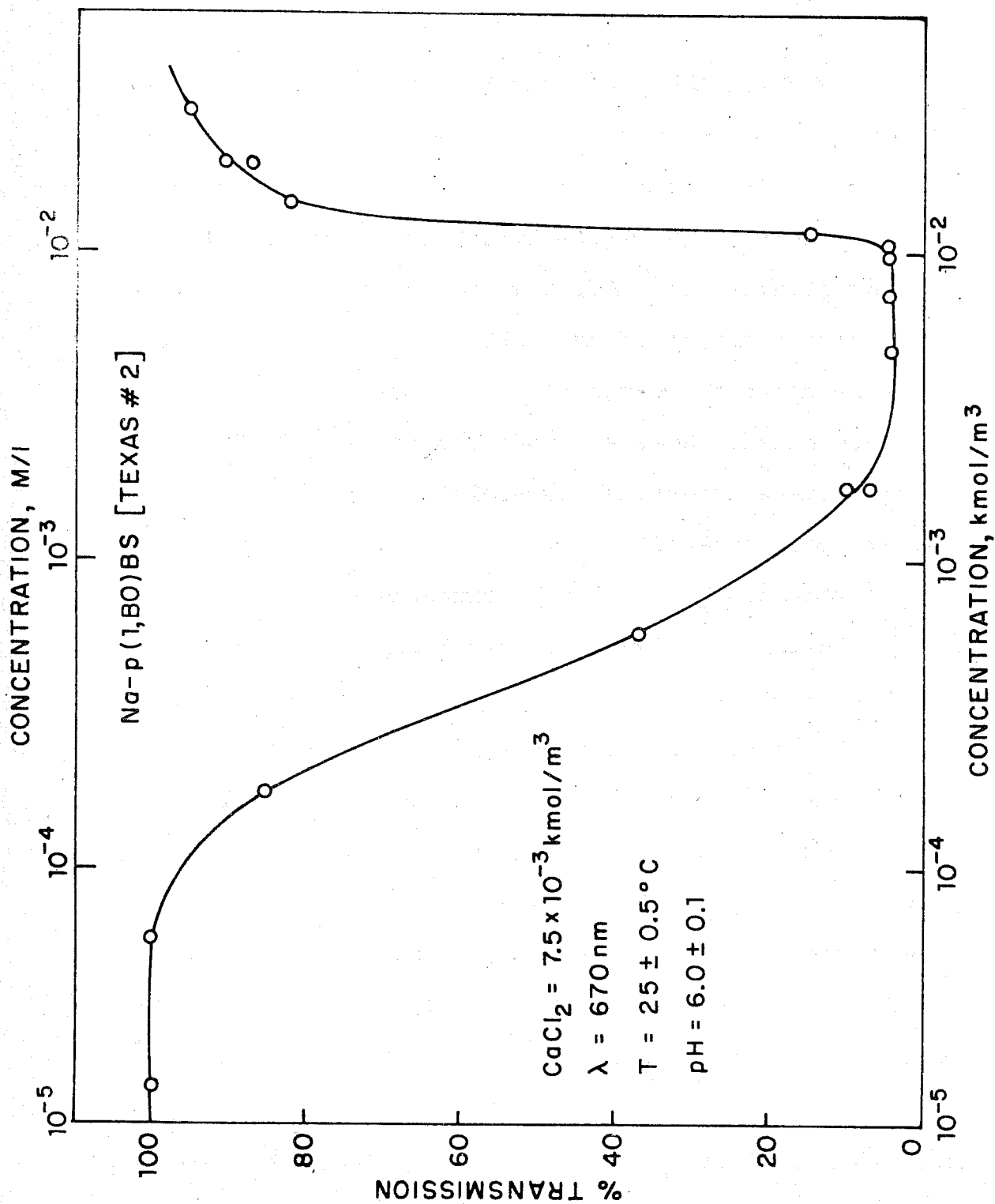


Figure II. 9. Percent Transmission of Texas#2 sulfonate solutions as a function of its concentration in the presence of  $7.5 \times 10^{-3} \text{ M/l CaCl}_2$ .

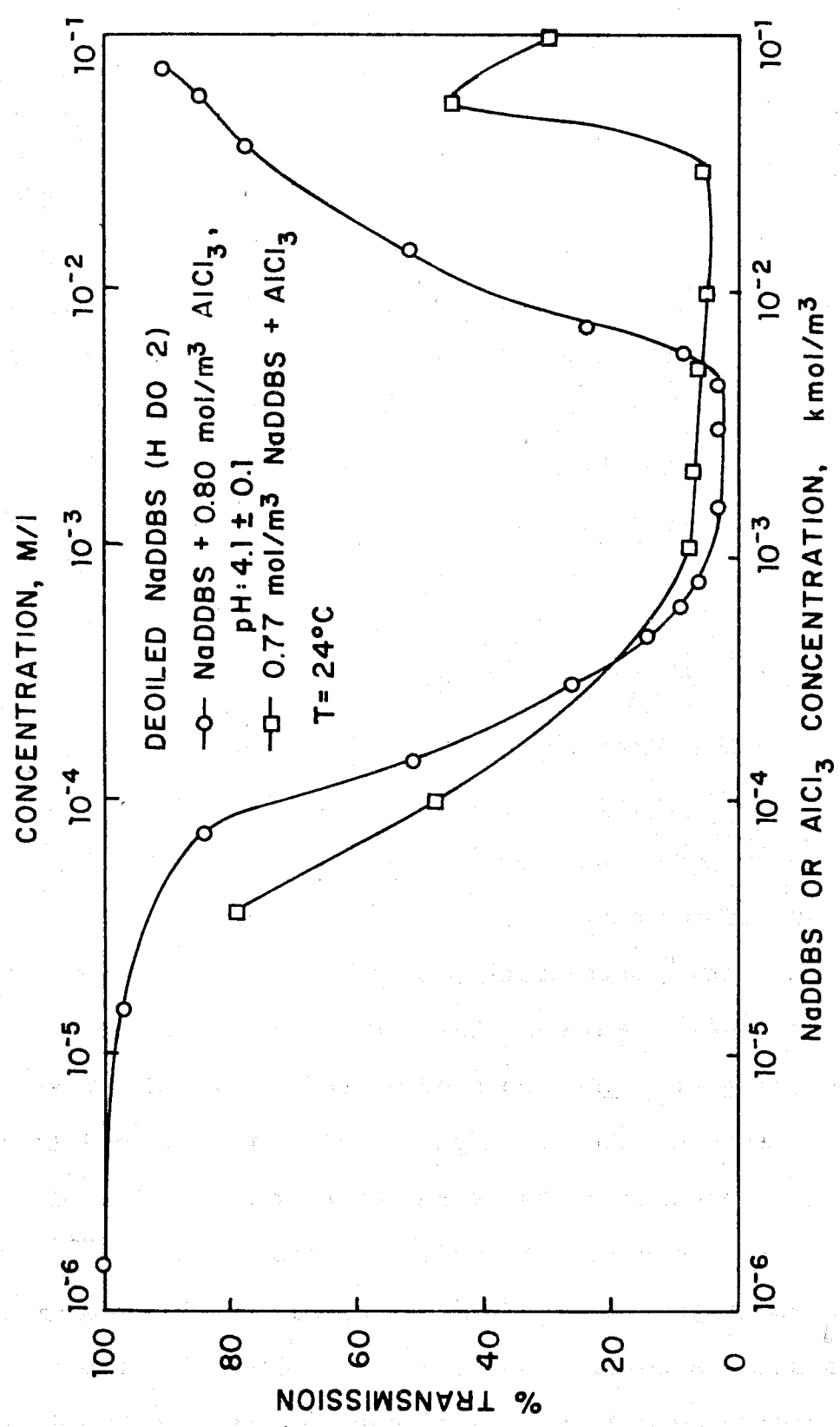


Figure II. 10. Percent light transmission as a function of added dodecylbenzene-sulfonate and AlCl<sub>3</sub> concentrations.

concentrations. This is probably a result of the specific associative interactions between the sulfonate and counter ions. Since the formation of dimers is more probable than trimers or multimers of sulfonate, the complete neutralization of  $Al^{+++}$  ions requires larger concentrations of sulfonate. The complete redissolution of aluminum sulfonate takes place only at a sulfonate to aluminum ratio of about 100.

The solubility product of the salts of the sulfonate was calculated with the help of the turbidity versus log concentration plots and the expression relating solubility product,  $K_s$ , to concentrations of ions:

$$K_s = [C_{M^{m+}}] [C_{S^{-}}]^n$$

where  $C_{M^{m+}}$  and  $C_{S^{-}}$  represent the salt cation and sulfonate

respectively. Using the data for the concentrations that correspond to the initial increase in turbidity, the solubility product was calculated to be  $2 \times 10^{-11}$  M for calcium and  $4 \times 10^{-19}$  M for aluminum sulfonates.

Increase of the concentration of  $AlCl_3$  to a sulfonate solution on the other hand was observed to cause partial redissolution only at higher concentrations. This decrease in turbidity which resulted in apparent partial redissolution is essentially dependent on the kinetics of coagulation of precipitates. Introduction of sufficient amounts of  $Al^{+++}$  ions can be expected to produce a charge reversal of the precipitate particulates above a certain concentration where the formation of positive sol occurs; this in turn can indeed cause redispersion

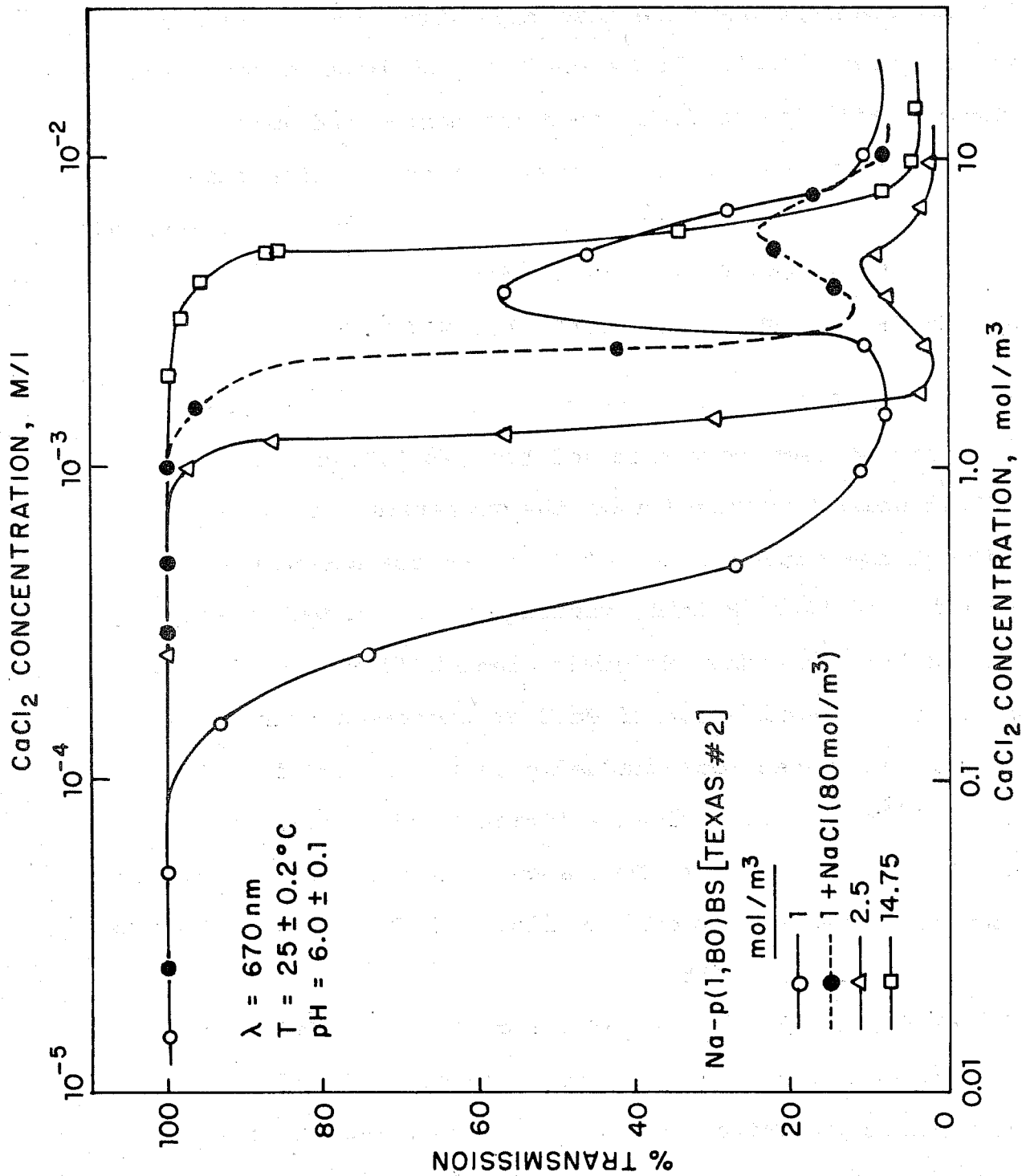


Figure II. 11. Percent light transmission as a function of added CaCl<sub>2</sub> concentrations of Texas #2 sulfonate.

of the precipitate and decrease the turbidity of the solution.

Similar observations were also made with calcium ions as shown in Figure II.11. It is seen that at lower concentrations of sulfonate, addition of  $\text{CaCl}_2$  produces maxima and minima in the turbidity versus log calcium salt concentration curves. Interestingly these effects disappear at higher concentrations of sodium dodecylbenzenesulfonate (14.35 mM).

#### B.4 ADDITION OF MONO AND MULTIVALENT SALT MIXTURES

The effect of NaCl additions on calcium sulfonate precipitates that have already been formed in solution is illustrated in Figure II.12 where transmission of the suspension is plotted as a function of the concentration of NaCl. In the absence of NaCl, addition of  $5 \times 10^{-3} \text{ M}$   $\text{CaCl}_2$  results in significant precipitation of  $10^{-3} \text{ M}$  and  $5 \times 10^{-3} \text{ M}$  sodium dodecylbenzenesulfonate solutions. However, as the concentration of NaCl is increased, turbidity of the resultant suspensions gradually decreases and finally at about  $5 \times 10^{-2} \text{ M}$  of NaCl a clear solution is obtained. Increasing the concentration of NaCl above  $0.3 \text{ M}$  apparently causes the system to exceed the solubility limit of the sodium sulfonate and hence to precipitate out.

An explanation for this interesting effect of NaCl salts can become evident when examining the possible role of micellization/solubilization phenomena in the present system under investigation here. For complete redissolution of calcium sulfonate precipitates, it has been found earlier that at least

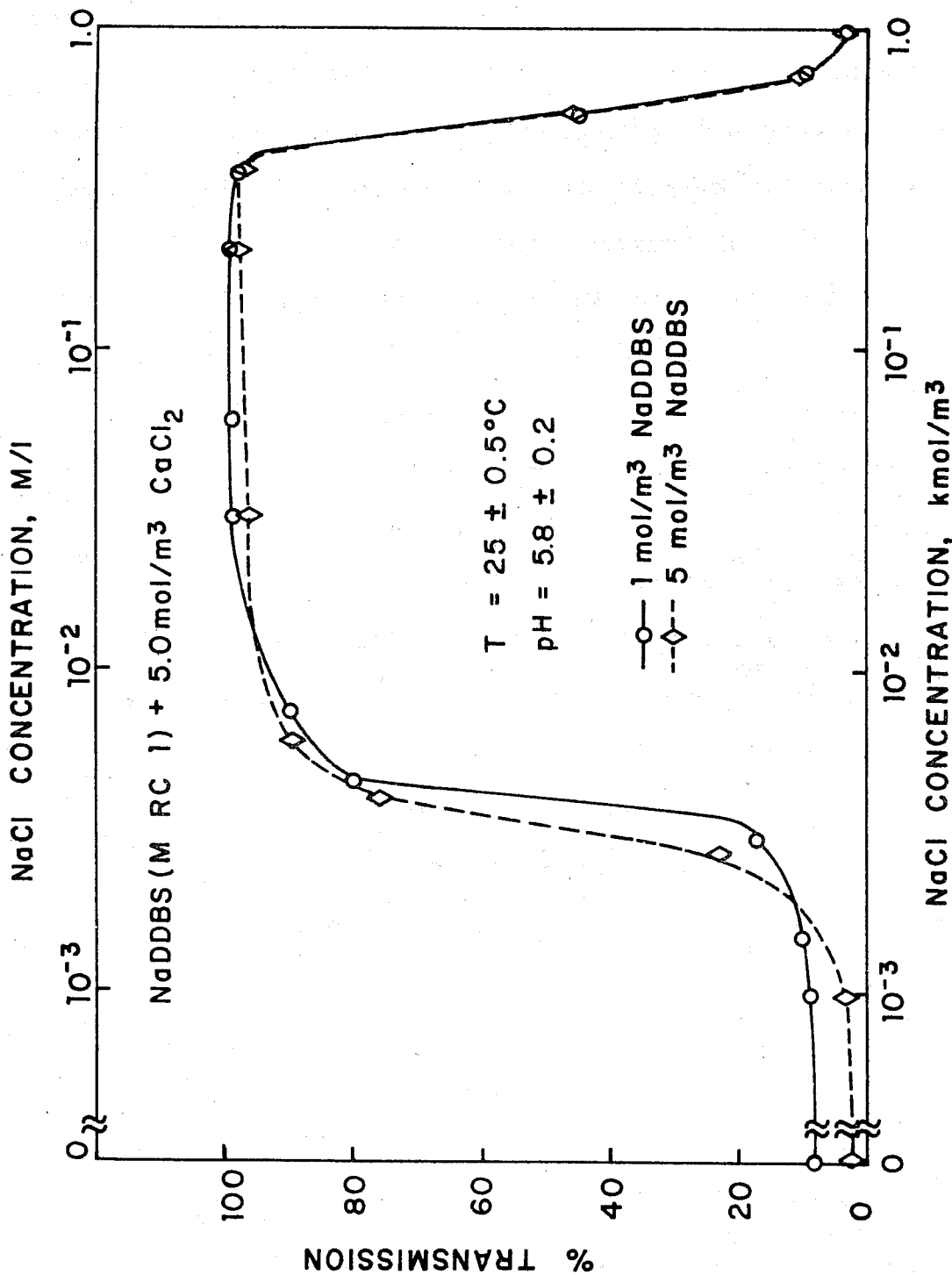


Figure II. 12. Percent light transmission as a function of added concentration of NaCl for two concentrations of sodium dodecylbenzenesulfonate in the presence of 5x10<sup>-3</sup>M CaCl<sub>2</sub>.

five times of sulfonate to calcium ratio is required. Since the solution considered here contains only  $10^{-3}$  M of sulfonate, it is evidently unable to cause redissolution of the precipitates. If the redissolution mechanism is due to the formation of micelles and subsequent solubilization of precipitates in them, addition of NaCl can however be expected to lower the cmc of sulfonate and in turn enhance the formation of micelles. Then such enhanced micellization due to the addition of NaCl can be expected to cause redissolution by solubilization.

The implication of these phenomena of precipitation and redissolution to adsorption is important since NaCl is generally added as brine solution to adsorption systems. Release of multivalent ions such as  $\text{Ca}^{++}$ ,  $\text{Mg}^{++}$  or  $\text{Al}^{+++}$  in the presence of NaCl can produce precipitation and redissolution regions and thereby generate apparent adsorption ~~maxima~~ or minima in adsorption isotherms. Furthermore, precipitation of sulfonates can conceivably lead to plugging of pores or reservoirs with serious consequences. The potential role of redissolution in such cases appears to deserve careful examination.

## C. Mechanisms of Precipitation/Redissolution

### Phenomena: Surface Tension Studies

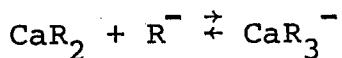
#### C.1 INTRODUCTION

The redissolution of the surfactant/multivalent ion precipitates at high surfactant concentrations can be caused by a number of possible reasons such as (1,8):

a) Solubilization of the precipitates in surfactant micelles which are formed in solution at some concentration above the equivalent surfactant concentration for the complete precipitation of multivalent ions.

b) Recharging and the consequent redispersion of the almost neutral, coagulated micelles, the recharging being due to the adsorption (or solubilization) of the charged monomers on the micelle.

c) Formation of charged complexes between the precipitate and the surfactant monomer - eg.



It is possible that more than one mechanism may govern the redissolution process. A characteristic property that may yield important information on the mechanisms of redissolution process is the surface tension of surfactant solutions in the presence of various multivalent ions. For example, if mechanism (a) governs the process, the surface tension vs log (concentration)

curve can be expected to exhibit 4 regions - initial decrease in  $\gamma$  followed by a region of constant  $\gamma$  corresponding to the precipitation region, a third region where  $\frac{\partial \gamma}{\partial \log C_T}$  will be same as or higher than that of region 1 and finally an almost constant  $\gamma$  region corresponding to micellization. Precipitation region followed by a decrease in  $\gamma$  where  $\frac{\partial \gamma}{\partial \log C_T}$  is lower than that of region 1 may suggest mechanism (c). Since (b) involves micellization before precipitation, no significant decrease in  $\gamma$  can be expected in the redissolution region. It appears that surface tension results can be useful in investigating the mechanisms of redissolution process. In addition, these studies can also yield information on the energy of interaction of multivalent ions with the charged surfactant interfaces. Since micellar/solution interface is similar to the liquid/air interface (but for the differences in curvature), such results may be useful in revealing the specific nature of counter ion adsorption at the micellar surface. A mathematical approach described below suggests how surface tension results can be exploited to study the counter ion adsorption at charged interfaces.

## C.2 THEORY

Consider the surfactant RM in solution in the presence of (a) a uni-univalent inorganic electrolyte MX and (b) a bi-univalent inorganic electrolyte  $BX_2$ . Let RM be a highly ionizable surfactant such as sulfonate or sulfate. Aqueous species included in the following treatment are:  $R^-$ ,  $M^+$ ,  $X^-$ ,  $B^{2+}$ ,  $H^+$ ,  $OH^-$  and  $H_2O$ . Species such as  $RH$  and  $R_2H^-$  are expected to influence

the surfactant behavior in the near micellar region only at pH values below about 3 (9). Premicellar aggregates such as dimers ( $R_2^{2-}$ ) have not been included in the model at present. If necessary, they can be incorporated in the treatment as and when more thermodynamic information about them becomes available.

Gibbs equation for the adsorption of various species at the interface (see equation 19) can be applied to this system with the standard convention that  $\Gamma_{H_2O} = 0$ . Using a similar procedure outlined in section A for the uni-univalent electrolyte/surfactant system (a) and the bi-univalent electrolyte/surfactant system (b) separately, the relevant equations relating the surface excess to surface tension and chemical potential of different species can be obtained. Since the specific adsorption of  $H^+$  and  $OH^-$  are not to be expected in the case of a highly ionizable surfactant and since the concentrations of  $H^+$  and  $OH^-$  are relatively low compared to  $M^+$  and  $X^-$  ions, the terms involving  $\Gamma_{H^+}$  and  $\Gamma_{OH^-}$  can be neglected. By incorporating the conditions from bulk chemical equilibria as well as the electrical neutrality at the interface, the mathematics of the system can be further simplified. The resulting expressions are:

For system (a)

$$\begin{aligned}
 - \frac{\partial \gamma}{RT} = & \left[ \Gamma_{R^-} - \Gamma_{X^-} \cdot \frac{C_{R^-}}{C_{X^-}} \right] \partial \ln C_{R^-} \\
 & + \left[ \Gamma_{M^+} + \Gamma_{X^-} \cdot \frac{C_{M^+}}{C_{X^-}} \right] \partial \ln C_{X^-} \\
 & + 2\Gamma_{M^+} \partial \ln f_1
 \end{aligned} \tag{62}$$

and for system (b)

$$\begin{aligned}
 - \frac{\partial \gamma}{RT} = & \left[ \Gamma_{R^-} + \Gamma_{M^+} \right] \partial \ln C_{R^-} \\
 & + \left[ \Gamma_{B^{2+}} + \Gamma_{X^-} \right] \partial \ln C_{B^{2+}} \\
 & + \left[ \Gamma_{M^+} + \Gamma_{B^{2+}} \right] 2 \partial \ln f_1 \\
 & + \left[ \Gamma_{B^{2+}} \partial \ln f_2 \right]
 \end{aligned} \tag{63}$$

where  $f_1$  and  $f_2$  are the activity coefficients for singly charged and doubly charged ions respectively. Systems (a) and (b) are analyzed separately in the following sections.

System (a) Uni-univalent electrolyte and surfactant. Equation 62 under constant  $C_{R^-}$  conditions can be reduced to:

$$- \frac{\partial \gamma}{RT \partial \ln C_{M^+}} = \Gamma_{M^+} + \left[ 1 + 2 \frac{\partial \ln f_1}{\partial \ln C_{M^+}} \right] \frac{\Gamma_{X^-} \cdot C_{M^+}}{C_{X^-}} \tag{64}$$

Since the monolayer potential is expected to be negative,  $\Gamma_{X^-}$  can be assumed to be negligible and hence  $\Gamma_{M^+}$  can be evaluated from the experimental data for  $\gamma$  vs  $C_{M^+}$  using equation 69. The above assumption can be checked by measuring  $\Gamma_{X^-}$  independently using labelled electrolytes.

Under constant  $C_{M^+}$  conditions,

$$- \frac{\partial \gamma}{RT \partial \ln C_{R^-}} = \Gamma_{R^-} - \Gamma_{X^-} \cdot \frac{C_{R^-}}{C_{X^-}} \tag{65}$$

Since  $\partial \ln f = 0$  when  $C_{M^+}$  is constant and approximately two orders of magnitude higher than  $C_{R^-}$ . Since  $C_{R^-}/C_{X^-}$  also would be small under these conditions, the 2nd term on the right hand side can be neglected. Therefore,

$$- \frac{\partial \gamma}{RT \partial \ln C_{R^-}} = \Gamma_{R^-} \tag{66}$$

Thus, surface tension results under appropriate conditions can yield both  $\Gamma_{R^-}$  and  $\Gamma_{M^+}$ .

System (b) Bi-univalent electrolyte and surfactant.

Equation which is applicable for this system can be written under constant  $C_{R^-}$  conditions as:

$$\frac{-\partial\gamma}{RT \partial \ln C_{B^{2+}}} = \Gamma_{B^{2+}} \left[ 1 + \frac{2 \partial \ln f_1}{\partial \ln C_{B^{2+}}} + \frac{\partial \ln f_2}{\partial \ln C_{B^{2+}}} \right] + \Gamma_{X^-} + 2\Gamma_{M^+} \frac{\partial \ln f_1}{\partial \ln C_{B^{2+}}} \quad (67)$$

For the case where  $BX_2$  concentration is relatively large compared to  $RM$ ,  $\Gamma_{M^+}$  can be considered to be negligible in comparison to that of  $\Gamma_{B^{2+}}$ .  $\Gamma_{X^-}$  is also expected to be small, but if necessary can be estimated. Thus, surface tension data can yield information on the adsorption of  $B^{2+}$  ions at the interface.

If  $C_{BX_2}$  is constant,

$$\partial \ln C_{B^{2+}} = 0 \text{ and} \quad (68)$$

$$\partial \ln C_{X^-} = 0 \quad (69)$$

If the concentration of  $BX_2$  is high enough to control the ionic strength of the system,  $\partial \ln f_1 = 0$  and  $\partial \ln f_2 = 0$ . Thus, equation 72 can be reduced to the form,

$$\frac{-\partial\gamma}{RT \partial \ln C_{R^-}} = \Gamma_{R^-} + \Gamma_{M^+} \quad (70)$$

Thus the surface tension measurements under appropriate conditions can yield the adsorption of different species at the interface. This valuable information from the surface tension data can be further analyzed using ap-

appropriate models for the adsorption of counter ions at charged interfaces. In the present treatment, as a first approach the Stern model for adsorption has been used as discussed below.

Assuming that the penetration of counter ions into the charged monolayer is negligible,

$$\sigma_0 = \Gamma_{R^-} \cdot e \quad (71)$$

where  $\sigma_0$  is the charge density of the monolayer and  $e$  is the fundamental unit of charge. If  $\sigma_1$  and  $\sigma_2$  are the charge densities at the stern layer and the diffused double layer,

$$\sigma_0 = \sigma_1 + \sigma_2 \quad (72)$$

$$= 2\Gamma_{B^{2+}} + \Gamma_{M^+} \quad (73)$$

Also using the following relations from Davies and Ridel (3),

$$\sigma_0 = \frac{D'}{4\pi\delta} [\psi_0 - \psi_\delta] \quad (74)$$

and

$$\psi_\delta = \frac{2kT}{e} \sinh^{-1} \left[ \frac{\sigma_2}{C_i^{1/2}} \left( \frac{500\pi}{DRT} \right)^{1/2} \right] \quad (75)$$

where  $D'$  is the dielectric constant in the fixed part of the double layer (stern layer),  $D$  is the bulk dielectric constant,  $\delta$  is the thickness of the stern layer,  $R$  is the gas constant and  $T$  is the absolute temperature.

The variables from the above equations are:  $\Gamma_{R^-}$ ,  $\Gamma_{M^+}$ ,  $\Gamma_{B^{2+}}$ ,  $\sigma_0$ ,  $\sigma_1$ ,  $\sigma_2$ ,  $\psi_0$  and  $\psi_\delta$ . The thickness of the stern layer  $\delta$  can be estimated from the considerations of the size of the ions. Equations 67 and 70 to 75 provide only seven relations among the eight variables mentioned above and hence one more

equation is necessary to obtain the solution. Measurements of surface potential cannot solve this problem as it would introduce the dipole moments of the adsorbed species as new variables.

If the assumptions that bivalent ions are strongly adsorbed in the stern layer and that monovalent ions are present in the double layer (which are reasonable) are made, then,

$$\sigma_1 = 2\Gamma_B^{2+} e \quad (76)$$

and,  $\sigma_2 = \Gamma_M^+ e \quad (77)$

This system can now be solved satisfactorily to obtain the various parameters involved. In addition, the specific adsorption energy of multivalent ions can be obtained using the equation for adsorption in the stern layer (3):

$$\Gamma_B^{2+} = \Gamma_R^- \left[ 1 + \frac{1000}{\bar{M} C_B^{2+}} \text{Exp} \left( \frac{2 \cdot e \cdot \psi_\delta - w}{kT} \right) \right]^{-1} \quad (78)$$

where  $\bar{M}$  is the molecular weight of the solvent and  $w$  the specific interaction energy of the multivalent ion.

The discussion above clearly shows that surface tension data can be interpreted to yield useful information on the interaction of multivalent ions with the charged interfaces. Since the micellar solution interface is charged, interaction of multivalent ions with the micellar surface can be similar to that with the liquid/air or oil/water interfaces provided, the effect of shape of the micelle can be accounted for. It is important to note that such an approach can help in providing one with the mechanism involved in the interaction of micelles and multivalent ions, leading to precipitation/redissolution phenomenon.

### C.3 EXPERIMENTAL

Investigation of the surface tension behavior of dodecylbenzenesulfonate solutions in the presence of multivalent ions is in progress at present. Wilhelmy plate technique is employed for surface tension measurements. Under the precipitation conditions, the surface tension measurements are conducted with the supernatant solution obtained after the settling or the centrifugation of the precipitates.

### C.4 RESULTS AND DISCUSSION

The data obtained for the dependence of surface tension on the total concentration of dodecylbenzenesulfonate solutions in the presence of  $10^{-3}$  M calcium chloride are plotted in Figure II.13. The surface tension curve, in addition to a minimum in the region of precipitation, exhibits several regions with distinctively different slopes. In region 1, as shown in Figure II.13,  $\gamma$  decreases and  $\partial \gamma / \partial \log C_T$  increases with increases in the sulfonate concentration.

In region 2, the surface tension continues to decrease, but  $\partial \gamma / \partial \log C_T$  is also found to decrease upon increasing the concentration. This behavior continues even into the precipitation region till the added sulfonate concentration attains the value that is equivalent to calcium present in solution for complete precipitation. Further increase in sulfonate concen-

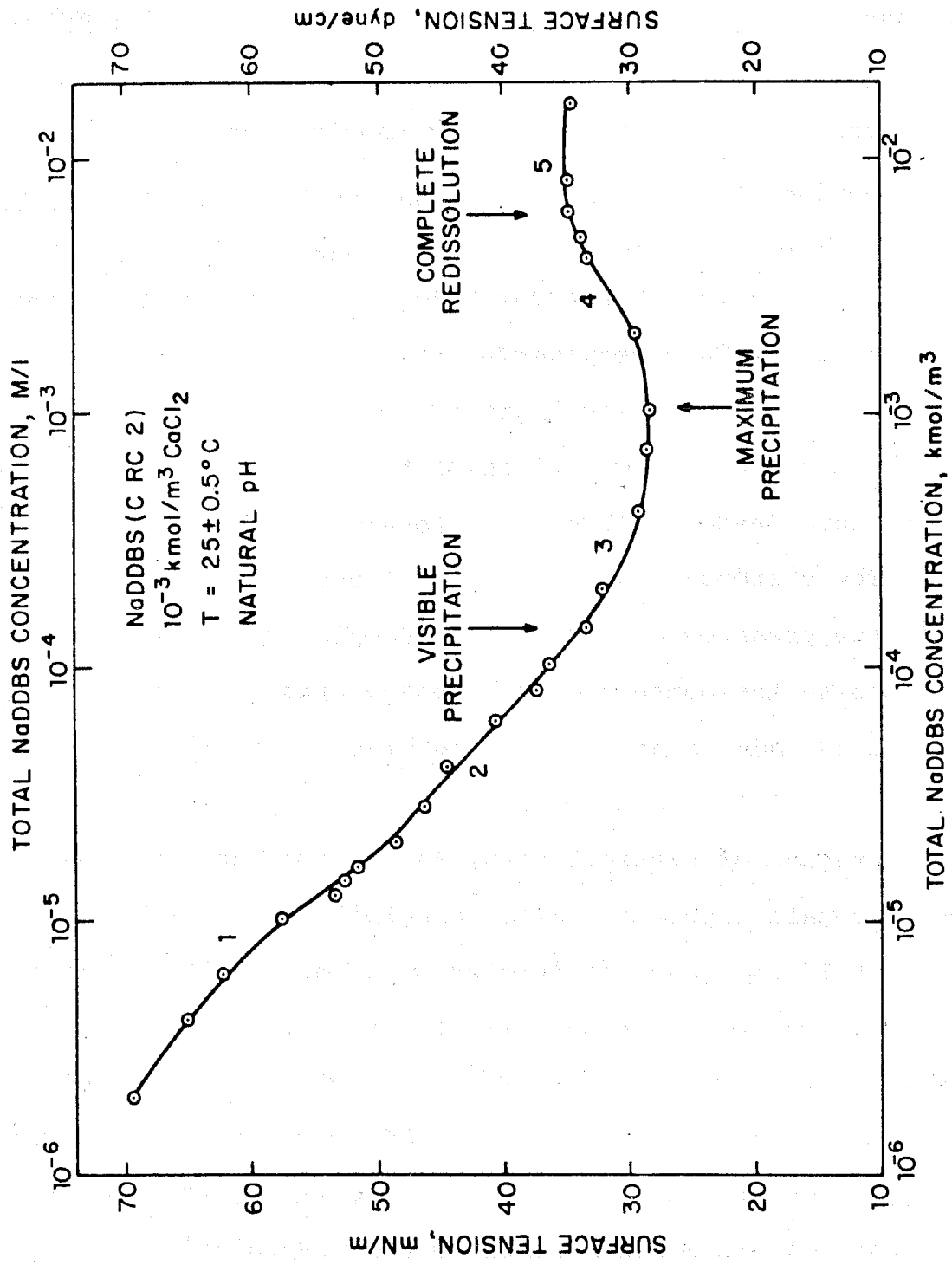


Figure II. 13. Surface tension as a function of the total concentration of NaDDBS in the presence of  $10^{-3}$  M CaCl<sub>2</sub>.

tration results in an increase in surface tension, till complete redissolution of the precipitate is achieved. At still higher concentrations in the tested region,  $\gamma$  remains constant.

It is evident from Figure II.13 that in  $10^{-3} \text{M}$   $\text{Ca}(\text{Cl}_2)_2$  solutions, a distinct micellization region does not occur prior to the precipitation of Ca-dodecylbenzenesulfonate. This suggests that the kraft point for Ca-dodecylbenzenesulfonate is above  $25^\circ\text{C}$ .

The decrease in  $\partial \gamma / \partial \log C_T$  in region 2 can be due to the increased association of sulfonate species in the bulk, possibly to form Ca-dodecylbenzenesulfonate species in solution. The thermodynamic treatment of surface tension in the presence of association complex as discussed earlier supports the contention that the decrease in  $\partial \gamma / \partial \log C_T$  could be due to such association of surfactant species in the bulk.

In the region of precipitation, the monomer activity is expected to remain constant. Also, precipitation is expected to continue till the level of calcium is brought below a value that is determined by the solubility product of Ca-dodecylbenzenesulfonate. Further addition of sulfonate will indeed cause an increase in the activity of sulfonate species in solution and will also lead to the formation of micelles in the system. In such an event, micelles can solubilize the precipitates of Ca-dodecylbenzenesulfonate and result in their redissolution. Increase in monomer activity, however, should be expected to decrease the surface tension further which is contrary to the

- 117 -

actual observation. This anomaly could be explained if the role of Ca-sulfonate in this system can be considered to be analogous to that of a surface active impurity in a normal surfactant system. The impurity gets adsorbed at the L/A interface prior to micellization and gets solubilized in the micelle at higher concentration. Such a phenomenon can mask any possible decrease in surface tension due to the increase in monomer activity. Thus, the surface tension behavior of Na-DDBS in the presence of  $10^{-3}$  M calcium chloride seems to support the mechanism of redissolution by a solubilization process with micelles.

Unlike in the presence of calcium chloride, the surface tension vs  $\log C_T$  curve (see Figure II.14) in the presence of  $5 \times 10^{-4}$  M  $Al(NO_3)_3$  exhibits an apparent micellization region. The following interesting features of this curve should be noted:

1. The value of apparent CMC under these conditions is approximately two orders of magnitude lower than that for pure Na-dodecylbenzenesulfonate.
2. The surface tension in the above region here is about 50 dynes/cm which is almost 15 dynes/cm higher than the corresponding value for pure NaDDBS.
3. A significant decrease of about 20 dynes/cm is observed in the initial part of the visible precipitation region. Surface tension however remained constant from  $2 \times 10^{-4}$  M to  $2 \times 10^{-3}$  M sulfonate where precipitates continued to remain stable. In the redissolution region an increase in surface tension of about 3 dynes/cm is observed.

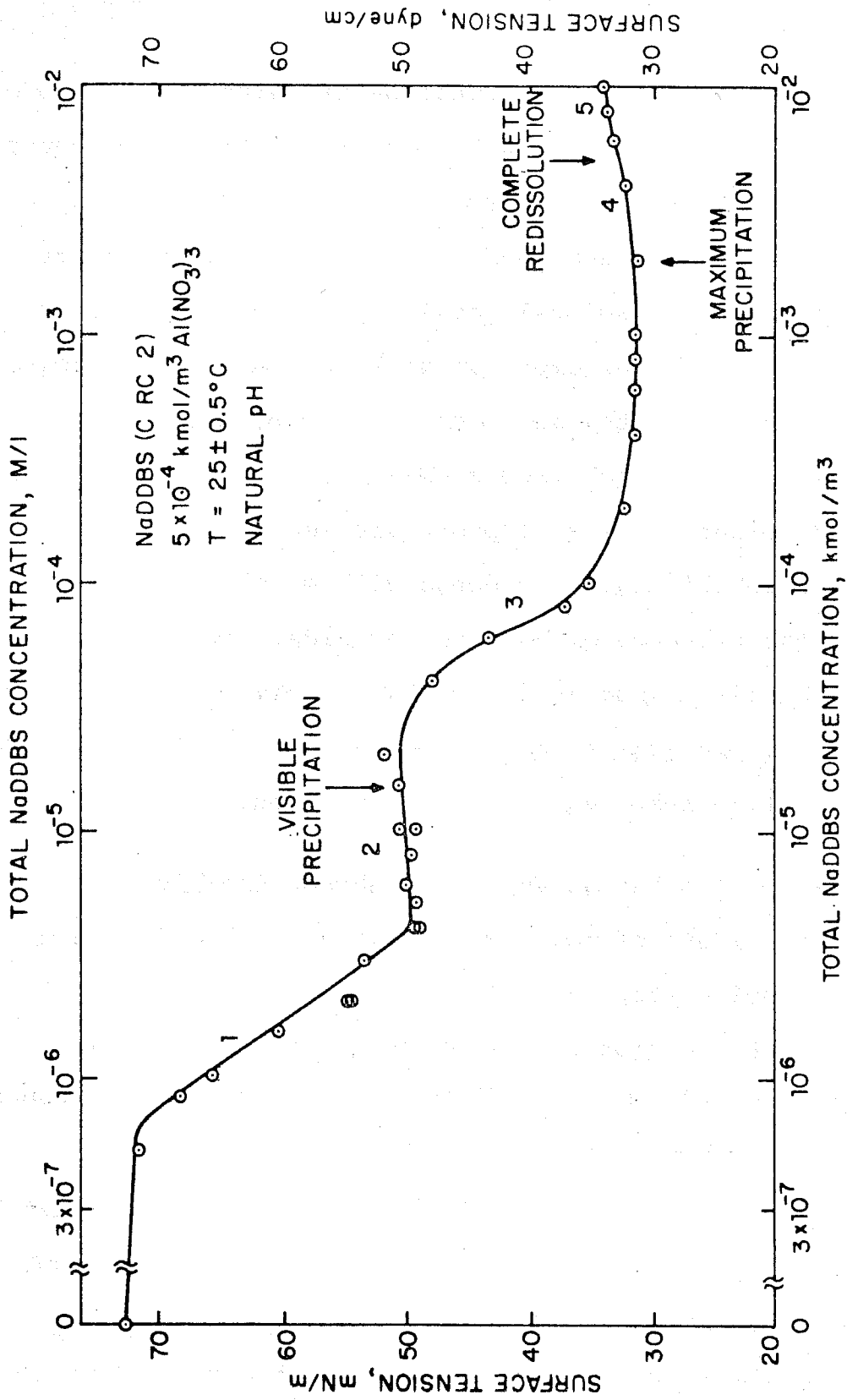


Figure II. 14. Surface tension as a function of the total concentration of NaDDBS in the presence of  $5 \times 10^{-4}$  M Al(NO<sub>3</sub>)<sub>3</sub>.

It was found that the rates of surface tension decay in regions 1 and 2 (Figure II.14) were low when compared to those in regions of higher sulfonate concentrations. In regions 1 and 2, as much as one hour was needed for equilibrium to be attained where as about ten to twenty minutes were sufficient in the other regions.

Surface tension measurements were conducted under natural pH conditions. The pH of different test solutions varied in the range of 3.8 to 5.1 in a random manner. It is recognized that such a change in pH can influence the nature and form of aluminum species in solution and hence can affect their interactions with the sulfonate. It might be noted that Surface tension of dodecyl-sulfate, has also been reported in the past to be influenced by pH below 4 (9). Experiments are in progress at present under constant pH conditions in order to isolate the effects of pH changes from the real interaction effects.

The results for the surface tension behavior of sulfonate solutions in the presence of aluminum species indeed exhibit an interesting behavior and are expected to yield valuable information on the precipitation/redissolution phenomenon. Any mechanistic interpretation of these results will have to await the results from further experimentation under controlled conditions.

## C.5 CONCLUSIONS

Kinetics of precipitation was studied as a function of electrolyte concentration. It was found that the equilibration time was markedly dependent on the experimental conditions such as degree of stirring.

Monovalent cations such as  $\text{Na}^+$  caused the precipitation of sulfonates upon increasing the sulfonate concentration. Sulfonate exhibited lesser tolerance to  $\text{Na}^+$  and  $\text{K}^+$  ions when compared to  $\text{NH}_4^+$  and  $\text{Li}^+$  ions. Multivalent ions such as  $\text{Ca}^{++}$ ,  $\text{Al}^{+++}$ , on the other hand, precipitated and then redissolved upon a further increase in sulfonate concentration. It appears that the concentration at which complete redissolution occurs is a function of the valency of the multivalent ion. The solubility products of the salts of sulfonate were determined from the turbidity measurements; calcium and aluminum sulfonates have the solubility products of  $2 \times 10^{-11} \text{M}$  and  $4 \times 10^{-19} \text{M}$  respectively. In the case of mono and multivalent ion mixtures, an interesting observation was made when  $\text{NaCl}$  was added to an already formed calcium sulfonate precipitate. Addition of  $\text{NaCl}$  caused the redissolution of the calcium sulfonate precipitates. Addition of  $\text{Na}^+$  ions is believed to lower the cmc of sulfonate and lead to the formation of micelles in which the calcium precipitates can get solubilized.

Possible mechanisms suggested for the redissolution pheno-

menon are: solubilization of precipitates in micelles, redissolution by complexation and redispersion of the already coagulated micelles due to the development of charge resulting from the adsorption of sulfonate on the precipitates. Surface tension results obtained in the presence of calcium ions support the mechanism of solubilization in micelles, whereas results obtained in the presence of aluminum salt seem to exhibit precipitation/redissolution after the micellization process. Further investigation along similar lines is expected to yield more information towards the understanding of the precipitation/redissolution process.

## D. Surfactant-Polymer Interactions

### D.1 INTRODUCTION

In micellar flooding, surfactant-polymer interactions can lead to precipitation of surfactant or polymer and phase separations. If the interfacial tension between the sulfonate containing phases is sufficient then additional loss of the surfactant could occur due to phase trapping in the porous matrix. Furthermore surfactant-polymer interactions can modify the adsorption behavior of both the polymer and surfactant on the reservoir rock and also produce changes in the interfacial rheological behavior in such a way so as to become a significant factor in determining the recovery of surfactant trapped in the rock (10). Earlier results (11) had shown that while increased additions of the surfactant can result in general only in a nominal decrease in the adsorption of the polymer on kaolinite, the addition of polymer can produce a marked decrease on the adsorption of surfactant itself. Adsorption of sulfonate in the presence of polymer was in fact negligible under the only condition that was studied for exploratory purposes at that time. The results had at least shown that it is important to investigate the modifications in the bulk and interfacial properties due to surfactant-polymer interactions that might lead to minimum surfactant losses.

### D.2 RELATIVE VISCOSITY MEASUREMENTS

Surfactant-polymer incompatibility can result in the formation

of phases of different viscosities and mobilities. Modifications in bulk properties due to interaction between surfactant and polymer molecules have been investigated in the past by surface tension (12-14), precipitation (12-13), dye solubilization (15), electrophoresis (16), conductivity (14,17) and relative viscosity measurements (12-14,17).

Viscosity behavior of sodium dodecyl sulfonate (NaDDS) was studied during the current year as a function of polyacrylamide (PAM) concentration using a capillary viscometer. It can be seen in Figure II.15 that relative viscosity of a given concentration of the polyacrylamide (1000 ppm) did not change significantly when up to  $2.5 \times 10^{-3}$  M/l of surfactant was present in the mixture. The preliminary results obtained here suggest that further work in a wider concentration range of the surfactant at different levels of ionic strength, temperature and pH might provide information that could prove useful in developing our understanding of the role of polymer-surfactant interactions under conditions relevant to micellar flooding.

### D.3 SURFACE TENSION STUDIES

Surface tension data can be profitably used for evaluating driving forces for different molecules to migrate preferentially to solid-fluid interfaces.

Surface tension of sodium dodecyl sulfonate (NaDDS), polyacrylamide (PAM) and of a mixture of the two was measured using

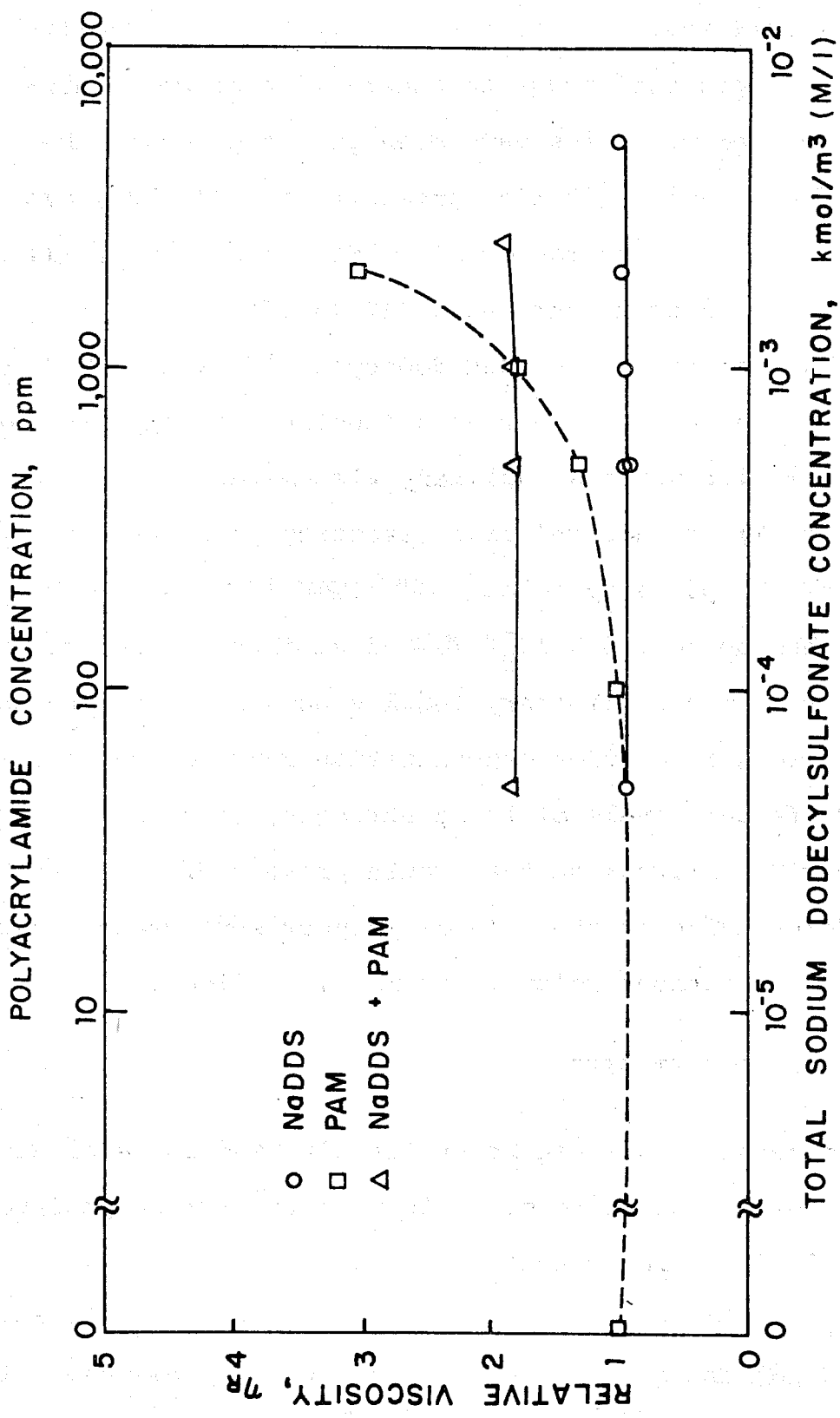


Figure II. 15. Relative Viscosity of 1,000 ppm of polyacrylamide (PAM) as a function of concentration of sodium dodecylsulfonate (NaDDS).

the Wilhelmy Plate method. As shown in Figure II.16, polyacrylamide did not produce any significant change in surface tension indicating absence of surface activity. Surface tension of sodium dodecyl sulfonate, however, decreased significantly in the presence of polymer indicating an increase in the concentration of surface active species at the liquid-gas interface. Presence of polymer molecules can modify surface tension behavior of sulfonate solution as discussed below:

1. No surface interaction between nonionic polymer and anionic surfactant. Presence of polymer molecules can change the solvent power of the aqueous medium making it more favorable for surfactant molecules to migrate to the liquid-gas interface and thereby producing a decrease in the surface tension. It can also result in mutual association of the surfactant molecules in the bulk which may or may not affect the surface tension behavior

2. Surface Association between surfactant and polymer molecules: Hydrogen bonding of surfactant molecules to charged sites of polymer or hydrocarbon chain interaction between polymer and surfactant molecules can result into the formation of polymer surfactant complexes. Generally this type of association is expected to result in an increase in the surface tension of surfactant solution under present experimental conditions. Since a significant decrease in surface tension of surfactant solution is observed in the presence of polymer molecules, effect of polymer on solvent power of the aqueous medium seems to be a

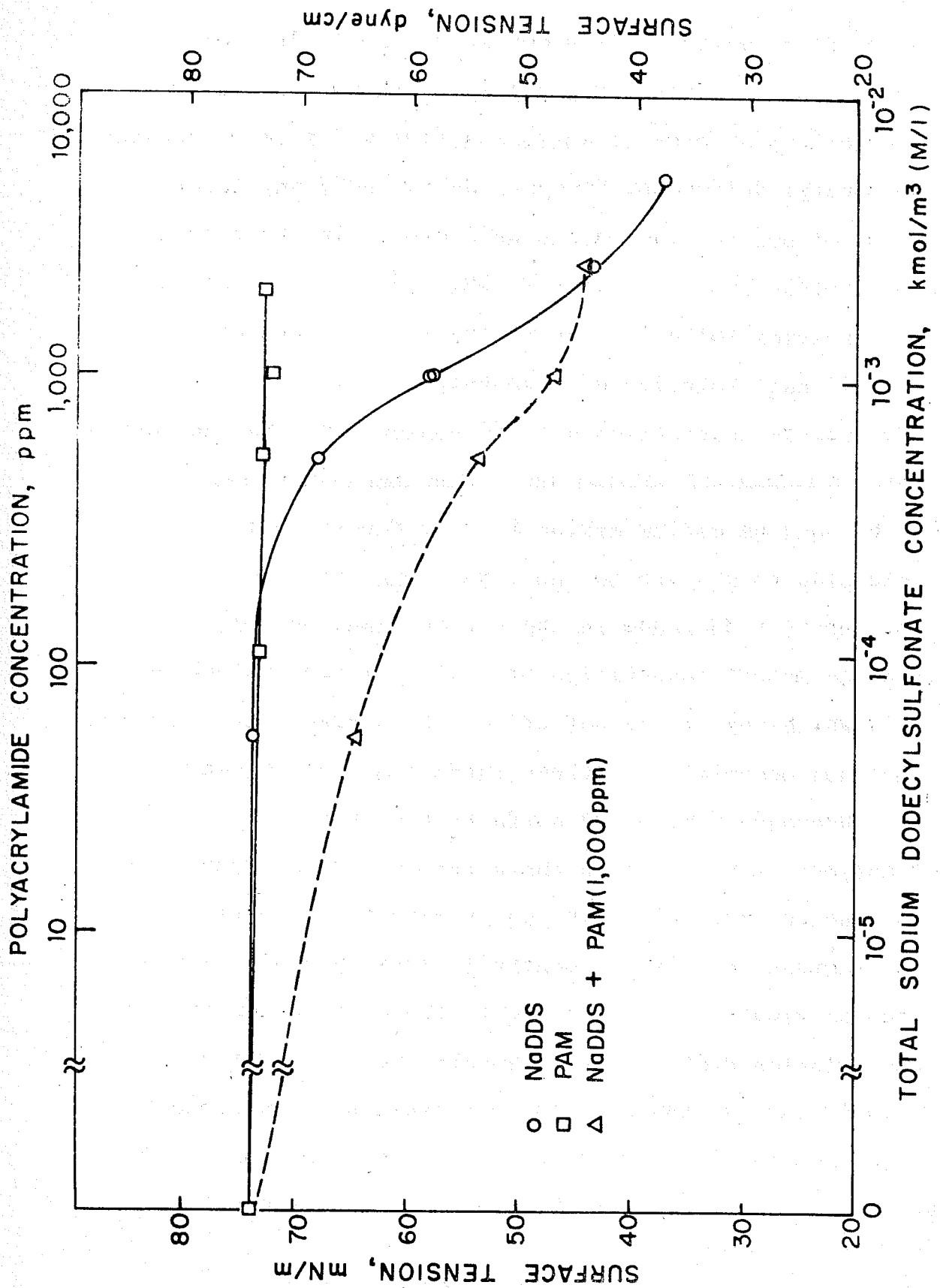


Figure II. 16. Surface tension of sodium dodecylsulfonate (NaDDS) in presence of 1,000 ppm of polyacrylamide (PAM).

predominant factor which is also supported by the relative viscosity measurements. Further work is required to understand the mechanistics of polymer-surfactant interaction and its impact on the surfactant trapped in the porous matrix as well as oil displacement efficiency of the micellar flood.

Symbols and Abbreviations

$A_i$	Hydrocarbon chain area of the species 'i' exposed to solution.
ALC	Analytical Liquid Chromatography.
$C_{b-i}$	Concentration of species 'i' in the bulk.
$C_i, c_i$	Concentration in moles/liter of species 'i'.
$C_{s-i}$	Concentration of species 'i' at the surface.
$C_T$	Total surfactant concentration.
D	Dialectric constant of the bulk solution.
D'	Dielectric constant at the interfacial region
d	a parameter related to the thickness of the adsorbed layer.
e	Fundamental unit of charge.
$f_1$	Activity coefficient of singly charged ions.
$f_2$	Activity coefficient of doubly charged ions.
$K_a$	Acid dissociation constant.
$K_{AD}$	Acid-soap formation constant.
$K_D$	Dimerization constant.
$K_s$	Solubility product.
k	Boltzmann Constant.
LC	Liquid Chromatography.
$l_o$	Length of a single $-CH_2-$ group in a hydrocarbon chain.
$\bar{M}$	Molecular weight of the solvent.

NaDDS	Sodium dodecylsulfonate
NaDDBS	Sodium dodecylbenzenesulfonate
n	Number of $-CH_2-$ groups in the hydrocarbon chain.
PAM	polyacrylamide
R	Gas Constant
RC	Recrystallized.
r	Cross sectional radius of the hydrocarbon chain.
T	Absolute temperature.
W	Specific Interaction Energy.
z	Charge on the species.
$\alpha$	Coefficient that accounts for the associative interactions in solution.
$\beta$	Coefficient that accounts for the associative interactions in solution.
$\Gamma_i$	Surface excess of species 'i'.
$\Gamma_{R-T}$	Total surface excess of surfactant.
$\gamma$	Surface tension.
$\Delta G^0$	Standard Free Energy Change.
$\delta$	Thickness of the Stern layer.
$\lambda_p$	Free energy change due to the transfer of the polar group to the interface.
$\mu_i$	Chemical potential of species 'i'.
$\sigma_0$	Charge Density of the Monolayer.
$\sigma_1$	Charge Density of the Stern layer.

- $\sigma_2$  Charge Density of the diffused double layer.
- $\phi_{-\text{CH}_2^-}$  Free energy change due to the transfer of a single  $-\text{CH}_2^-$  group to the interface.
- $\phi'_{-\text{CH}_2^-}$  Free energy change due to the transfer of unit area of hydrocarbon chain to the interface.
- $\psi_0$  Monolayer potential.

### III. DYNAMIC STUDIES OF THE INTERACTION OF POLYMER AND SURFACTANT WITH CORE MINERALS

#### A. Adsorption Characteristics of Poly(acrylamide) on Sodium Kaolinite

##### A.1 INTRODUCTION

High molecular weight polymers play a major role in water treatment,<sup>1</sup> flocculation of colloidal suspensions,<sup>2,3</sup> and mobility control in micellar-polymer flooding technology.<sup>4,5</sup> These applications have been the subject of recent reviews.<sup>6-8</sup> Poly(acrylamide) and its copolymers hold special importance because of their use in all of these areas. However, as mobility control agents in enhanced oil recovery techniques, the efficiency of poly(acrylamide) is reduced for two reasons. First, the polymer is degraded in the shear flow that is most severe at the points of injection into the well; second, the polymer is irreversibly retained within the porous structure of the reservoir material.<sup>9,10</sup> Its retention results from physical entrapment and chemical adsorption on the mineral surfaces. This report will focus on the problems of polymer adsorption.

Polymer interaction with solid surfaces is well documented in the literature.<sup>11</sup> The adsorption of highly charged polyelectrolytes such as poly(styrene sodium sulfonate) to latex particles has been studied.<sup>12</sup> The characteristics of the adsorption of poly(vinyl alcohol), a non-ionic hydrophilic polymer, has been studied in relation to several different surfaces - for example, silver iodide,<sup>13</sup> aluminum oxide,<sup>14</sup> and silica.<sup>15</sup> Studies of the adsorption of poly(acrylamide) and its hydrolytic decomposition products have also been conducted for a large number of different substrates, including calcium carbonate,<sup>16</sup> china clay,<sup>17</sup> calcium phosphate,<sup>18</sup> cellulose,<sup>19</sup> and kaolinite.<sup>20-24</sup>

However, in most of these instances, the characterization of the surface or of the polymeric component is not always complete. In this report, we will focus on the adsorption of poly(acrylamide) on well characterized sodium kaolinite. Although the mineral in most oil reservoirs is Berea sandstone, the adsorption of polymer in this strata is most often due to the presence of minor components, such as clay. Although present only in small amounts, the clay component comprises a large fraction of the exposed surface area within the reservoir. (Griffith<sup>25</sup> indicates that common Berea sandstone contains about 3-7 percent kaolinite with minor amounts of montmorillonite and illite.) Thus, this work investigates the effects of ionic strength, pH, and polymer charge on the adsorption characteristics of poly(acrylamide) copolymers.

## A.2 EXPERIMENTAL PROCEDURES

### A.2.a Preparation of Acrylamide Copolymers

Acrylamide (Eastman, electrophoresis grade) and 2-acrylamido-2-methyl propane sulfonic acid (Lubrizol Chemicals, research grade) were obtained as crystalline powders and used without further purification. Acrylamide labeled in the 1-position with carbon-14 was obtained from New England Nuclear with a specific activity of 0.1995 millicuries per millimole. It was used also as a received.

Because of the difficulty of purifying polymer and radioactive monomer in a solution polymerization, the tagged

poly(acrylamide) PAM and its copolymer with the sulfonated monomer, PAMPS, were prepared following the procedure for a precipitation polymerization as described by Wada, Sekiya, and Machi.<sup>26</sup>

Acrylamide (19.9 gm) and C-14 labeled acrylamide (0.06 gm) were dissolved in an acetone water solution (45/55, v/v) to yield a solution that was 2.5 molar in monomer. The solution was placed in a polymerization tube where nitrogen was bubbled for 30 minutes under conditions which did not alter the monomer or solvent composition. The reaction mixture was sealed and irradiated with a cobalt 60 irradiation source at a dose rate of 0.6 krad/hr for a total dose of 28.8 krad (48 hours). The polymer yield was 87 percent. The unreacted monomer was removed by repeated washing of the precipitate in a blender with acetone. The polymer was then freeze-dried to a fine white powder and stored at 4° prior to use.

A similar procedure was followed in the preparation of the sulfonated copolymer. Acrylamide (15.94 gm), tagged acrylamide (0.06 gm), and the AMPS monomer, 2-acrylamide-2-methyl propane sulfonic acid (4 gm), were dissolved in an acetone water mixture (50/50, v/v) and polymerized for a similar period of time to give a 67 percent yield of polymer. The polymerizations were repeated for untagged materials with similar yields. All polymers were characterized by measuring their intrinsic viscosities in either water or NaCl solution at 30°. Elemental analysis indicated that the PAMS polymer was 6.8 percent AMPS, which agrees well with the overall starting composition (12 percent AMPS).

Intrinsic viscosities were measured at 30° in a standard Ubbelohde viscometer. The data reported here were not corrected for the shear rate effect on the viscosity, which is expected to be small but significant for high molecular weight polymers such as those used in this work. In distilled water, the Mark-Houwink viscosity parameters for poly(acrylamide) are  $K = 6.31 \times 10^3$  dl/gm and  $a = 0.8$  at 30°. <sup>27</sup> Similar parameters are not available for the acrylamide copolymers.

#### A.2.b Preparation of Sodium Kaolinite

Our starting material was a well crystallized sample of Georgia kaolinite (from the University of Missouri repository), having a surface area of 9.82 m<sup>2</sup>/gm as determined by nitrogen adsorption. The dry clay was treated with water for 10 minutes in a high speed mixer at a solid-to-liquid ratio of 0.5, then diluted with distilled water to 5 percent solids and allowed to settle. The kaolinite was repeatedly washed with intense agitation until there was no change in the conductivity of the supernatant water. A NaCl solution (2M) was added to the solids and agitated at a high solid-to-liquid ratio for 30 minutes, then diluted and agitated again for 2 hours, allowed to settle, and the supernatant decanted. The washing procedure was repeated until a pH of 7 and a constant conductivity were observed in the supernatant. The kaolinite was repulped with 1M NaCl at pH 3, agitated for another 30 minutes, diluted with water, agitated for 2 hours, allowed to settle, and washed with distilled water to pH 7 and constant supernatant conductivity. The ion exchange procedure was repeated

twice with the 1M NaCl, each time being followed with the same washing procedure. The final washings were with triple distilled water. The fine clay particles were then separated from the coarse ones by decantation. The fine particles were recovered and repeatedly washed with triple distilled water until the conductivity of the clay suspension became identical to that of the triple distilled water. The sodium kaolinite was allowed to settle, and the thick suspension was freeze-dried to yield a powder that was stored in a dessicator prior to use.

#### A.2.c Procedure for Polymer Adsorption

Approximately 1 gm of freeze-dried sodium kaolinite was weighed into a glass vial having a Teflon-lined screw cap. A 2000 ppm polymer solution in the appropriate electrolyte concentration was prepared. To the clay in the vial was added 2.5 ml of the supporting electrolyte (polymer free); this solution was kept at 30° with agitation for 2 hours. HCl or NaOH was then added to adjust the pH of the solution. After this conditioning step, a solution comprising a mixture of the polymer solution and a polymer-free solution having the same electrolyte concentration with the required polymer amount was added to the clay. The total liquid volume was 10 ml.

The adsorption time began at this point. The vial was agitated for a time in a constant temperature incubator. At the end of the experiment, the sample was centrifuged at 1500 g for 20 minutes. A 1 ml sample of the supernatant was mixed with 13 ml of Aquasol-2 liquid scintillation cocktail (dioxane-based, New England Nuclear) in a polyethylene scintillation vial. The

sample was analyzed in an LS-100 C liquid scintillation system. This scintillation procedure could tolerate ionic strengths up to 3M. Using 1 ml samples of 10 ppm pure tagged polymer solutions in the absence of adsorption, the poly(acrylamide) polymer, PAM, gave 178 cpm and the copolymer containing the sulfonate, PAMS, gave 150 cpm.

When experiments were performed at 60°, the procedure was slightly modified. The samples were equilibrated with the sodium kaolinite at 60° with shaking for 24 hours. The samples still at 60° were allowed to settle for a period of 24 hours. The supernatant was centrifuged in an insulated centrifuge tube for 10 minutes, during which time the temperature was observed to fall about 8° to 52°. A 1 ml aliquot of this solution was used for the scintillation measurement.

### A.3 DISCUSSION OF RESULTS

Before considering the interaction between the poly(acrylamides) and the sodium kaolinite surface, it is necessary to describe the properties of each material as it exists alone in the experimental medium. The properties of both components are dependent on the nature of the medium, the ionic strength, pH, and temperature. Kaolinite is an aluminosilicate ( $\text{Al}_4\text{Si}_4\text{O}_{10}(\text{OH})_8$ ) whose crystal structure contains alternate sheets of alumina and silica oxides. As the crystal units have planar habits, there are two principal surfaces: the edge containing exposed metal ions, and the oxide surfaces. Kaolinite exchanges cations and, in this work, the sodium form of the mineral was prepared. Buchanan and Oppenheim<sup>28</sup> investigated the stability of kaolinite in aqueous

suspensions. With  $\text{pH} < 4$ , the aluminum cations may be dissolved from the lattice; in the  $\text{pH}$  range 4-9, a  $\text{Si}(\text{OH})_4$  entity in some form is leached away; and at higher  $\text{pH}$  values, the aluminate ions become freed. In our preparation of sodium kaolinite, care was taken to maintain the clay during the washing and conditioning steps between  $\text{pH}$  4.5 and 7 in order to minimize the leaching of aluminum ions from the crystal matrix. However, despite carefully controlled conditioning steps, kaolinite is unstable in electrolyte solutions such as those used in the adsorption experiments here considered. As determined by Williams and Williams<sup>29</sup> and by Hunter and Alexander<sup>30</sup> from electrophoretic mobility measurements, the surface charge of kaolinite is a function of solution  $\text{pH}$  and solution ionic strength. At high  $\text{pH}$ , the surface is negatively charged; the magnitude of the charge drops slightly as the ionic strength is increased from  $10^{-4}$  to  $10^{-2}$  molar  $\text{NaCl}$ . At  $\text{pH}$  5, the surface charge, still negative, is nearly independent of the electrolyte ionic strength. At  $\text{pH}$  3, the surface is slightly negatively charged in the presence of electrolyte, but becomes positive at very dilute electrolyte concentrations. The positive charge is attributed to the metal ions on the edges of the kaolinite crystal lamellae. Although heterogeneous surface charge is indicated from crystal structure considerations, in this work we will interpret the results solely in terms of the overall kaolinite surface charge. No measurements have been made in this work on the electrophoretic mobility of sodium kaolinite to which polymer is adsorbed.

Polymerization was carried out with initiation by  $\gamma$  irradiation in a medium free of all components but the monomers and solvent system. The polymers so produced were free from impurities which might alter their interactions with adsorbing surfaces. At the low doses used, no significant branching occurs during the radiation-induced synthesis. A combination of chains scission and chain branching is expected as side reactions at much higher levels.<sup>73</sup> Although the reactivity ratios for this copolymerization are not known, they may be reasonably approximated by those for acrylamide ( $r_1 = 1.1$ ) and sodium acrylate ( $r_2 = 0.3$ ), as reported by Plochocka and Wojnarowski.<sup>74,75</sup> The ideal copolymer equation predicts that the initial copolymer composition from a 12 percent by mole AMPS monomer mixture in acrylamide would be 10 percent AMPS, and that the composition of copolymer being produced at 60 percent conversion would be about 13 percent. Although the analyzed composition of 6.8 percent AMPS is somewhat lower, it nevertheless is consistent with the predictions of the copolymer equation. Because of the economics of making C-14 labeled materials, these copolymerizations were taken to a high conversion. The application of the ideal copolymer equation is not strictly correct, since precipitation occurs during the growth of the polymer chain. In order to interpret the adsorption results for the copolymer, we will assume homogeneous polymer composition and molecular weight.

Two poly(acrylamide) polymers were used in the adsorption studies -- a homopolymer PAM, and a copolymer PAMS contained 6.8 percent of the AMPS. The PAM was prepared as an uncharged

polymer without any significant degree of hydrolysis of the pendant amide groups to carboxylic acid form. The intrinsic viscosity of PAM determined at 30° (Fig. 1(a)) is independent of the ionic strength of the solution in which the viscosities were determined.

This intrinsic viscosity is a measure of the effective hydrodynamic volume of the polymer coil in solution.<sup>76</sup> For the PAM in these experiments, the expansion of the coil is independent of the electrolyte concentration. However, the PAMS containing 6.8 percent by mole of monomer with a strongly ionic sulfonate group have an intrinsic viscosity that increases sharply as the ionic strength of the solution decreases to  $10^{-2}$  molar NaCl (Fig. 1(a)). Coulombic repulsion along the polymer chain becomes more significant at low concentrations of supporting electrolyte.<sup>77,78</sup> This electrostatic repulsion causes an expansion of the polymer coil and an increase in its effective hydrodynamic volume in solution. In contrast to the PAM, the PAMS is expected to exclude coions from the domain of the polymer coil in a Donnan-like manner at low ionic strengths of the supporting electrolyte.

Figure 1(b) shows the effect of pH on the intrinsic viscosity of PAM, PAMS, and a copolymer of acrylamide and acrylic acid having approximately the same composition as the PAMS. The PAM's intrinsic viscosity at both low and high ionic strength is independent of the solution pH. The PAMS has a significantly higher intrinsic viscosity which passes through a shallow maximum at pH 6. The sulfonate polymer, while exchanging its counter ions readily as the pH changes, is much less sensitive to pH than is the corresponding carboxylate-containing copolymer. The weakly acidic

carboxylate-containing copolymer has an intrinsic viscosity at low pH which approaches that of the PAM. Most of the carboxylate groups are in the associated hydrogen form. However, at high pH, as they ionize with the sodium counterion, the polymer coil is expanded and the intrinsic viscosity approaches that of the PAMS. The ionization of the PAMS is believed to be independent of pH.

Since the adsorption experiments extended over long periods of time, it was necessary to consider the possibility that the polymers used in this work had decomposed under experimental conditions. Palit and coworkers<sup>79</sup> have presented data which indicate rapid hydrolysis of PAM in strongly alkaline solutions. Under milder conditions, Shyluk and Stow<sup>80</sup> have shown that PAM undergoes an aging which results in a drop in solution viscosity. In Fig. 2, the relative specific viscosities are given for a 2000 ppm PAM solution as a function of equilibration time at the indicated conditions. Equilibrium adsorption measurements normally required 72 hours contact time with the kaolinite suspension. At both 30° and 60°, PAM retained its viscosity near its initial value. Over longer times at 60°, an increase in viscosity was observed when measured in a solution of zero ionic strength. At the same equilibration conditions (save for being in 1 molar in NaCl), the PAM retained a more constant relative viscosity. Hydrolysis is indicated. In the absence of NaCl, the polyelectrolyte effect causes an increase in viscosity. In salt, this expansion of the coil is not observed. This constant viscosity, however, indicates that no chain scission occurs during the equilibration time. Under conditions of high pH and

long equilibration times, it was sometimes observed that the amount of polymer adsorbed slowly decreased over time<sup>42</sup>. This decline may be attributed to the effects of hydrolysis and of the hydrolysis products on the adsorption equilibrium.

In Fig. 3, the amount of PAM adsorbed on sodium kaolinite is plotted as a function of time for experiments performed at 30°. The ionic strength (I) refers to concentration of NaCl in ppm. In all but one of the experiments, the solid-to-liquid ratio (S) was 0,1. The amount adsorbed (mg/g) was less when the solid-to-liquid ratio was high for a given initial polymer concentration. All other conditions being the same, the final equilibrium polymer concentration was lower for higher solid-to-liquid ratio. The reported pH represents the final hydrogen concentration which resulted from the adsorption process as in Fig. 3 no adjustment was made in the solution pH. The rate of adsorption of PAM on sodium kaolinite was rapid - approximately 80 percent occurring within the initial 15 minutes of contact time. An adsorption plateau was established after 100 minutes, and was maintained with only a slight drift over a long period of time. The rate of adsorption was independent of initial conditions. During these adsorption experiments, the concentration of polymer in solution dropped to a low value. The analysis by Jankovics<sup>18</sup> of the kinetics of a Langmurian adsorption was not applied to these data because the adsorption was too rapid. Although data at very short times is most useful for determining the adsorption kinetic parameters, it was not obtained. To ensure full equilibration of the surface with the components in solution, equilibration times of 72 hours (4320 minutes) were used in adsorption experiments performed at 30° with both PAM and PAMS.

In Figs. 4(a)-(e), adsorption isotherms at 30° for PAM on sodium kaolinite are plotted as a function of the equilibrium polymer concentration. Isotherms are given for adsorption at natural pH (resulting when no HCl or NaOH are added to the system) and for higher and lower pH values (resulting from addition of acid or base to the kaolinite during the conditioning step). The pH did not shift more than 0.2 pH units during the course of a typical adsorption experiment; all of the reported pH data refer to the final equilibrium pH of the solutions.

The adsorption studies were performed in a supporting electrolyte, NaCl, which varied in concentration from 0 (for distilled water) to 3M. In solutions of high ionic strength (Fig. 4(a)), the adsorption isotherm shifts to lower absolute adsorptions as the solution pH increases. At low ionic strengths, the decrease in adsorption that accompanies a change in pH from pH 2.2 to pH 7.2 is small. A very significant drop occurs in the high pH ranges. Under these experimental conditions, the essentially non-ionic PAM does not significantly change its equilibrium shape in free solution. This is confirmed by the intrinsic viscosity data for PAM in these same polymer solutions. Michaels and Morelos<sup>23</sup> have reasoned that the interactions between PAM and surfaces such as kaolinite result from hydrogen bonding between the amide hydrogen atoms and the oxygen groups on the aluminosilicate surface. In the absence of any significant charging effect on the PAM, this surface interaction results in a very favorable partitioning of the polymer from its condition in free solution to an aggregation in a domain next to the mineral water interface. The pH effect observed results from the changes in the surface

character of the kaolinite. Between pH 2 and 7, the kaolinite has a surface charge which changes from a near positive to a moderately negative value.<sup>29</sup> Under these conditions, there is only a slight shift in the adsorption of the PAM, implying only a slight alteration of the interaction between the kaolinite and the PAM. However, when the surface charge on the kaolinite reaches highly negative magnitudes, the basic attractive interaction of the uncharged PAM with the kaolinite surface is weakened. The kaolinite-PAM interaction is reduced in the strongly ionic domain of the interface at high pH conditions. The slight drop in PAM adsorption, as the ionic strength is increased at constant pH, is also consistent with this. The natural pH of adsorption of PAM on sodium kaolinite is a function of solution ionic strength. In Fig. 4(a), ionic strength 3 molar NaCl, the natural pH is 4.4. As the ionic strength is reduced to zero (Fig. 4(e)), the natural pH shifts to 6.9. At high electrolyte concentration, there is an exchange of the hydrogen ions of the clay with the sodium ions in the water resulting in a lower pH.

In most cases, the adsorption increased sharply as the equilibrium solution polymer concentration increased to 100 ppm. The isotherms did not, however, level off to a plateau of constant polymer adsorption, but slowly increased as the polymer in solution rose to 500 ppm. For PAM, only at the very high values could a definite plateau limit in the adsorption be observed. Using the standard correlation, these adsorption data did follow a Langmuirian pattern. No evidence of a multilayer adsorption of the PAM was encountered. Adsorption isotherm shape for the PAM

indicates no significant cooperative interaction between the PAM on the interface and those about to be adsorbed from the solution. The PAM on the surface occupy lattice spaces independently of the other polymer molecules already on the surface.

In Figs. 5(a)-(b), the equilibrium adsorption isotherms are given for the ionic PAMS polymer as a function of polymer concentration, solution ionic strength, and pH. Although the shape of the adsorption isotherms is similar to those of the PAM, two important differences should be noticed as polymer concentration is increased. For a given ionic strength in the supporting electrolyte, the adsorption drops off in a regular manner as the pH is increased from 2 to 9. This reflects the increase in Coulombic repulsion as the surface charge on the kaolinite becomes more negative in the regions of high pH. The ionic character of the PAMS backbone does not change substantially as the pH is changed in this region.

In addition to the pH effect, there is a very strong ionic strength effect on the absolute amount of polymer adsorbed. At low ionic strengths, the adsorption is near zero as the electrostatic repulsion between polymer and surface is high. As the ionic strength is increased, the supporting electrolyte suppresses the extent to which the fixed charges on the polymer and surface can dominate the interactions. In a 1 molar solution, although the effect of pH is still observed, the absolute adsorption of the PAMS is in the same range as that observed for the uncharged PAM.

Figure 6 summarizes the adsorption characteristics of the two polymers on sodium kaolinite at an equilibrium polymer

concentration of 100 ppm. Unlike the PAM, the PAMS has an adsorption which is suppressed under conditions of low ionic strength in the supporting electrolyte. The absolute adsorption of the PAMS increases at high ionic strengths into a region comparable (although still lower) to the PAM. The effect of ionic strength on the adsorption of the PAMS follows a commonly encountered pattern for electrostatic rejection of a charged body from a similarly charged polyelectrolyte.

It was difficult to measure the adsorption of these polymers at elevated temperatures because a room temperature centrifuge had to be used. With proper insulation of the centrifuge tube, a temperature drop of less than  $8^{\circ}$  was observed. The data in Figs. 7(a)-(b) refer to experiments that were performed at  $30^{\circ}$  and  $60^{\circ}$  as a function of polymer concentration solution and ionic strength at natural pH. The solutions were equilibrated at  $60^{\circ}$  for 24 hours, allowed to settle for another 24 hours, and the supernatant was centrifuged under conditions where the final solution temperature after centrifugation was about  $52^{\circ}$ . This change in the temperature has an insignificant effect on the observed equilibrium isotherms. There is no observed change in the adsorption of PAMS as a function of temperature for solutions of different ionic strength, even in the region of high ionic strength where much of the Donnan repulsion is suppressed. The Coulombic effects still dominate the adsorption in a manner where temperature does not change the isotherm. In Fig. 7(b), similar data are given for the uncharged PAM. For both conditions of low and high ionic strength, the adsorption isotherm is lowered as the

temperature is increased from 30° to 60°. Significant hydrolysis of the PAM under these conditions is doubted because of the data given in Fig. 2, and because a hydrolyzed PAM being ionic should give a temperature effect analogous to the PAMS. This reduction in the adsorption isotherm for the uncharged polymer is consistent with the hypothesis that a form of hydrogen bonding is responsible for the attraction of the PAM to the sodium kaolinite. Such interactions are exothermic and thus are expected to weaken as the temperature is increased.

Adsorption of flexible chain polymers such as poly(acrylamide) is rapid and, in most reports, the reverse desorption under normal conditions is very slow. At moderate pH, this adsorption is independent of ionic strength of the solution. This suggests a form of hydrogen bonding as the basis of the interaction between polymer and surface. However, it is generally believed that a randomly coiled polymer such as poly(acrylamide), if associated with a surface, cannot have a significant fraction of its chains attachments to the surface without a resulting very large decrease in configurational entropy. Silberberg<sup>81</sup> has presented a picture of chain segments attached at specific points along the chain with long loops of polymer in a more or less random conformation extending out into solution. However, with poly(acrylamides) there is no reason to suspect that any one site on the polymer chain has any more preference for the surface than any other one. Given the kinetic turmoil that exists within a random coil as it moves through its ensemble of conformation shapes, it is reasonable to suspect that the interactions with the surface are

transient. The hydrogen bonding at different sites is being continually made and broken, although on the average maintaining a certain number of interactions with the surface. The interaction between the oxygens of the surface and the acrylamide may be analogous to the interactions that occur in solution between the oxygens of poly(oxyethylene) and the carboxylic acid hydrogens of unionized poly(acrylic acid.)<sup>82</sup> These polymers form a coacervate in aqueous solution. The interaction energy between the ether oxygens and low molecular weight carboxylic acid groups has been found from melting point depression measurements to be about 6 cal/cc and exothermic.<sup>83</sup> As with PAMS, a change in the ionic character of the poly(acrylic acid) leads to a weakening of the association between the two components.

Desorption of polymers from such a surface is slow, as it is highly unlikely that all of the points of interaction of the polymer and surface will be simultaneously broken. For high molecular weight polymers in which there are on average a great number of interactions with the sites on the surface, total desorption of the molecule is impossible. This does not mean that the polymer molecule cannot move over the surface as the coverage of the surface increases. Surface diffusion envisioned as a rolling of the random polymer coil over the surface can easily occur without any need for total desorption of the polymer coil from the surface.

The effects of charge on the polymer-surface interaction may be viewed as a secondary interaction between the components whose effect is superimposed. The negative surface charge and the

negative polymer fixed charge cause a reduction in the ability of the amide groups to hydrogen bond with the surface.

The electrostatic repulsions keep more of the chain elements of the coil away from the surface, particularly at conditions of low ionic strength. This makes it more difficult for polymer-surface hydrogen bonds to form. The result is a reduction in the effective adsorption at a given polymer concentration. As the supporting electrolyte concentration is increased, the Debye layer is suppressed, the polymer can approach the surface more closely, and the amide groups along the PAMS chain can once again form a complement of bonds with the surface. The absolute adsorption of the PAMS to the surface is reduced somewhat from that of the PAM<sup>-</sup> at conditions of high ionic strengths because this polymer contains 10 percent by mole of a non-hydrogen bonding monomer in its backbone.

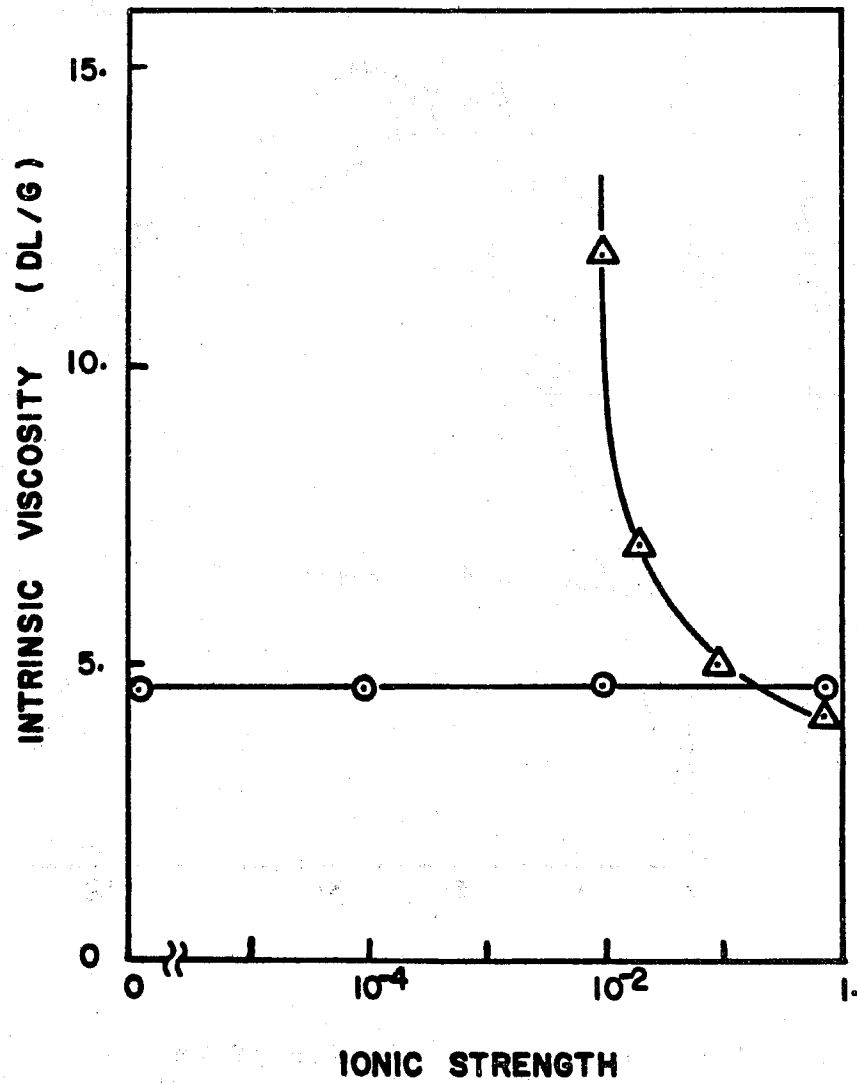


Figure 1(a) Intrinsic viscosity of poly(acrylamide) and the copolymer PAMS as a function of ionic strength. Electrolyte: NaCl ; Temperature 30°C.

○ PAM ;                      △ PAMS.

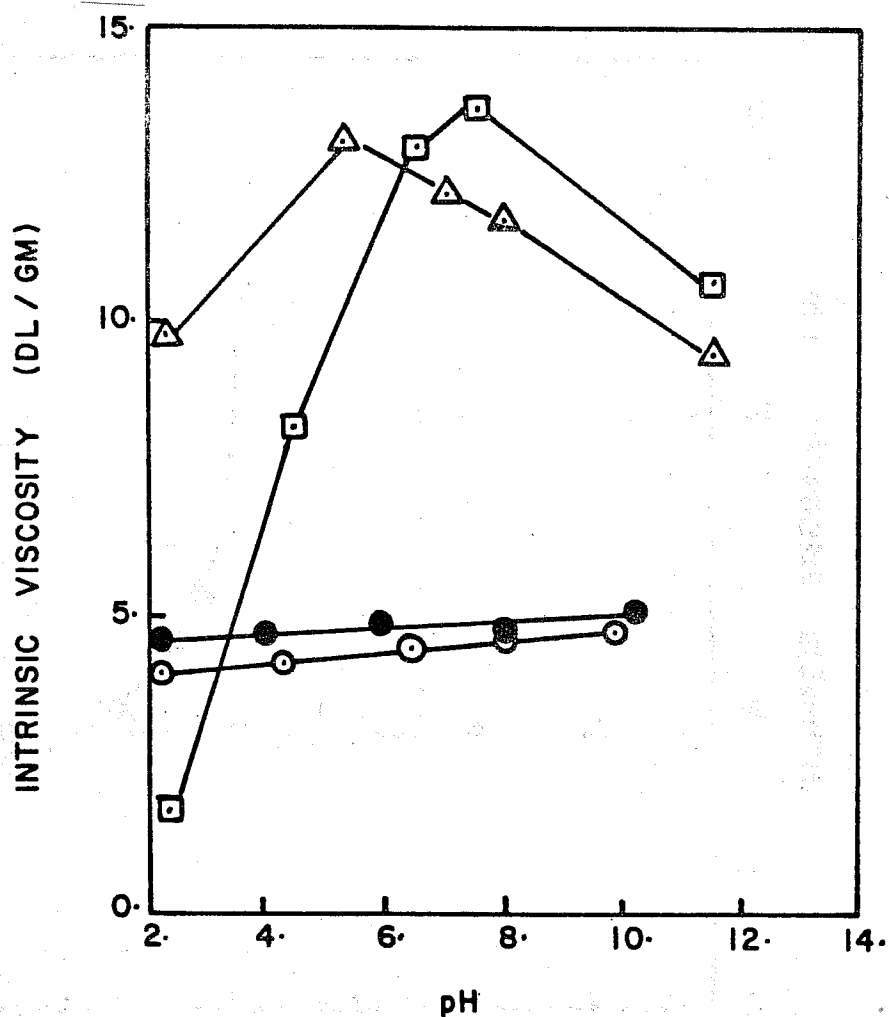


Figure 1(b) Effect of solution pH on the intrinsic viscosity of poly(acrylamide) and its copolymers Temperature 30°C .

- △ PAMS in 10<sup>-2</sup> molar NaCl
- PAMC in 10<sup>-2</sup> molar NaCl
- PAM in 1 molar NaCl
- PAM in distilled water

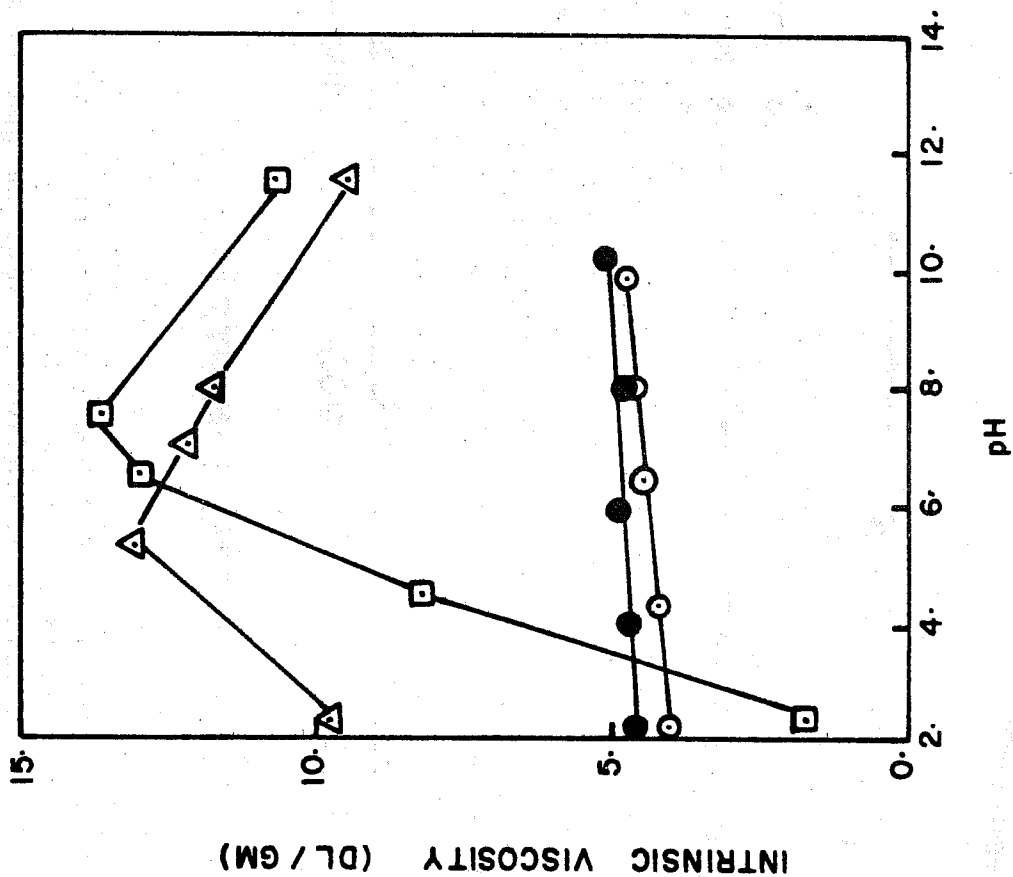


Figure 2 Relative viscosity of a 2000 ppm PAM solution as a function of equilibration time without agitation: in distilled water at 60°C ○ ; and at 30°C ● and in 1 molar NaCl at 60°C △ .

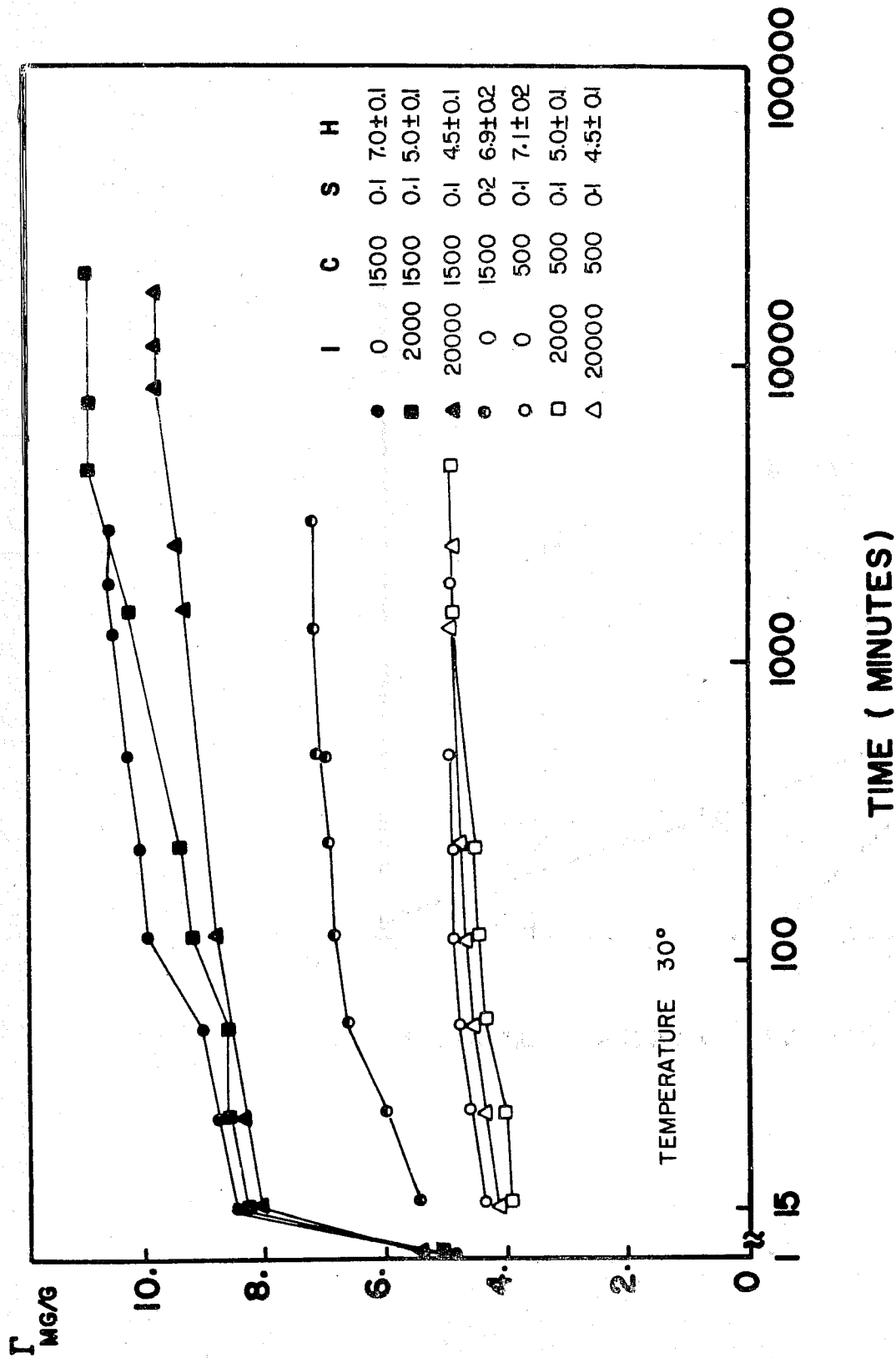


Figure 3 Kinetics of PAM adsorption on sodium kaolinite at the conditions indicated. (I is concentration of NaCl in ppm; C is the initial PAM concentration in ppm; S is the solid to liquid ratio and H is the initial solution pH)

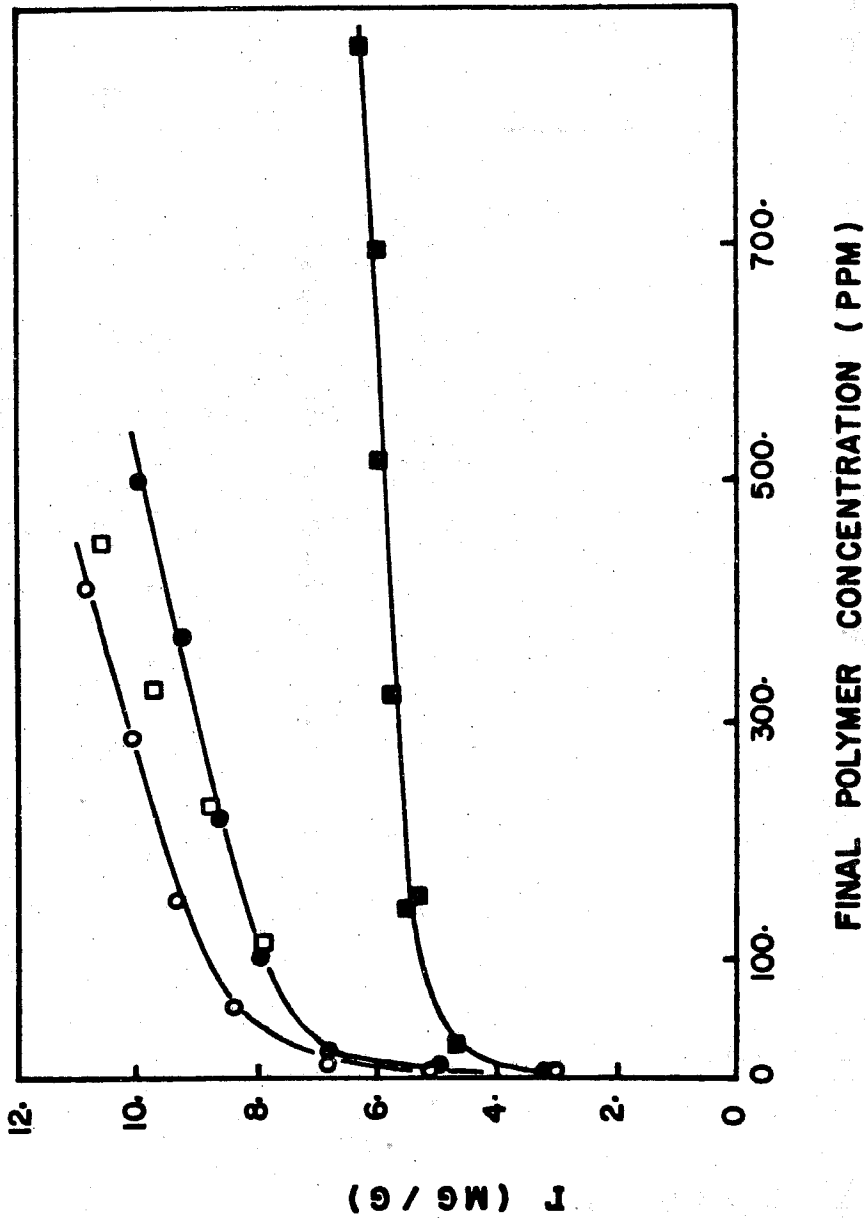


Figure 4 Equilibrium adsorption of PAM on sodium kaolinite as a function of final polymer concentration. ( Temperature is 30°C; S is 0.1 ; equilibrium time is 72 hours; indicated pH is final equilibrium value )

(a) Ionic strength is 3 molar NaCl

○ pH 1.6; □ pH 4.4 (natural); ● pH 6.7; ■ pH 11.3

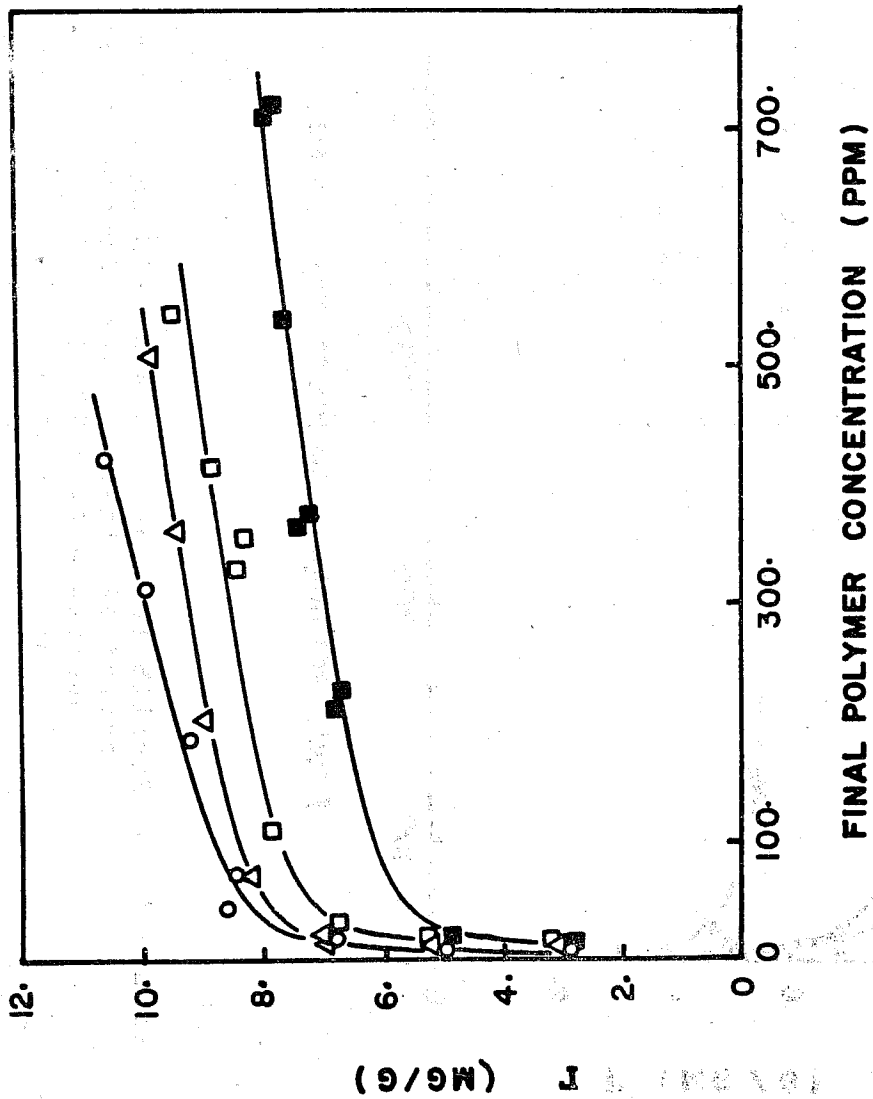


Figure 4 (b) Ionic strength is 1 molar NaCl.  
O pH 2.0; Δ pH 4.5 (natural); □ pH 6.6; ■ pH 10.3

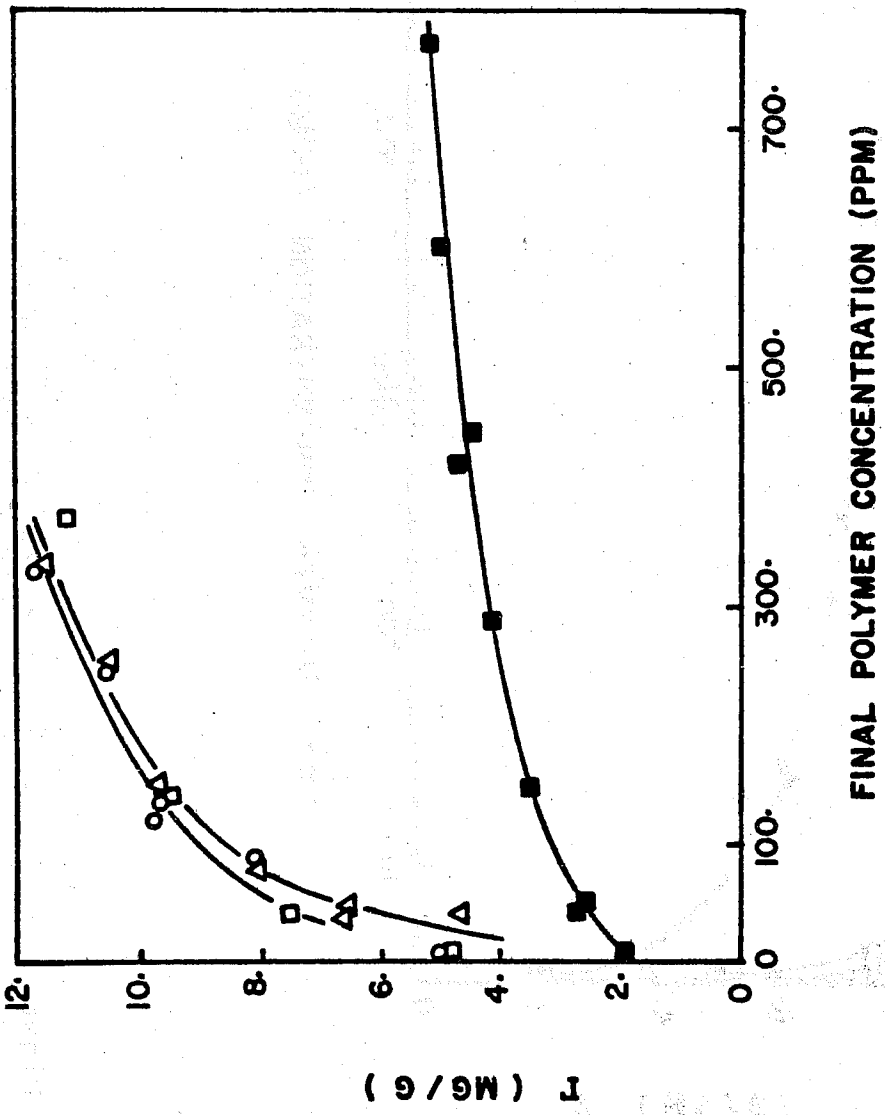


Figure 4 (c) Ionic strength is 0.1 molar NaCl

O pH 2.3; Δ pH 4.7 (natural); □ pH 7.4 ; ■ pH 11.9

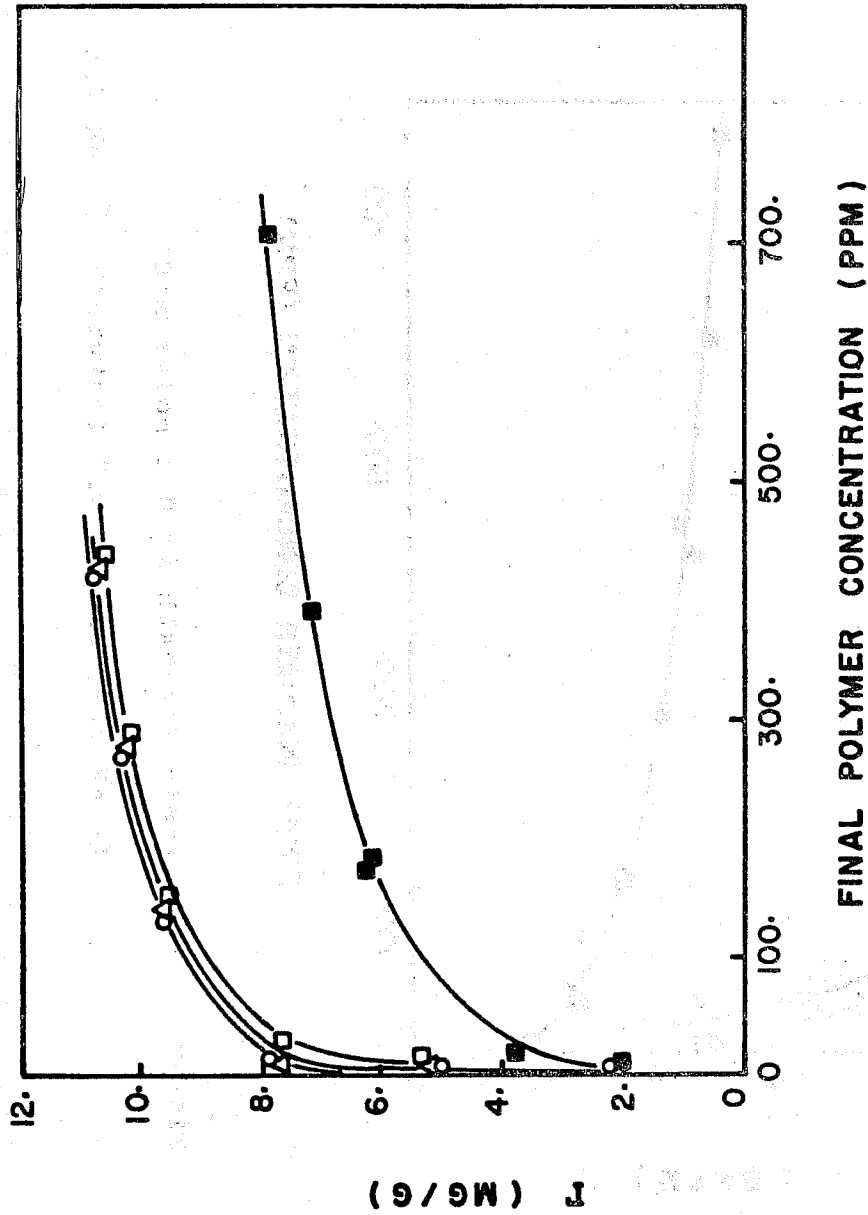


Figure 4 (d) Ionic strength is  $10^{-2}$  molar NaCl.

○ pH 2.2; △ pH 5.4 (natural); □ pH 7.2; ■ pH 10.9.

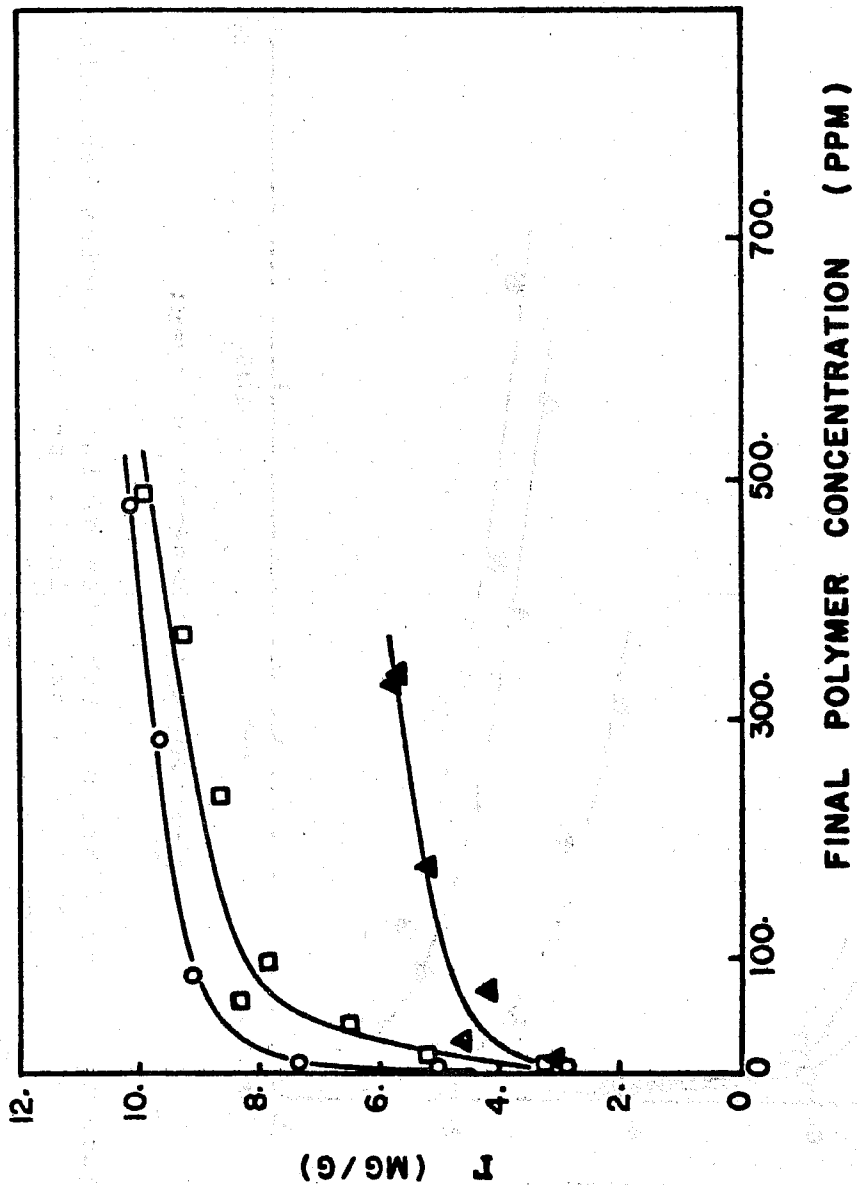


Figure 4(e) Distilled water

○ pH 2.3; □ pH 6.9 (natural); ▲ pH 10.8 .

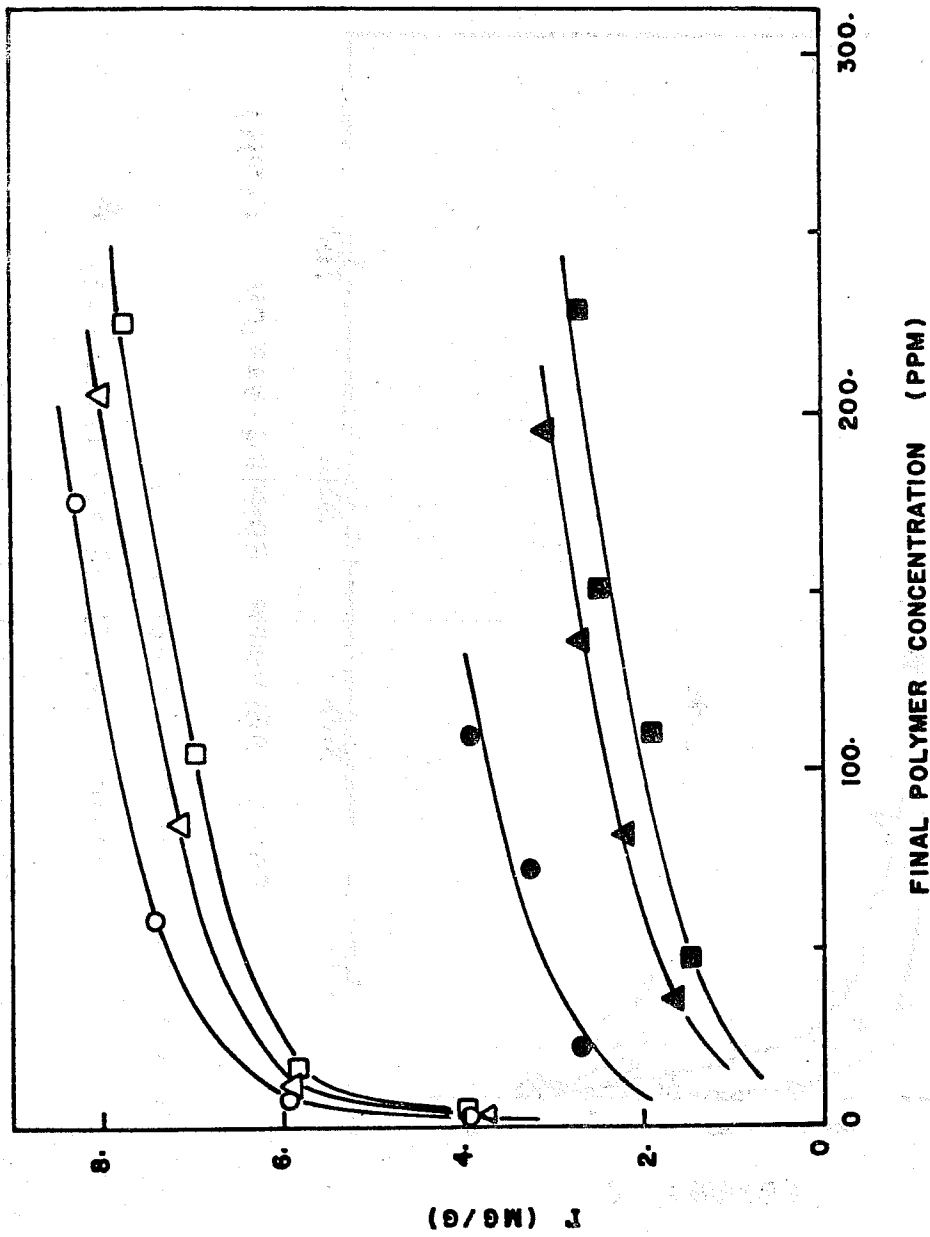


Figure 5 Equilibrium adsorption of PAMS on sodium kaolinite as a function of final solution polymer concentration. ( conditions as in Figure 4 )

(a) in 1 molar NaCl - O pH 3.8;  $\Delta$  pH 6.5;  $\square$  pH 8.7 .  
 in  $10^{-2}$  molar NaCl -  $\bullet$  pH 4.9;  $\blacktriangle$  pH 7.5;  $\blacksquare$  pH 9.4 .

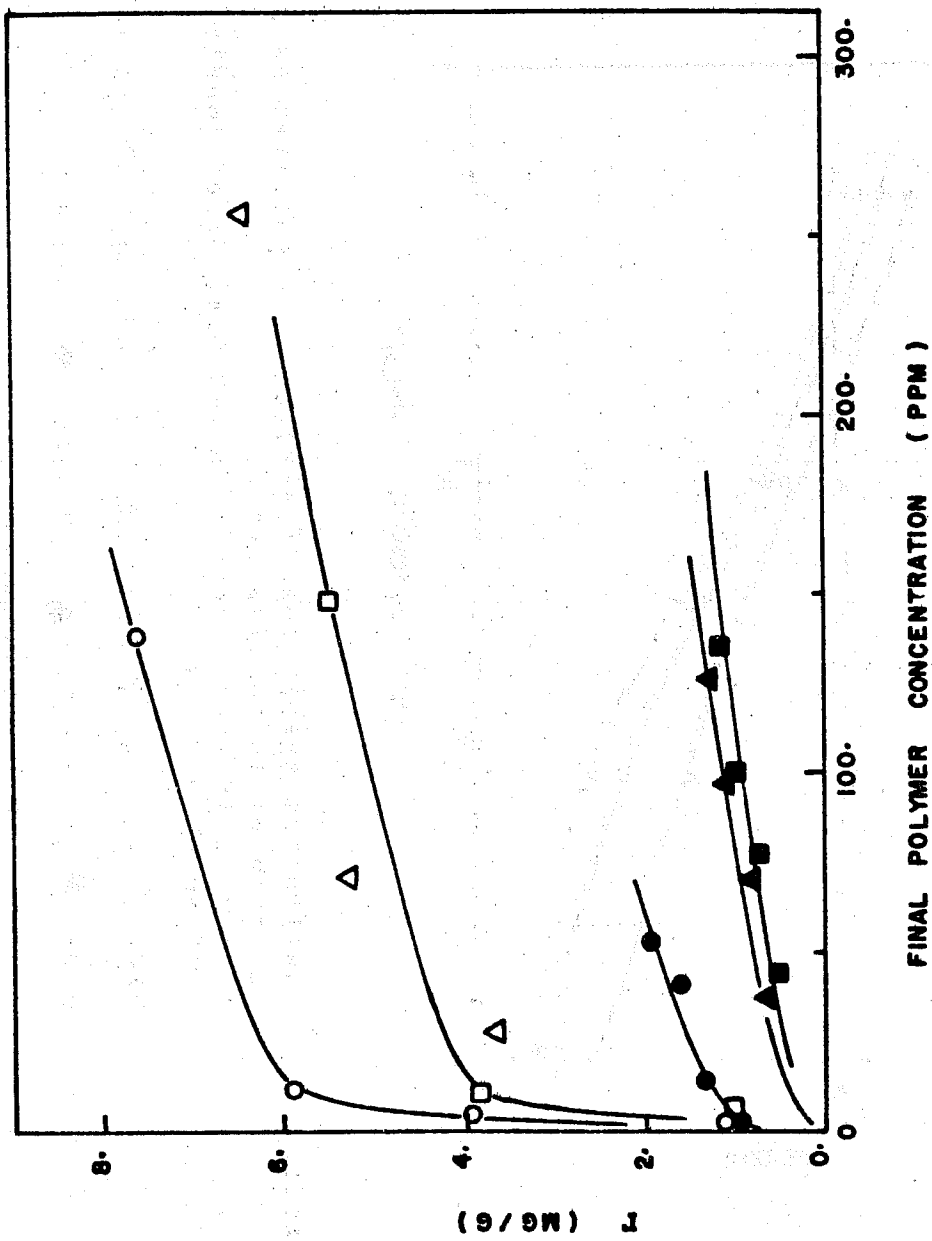


Figure 5 (b) in 10<sup>-1</sup> molar NaCl - ○ pH 2.5; △ pH 4.4; □ pH 7.7 .  
in 10<sup>-4</sup> molar NaCl - ● pH 5.0; ▲ pH 7.7; ■ pH 10.0 .

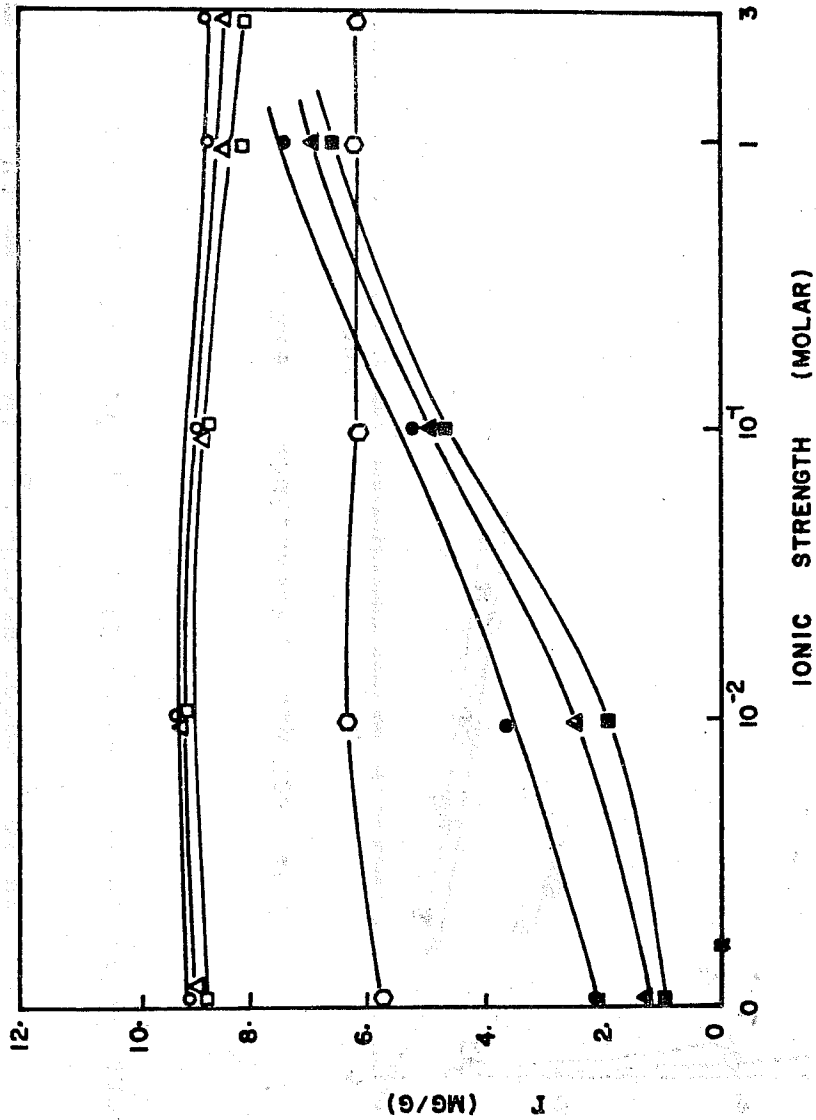


Figure 6 Equilibrium adsorption of acrylamide copolymers as a function of ionic strength ( final polymer concentration 100 ppm; other conditions as in Figure 4 )

PAM: ○ pH 2.5; △ pH 5.0; □ pH 7.0; ◇ pH 10.5 .

PAMS: ● pH 5.0; ▲ pH 7.0; ■ pH 8.5 .

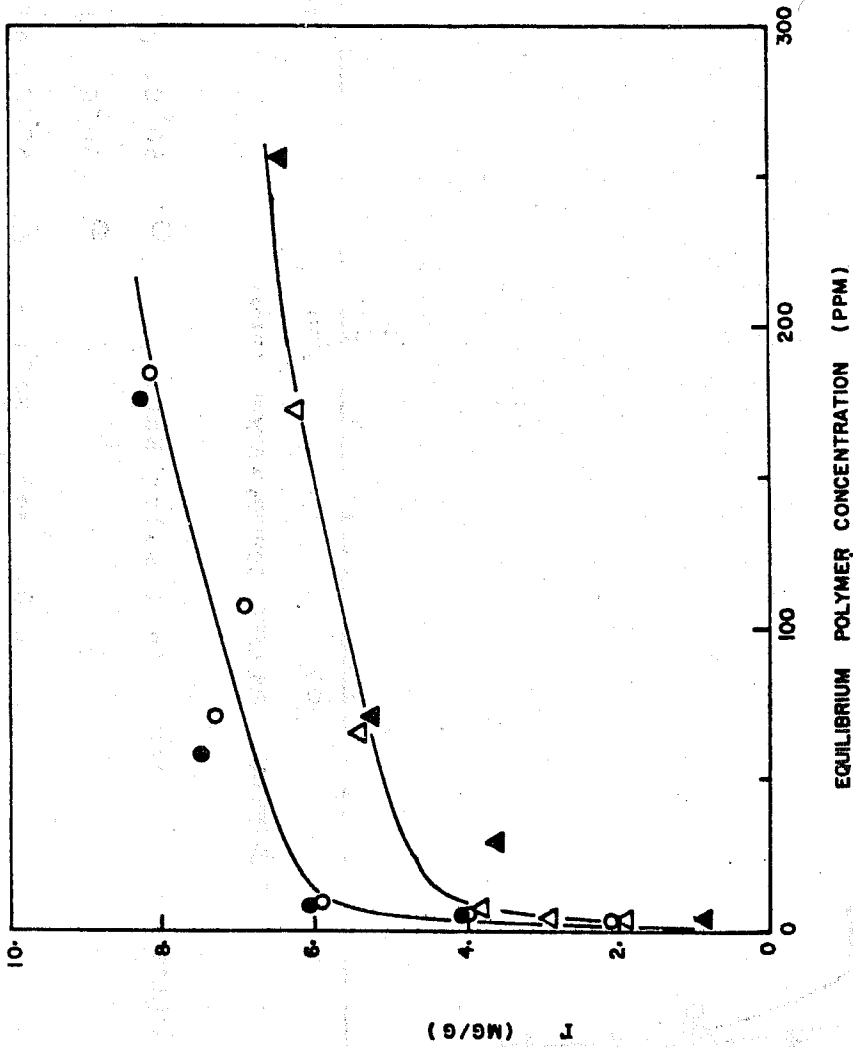


Figure 7 Effect of temperature on the adsorption of acrylamide copolymers on sodium kaolinite

(a) PAMS : in 1 molar NaCl - ○ 60°C, pH 4.0; ● 30°C, pH 3.8 .  
in 0.1 molar NaCl - △ 60°C, pH 4.4; ▲ 30°C, pH 4.4 .

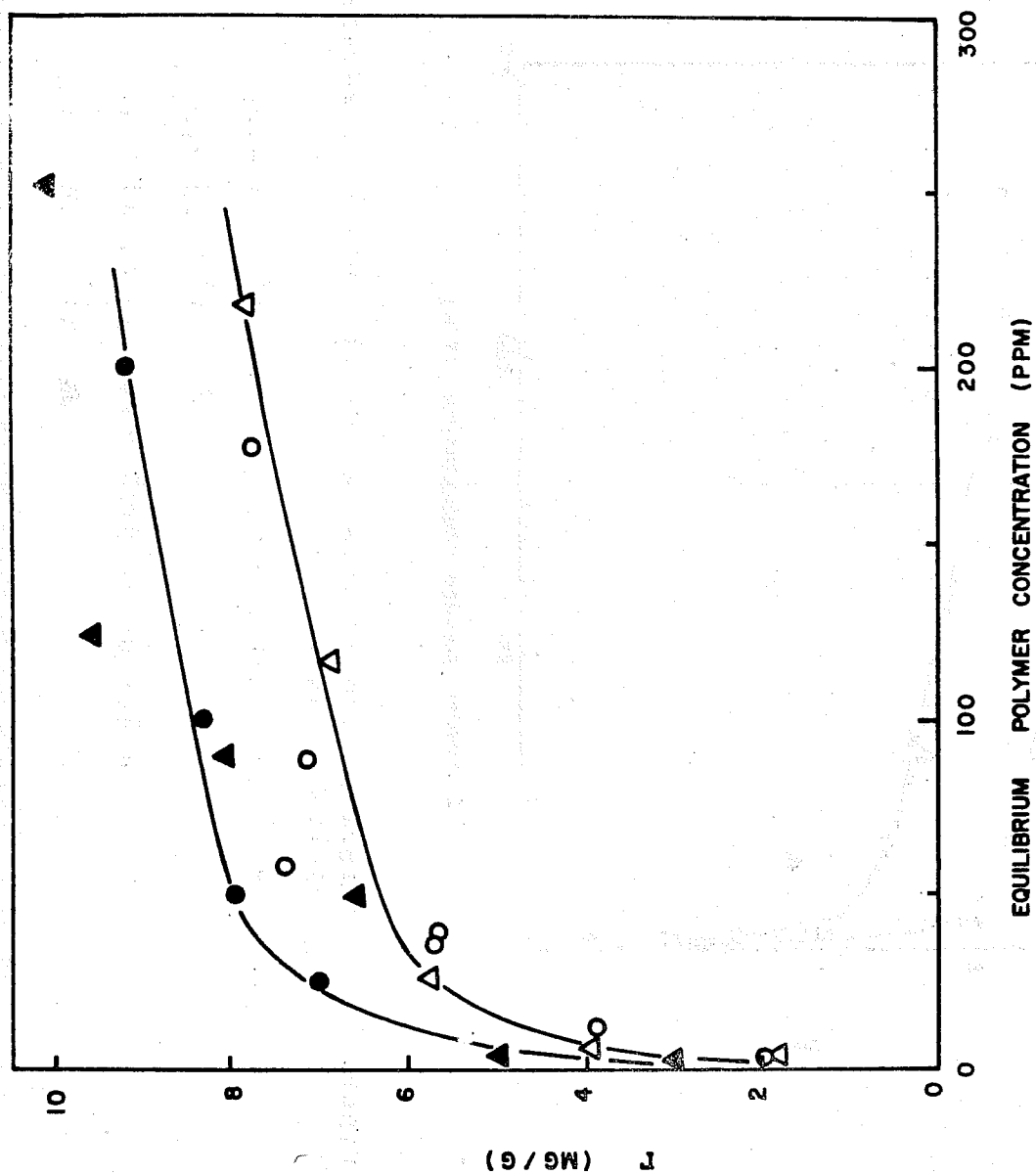


Figure 7 (b) PAM: in 1 molar NaCl - ○ 60°C, pH 4.2;  
● 30°C, pH 4.5  
in 0.1 molar NaCl - △ 60°C, pH 3.7  
▲ 30°C, pH 4.7.

## B. Polymeric Flow Distributions in Consolidated Sandstone

### B.1 INTRODUCTION

In order to study the interactions during the flow of reagents through a reservoir, we have selected a virgin Berea sandstone core as the basic matrix. Since the flow distribution is important and since the flow distribution is in fact controlled by the polymeric mobility control agent, we have selected to begin our investigation with a study of the interaction of the polymer within the core. From the output concentration profile, the following information can be derived:

1. From the area of the peak, the total polymer retained in the core (related to retention due to physical processes and adsorption) can be calculated.
2. From the average residence time, the inaccessible pore volume can be calculated in those cases where adsorption is not a problem.
3. From the shape of the peak characterized by the various moments of the residence time distributions, some physical parameters are obtained.

The shape of the output is useful to describe the structure and the physical processes that are occurring in the micro-environments within the porous matrix of the Berea core. We must assume that the change in shape of the pulse injected into the core during its residence in the core is related to the following factors:

1. Within each channel there is local Poiseuille flow, and thus, within a given channel there is a tendency for the solute molecules at the center line to move faster than those next to the walls.
2. There is a distribution in the size of the channels and thus there is a distribution in the average solute velocities in channels of different size.

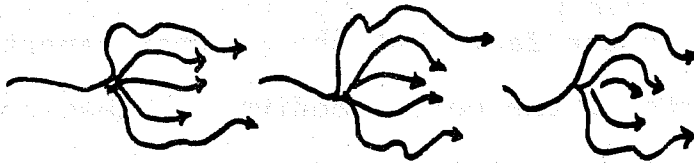
For a given pressure drop, the flow will prefer the larger channels.

3. In addition to the convective terms described, there is molecular diffusion in which solute in regions of high concentration will diffuse into regions of low solute concentration.

These factors tend to spread out the solute pulse that was injected into the core. However, there are other phenomena which must be taken into account.

4. A core is not a series of single capillaries of different sizes. It is a series of channels which converge and diverge in a periodic manner as the flow progresses around and through the granular texture of the conglomerate. Thus, there is mixing of the streams passing through the channels of different flow velocities.
5. Since there is a range of size in the channels, there is for the large polymeric solutes a range of pore regions which are inaccessible due either to a physical exclusion or to a double layer exclusion. It is observed that a high molecular weight poly(acrylamide) is accessible to only about 70 percent of a Berea core under ideal conditions.
6. In the regions in which the polymer can reach (or any other solute for that matter), there is an interaction between the mineral surface and the solute which leads either to a physical retention or to an actual adsorption.

In order to analyze in any rational manner the dynamic data that is obtained from a core experiment, it is necessary to construct a model which contains the elements discussed above. Since we do not know the relative importance of these factors, it is necessary to postulate a model with many parameters in it and devise experiments which permit some evaluation of the magnitude of their effect. In the figure below, we diagram in the simplest sense the converging and the diverging flows which characterize a porous medium.



It is reasonable to consider an array of capillaries of different size (reflecting the permeability distribution and diverging regions) which are connected by a mixing zone (representing the converging points). The physical size of these parameters must be described in terms of available experimental data. This complexity is not warranted if only the shape of a given output is required. However, in the present work we are concerned more with a study of the detailed structure of the various regions of the core. Thus, from many different experimental outputs we will attempt to describe the complex components of a core. This analysis will ultimately permit the analysis of binary interactions between solutes such as polymer-surfactant. At present, we do not easily expect to be able to introduce two-phase flow and the surface tension effects associated with the actual flooding operation.

## B. 2 EXPERIMENTAL DEVELOPMENT

### B.2.a Background

#### B.2.a.1 Polymer Flooding

Investigators have conducted laboratory experiments for core floodings.<sup>31,32,33</sup> Economic, process, and operational difficulties have been recognized in connection with polymer flooding. Not all the polymer that is injected is recovered. This phenomenon was attributed to adsorption by some authors who studied static polymer adsorption on solid surfaces.<sup>34,35,36</sup> Polymer loss may also be

due to retention in the pores.<sup>37,38</sup> The second problem associated with polymer flooding is the fact that the polymer cannot penetrate into certain parts of the porous medium.<sup>39</sup> These constricted regions are termed the inaccessible pore volume (IPV). The oil trapped in the IPV (about 20-30 percent of the total pore volume) will not be driven by the micellar-polymer flood. The third problem with the polymer is its plugging some porous space in the reservoirs, its degrading due to shearing, scission, or thermal and/or bacterial attack.

#### B.2.a.2 Porous Media

Permeability, which is a measure of the fluid conductivity, is one of the most important characteristics of porous media.

Darcy was the first investigator to study the permeability effect in water purification.<sup>40</sup> Darcy's law is:

$$\frac{Q}{A} = \frac{k}{\mu} \times \frac{\Delta P}{L} \quad (1)$$

where

- k = permeability constant of the medium
- Q = flow rate
- A = cross-sectional area
- $\Delta P/L$  = pressure gradient
- $\mu$  = viscosity of the fluid

The permeability unit is a "darcy" (in length squared) which defines the case of a fluid with a viscosity at one centipoise moving across a 1 cm<sup>2</sup> with a flow rate of 1 cm<sup>3</sup>/sec under 1 atm/cm pressure gradient.

Kozeny<sup>41</sup> developed another expression for k as he assumed that the porous medium consisted of an array of parallel

capillaries. Muskat<sup>42,43</sup> adapted the equation of continuity and the equations of motion for porous media. Numerous authors have investigated the continuous permeability distributions within a single porous medium, i.e., sandstone cores.<sup>44,45,46</sup>

### B.2.a.3 Residence Time Distributions

Danckwerts<sup>47</sup> was one of the first investigators who studied residence time distributions through tracer experiments. The total tracer eluting by a carrier solvent is given as:

$$T_{out} = \int_0^{\infty} Q C_{out} dt \quad (2)$$

where  $C_{out}$  is the exiting concentration and  $Q$  is the flow rate. The average residence time is defined as the first moment of the exit age distribution, or,

$$\bar{t}_{conc} = \frac{\int_0^{\infty} t C_{out} dt}{\int_0^{\infty} C_{out} dt} \quad (3)$$

The variance ( $\sigma^2$ ) about the mean is the difference between the second moment of the exit age distribution and the square of the mean residence time.

### B.2.b Apparatus

The system, given in Figure 8, is modified liquid chromatography where a packed column is replaced by a consolidated Berea sandstone core (2" diameter and 10" long). Solutes that are injected into the core by an injection valve are eluted through the continuously pumped salt solution. The transient concentration is monitored by a differential refractometer and the output signal

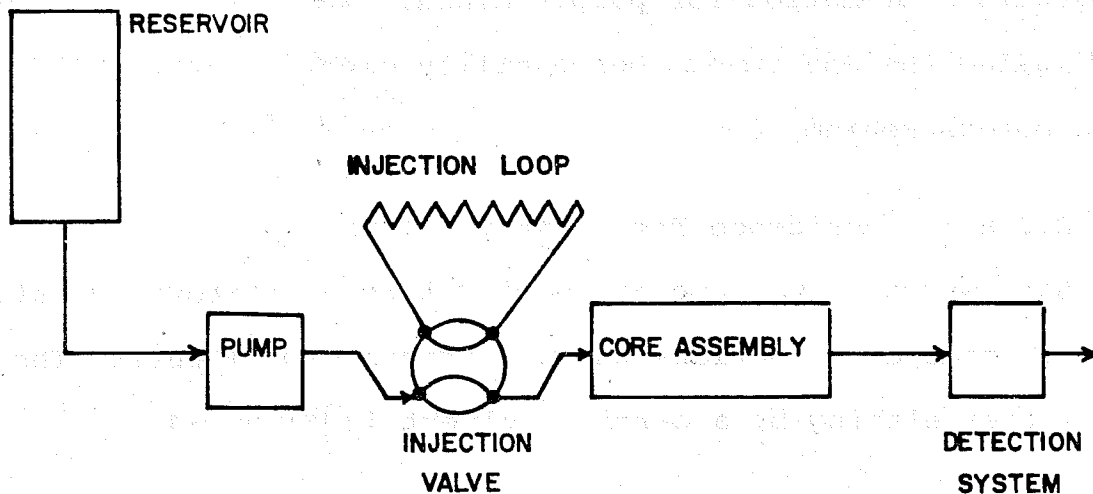


Figure 8 Schematic Representation of Experimental System (49).

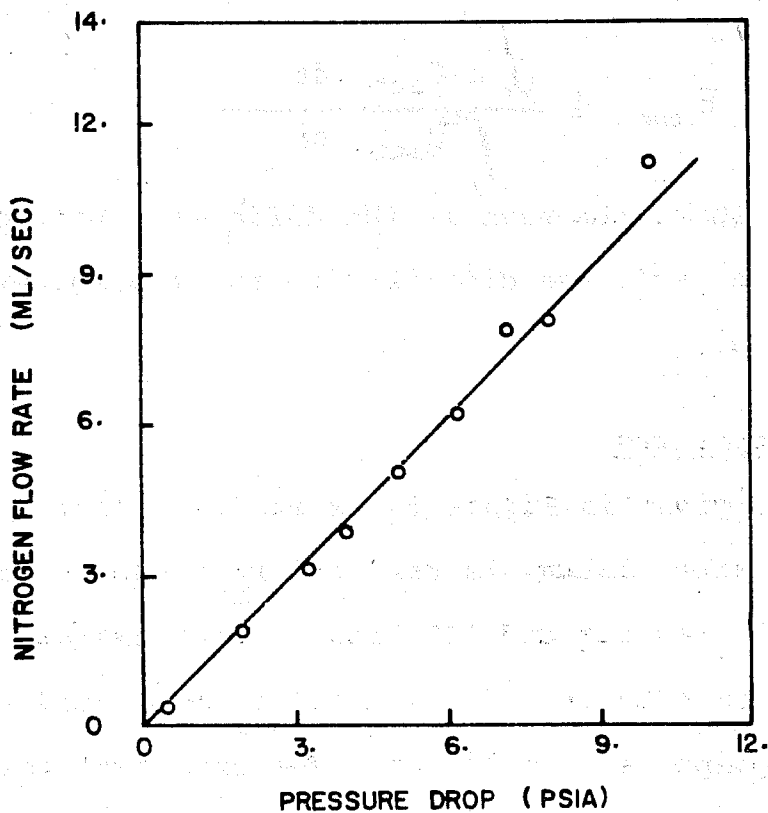


Figure 9 Core Permeability Test with Nitrogen Gas (49) Berea Sandstone, 333 millidarcy.

is plotted on a strip chart recorder. Thus, the indicator dilution technique is applied to study adsorption and dynamic flow through porous media. For a more detailed review of the experimental design, the reader is referred to the Annual Report of July 1978.<sup>48</sup>

#### List of Apparatus

Solvent reservoir  
Pump (Instrumentation Specialties Company)  
Injection valve (Glenco Scientific, Incorporated)  
Core assembly (Berea sandstone core: Cleaveland Quarries Company; aluminum holder: machined in Chemical Engineering Shop)  
Differential refractometer (Laboratory Data Control)  
Strip-chart recorder (Leeds and Northrup)  
Constant temperature circulatory bath

#### B.2.c Experiments

The experiments described here were conducted initially by Dick Jung,<sup>49</sup> who was an M.S. student and my predecessor on the project.

##### B.2.c.1 Calibration

The individual instruments were calibrated in order to convert output signals into concentration units. Details are to be found in the Annual Report of July 1978.<sup>48</sup>

##### B.2.c.2 Characterization of the Core

###### B.2.c.2.a Permeability

The volumetric flow rates of nitrogen through the core at low pressure drops were measured and plotted (Fig. 9). The average permeability of the core was calculated (Eq. 1)<sup>40</sup> from the slope of this plot through linear regression.

### B.2.c.2.b Total Pore Volume

After the core was evacuated, it was saturated with a saline solution (1996 ppm NaCl in distilled water). The amount of salt solution that penetrated the core was measured volumetrically and compared to the value obtained from the weight difference of the core before and after saturation. The latter is known as the imbibition method.<sup>50</sup>

### B.2.c.3 Dynamic Flow through the Core

#### B.2.c.3.a Sucrose Runs

1.39 ml of a solution consisting of 4990 ppm sucrose in 1996 ppm NaCl solution was injected into the core and the concentration as a function of time was continuously recorded. These runs served two purposes. The pore volume was obtained from the following equation:

$$\bar{V} = \bar{t} Q \quad (4)$$

where  $Q$  is the flow rate and  $\bar{t}$  is the mean residence time calculated from Eq. (3) in which the experimental concentration profile is substituted. The integrals are approximated by the trapezoidal rule. Percent solute recovery was calculated from:

$$\% \text{ Recovery} = \frac{(100) T_{\text{out}}}{T_{\text{in}}} \quad (5)$$

where  $T_{\text{out}}$  is obtained from Eq. (2) and  $T_{\text{in}}$  is the total solute injected:

$$T_{\text{in}} = Q C_o t_{\text{inj}}$$

where  $C_0$  is the initial concentration and  $t_{inj}$  is the time interval for injection.

The pore volume  $\bar{V}$  was very close to the total pore volume measured above. % Recovery was very high. Thus, since sucrose behaved like an ideal tracer, the experimental concentration profiles could be compared to the proposed model (Section B.3) results.

#### B.2.c.3.b Polymer Runs

1.39 ml of a poly(acrylamide) solution (2120 ppm in 1996 ppm NaCl solution) was injected into the core and the concentration was plotted continuously on the strip chart recorder. The accessible pore volume was calculated from Eq. (4),  $V_{acc} = \bar{V}$  polymer. The percentage of inaccessible pore volume (IPV) was:

$$IPV\% = \frac{V - V_{acc}}{\bar{V}} \quad (100) \quad (6)$$

where  $\bar{V}$  was obtained from the sucrose runs. The total amount of polymer recovered could be approximated from Eq. (5). Therefore, these experiments allowed the calculation of the IPV and amount of polymer adsorbed. By incorporating these parameters into the model (Section B.2), theoretical and experimental results can be compared.

#### B.2.d Results and Discussion

##### B.2.d.1 The Total Pore Volume

The total pore volume ( $V_p$ ) was measured to be  $108 \pm 2$  ml. This volume is compared to the pore volume ( $\bar{V}$ ) obtained from the mean residence time of a tracer (i.e., sucrose).

TABLE I  
Sucrose Run 149

t (min)	C (ppm)	$\frac{C}{C_{MAX}}$	$\frac{t}{T}$
149.67	0.0	0.0	0.604
159.67	0.81	0.00692	0.645
169.67	17.2	0.147	0.685
179.67	44.9	0.384	0.725
189.67	76.9	0.657	0.766
199.67	92.1	0.787	0.806
209.67	102.8	0.879	0.846
219.67	113.4	0.969	0.887
229.67	117.0	1.000	0.927
239.67	114.9	0.982	0.968
249.67	110.4	0.944	1.008
259.67	104.3	0.891	1.048
269.67	95.2	0.814	1.089
279.67	83.0	0.709	1.129
289.67	67.8	0.579	1.169
299.67	52.5	0.449	1.210
309.67	44.9	0.384	1.250
319.67	34.1	0.291	1.291
329.67	28.0	0.239	1.331
339.67	20.3	0.174	1.371
349.67	12.5	0.107	1.412
359.67	6.31	0.0539	1.452
369.67	3.18	0.0272	1.492
379.67	0.0	0.0	1.533

Q = 25 ml/hr  
 Dose = 1.39 ml of 4990 ppm solution  
 RI Scale "2", 20 mv F.S.  
 $C_{MAX}$  = 117 ppm  
 $T$  = 247.7 minutes  
 $V_{access}$  = 103.5 ml  
 Recovery of solute injected = 80.5%

TABLE II  
Polymer Run 149

t (min)	$\frac{C}{C_{MAX}}$	$\frac{t}{T}$
405	0.0	0.457
455	0.0526	0.513
505	0.187	0.569
555	0.330	0.626
605	0.391	0.682
655	0.534	0.738
705	0.717	0.795
755	0.869	0.851
805	1.000	0.907
855	0.889	0.964
905	0.848	1.020
955	0.798	1.077
1005	0.686	1.133
1055	0.534	1.189
1105	0.503	1.246
1155	0.330	1.302
1205	0.269	1.358
1255	0.228	1.415
1305	0.197	1.471
1355	0.177	1.528
1405	0.0421	1.584
1455	0.0	1.640

Q = 5 ml/hr  
 Dose = 1.39 ml of 2120 ppm solution  
 RI Scale "2", 5 mv F.S.  
 $C_{MAX}$  = 38.0 ppm  
 $T$  = 38.0 ppm  
 $V_{access}$  = 73.9 ml (IPV = 28.4%)

TABLE III  
Experimental Results

Solute	Flow Rate (ml/hr)	Dose Volume for S (ml)	$V_{acc}$ for P (ml)	IPVZ for P	Retention Volume (ml)	Z Recovery
S	25	103.5	-	-	62.4	80.5
S	25	102.3	-	-	55.0	97.2
S	10	110.3	-	-	63.7	109.0
S	35	117.4	-	-	61.7	100.2
S	20	108.7	-	-	55.0	102.8
S	5	103.2	-	-	64.7	102.5
P	5	-	73.9	28.4	33.8	51.4
P	5	-	66.7	35.4	16.5	45.5
S	5	93.9	-	-	45.9	72.6
P	5	-	40.8	60.0	4.2	33.5

S = Sucrose (4990 ppm)

P = Polymer (2120 ppm)

#### B.2.d.2 Average Porosity and Permeability

The average porosity ( $\bar{\phi}$ ) is  $V_p/V_B$ <sup>52</sup> where  $V_B$  is the bulk volume measured from geometrical dimensions in this case.  $\bar{\phi}$  is calculated to be 0.21. The average permeability ( $\bar{k}$ ) from Darcy's law was  $333 \pm 5$  md. Both the porosity and permeability are significant parameters characterizing a consolidated Berea sandstone core. Porosity and permeability distributions for porous material have been obtained in the literature.<sup>46,50</sup> The permeability as a function of porosity can be representative of a flow distribution as well.<sup>46</sup> Thus, the mean values obtained experimentally can be compared to mean values obtained from distributions of actual field studies.

#### B.2.d.3 Sucrose Runs

A typical sucrose run data is presented in Table I. The summary of the calculated results are given in Table III. The retention volume is defined as the initial value of the volume increment where the solute can be first detected. The average pore volume of the ten runs is  $108 \pm 5$  ml. It can be deduced from this that sucrose flows through all the pores of the core. The average recovery is 96 percent, indicating that there is no significant interaction between the core and sucrose. Thus, the sucrose can be considered an excellent tracer to characterize the flow through the core. The % recovery exceeding 100 percent could be due to inaccuracy of measuring concentration (from the chart paper) due to noise in the input signal. However, when the % recovery is averaged out over a large number of runs, the

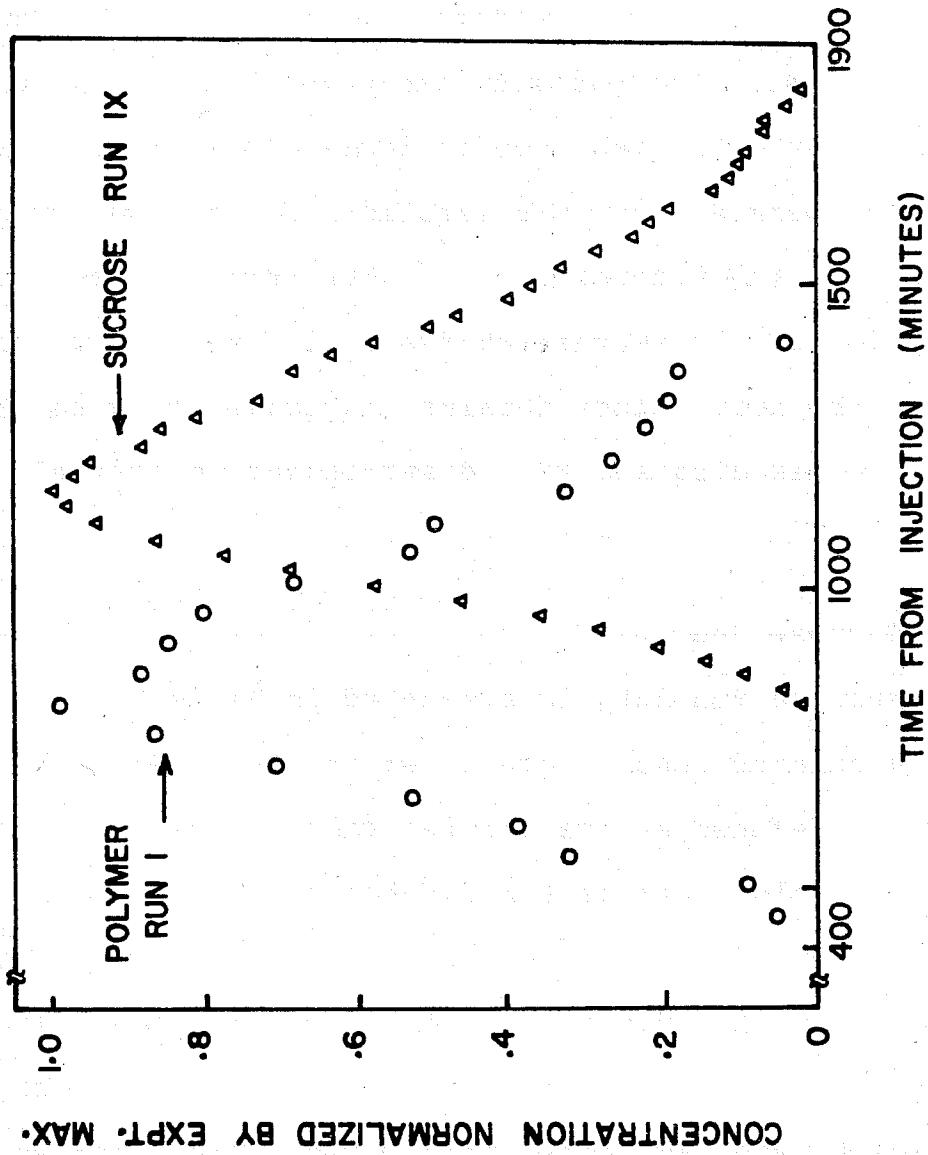


Figure 10 Typical Sucrose and Polymer Core Residence Time Distribution Profiles that Result from Pulse Injection into Berea Core (49)

measurement errors tend to phase out each other. The last run was between two polymer runs. The decrease in the retention volume implies the possibility of the core being partially plugged by the polymer.

#### B.2.d.4 Polymer Runs

Table II represents a typical set of data on polymer runs. Table III gives the summary of results obtained from the polymer runs. The average IPV for the polymer was 32.4 percent (based on  $\bar{V} = 103.2$  ml). This result is in excellent agreement with reported values.<sup>47,48,49,51</sup> There is a trend of decreasing accessible volume and retention volume for the chronological polymer runs. The last sucrose run yielded a low recovery, probably due to entrapment of sucrose in pores plugged by the polymer.

In Fig. 10, the polymer and sucrose are plotted on the same set of coordinates. Concentration is dimensionalized by the maximum value. The polymer eluting sooner than the sucrose is consistent with the idea of inaccessible pore volume. However, the two curves are quite superimposable. This implies that the core has a consistent porosity and permeability distribution, even though there are small pores which the polymer cannot penetrate due to steric hindrance.

### B.3 MODEL DEVELOPMENT

#### B.3.a Background

Investigators have developed theoretical models describing transport through porous media. Three major trends in these developments can be detected. The first type of design is known

as the capillary bundle model.<sup>50</sup> The second and third types of considerations can be divided as diffusional and mixing cell models.

In the capillary bundle model, the porous medium consists of an array of parallel tubes of varying sizes.<sup>41</sup> Each tube can represent a different permeability. The bundle as a whole displays an average permeability representing the entire medium. The capillary model has been modified by various investigators.<sup>52,53,54</sup> This model has been quite recently applied to an actual oil field consisting of various horizontal rock permeabilities.<sup>55</sup>

The diffusional models make use of the equation of continuity.<sup>56</sup> Plug flow with constant physical properties is assumed and the reaction terms are omitted since inert tracers are used. From the equation of continuity, the transient concentration functions which are the responses to various inputs into consolidated cores are obtained.<sup>57-61</sup> In liquid chromatography, where this approach has been used, analogous profiles are given for unconsolidated packing.<sup>52</sup>

In the mixing cell models, networks of ideal CFSTRs are arranged in series and/or in parallel. The first model consists of a series of CFSTRs.<sup>57,61</sup> Other investigators have modified this arrangement to include stagnant regions.<sup>62-66</sup> Levich<sup>65</sup> also compares the equations obtained from diffusional and mixing models. Rogers and Gradner<sup>67</sup> developed a model consisting of finite stages with a repeating unit in which there are two interconnected (one of which incorporates stagnant regions) CFSTRs in series with a plug flow tank.

### B.3.b Mathematical Development

#### B.3.b.1 Analytical Solution

The original model was proposed by Jung and Gryte.<sup>49</sup> The core consists of M number of repeating units. The repeating unit consists of two capillary bundle sections connected by a mixing chamber. All the chambers are CFSTRs. The input flow is split by a hypothetical zero volume splitter block in analogy to a physical divergent flow around solid regions. The two capillary bundles each consist of N number of parallel mixing chambers which are accessible to polymer flow. In addition, as Dawson and Lantz proposed, a core consists of constricted pores inaccessible to the polymer.<sup>39</sup> These regions are also incorporated into the capillary bundles. The flows exiting the capillary chambers are joined in a zero volume hypothetical adder block unit. This is analogous to intersecting and instantaneously mixing streams. The existing stream from the adder enters an actual mixing chamber, which can incorporate radial or prolonged mixing. This unit has a physical significance, since all streams will mix eventually before exiting. In all the chambers, the adsorption is assumed to be a homogeneous reaction governed by Henry's Law for dilute solutions.

The transfer function for the core consisting of M repeating units in series is derived as:<sup>39</sup>

$$\frac{\hat{C}_{out}}{\hat{C}_{in}} = \left[ \frac{A_1}{s + g_1} + \frac{A_2}{s + g_2} \right]^{2M} \frac{\delta^M}{(s + b)^M} \quad (7)$$

where  $A_i = \frac{Q_i/Q}{V_i/Q_i}$

$g_i = \frac{Q_i}{V_i} + k_{ads}$

$\delta = Q/V_M$

$b = Q/V_M + k_{ads}$

$\hat{C}_{out}, \hat{C}_{in}$  = the concentration profiles in the Laplace domain of the streams exiting from the last stage and entering the first stage, respectively.

In the original model, there are two parallel chambers besides the inaccessible pore volume. This repeating unit is given in Fig. 11.<sup>39</sup> The input function, approximated as the unit impulse function, has the following Laplace transform,

$$\hat{C}_{in} = \hat{C}_o t_{inj} \quad (8)$$

where  $C_o$  = the initial concentration

$t_{inj}$  = the time of injection

(This approximation is valid since  $t_{inj} \sim 17$  minutes, while the width of the response is about 1000 minutes. Recall Fig. 10.)

In the previous work, this Laplace transform was inverted analytically, making use of the binomial expansion, the convolution theorem, and incomplete  $\gamma$  functions. The final exiting concentration profile in dimensional form was obtained as:<sup>39</sup>

$$C_{out} = C_0 \tau_{inj} \delta^M \sum_{j=0}^{M-1} \frac{(-1)^j \tau^{M-1-j} e^{-bt}}{(M-1-j)! j!} \left\{ \sum_{l=1}^{2M-1} \frac{(2M)! A_1^{2M-l} A_2^l}{(2M-l)! l! (l-1)!} \right. \quad (9)$$

$$\left[ \sum_{k=0}^{2M-l-1} \frac{(-1)^k}{(2M-l-1-k)! k!} \left( \frac{(l+k-1)!}{(g_2-g_1)^{l+k}} \frac{\gamma(2M-k-l+j, (g_1-b)\tau)}{(g_1-b)^{2M-k-l+j}} \right. \right.$$

$$\left. \left. - \sum_{r=0}^{l+k-1} \frac{(l+k-1)!}{(l+k-1-r)!} \frac{\gamma(2M-r+j-1, (g_2-b)\tau)}{(g_2-g_1)^{r+1} (g_2-b)^{2M-r+j-1}} \right) \right] + \frac{A_1^{2M} \gamma(2M+j, (g_1-b)\tau)}{(2M-1)! (g_1-b)^{2M+j}}$$

$$+ \left. \frac{A_2^{2M} \gamma(2M+j, (g_2-b)\tau)}{(2M-1)! (g_2-b)^{2M+j}} \right\}$$

where  $\gamma$  is the incomplete  $\gamma$  function.

Due to the complexity of this function, it was not possible to simulate the output in the computer efficiently within the given time limitation. Therefore, we have investigated alternate ways of computing the concentration time function by inverting the following expression:

$$\mathcal{L}[c(t)] = \hat{C}_{out} = \hat{C}_{in} \int_0^{\infty} e^{-st} c(t) dt \quad (10)$$

### B.3.b.2 Numerical Solution

The Laplace transform is inverted numerically by adapting Seinfeld's and Lapidus's<sup>68</sup> revised version of Piessen's algorithm.<sup>69</sup> The Legendre-Gauss quadrature is applied to approximate the Laplace integral. Furthermore, the Vandermonde coefficient matrix is inverted using the method which was developed by Bellman et al.,<sup>70</sup> and later modified by Piessens. A more detailed discussion can be

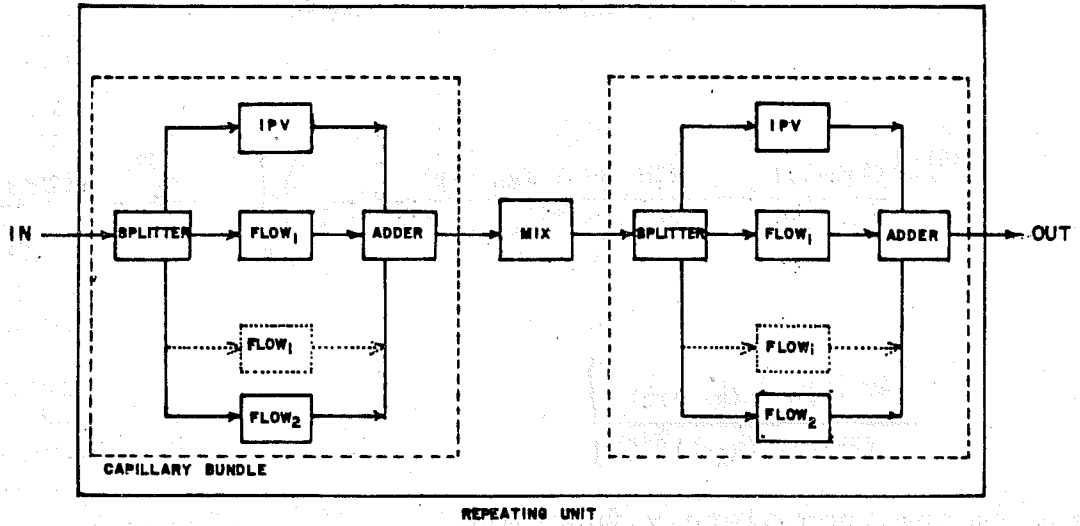


Figure 11 Schematic Representation of Repeating Unit for Proposed Model of Core Transport (49).

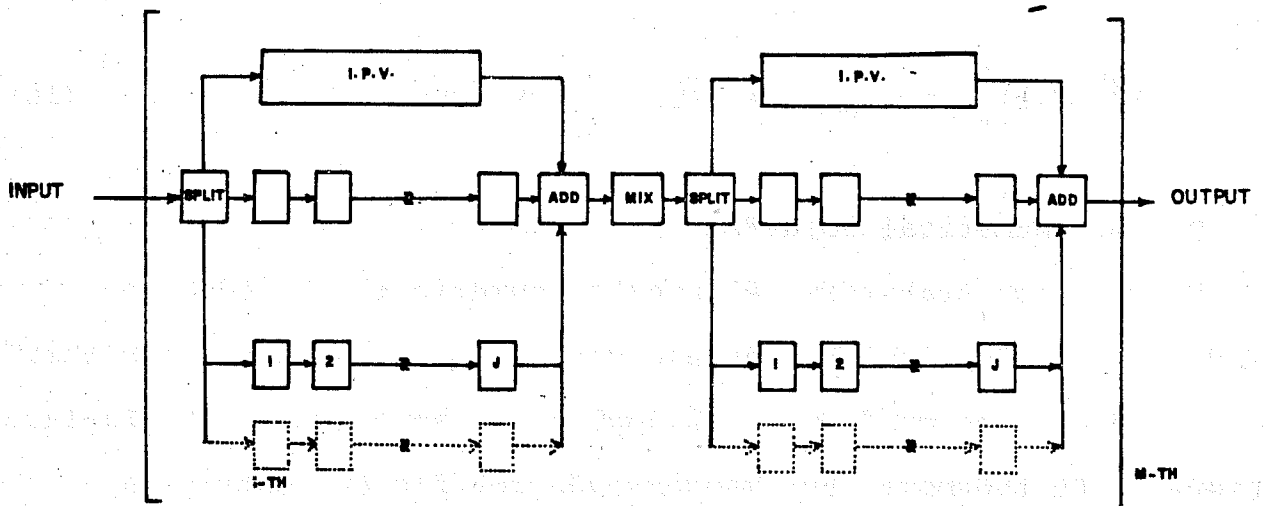


Figure 12 Modified Repeating Unit wherein Series CFSTR Units Simulate Capillary Plug Flow.

found in the doctoral proposal presented in May, 1979.<sup>71</sup> The readers are also referred to Carnahan<sup>72</sup> and Seinfeld<sup>68</sup> for further information on the development of this approach.

### B.3.b.3 Modification

With the numerical solution, the model can be modified to yield a more realistic approach to the actual determination of the physical situation.

The first modification is the replacement of single parallel mixers in the capillary bundle element with several mixers in series, as shown in Fig. 12. The specific case tried was ten mixers in series, and two of these series in parallel in addition to the inaccessible pore volume. The results related to this modification are given in Section B.3.c (Fig. 21). The adsorption in the pores takes place along the length of the pores. By incorporating quite a few mixers in series, the plug flow reactor is approached. The flow rate is constant and if the mixers are assumed to be of equal volume, no new critical parameters are introduced into the model.

The number of the parallel flow chambers can be increased to modify the radial dispersion of the branching streams. However, with each parallel chamber, two new parameters - namely, the volume of the chamber and the flow rate associated with it - are introduced. Therefore, a method should be devised to estimate the parameters before modifications increasing the number of unknown variables are incorporated into the model.

### B.3.b.4 Estimation of Parameters

In order to obtain a good correlation between experimental and theoretical results, the parameters have to be optimally selected. The parameters of the model may be grouped in three categories: (1) the experimental set or determined parameters, (2) estimated parameters by optimization, and (3) calculated parameters by solving identity functions. The technique in approximating the parameters in the second category will be adapted from the recent work of Rogers and Gardner.<sup>67</sup>

All the parameters and the way they are obtained are summarized in Fig. 13. The original model has the following parameters: flow rates ( $Q$ ,  $Q_1$ ,  $Q_2$ ), holdups ( $V_1$ ,  $V_2$ ,  $V_M$ ), and the number of stages  $M$ . First of all,  $Q$  is experimentally fixed, and  $V_T$  is the total pore volume which can be determined from the experimental concentration profile. From identity relationships:

$$Q = Q_1 + Q_2 \quad (11)$$

and

$$V_T = M V_M + 2 M V_1 + 2 M V_2 \quad (12)$$

Furthermore, the standard deviation for the model can be shown to be:<sup>49</sup>

$$\sigma^2 = - \frac{(2MV_1 + 2MV_2)^2}{2Q^2M} + \frac{1}{MQ} \left\{ \frac{(2MV_1)^2}{Q_1} + \frac{(2MV_2)^2}{Q_2} \right\} + \frac{V_M^2}{MQ^2} \quad (13)$$

Eq. 13 is an inequality constraint because  $\sigma^2$  cannot be less than zero. The ratio of the total volume of the mixing chambers to the total volume of the capillary bundle chambers approaches a very high value for high  $M$  values to meet this criterion. Thus,

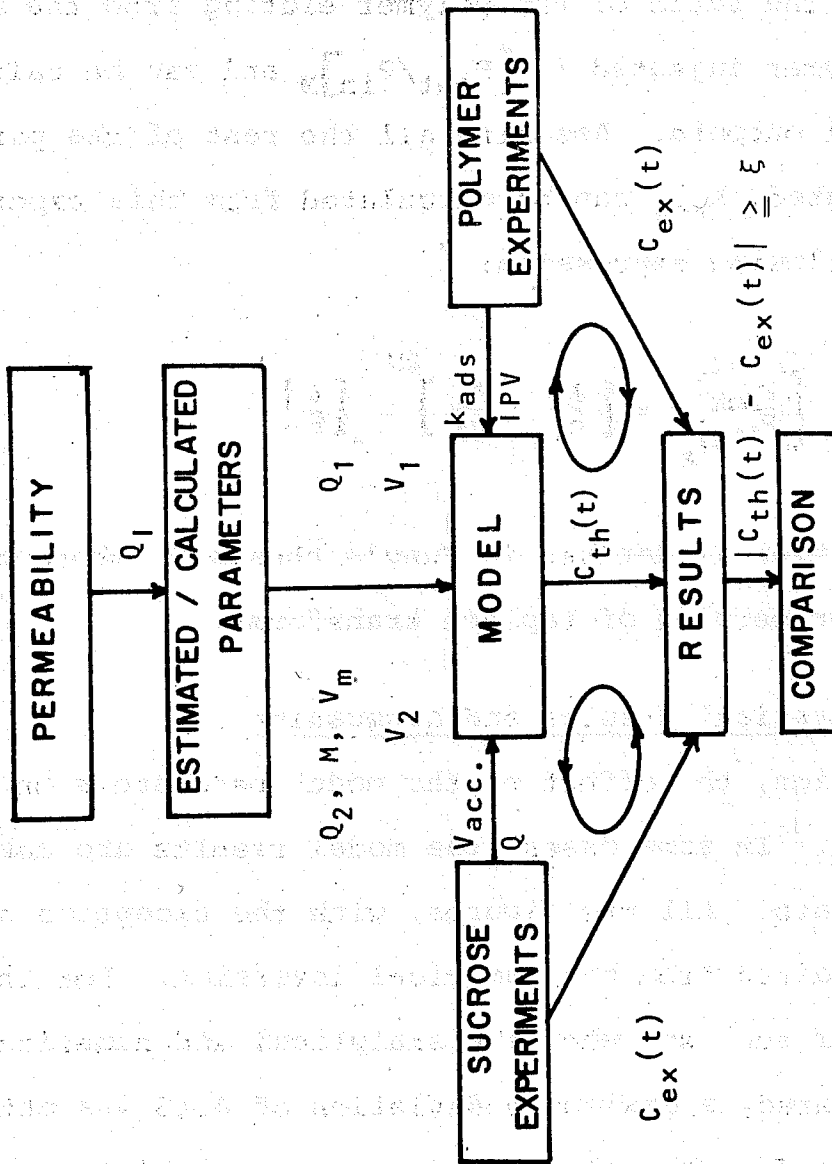


Figure 13 Informational Flow Diagram Relating the Experimental Results to the Core Model.

although parameters like  $M$ ,  $Q_1$ ,  $V_1$ , and  $V_M$  are to be optimized, still  $V_1$  and  $V_M$  are not independent. In the case of polymer runs, the additional parameters,  $k_{ads}$  and  $IPV\%$ , can be determined from experimental results.  $IPV\%$  was described earlier in the experimental section. The ratio of the polymer eluting from the  $M$ th stage to the polymer injected is  $\left[ \frac{P_{out}}{P_{in}} \right]_M$  and can be calculated from experimental outputs. Assuming all the rest of the parameters are estimated,  $k_{ads}$  can be calculated from this experimental ratio and the following expression:

$$\left[ \frac{P_{out}}{P_{in}} \right]_M = \left[ \frac{A_1}{g_1} + \frac{A_2}{g_2} \right]^{2M} \left[ \frac{\delta}{b} \right]^M \quad (14)$$

An analogous equation is derived in Jung's thesis,<sup>49</sup> where he has made use of the properties of Laplace transforms.

### B.3.c Theoretical Results and Discussion

In this section, the effect of the model parameters on the output is studied. In some cases, the model results are compared to experimental data. All the figures, with the exception of Fig. 24, were obtained from the numerical inversion. For the case of nine stages for sucrose when the analytical and numerical results were compared, a maximum % deviation of 0.15 was obtained. The concentrations for the polymer and sucrose solutions are normalized by the corresponding experimentally determined maxima. However, the time is dimensional.

The effect of number of repeating units  $M$  is given in Fig. 14. As  $M$  increases, the maximum concentration increases and shifts to

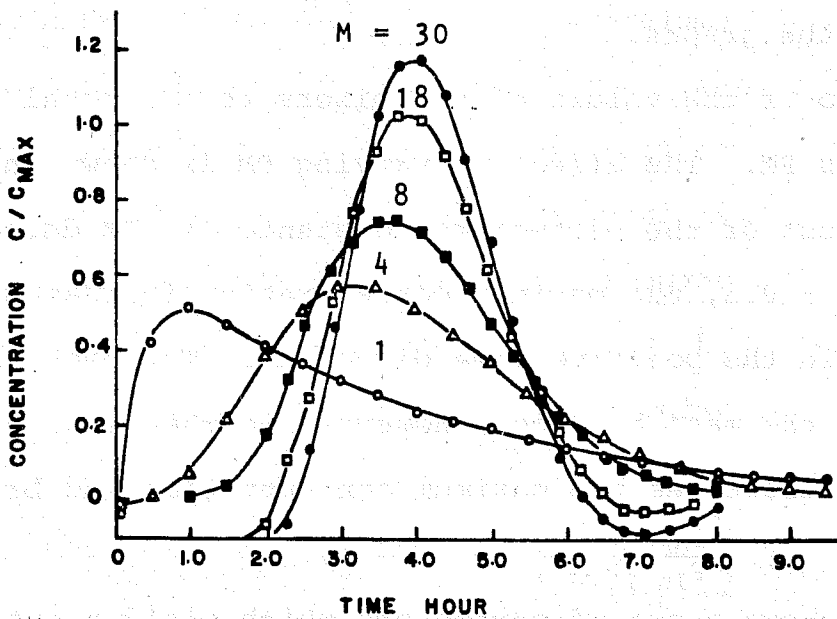


Figure 14 Effect of Number of Stages on Model Predicted Exit Concentration Profile  
 $Q = 25 \text{ ml/hr}$ ;  $Q_1 = 8.5 \text{ ml/hr}$ ;  $PM = 0.9$ .

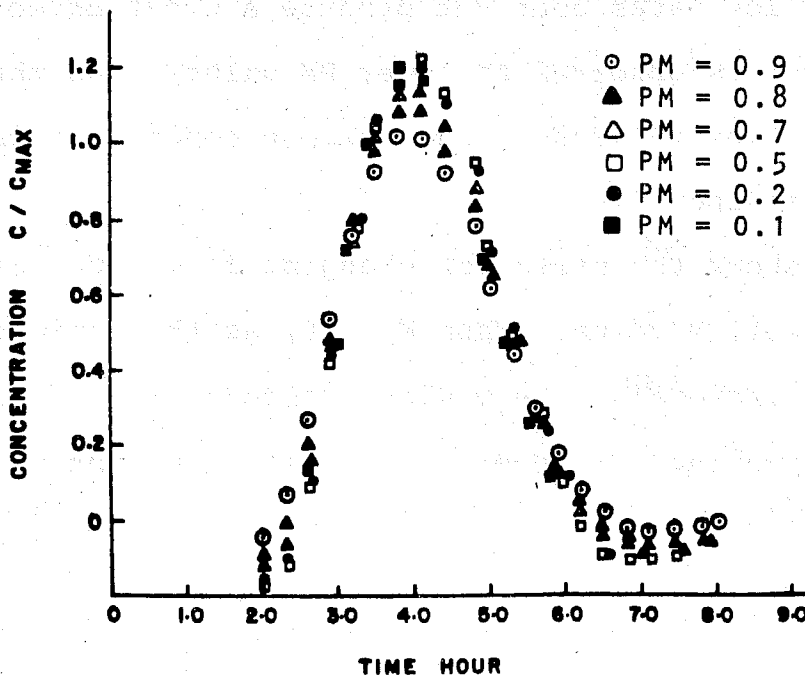


Figure 15 Effect of Mixing Volume Fraction PM on Model  
 $M = 18$ ;  $Q = 25 \text{ ml/hr}$ ;  $Q_1 = 8.5 \text{ ml/hr}$ .

the right on the positive time scale. The peak sharpens to comply with the mass balance. The variables that are kept constant are shown on the graphs.

The ratio of the volume of the mixers to the total volume is represented as PM. The effect of varying PM is shown in Fig. 15, keeping the rest of the parameters constant. As PM decreases in the range 0.9 - 0.5, the maximum concentration increases and moves to the right in the positive time direction. The peak sharpens again to keep the mass balance. However, in the range 0.5 - 0.1, decreasing PM decreases the maximum concentration and broadens the curve.

Fig. 16 shows a set of parameters which yield a good fit in comparison to the experimental data. At  $M = 18$ , no effect of flow rates into individual chambers is depicted.

Fig. 17 represents a combination of effects. As PM decreases, the effect of changing M is diluted. In other words, with small M and PM values, it is also possible to get a good approximation. Changing the flow rates does not produce a great effect; however, a larger change is observed at lower PM values. As the ratio of the two flow rates increases, the maximum concentration increases and the peak sharpens.

Fig. 18 shows the effect of changing flow rates at a different (lower) M value. When  $M = 10$ , as the ratio of the two flow rates is increased, the maximum concentration increases with some peak sharpening. However, the position of the maximum in time remains constant.

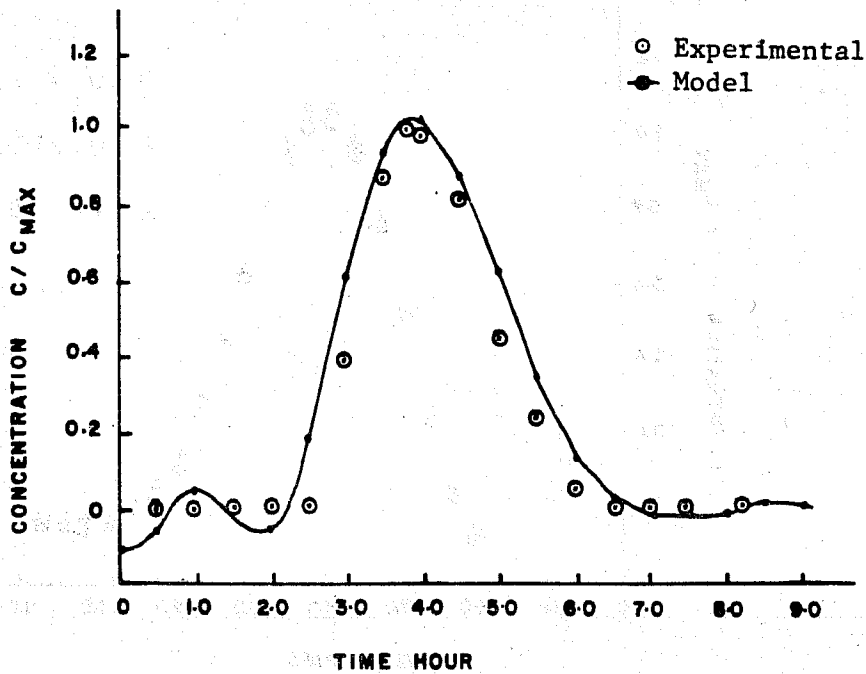


Figure 16 Comparison of Experimental Results and Model Prediction at  $M = 18$ ;  $PM = 0.9$ ;  $Q = 25$  ml/hr;  $Q_1 = 11$  ml/hr.

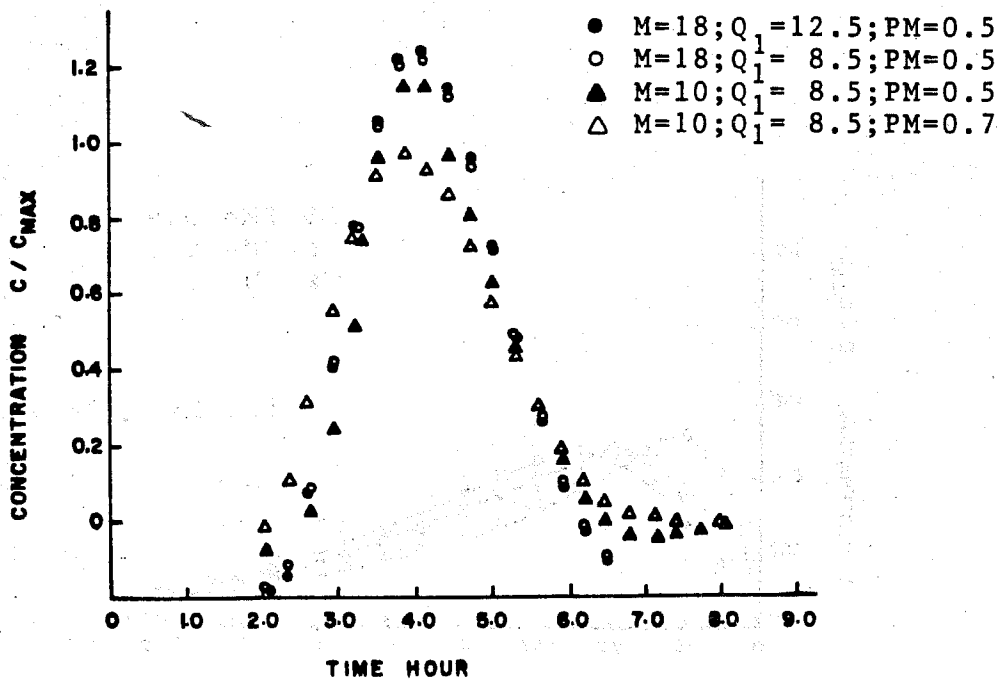


Figure 17 Sensitivity to Model Parameters :  $M$ ,  $Q_1$  and  $PM$ .

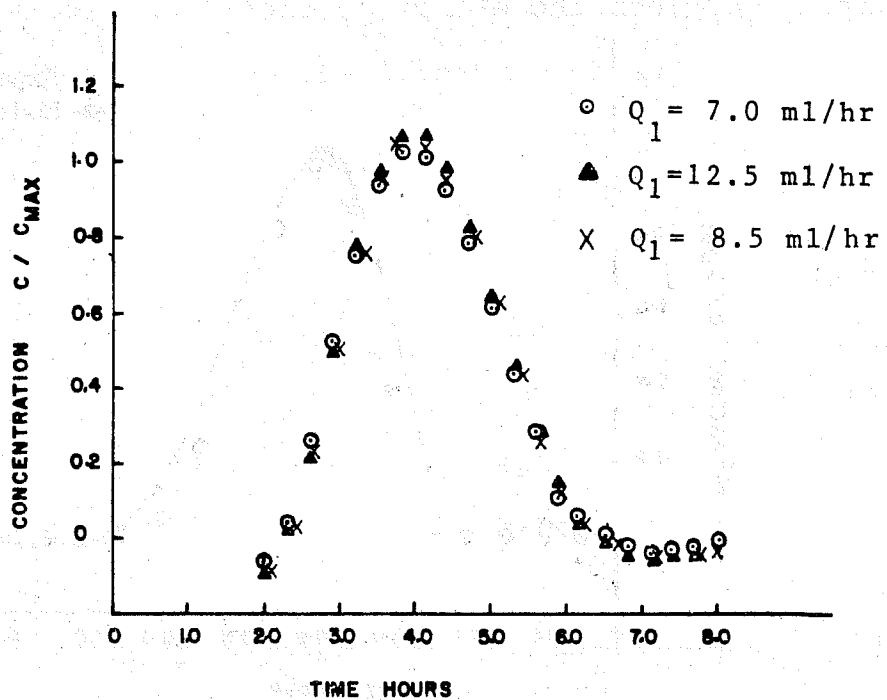


Figure 18 Effect of Flow Rate Distribution on Output for a Model with 10 Stages  
M = 10; PM = 0.5; Q = 25 ml/hr.

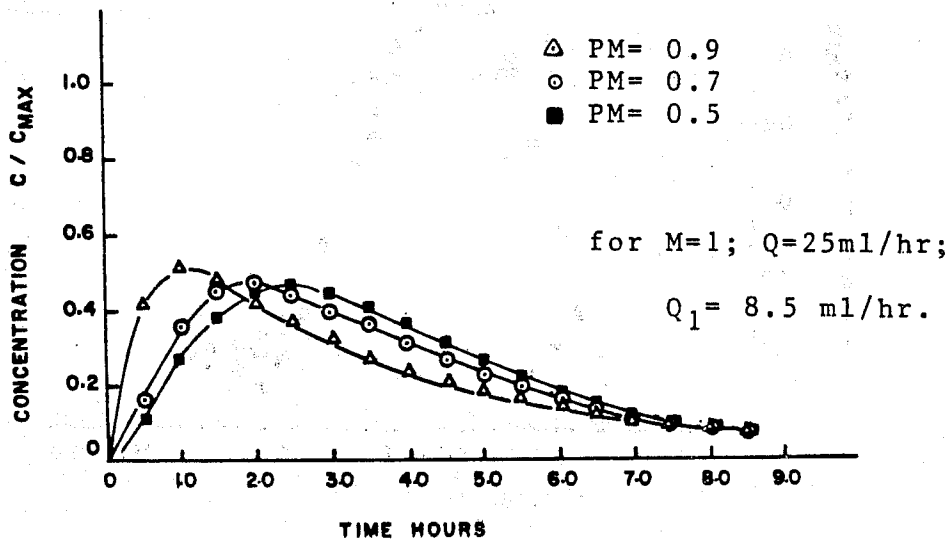


Figure 19 Effect of Mixing Volume Fraction, PM on Output from a Single Stage

Fig. 19 depicts the effect of the model parameters for one stage ( $M = 1$ ). The flow rate effect is within 2 ppm. As the PM value decreases, the maximum concentration decreases and shifts to the right on the time axis. The peak broadens as dispersion increases.

The effect of the parameters of the specific computer program is shown in Fig. 20. A is a parameter changing the amplitude of iterations. As A increases, the oscillating concentrations at the tails of the peak dampen and negative concentrations are thus nulled out. NUM is the order of the approximation for the polynomial in inverting the transform. As NUM decreases, the model profile does not approach the experimental profile.

Fig. 21 introduces a modification into the model. The single parallel capillary chambers are replaced by ten mixers in series. The effects of A and flow rates are studied in comparison to the original model. The new model which approaches plug flow behavior yields a higher maximum, shifted to the right in comparison to the old one. Flow rates do not produce a large deviation. Increasing A causes the dampening of the oscillations.

Fig. 22 is a representation of outputs from cores with varying sizes. The fixed parameters are obtained from a set of results yielding a good fit. The first curve is for a core of one repeating unit; the second, two units; the third, four; the fourth, six; the fifth, eight; and finally, the last curve is for a core with ten repeating units. The signal moves to the right on the positive time scale. The first one is very sharp and very similar to the response of a CFSTR. As M increases, the peaks

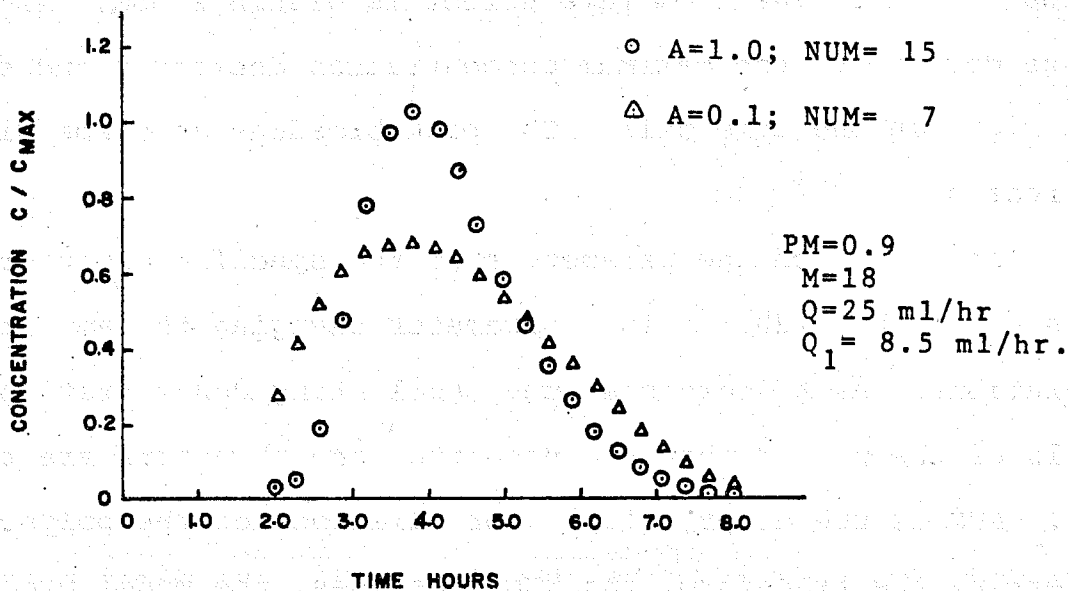


Figure 20 Effects of System Parameters

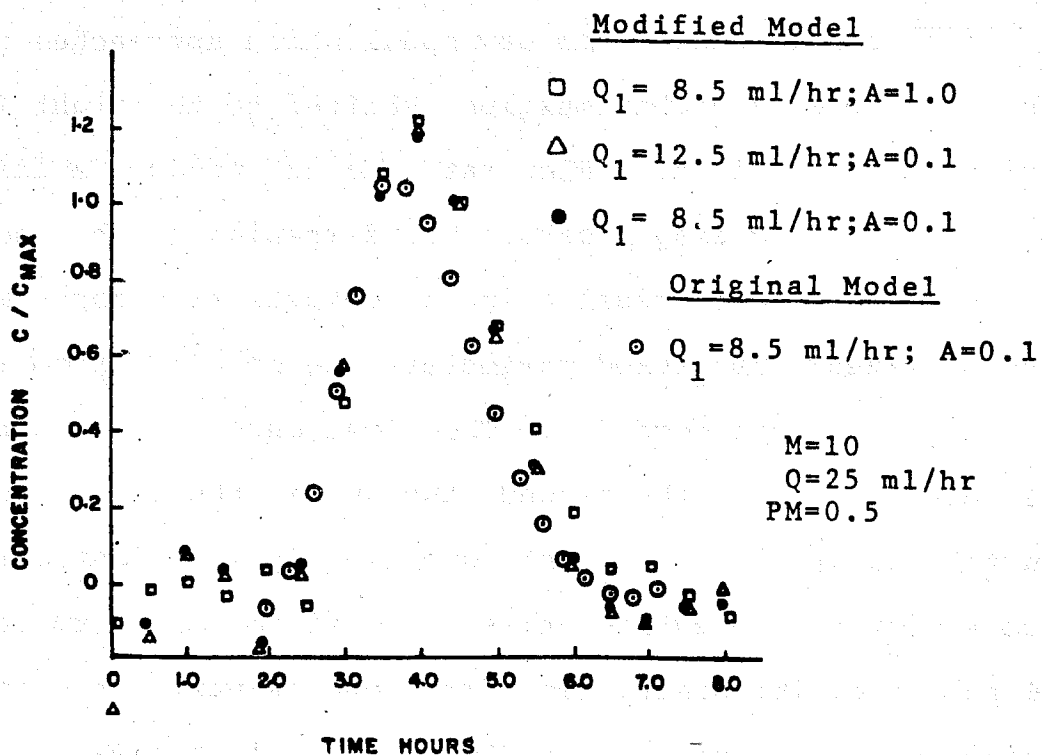


Figure 21 Modified and Original Model Compared

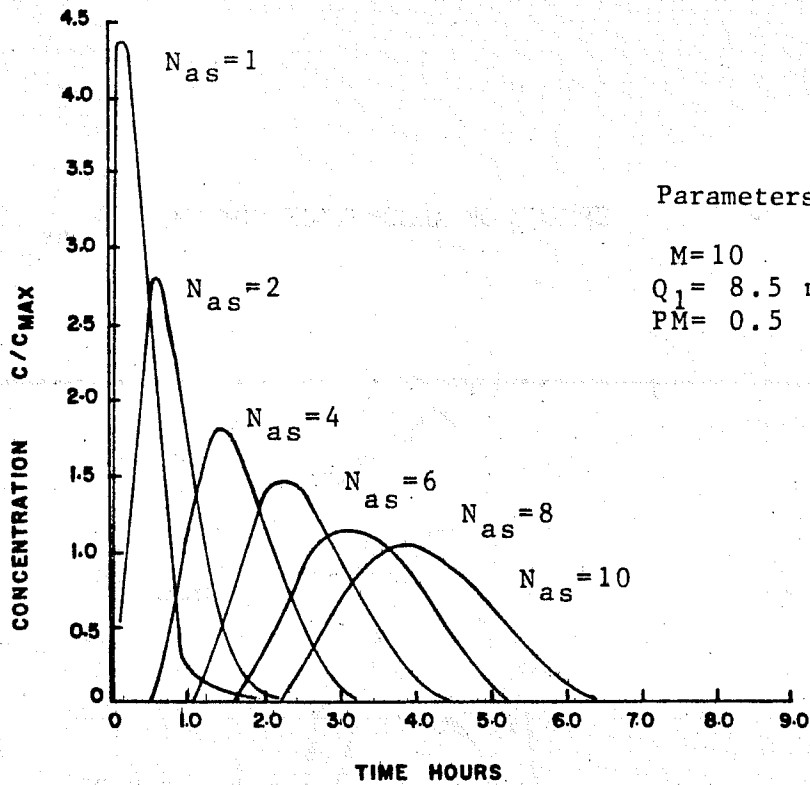


Figure 22 Simulated Output from Cores of Different Length for Pulse Injection of Sucrose.

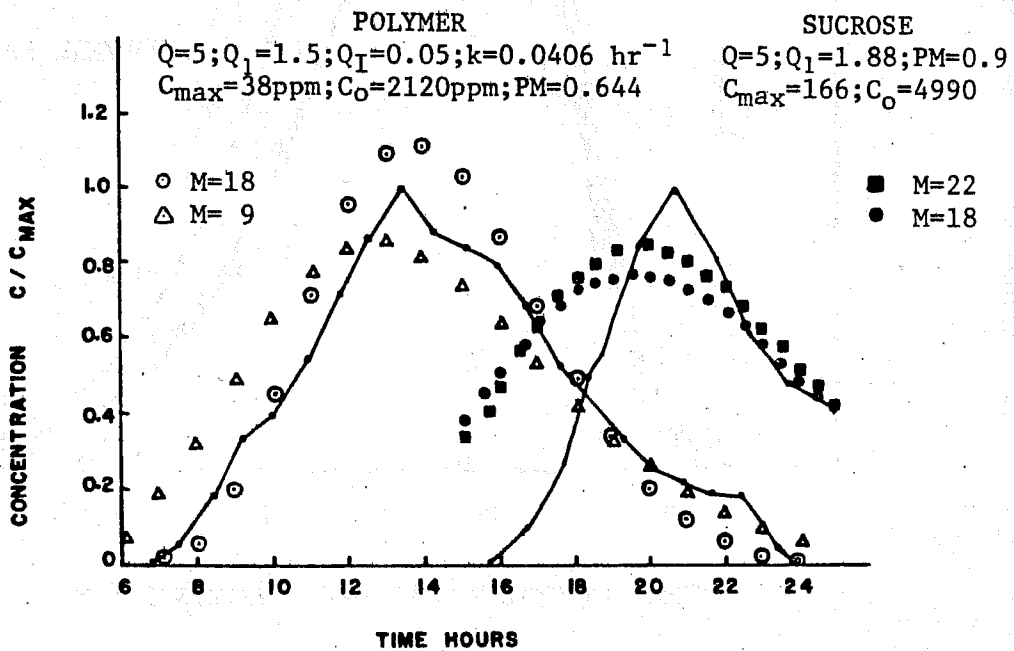
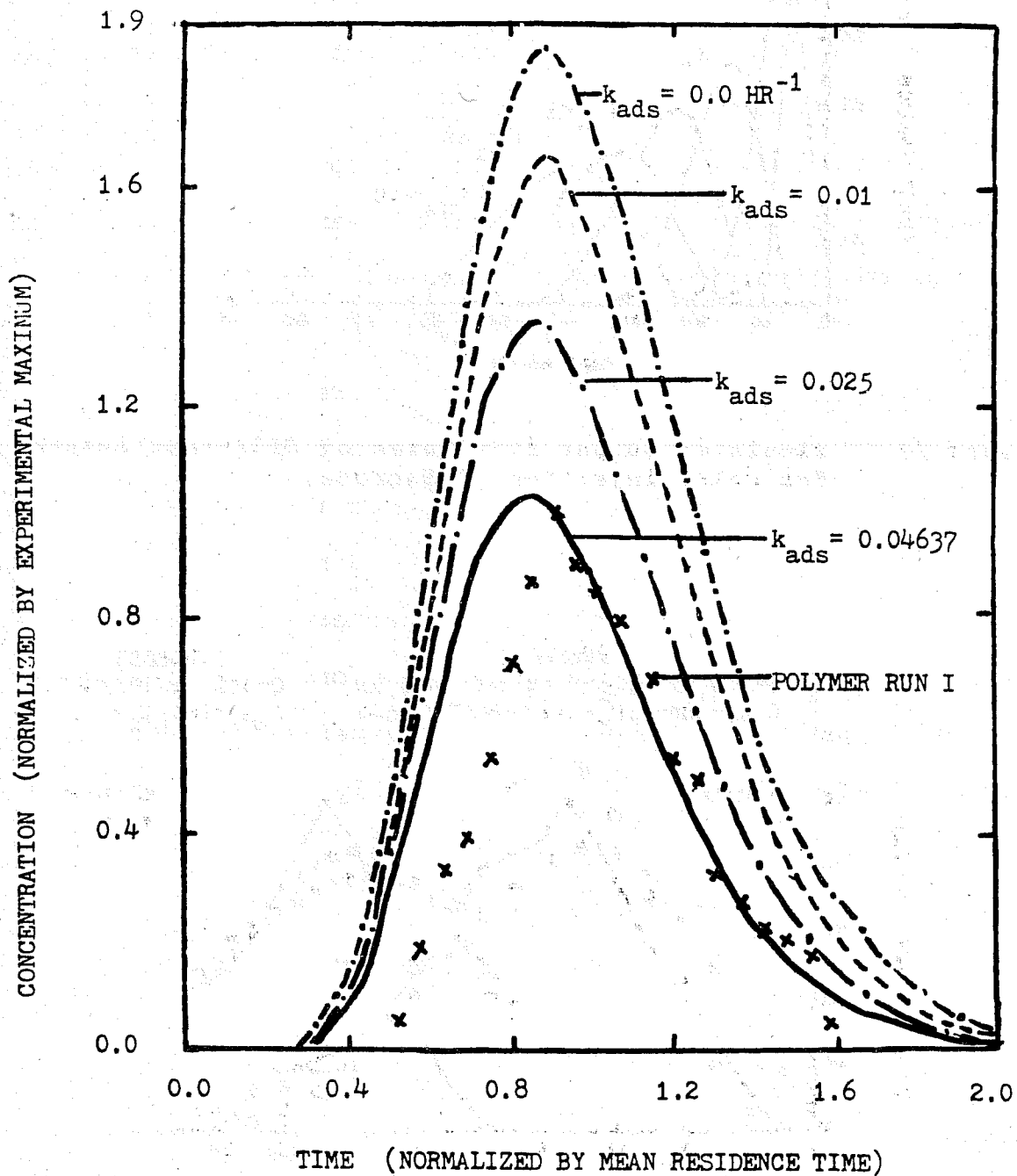


Figure 23 Sucrose and Polymer Signals

FIGURE 24 EFFECT OF ADSORPTION CONSTANT,  $k_{ads}$  (49)



broaden and spread. Since these were obtained for sucrose, the area under each curve remained the same.

In Fig. 23, the polymer and the sucrose are plotted on the same set of axes. The total flow rate is slower. The polymer elutes sooner than sucrose. The effect of increasing  $M$  gives the same result as before. The parameters selected do not represent a good fit in either case.

Fig. 24<sup>9</sup> shows the effect of the adsorption constant. As the adsorption constant increases, a lower maximum shifted to the left in the positive time scale is obtained. The peak broadens in accordance with the material balance.

In this development, the number of discrete stages ( $M$ ) and the ratio of the volume of the mixers to the total volume ( $PM$ ) were the parameters that affected the output most. The individual flow rates into the parallel capillaries did not have a substantial influence. By modifying the model, the permeability effect will be incorporated. Although certain combinations of parameters yield results in good agreement with the experimental results, the variables are not unique. This is especially observed when the flow rate is altered or the polymer is used; the experimental and theoretical results diverge (i.e., Fig. 23). Optimization is essential for the estimation of unique parameters. Fig. 20 shows that varying the core sizes will be a significant experiment showing the extent of dispersion. Fig. 24 shows that adsorption is an unresolved phenomenon. We must design experiments to characterize polymer core interactions further.

SYMBOLS IN THE FIGURES

- A = distance between interpolation points
- C = concentration of solute in ppm
- $C_{\max}$  = maximum concentration of solute in ppm
- $k_{\text{ads}}$  = adsorption constant in  $\text{hr}^{-1}$
- M = number of repeating units
- $N_{\text{as}}$  = number of assumed repeating units
- NUM = order of approximation of interpolating polynomial
- NUMM = number of data points
- PM = ratio of volume of mixing chambers to the total volume
- Q = flow rate of stream going into the repeating unit in ml/hr
- $Q_1$  = flow rate of stream going into first flow chamber in ml/hr
- $Q_2$  = flow rate of stream going into second flow chamber in ml/hr
- $Q_I$  = flow rate of stream going into the inaccessible region in ml/hr
- T = time in hr

## C. Tomographic Observation of Oil Displacement

### C.1 INTRODUCTION

Computer axial tomography (CAT) is a technique whereby the electron density over a planar surface can be reconstructed from the information supplied by a multitude of transmission X-ray measurements. A tomographic plane or slice is divided into picture elements (pixelles). It is the purpose of this method to calculate the electron density of each element and thereby to reconstruct an image of the cross-section. By convention, the electron density is given in CT numbers. These are proportional to the deviation of the pixelle X-ray linear attenuation coefficient from that of water ( $CT_{H_2O} = 0$ ). In the present instrument, the pixelles have dimensions  $0.75 \times 0.75$  mm in the plane of the slice and 1 cm in depth. The depth is related to the X-ray beam width and detector geometry. This pixelle volume represents the resolving power of the machine, since the electron density in each pixelle is assumed to be uniform. The present machine is optimized for patient use; thus the exposure dose is minimal and the computation code is optimal for electron densities characteristic of animal tissue (CT numbers of 100). Since silica has a higher atomic number, its CT values are in the range 1000-2000. Thus, all measurements of X-ray density must be calibrated, since we are operating out of the linear range of the machine. This technique was first used in a medical environment in 1973 at the Mayo Clinic for the purpose of identifying tumor regions in the brain.

## C.2 PROCEDURE

### C.2.a Calibration of CAT Scan

Solutions were prepared having different characteristic electron densities. Toluene and carbon tetrachloride and their mixtures represent extremes in electron density for hydrophobic oil-like components. For aqueous systems, solutions of both KI and KCl at 0.1 N and 1.0 N were used as electrolytes.

Ottawas sand (20-60 mesh) was mixed with a solution and poured as a slurry into a test tube (25 mm I.D. × 20 cm) and allowed to settle. Sand was continuously added until there was no free liquid remaining at the top of the tube. Similar tubes were prepared for all of the mineral solutions (36 in all). These tubes were stoppered and placed in a cylindrical container (20 cm I.D. × 23 cm depth). The spaces between the test tubes were filled with dry sand. The container, which was covered and sealed, was used as a test object for the CAT scanning experiments. It was positioned in the scanner with the axis of the cylinder normal to the direction of the tomographic plane, in such a way that the slice would cut through the mid-point of all the test tubes. The results for the CT numbers found at the centerpoint of the different tubes given in Fig. 25.

### C.2.b CAT Scan of Oil Displacement

A Berea sandstone core (300 millidarcy, air; 2 inch diameter, 10 inch length; dried 24 hours, vacuum 100<sup>0</sup>; from Cleveland Quarries) was encapsulated with a thin coat of epoxy (Epon 828). As illustrated in Fig. 26, an epoxy endcap (0.5 inches thick) was formed at one end of the core. After curing, the exit end was cut

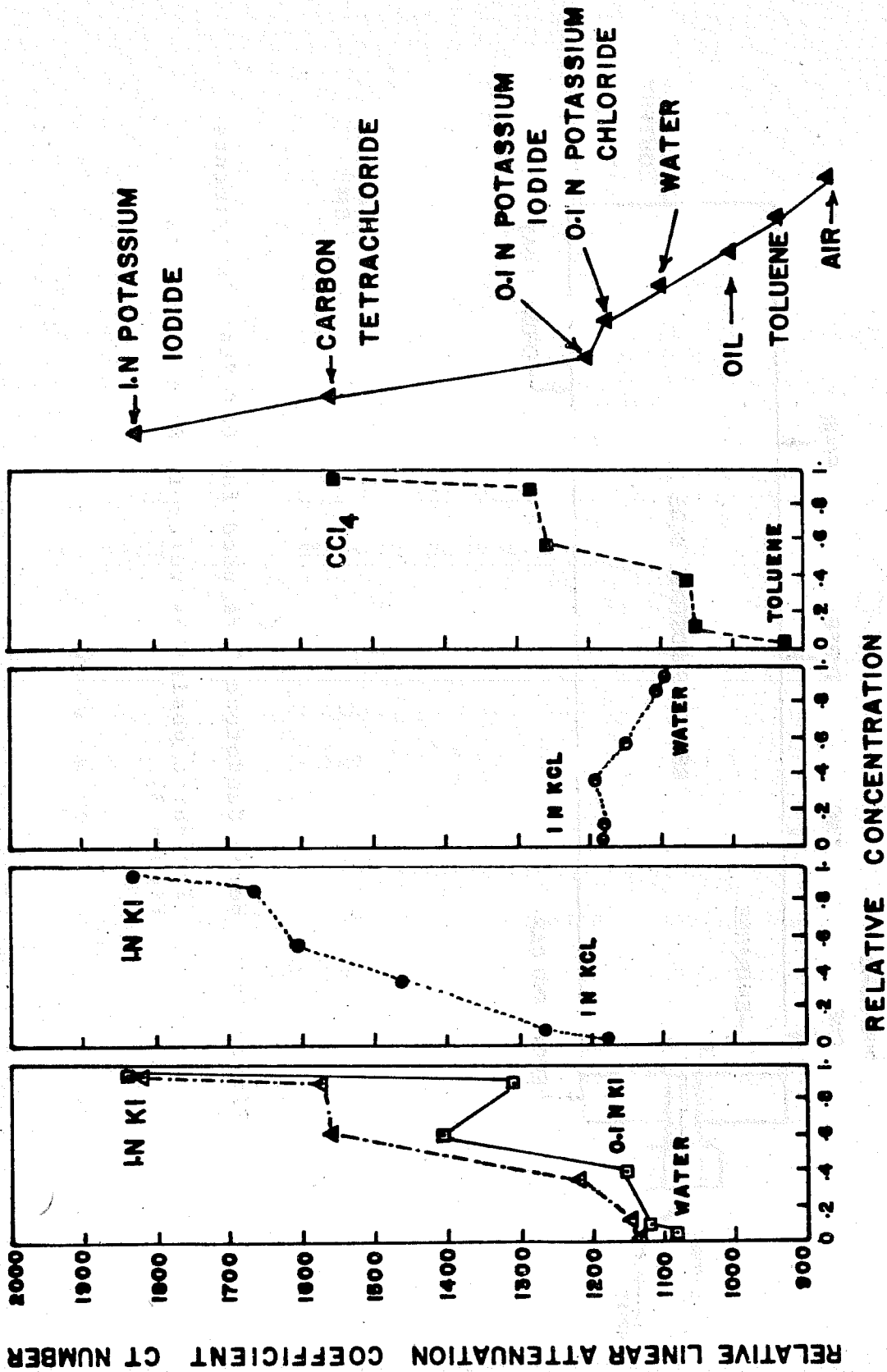


Figure 25 CT Numbers as a Function of Solution Composition for Sand Packed Beds

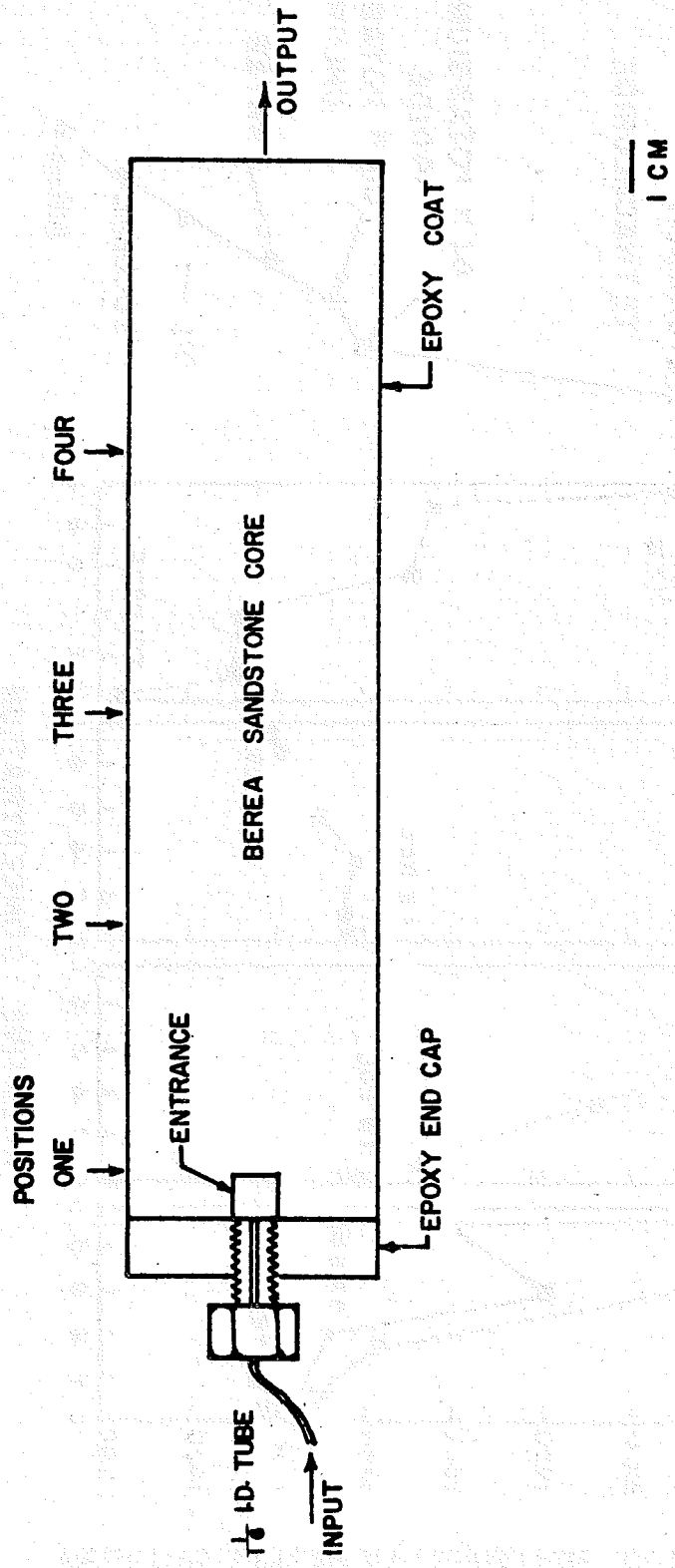


Figure 26 Berea Sandstone Core used for CAT Scan Experiments  
(Indicated positions refer to Scan Images in Figure 3)

off to expose the virgin Berea sandstone. The endcap was drilled and tapped for a 1/4 inch standard pipe to tube connector. At the entrance region, a hold was made approximately 0.75 inches into the core to provide an entry region. The core was evacuated to 100 microns and filled with a light oil (from Texaco, Dr. Morduchowitz). The oil flow-pressure drop was measured using this filtered oil.

A 1 N KI solution was prepared and pumped at a rate of 7 cc/hr into the core. The volume of oil and water coming out of the core was collected. After 100 cc had passed through the core (30 of oil recovered), the apparatus was stopped and the core was taken to the St. Luke's Hospital Center for the CAT Scan. The scan was made approximately 1 hour after the flow was stopped.

### C.3 DISCUSSION OF RESULTS

In Fig. 25 the CT numbers represent the average over to the domain within the sand-packed tubes. The void spaces contain the indicated solutions. For example, there are tubes containing toluene or carbon tetrachloride. The one containing pure  $\text{CCl}_4$  and sand has the highest electron density and thus a CT number of 1500. The tube with toluene and sand has a corresponding CT number of 920. The mixtures of these solutions have electron densities as indicated in Fig. 25. Though these data are taken in a region in which the SCAT scanner is not calibrated, the data are reasonable. Within the calibrated zone (CT less than 1000), the CT numbers are accurate to within  $\pm 0.5$  percent. It is evident that one sees the interface between  $\text{CCl}_4$  and toluene. In fact, it is evident that with this technique, many of the common fluids

used in oil recovery technology have electron density differences which permit their direct observation with CAT scanning techniques.

In Fig. 27, a photographic representation of scans is given for the four positions on the core identified in Fig. 26. These scans were taken one after another within about a 20 minute period during which time there was no flow through the core. In the initial scan, the entry well is observed. The 1 N KI solution is seen as a black region. Evidently there is an air bubble in the injection well. It is seen as a white region. The KI solution has permeated the domain around the injection well, and we feel that only the narrow band around the core periphery is oil filled. In the succeeding sections, the fingering of the 1 N KI solution is evident. The dark zones are KI rich; the light regions are oil rich. It is evident that there are definite preferred paths and that these paths are aligned in definite directions. That this is not a machine artifact was proven by a rotation of the core sample. The stratification of the porous regions may be of geologic origin. However, this was an isolated core and thus, more work is needed to confirm this observation. There is a definite correlation of the pattern from slice to slice and thus, one concludes that the KI regions represent continuous channels in the Berea structure.

Although area histograms were not available at the time of writing this report, it is possible to do an intensity survey to allocate the number of pixelles in each of the different CT categories. In addition, we anticipate carrying these experiments in a dynamic mode and continuously observing the development of

Figure 27

CAT Scan of Water-Flooded Berea Sandstone Core

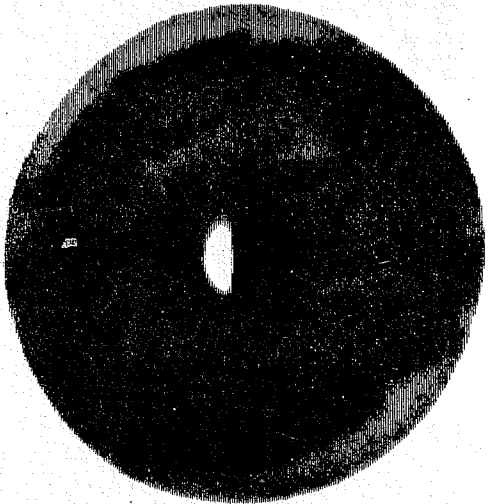
- 
- Positions 1-4 identified in Fig. 26.
  - Intensity Bar Spans from CT = 2000 (Black) to CT = 0 (White).
  - Black regions contain 1 N KI; gray regions are oil filled.



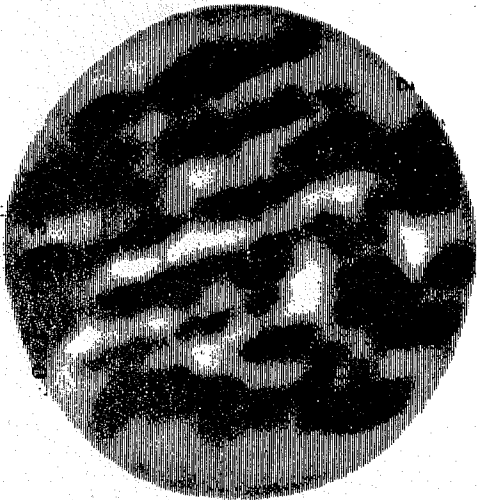
POSITION  
TWO



POSITION  
FOUR



POSITION  
ONE



POSITION  
THREE

the displacement geometry, not only with water flooding but also with micellar and polymer flows.

REFERENCES

Chapter I

1. Powers, G.W., "The Volumetric Determination of Organic Sulfonates or Sulfonates by the Double Indicator Method," Amoco Method C-225, 1970.
2. Reid, V.W., Longman, G.F. and Heinerth, E., "Determination of Anionic-Active Detergents by Two-Phase Titration," *Tenside*, 4, No. 9, 292-294, 1967.
3. Reid, V.W., Longman, G.F. and Heinerth, E., "Determination of Anionic-Active Detergents by Two-Phase Titration," *Tenside*, 5, No. 3-4, 90-96, 1968.
4. Somasundaran, P., "Adsorption from Flooding Solutions in Porous Media - A Study of Interactions of Surfactants and Polymers with Reservoir Minerals," Annual Report to the National Science Foundation and a Consortium of Supporting Industrial Organizations, Columbia University, August 1977.
5. McBain, J.W., Advances in Colloid Science, 1, Interscience, New York, 1942.
6. Mysels, K.J. and Otter, R.J., "Thermodynamic Aspects of Mixed Mycelles - Application to an Empirically Established Equilibrium," *J. Coll. Sci.*, 16, 74-480, 1961.
7. Trogus, F.J., Schechter, R.S. and Wade, W.H., "A New Interpretation of Adsorption Maxima and Minima," submitted to *J. Colloid and Interface Sci.*, July 1977.
8. Trogus, F.J., Schechter, R.S., and Wade, W.H., "Adsorption of Mixed Surfactant Systems," SPE Paper 6845 presented at 52nd Annual Fall Meeting of SPE, Denver, 1977.
9. Kitchener, J.A., "Mechanisms of Adsorption from Aqueous Solutions: Some Basic Problems," *J. Photographic Sci.*, 13, 152-158, 1965.
10. Somasundaran, P., "Adsorption from Flooding Solutions in Porous Media - A Study of Interactions of Surfactants and Polymers with Reservoir Minerals," Annual Report to the National Science Foundation and a Consortium of Supporting Industrial Organizations, Columbia University, July 1978.

## Chapter II

1. "Adsorption from Flooding Solutions in Porous Media," Annual Report submitted to the National Science Foundation and a Consortium of Supporting Industrial Organizations, Columbia University, N.Y., 1978.
2. Ananthapadmanabhan, K.P., "Associative Interactions in Surfactant Solutions and their Role in Flotation," Doctoral Research Proposal, Columbia University, N.Y., 1979.
3. Davies, J.T. and Rideal, E.K., Interfacial Phenomena, Academic Press, N.Y., 1963.
4. Bangs, L.B., "Surfactant Dimers and Their Adsorption," Ph.D. Dissertation, MIT, 1964.
5. Rijnbout, J.B., "Adsorption and Dimerization of Hexadecyltrimethylammonium Bromide from Surface Tension Measurements," J. Coll. Interface Science, 62, (1), 81, 1977.
6. Kulkarni, R.D. and Somasundaran, P., "Kinetics of Oleate Adsorption at the Liquid/Air Interface and its Role in Hematite Flotation," in Adv. in Adv. in Interfacial Phenomena on Particulate/Solution/Gas Systems, Applications to Flotation Research, Somasundaran, P. and Grieves, R.B., eds., AIChE symp. series, No. 150, 1975, pp 124-33.
7. Horne, R.W., Ottewill, R.H., "Studies on the Precipitation of Metallic Salts of Tetradecyl Sulfate," World Congress on Surface Active Agents, Vol. 1-2, 1960, pp. 103-108.
8. O'Brien, E.F., and Wiers, G.H., "Precipitation Boundaries in Calcium-Alkylbenzenesulfonate Systems," Preprints, 48th National Coll. Symp., 220, 1974.
9. James, J.W. and Pethica, B.A., "Ion Exchange at Surfaces Containing Laurylsulfate," in World Congress on Surface Active Agents, Vol. 1-2, 1960, pp 227-32.
10. Wasan, R.T. and Mohan, V., "Interfacial Rheological Properties of Fluid Interfaces Containing Surfactants," in Improved Oil Recovery by Surfactant and Polymer Flooding, D.O. Shah and R.S. Schechter Academic Press, New York, 1977.
11. Somasundaran, P., "Adsorption from Flooding Solutions in Porous Media," Annual Report submitted to the National Science Foundation and a Consortium of Supporting Industrial Organizations, July 1978; Columbia University, New York.

12. Goddard, E.D., Phillips, T.S. and Hannan, R.B., "Water Soluble Polymer-Surfactant Interaction - Part I," J. Soc. Cosmet. Chem., 26, 461-476, 1975.
13. Goddard, E.D. and Hannan, R.B., "Polymer/Surfactant Interactions," J. Am. Oil Chem. Soc., 54, 561-566, 1977.
14. Jones, M.N., "The Interaction of Sodium Dodecylsulfate with Polyethylene Oxide," J. Colloid Interface Sci., 23, 36-42, 1967.
15. Saiko, S., "Solubilization Properties of Polymer-Surfactant Complexes," J. Colloid Interface Sci. 24, 227-234, 1967.
16. Isemura, T. and Imamichi, A., "The Dissolution of Water-Insoluble Polymers in the Surfactant Solution, The Polyelectrolyte Behavior of the Dissolved Polymers," J. Polym. Sci., 33, 337-352, 1958.
17. Tadros, Th. F., "The Interaction of Cetyltrimethylammonium Bromide and Sodium Dodecylbenzenesulfonate with Polyvinyl Alcohol. Adsorption of the Polymer-Surfactant Complexes on Silica," J. Colloid Interface Sci., 46, 528-539, 1974.

### Chapter III

1. Stafford, A.E., "Polymers for Industrial Water Users," Brit. Polym. J., 4, 237-37,
2. Kitchener, J.A., "Action of Polymeric Flocculants," Brit. Polym. J., 4, 217-29
3. Anthony, A.J., P.H. King, and C.W. Randall, "The Effects of Branching and Other Physical Properties of Anionic Poly(acrylamide) on the Flocculation of Domestic Sewage." J. Appl. Polym. Sci., 19, 37-48, 1975.
4. Chang, H.L., "Polymer Flooding Technology Yesterday, Today, and Tomorrow." SPE Paper 70, Symp. of Improved Oil Recovery, of Soc. of Pet. Engrs. of AIME, Tulsa, Oklahoma, (April 16, 1978).
5. Guthrie, H.D., "Utilizing Enhanced Oil Recovery Technology." SPE Paper 7040, Symp. of Improved Oil Recovery, Soc. of Pet. Engr. of AIME, Tulsa, Oklahoma, (April 16, 1978).
6. Vincent, V.B., "Effects of Adsorbed Polymers on Dispersion Stability." Adv. Colloid and Interfac. Sci., 4, 193-277, 1974.

7. Eirich, F.R., "Conformational State of Macromolecules Adsorbed at Solid Liquid Interfaces." J. Colloid and Interfac. Sci., 58 (2), 423-436, 1977 .
8. Vrij, A., "Polymers at Interfaces and the Interactions in Colloidal Dispersions." Pure and Appl. Chem., 48, 471-83, 1976 .
9. Szabo, M.T., "Polymer Retention in Porous Media using Carbon 14 Tagged Hydrolyzed Poly(acrylamide)." Soc. of Pet. Engrs. Trans., 323-28, 1975 .
10. Morris, C.W. and K.M. Jackson, "Mechanical Degradation of Poly(acrylamide) Solutions in Porous Media." SPE Paper 7064, Symp. of Improved Methods of Oil Recovery, Soc. of Pet. Engrs. of A.I.M.E., Tulsa, Oklahoma (April 16, 1978).
11. Lipatov, Y.S. and L.M. Sergeeva, "Adsorption of Polymers from Concentration Solution." Adv. in Colloid and Interfac. Sci., 6, 1-92, 1976 .
12. Sarkar, N. and A.S. Teot, "Coagulation of Negatively Charged Colloids by Anionic Polyelectrolytes and Metal Ions." J. Colloid and Interfac. Sci., 43 (2), 370-81, 1973 .
13. Fleer, G.J., "Polymer Adsorption and its Effects on Colloidal Stability." Meded. Landbouwhogeschool Wageningen, 71 (20), 12-33, 1971 .
14. Koopla, L.K. and J. Lyklema, "Characterization of Polymers in the Adsorbed State by Double Layer Measurement." Faraday Discuss. of Chem. Soc., No. 59, 230-41, 1975 .
15. Tadros, T.F., "Adsorption of Poly(vinyl alcohol) on Silica at Various pH Values and its Effects on the Flocculation of Dispersions." J. Colloid and Interfac. Sci., 64(1), 36-47, 1978.
16. Sakaguchi, K. and K. Nagase, "Flocculation of Kaolin and Calcium Carbonate by Polymers." Bull. Chem. Soc. Japan, 39, 88-91, 1966 .
17. Dollimore, D. and T.A. Horridge, "Filtration of Beds of China Clay Flocculated by Poly(acrylamide). Powder Tech., 5, 111-14, 1971-72 .
18. Jankovics, L., "Kinetics of Poly(acrylamide) Adsorption on Calcium Phosphate." J. Polym. Sci., Pt. A.3, 3519-22, 1965 .
19. Nedelcheva, M.P. and G.V. Stoilkow, "Poly(acrylamide) Adsorption on Cellulose." Colloid and Polym. Sci., 255, 327-33 ,1977 .

20. Mortensen, J.L. "Adsorption of hydrolyzed Poly(acrylonitrile) on Kaolinite Clays and Minerals." Proc. Natl. Conf. Clays and Clay Minerals, 9, 530-45, 1961 .
21. Black, A.P., F.B. Birkner, and J.J. Morgan, "Effect of Polymer Adsorption on the Electrokinetic Stability of Dilute Clay Suspensions." J. Colloid and Interfac. Sci., 21, 626-48, 1966 .
22. Roberts, K., J. Kowalewska, and S. Friberg, "The Influence of the Interactions between Hydrolyzed Aluminum Ions and Poly(acrylamide) on the Sedimentation of Kaolin Suspensions." J. Colloid and Interfac. Sci., 48(3), 363-67, 1974 .
23. Michaels, A.S. and O. Morelos, "Polyelectronic Adsorption on Clays." J. Polym. Sci., Pt. C, Symp. No. 42, 553-62, 1973 .
24. Schamp, N. and J. Huylebroeck, "Adsorption of Polymers on Clays." J. Polym. Sci., Pt. C, Symp. No. 42, 553-62, 1973 .
25. Griffith, T.D., "Application of Ion Exchange Process to Reservoir Preflushes." SPE Paper 7587, 53rd Fall Technical Confer. Soc. Pet. Engrs. of A.I.M.E., Houston, Texas (October 1, 1978).
26. Wada, T., H. Sekiya, and S. Machi, "Synthesis of High Molecular Weight Poly(acrylamide) Flocculant by Radiation Polymerization." J. Appl. Polym. Sci., 20, 3233-40, 1976 .
27. Brandrup, J. and I. Immergut (eds.), Polymer Handbook. New York: Interscience, 1966 .
28. Buchanan, A.S. and R.C. Oppenheim, "Surface Chemistry of Kaolinite I, II, and III." Aust. J. Chem., 21, 2367-71, 1968 ; ibid., 25, 1843-47, 1975 ; ibid., 25, 1857-61, 1972 .
29. Williams, D.J.A. and K.P. Williams, "Electrophoresis and Zeta Potential of Kaolinite." J. Colloid and Interfac. Sci., 65(1), 79-87, 1978 .
30. Hunter, R.J. and A.E. Alexander, "Electrophoretic Mobility and Stability of Kaolinite Sols." J. Colloid and Interfac. Sci., 18, 820-32, 1963 .
31. Chang, Harry L., "Polymer Flooding Technology - Yesterday, Today, and Tomorrow," Soc. Petroleum Engineers of AIME, 7043, (April 1978), pp. 55-70.
32. Gogarty, Barney W., "Micellar/Polymer Flooding - An Overview," Paper SPE 7041, (April 1978).
33. Stanislav, J.F. and C.S. Kabir, "Polymer Flow Behaviour as Applied to Enhanced Recovery," J. Can. Petroleum Tech., 16 (2), (April-June 1977), pp. 91-97.

34. Smellie, Robert H. and Victor K. La Mer, *J. Colloid Sci.*, 13, 1958, pp. 589-99.
35. Peterson, C. and T.K. Kwei, *J. Phys. Chem.*, 65, (Aug. 1961), pp. 1330-33.
36. Jankovics, L., *J. Polymer Sci.: Part A*, 3, 1965, pp. 3519-22.
37. Szabo, M.T., *Soc. Petroleum Engineers J.*, 15, (Aug. 1975), pp. 323-37.
38. Szabo, M.T., *Soc. Petroleum Engineers J.*, 15, (Aug. 1975), pp. 338-46.
39. Dawson, Rapier and Ronald B. Lantz, *Soc. Petroleum Engineers J.*, 12, (Oct. 1972), pp. 448-52.
40. Darcy, H., *Les fontaines publiques de la ville de Dijon.* Paris: Dalmont 1856 .
41. Kozeny, J., *S.-Ber. Wiener Akad. Abt. II.a*, 136, 1927a, p. 271.
42. Muskat, Morris, *Flow of Homogeneous Fluids through Porous Media.* New York: McGraw-Hill Book Company, Inc. 1937 .
43. Muskat, Morris, *Physical Principles of Oil Production.* New York: McGraw-Hill Book Company, Inc. 1949 .
44. Law, J., *Trans. AIME*, 155, 1947, p. 200.
45. Pirson, Sylvain J., *Elements of Oil Reservoir Engineering.* New York: McGraw-Hill Book Company, Inc. 1950 .
46. Amyx, James W., Daniel M. Bass, and Robert L. Whiting, *Petroleum Reservoir Engineering -- Physical Properties.* New York: McGraw-Hill Book Company, Inc. 1960 .
47. Danckwerts, P.V., *Chem. Eng. Sci.*, 2 (1), (Feb. 1953), pp. 1-13.
48. Somasundaran, P. et al., Annual Report to the National Science Foundation (Grant Number: ENG-76-08756). Henry Krumb School of Mines, Columbia University, (July 1978)
49. Jung, Dick, M.S. Thesis (May 1979), under the supervision of Professor Carl C. Gryte.
50. Collins, Royal E., *Flow of Fluids through Porous Materials.* New York: Reinhold Publishing Corporation, 1961 .
51. Dominguez, Jose G. and Paul G. Willhite, "Polymer Retention and Flow Characteristics of Polymer Solutions in Porous Media," Paper SPE 5835 (March 1976).

52. Wyllie, M.R.J. and M.B. Spangler, Bull. Am. Assoc. Petrol. Geologists (Feb. 1952), p. 359.
53. Cornell, D. and D.L. Katz, Ind. Eng. Chem., 45, 1953.
54. Wyllie, M.R.J. and G.H.F. Gardner, "The Generalized Kozeny-Carman Equation," World Oil, (March and April 1958).
55. Vela, Saul, D.V. Peaceman, and E.I. Sandvik, Soc. Petrol. Engr. J., 16, April 1976, pp. 82-96.
56. Bird, Byron R., Warren E. Stewart, and Edwin N. Lightfoot, Transport Phenomena. New York: John Wiley and Sons, Inc. (1972).
57. Levelspiel, O., Chemical Reaction Engineering. New York: John Wiley and Sons, Inc. 1972.
58. Perkins, T.K. and O.C. Johnston, Soc. Petrol. Engr. J., 3, March 1963, pp. 70-84.
59. Aronofsky, J.S. and J.P. Heller, Petrol. Trans. AIME, 210, 1957, pp. 345-49.
60. Levenspiel, O. and W.K. Smith, Chem. Eng. Sci., 6, 1957, p. 227.
61. Hill, Charles G., An Introduction to Chemical Engineering Kinetics and Reactor Design. New York: John Wiley and Sons, Inc. (1977).
62. Turner, G.A., Chem. Eng. Sci., 7, 1957, pp. 156-65.
63. Aris, R., Chem. Eng. Sci., 11, (Nov. 1959), pp. 194-98.
64. Deans, H.A., Soc. Petrol. Engr. J., 3, (March 1963), pp. 49-52.
65. Levich, V.G., V.S. Markin, and Y.A. Chismadzhev, Chem. Eng. Sci., 22, 1967, pp. 1357-67.
66. Kyle, C.R. and R.L. Perrine, Soc. Petrol. Engr. J., 11, (March 1971), pp. 57-62.
67. Rogers, Reed S.C. and Robin P. Gardner, AIChE J., 25(2), (March 1979), p. 229.
68. Seinfeld, John H. and Leon Lapidus, Mathematical Methods in Chemical Engineering. Vol. III: Process Modeling, Estimation, and Identification. Englewood Cliffs, NJ: Prentice-Hall, Inc. 1974.
69. Piessens, R., "Report on Numerical Inversion of the Laplace Transform (Computer Program)." University of Leuven, Belgium, 1969.

70. Bellman, R., R.E. Kalaba, and J. Lockett, Numerical Inversion of the Laplace Transform. New York: American Elsevier 1966 .
71. Ayral, Seyda, "Doctoral Proposal." Chemical Engineering Department, Columbia University, (May 1979).
72. Carnahan, Brice, H.A. Luther, and James O. Wilkes, Applied Numerical Methods. New York: John Wiley and Sons, Inc. 1969 .
73. Henglein, A. "Crosslinking of Polymers in Solution under the Influence of Gamma Irradiation." J. Phys. Chem., 63, 1852-58 1959 .
74. Bourdais, J., "Réactivité de l'acide acrylique dans les copolymérisations." Bull. Soc. Chim. France, 95, 485-89 1955 .
75. Plochocka, K. and T.J. Wojnarowski, "The Effects of Li, Na, K Cations on the Reactivities of Acrylic Acid Salts and Acrylamide in Copolymerization in Aqueous Medium." European Polym. J., 7, 797-804 1971 .
76. Morawetz, H., in Macromolecules in Solution. Second Edition. New York: Interscience 1974 .
77. Overbeek, J.T.G., "Polyelectrolytes Past, Present, and Future." Pure and Applied Chem., 46, 91-101 1976 .
78. Rice, S.A. and M. Nagasawa, Polyelectrolyte Solutions. New York: Academic Press 1961 .
79. Mukhopadhyay, S., B.C. Mitra, and S.R. Palit, "Kinetics of Alkaline Hydrolysis of Poly(acrylamide)." Indian J. of Chem., 7, 903-904 1969 .
80. Shyluk, W.P. and F.S. Stow, "Aging and Loss of Flocculation Activity of Aqueous Poly(acrylamide) Solutions." J. Appl. Polym. Sci., 13, 1023-36 1969 .
81. Silverberg, A., "The Adsorption of Flexible Macromolecules." J. Phys. Chem., 66, 1872-1983 (1962); ibid., 66, 1884-1907.
82. Bailey, F.E., R.D. Lundberg, and R.W. Callard, "Some Factors Affecting the Molecular Association of Poly(ethylene Oxide) and Poly(acrylic Acid) in Aqueous Solution." J. Polym. Sci., Pt. A, 2, 845-51 1964 .
83. Gryte, C.C., unpublished results.

